Catarina Pereira Nobre

Licenciada em Bioquímica

Mestre em Energia e Bioenergia

Thermochemical upgrading of Refuse Derived Fuel

Dissertação para obtenção do Grau de Doutor em

Energia e Bioenergia

Orientadora: Maria Margarida Boavida Pontes Gonçalves, Professora Auxiliar, Faculdade de Ciências e Tecnologia, Universidade NOVA de Lisboa

Co-orientadora: Maria Cândida Lobo Guerra Vilarinho, Professora Auxiliar, Escola de Engenharia, Universidade do Minho

Júri:

Presidente: Doutora Maria Luísa Dias de Carvalho de Sousa Leonardo

Arguentes: Doutor Mário Manuel Gonçalves da Costa

Doutor João Luís Monney de Sá Paiva

Vogais: Doutora Helena Margarida Nunes Pereira

Doutor José Carlos Fernandes Teixeira

Doutor Paulo Sérgio Duque de Brito

Doutora Maria Margarida Boavida Pontes Gonçalves

FACULDADE DE CIÊNCIAS E TECNOLOGIA
UNIVERSIDADE NOVA DE LISBOA

Abril, 2019

Thermochemical upgrading of Refuse Derived Fuel

To my mother. Always.

Acknowledgements

The work presented in this thesis would not have been possible without my close association with many people. I take this opportunity to extend my sincere gratitude and appreciation to everyone who made this PhD thesis possible.

First and foremost, I would like to acknowledge my supervisor, Professor Margarida Gonçalves, whose passion for this work is a motivation for everyone around her. Thank you for sharing your knowledge, for your dedication and availability. Thank you for once again traveling this road with me.

To my co-supervisor, Professor Cândida Vilarinho, thank you for your professionalism and availability, for all your input into this work and for always having a kind word.

To Professor Benilde Mendes, coordinator of this PhD program and President of the Department of Science and Technology of Biomass (DCTB), thank you for your constant presence throughout these years, for all your help and for the interest you show with all your students.

I gratefully acknowledge all the professors and staff from DCTB. Professor Ana Luísa Fernando, Professor Paula Duarte, D. Lurdes, D. Rita and D. Rosa, thank you for all the support over the years and for making this department the best place to work in!

To everyone at CVR (Centro para a Valorização de Resíduos), at the Mechanical Engineering Department of Minho University and at the School of Technology and Management from IPPortalegre, thank you for your collaboration and for always being so welcoming.

Thank you to the BRISK project, for the financial support that allowed for the work conducted at the ECN facilities. And thank you to the people at ECN for all the technical support.

Thank you to CITRI, S.A, Project I&DT nº 24878 for financial support and for supplying the raw materials used throughout this work.

To all of my "brothers and sisters in arms": Ricardo Correia, Octávio Alves, Andrei Longo, Ana Paula Oliveira, Luís Durão, Liliana Serrano, Catarina Viegas, Carolina Rodrigues and João Pires. And, of course, to my "babies": Dieimes Resende, Margarida Santos, Mariana Paiva, Noelia Romero, Leonor Pina and Vasco Soares Jorge. Thank you for all our healthy discussions, for your help and advice, all the laughs, all the venting, all the coffee breaks, lunches, dinners and overall good times we had together! You guys really made this a lot more fun!

To the best friends anyone could have: António, Catarina, Dalila, Diogo, Estela, Joana C., Joana S., and Rui. Thank you for always being by my side, through thick and thin.

To my grandmother, my aunts Bia, Liva and Zezinha, my cousins Zé, Luís, João and Vânia, my godmother, Maria Ana and Luís Alberto, Isabel and Pedro. Thank you for encouraging and helping me every step of the way.

Tiago, I couldn't have done this without you. You also lived every single minute of this and I am truly grateful for your support and your patience. I love you.

To my dad, Tozézico "Master of the Seas", thank you for being the "best dad in the world" since 1986!

And finally, my most heartfelt acknowledgement goes to my mother. I wish she could share this moment with me. I miss her every single day. There you go Mãe, we did it!

Abstract

The main objective of this thesis was to study Refuse Derived Fuel (RDF) upgrading by torrefaction and carbonization and to evaluate composition, fuel properties and adsorbent properties of the produced RDF chars

RDF is a solid fuel produced from non-hazardous wastes, such as municipal solid wastes, construction and demolition wastes or regular industrial wastes, and it is destined for energy production through incineration or co-incineration. Despite the processing, RDF still exhibits unattractive fuel properties, namely high heterogeneity, high moisture and ash contents and low grindability.

In a first approach, torrefaction (200-300 ºC) and carbonization (350 and 400 ºC) were applied to an industrial RDF sample, at a laboratory scale, using residence times between 15 and 60 minutes. The produced chars were characterized for their proximate, elemental and mineral compositions, heating value and leaching behavior. The increase in temperature and residence time showed a positive effect on the decrease in volatile matter and increase in fixed carbon content, as well as carbon content and high heating value (HHV). Leaching tests of the produced chars showed that heavy metals are better retained by the char matrix than within the raw RDF. For temperatures in the torrefaction range, process energy yields were higher than 96.3 % and process energy efficiencies were higher than 85 %. Nevertheless, the HHV of these RDF chars were lower than 19.4 $MJ.kg^{-1}$. In the carbonization range, RDF chars presented HHV in the range of 20.1 to 26.2 $MJ.kg^{-1}$, with energy yields from 84.5 to 91.7 % and process energy efficiencies from 70.8 to 79.2 %.

Torrefaction and carbonization tests were also carried out on a pre-pilot scale at 300 and 400 °C, and all products, namely char, condensates and permanent gases were collected and characterized. Chars showed high carbon contents (61.6 % and 80.2 %, 300 ° C and 400 ° C, respectively) and high calorific values (19.9 $MJ.kg^{-1}$ and 23.5 $MJ.kg^{-1}$, at 300 °C and 400 °C, respectively). Nevertheless, the ash content of the produced chars increased when compared to the raw RDF, reaching a maximum value of 28.8 wt.%. The thermal treatment caused the organic chlorine present in the RDF to be converted into inorganic species which could be removed by washing with water at room temperature. Gaseous emissions were mostly composed of carbon dioxide and carbon monoxide, with lower amounts of methane and hydrogen. The process condensates showed very high COD values and consisted mainly of oxygenated organic compounds, such as acids, furans and phenols.

Although the chars produced by torrefaction and carbonization have presented improved fuel properties, hydrothermal carbonization was also tested in order to validate its potential in the production of hydrochars with reduced ash and chlorine contents. The effects of process temperature (250-300 °C), residence time (30 min and 120 min) and solid-to-water ratio (1:15 and 1:5) on the main characteristics of the hydrochars and process waters were evaluated. The hydrochars had a low ash content (3.3 % at 300 °C and 120 min) and good heating values (28.1 $MJ.kg^{-1}$ at 275 °C and 120 min). The HTC process also revealed a maximum dechlorination efficiency of 55 % at 300 °C for 120 min. The energy efficiency calculations showed that the conditions of 275 °C, 30 minutes with a solid-to-water ratio of 1:5 had lower energy requirements (5.6 MJ), presenting a positive net energy (8.5 MJ) and a higher process efficiency (52.6 %). The process waters presented acid pH, high COD (maximum 27.2 $gO_2.L^{-1}$) and significant concentrations of total phenolic compounds and total reducing sugars. Several organic compounds have been identified in process waters, mainly organic acids, alcohols, furan derivatives, phenolic compounds and aromatic hydrocarbons. Remediation of the HTC process water was attempted through chemical precipitation and adsorption using activated carbon and RDF derived char. Although

removal efficiencies for COD and phenolic compounds were higher for activated carbon, RDF char may be a more sustainable adsorbent to be used in the treatment of these liquid effluents, due to its availability and low cost when compared to activated carbon.

The evaluation of the energetic valorization of RDF char by gasification was carried out at a pre-pilot scale using pellets of pine waste fortified with 5 % and 10 % of RDF char. The gasification tests were carried out at the temperatures of 800 and 850 °C and equivalence ratios of 0.25 and 0.30. The product gas yield ranged from 1.5 to 2.5 $m^3.kg^{-1}$ and was higher for an equivalence ratio of 0.25. The carbon conversion efficiency and the cold gas efficiency ranged from 60.4 to 96.1 % and 42.2 to 73.5 %, respectively. The pellets with RDF char had a better gasification performance at 850 ºC and ER 0.25. The incorporation of RDF char increased the concentrations of heavy PAHs in the gasification tars.

Finally, the material valorization of the RDF char was tested through its use as a low-cost adsorbent for the removal of the dye methylene blue or the heavy metal chromium (VI) from aqueous effluents. The experiments were carried out in batch and column modes and process parameters were varied, namely, contact time, solution pH, adsorbent mass, contaminant concentration, test temperature or column height. RDF char showed potential to remediate methylene blue, and it has been found that the adsorption may follow a chemical adsorption mechanism. Activation of the RDF char by extraction with aqueous KOH improved its removal efficiency towards both analytes.

Keywords: RDF; Torrefaction; Carbonization; Hydrothermal carbonization; RDF char; Hydrochar; Gasification; Adsorption

Resumo

O principal objetivo desta tese consistiu no estudo do melhoramento das características físico-químicas de Combustíveis Derivados de Resíduos (CDR) através dos processos termoquímicos de torrefação e carbonização, de forma a avaliar as propriedades combustíveis e adsorventes dos carvões de CDR produzidos.

O CDR é um combustível sólido produzido a partir de resíduos não perigosos, tais como resíduos sólidos urbanos, resíduos de construção e demolição ou resíduos industriais, e é destinado à produção de energia através de incineração ou coincineração. Apesar do seu processamento, o CDR ainda exibe propriedades combustíveis pouco atraentes, tais como, elevada heterogeneidade, elevados teores de humidade e cinzas e baixa moabilidade.

Numa primeira abordagem, os processos de torrefação (200-300 °C) e carbonização (350 e 400 °C) foram aplicados a uma amostra CDR industrial, em escala laboratorial, utilizando tempos de residência entre 15 e 60 minutos. Os carvões produzidos foram caracterizados relativamente às suas composições imediata, elementar e mineral, poder calorífico e comportamento de lixiviação. O aumento da temperatura e do tempo de residência mostraram um efeito positivo na diminuição da matéria volátil e aumento do teor de carbono fixo, bem como no teor de carbono e no poder calorífico superior (PCS). Os testes de lixiviação dos carvões de CDR demonstraram que os metais pesados são retidos de forma mais eficaz pela matriz de carvão em comparação com o CDR original. Para temperaturas na gama da torrefação, os rendimentos energéticos do processo foram superiores a 96,3 % e as eficiências energéticas do processo foram superiores a 85 %. No entanto, o PCS dos carvões de CDR obtidos por torrefação foram inferiores a 19,4 $MJ.kg^{-1}$. Na gama da carbonização, os carvões de CDR apresentaram PCS de 20,1 a 26,2 $MJ.kg^{-1}$, com rendimentos energéticos de 84,5 a 91,7 % e eficiências energéticas de 70,8 a 79,2 %.

Foram também realizados testes de torrefação e carbonização em escala pré-piloto a 300 e 400 ° C, e todos os produtos, ou seja, carvão, condensados e gases permanentes foram recolhidos e caracterizados. Os carvões de CDR apresentaram elevados teores de carbono (61,6 % e 80,2 %, a 300 ° C e 400 ° C, respetivamente) e elevado PCS (19,9 $MJ.kg^{-1}$ e 23,5 $MJ.kg^{-1}$, a 300 ° C e 400 ° C, respetivamente). No entanto, o teor de cinzas dos carvões produzidos aumentou significativamente quando comparado com o CDR original, atingindo um valor máximo de 28,8 %. O tratamento térmico fez com que o cloro orgânico presente no CDR fosse convertido em espécies inorgânicas que foram removidas por lavagem com água à temperatura ambiente. As emissões gasosas foram compostas maioritariamente por dióxido de carbono e monóxido de carbono, com menores quantidades de metano e hidrogénio. Os condensados produzidos demonstraram valores muito elevados de carência química de oxigénio (CQO) e consistiram principalmente de compostos orgânicos oxigenados, como ácidos, furanos e fenóis.

Embora os carvões produzidos por torrefação e carbonização tenham apresentado propriedades combustíveis melhoradas, a carbonização hidrotérmica (HTC) foi também testada para validar o seu potencial na produção de hidrocarvões com teores reduzidos de cinzas e cloro. Os efeitos da temperatura do processo (250-300 ° C), tempo de residência (30 min e 120 min) e relação sólido-água (1:15 e 1: 5) nas principais características dos hidrocarvões e águas de processo foram avaliados. Os hidrocarvões apresentaram teores de cinza reduzidos (3,3% a 300 ° C e 120 min) e PCS elevados (28,1 $MJ.kg^{-1}$ a 275 ° C e 120 min). O processo HTC também revelou uma eficiência máxima de descloração de 55 % a 300 ° C e 120 min. Os cálculos de eficiência energética demonstraram que as condições de 275 ° C, 30 minutos com relação sólido-água de 1:5 apresentaram menores necessidades energéticas (5,6 MJ), apresentando uma energia líquida positiva (8,5 MJ) e uma maior eficiência do processo (52,6 %). As águas de processo apresentaram pH ácido, elevados valores de CQO (máximo 27,2 $gO_2.L^{-1}$) e concentrações

significativas de compostos fenólicos totais e açúcares redutores totais. Diversos compostos orgânicos foram identificados nas águas de processo, principalmente ácidos orgânicos, álcoois, derivados de furano, compostos fenólicos e hidrocarbonetos aromáticos. A remediação da água do processo HTC foi realizada através de precipitação química e adsorção usando carvão ativado comercial e carvões derivados de CDR. Embora as eficiências de remoção de CQO e compostos fenólicos tenham sido mais elevadas para o carvão ativado, os carvões de CDR podem ser considerados adsorventes mais sustentáveis para o tratamento destes efluentes, devido à sua disponibilidade e baixo custo quando comparados ao carvão ativado.

A avaliação da valorização energética do carvão de CDR através de gaseificação, foi realizada em escala pré-piloto utilizando *pellets* de resíduos de pinho com 5 % e 10 % de incorporação de carvão de CDR. Os testes de gaseificação foram realizados nas temperaturas de 800 e 850 ° C e razões de equivalência (ER) de 0,25 e 0,30. O rendimento de gás produto variou entre 1,5 e 2,5 $m^3.kg^{-1}$ e foi maior para uma razão de equivalência de 0,25. A eficiência de conversão de carbono e a eficiência de gás frio variaram entre 60,4 e 96,1% e 42,2 a 73,5%, respetivamente. Os *pellets* com incorporação de carvão de CDR tiveram um melhor desempenho de gaseificação a 850 °C e ER 0.25. A incorporação de carvão de CDR aumentou as concentrações de hidrocarbonetos aromáticos policíclicos (PAHs) pesados nos *tars* de gaseificação.

Por fim, a valorização material do carvão de CDR foi testada através da sua utilização como adsorvente de baixo custo, para a remoção do corante azul de metileno ou do metal pesado crómio (VI) de efluentes aquosos. As experiências foram realizadas em descontínuo (*batch*) e em contínuo (coluna) e parâmetros do processo foram variados, nomeadamente, tempo de contato, pH da solução, massa de adsorvente, concentração de contaminante, temperatura de teste ou altura da coluna. O carvão de CDR demonstrou potencial para remediar o azul de metileno e verificou-se que a adsorção pode seguir um mecanismo de adsorção química. A ativação do carvão de CDR por extração com KOH aquoso melhorou a sua eficiência de remoção para ambos os analitos.

Palavras-chave: CDR; Torrefação; Carbonização; Carbonização hidrotérmica; carvão de CDR; Hidrocarvão; Gaseificação; Adsorção

Table of contents

List of figures

List of tables

List of abbreviations, symbols and units

Abbreviations

ar	As received basis
ASTM	American Society for Testing and Materials
BET	Brunauer-Emmet-Teller
BFBG	Bubbling Fluidized Bed Gasifier
BOD_5	Biochemical Oxygen Demand (5 days)
BS EN	British Standard European Norm
BSA	N,O-Bis(trimethylsilyl)acetamide
CCE	Carbon Conversion Efficiency
CDW	Construction and Demolition Wastes
CEN/TS	European Committee for Standardization Technical Specification
CGE	Cold Gas Efficiency
CHP	Combined Heat and Power
CITRI	Centro Integrado para o Tratamento de Resíduos Industriais
COD	Chemical Oxygen Demand
cRDF	Carbonized Refuse Derived Fuel
daf	dry ash free basis
db	dry basis
EBCT	Empty Bed Contact Time
EC	European Commission
ECN	Energy Center of the Netherlands
ER	Equivalence Ratio
EU	European Union
EWL	European Wastes List
FGR	Flue Gas Recirculation
FID	Flame Ionization Detector
FT-IR	Fourier Transform – Infrared Spectroscopy
GC-MS	Gas Chromatography – Mass Spectrometry
GHG	Greenhouse Gas Emissions
HHV	High Heating Value
HMF	Hidroxymethylfurfural
HTC	Hydrothermal Carbonization
IUPAC	International Union of Pure and Applied Chemistry
LHV	Low Heating Value
MB	Methylene Blue
MBT	Mechanical and Biological Treatment
MRF	Materials Recycling Facility
MSW	Municipal Solid Wastes
MT	Mechanical Treatment
MTZ	Mass Transfer Zone
PAHs	Polycyclic Aromatic Hydrocarbons
PCDD/Fs	Polychlorinated Dibenzodioxins/Dibenzofurans
PDF	Plastic Derived Fuel
PE	Polyethylene
PEE	Process Energy Efficiency
PGY	Producer Gas Yield
PERSU	Plano Estratégico para os Resíduos Urbanos
PET	Polyethylene terephthalate
PP	Polypropylene
PPF	Paper and Plastic Fuel
PS	Polystyrene
PVC	Polyvinyl chloride
PZC	Point of Zero Charge
RDF	Refuse Derived Fuel
RIW	Regular Industrial Wastes

RPF	Refuse Plastic/Paper Fuel
SEM-EDS	Scanning Electron Microscopy - Energy-Dispersive X-ray Spectroscopy
SRF	Solid Recovered Fuel
TGA/DSC	Thermogravimetric Analysis - Differential Scanning Calorimetry
TOC	Total Organic Carbon
VFBC	Vortexing Fluidized Bed Combustor
WtE	Waste-to-Energy
XRF	X-Ray Fluorescence

Symbols

A	Area above the breakthrough curve
B/A	Base-to-Acid ratio
B_T	Heat of adsorption constant
C_e	Dye concentration at equilibrium
C_p^x	Specific heat of a given substance (x)
Fu	Fouling index
h_0	Initial adsorption rate
$H_{w,HT}$	Water enthalpy at hydrothermal temperature
$H_{w,RT}$	Water enthalpy at room temperature
k_1	First-order rate constant of adsorption
k_2	Second-order rate constant of adsorption
k_f	Freundlich's constant
k_L	Langmuir's constant
k_T	Temkin's constant
k_{TH}	Thomas' constant
m	Mass
Q	Flow rate
q_e	Dye adsorbed at equilibrium (e)
Q_{input}	Total energy requirements
$q_{máx}$	Maximum dye uptake
Q_{net}	Net energy generation
Q_{output}	Energy contained in the process products
q_t	Amount of dye adsorbed at a given time (t)
Q_x	Energy requirement of a given process step (x)
R	Universal gas constant
R (%)	Removal efficiency
T	Temperature
t	Time
W_{total}	Total amount of adsorbate retained in the column
Z	Bed height
ΔG	Gibbs free energy
ΔH	Enthalpy change
ΔS	Entropy change
ΔT	Temperature change
ρ	Pearson's correlation coefficient

Units

cm	Centimeter
g	Gram
h	Hour
J	Joule
K	Kelvin
kg	Kilogram
L	Liter
m	Meter

mg	Miligram
min	Minute
MJ	Megajoule
mL	Mililiter
mol	Mol
s	Second
ton	Tonne
°C	Degree Celsius
µg	Microgram
%	Percentage

Chapter 1

General Introduction

1.1. Relevance of the study

Population growth and fast technological development have led to an increased consumerism which translates into a higher resource consumption and a consequent high waste production (Couto *et al.*, 2016; Teixeira *et al.*, 2014). There is a projected increase in the production of municipal solid wastes (MSW) of 2.2 billion tons by 2025 (Bolyard and Reinhart, 2016). In Portugal alone, around 4.75 million tons of MSW were produced in 2017 (Fernandes *et al.*, 2018). The ever-growing waste production is becoming a serious social and environmental problem, triggering the need to develop an improved waste management strategy.

Waste management largely focuses on treatment and final disposal of waste streams from all sectors of society, but nowadays it also contributes greatly to energy provision and secondary resource recovery (Astrup *et al.*, 2014). European Union (EU) guidelines and strategy for waste management, present in Directive 2008/98/EC, state that "the following waste hierarchy shall apply as a priority order in waste prevention, management legislation and policy: prevention, preparing for re-use, recycling, energy recovery and disposal" (Lombardi *et al.*, 2014). This hierarchy ranks valorization operations higher than disposal methods such as landfilling.

According to the Decree Law n. º 183/2009, that transposes Directive 1999/31/EC, landfilling must be brought to a minimum. Landfilling presents many environmental disadvantages, like the generation of highly contaminated liquid effluents and gaseous emissions. Furthermore, this practice also represents loss of resources and it has significant associated economical costs, depending on the type of waste. Currently there are three landfill typologies, namely, inert, non-hazardous and hazardous and the cost of depositing in each of the typologies is higher as the wastes are more reactive (hazardous) (Ministry of Environment, Regional Ordinance and Regional Development, 2009).

In spite of all the negative characteristics, sanitary landfilling is still recognized as the most common waste management strategy to deal with urban and industrial solid wastes throughout the globe (Abood *et al.*, 2014; Foo and Hameed, 2009; Rivas *et al.*, 2006). Directive 1999/31/EC stated that the amount of biodegradable material sent to landfill ought to be reduced to 35 % of the 1995 level by 2016. For the Member States that were landfilling more than 80 % of MSW in 1995 (which included Portugal) there was a four-year derogation period (Teixeira *et al.*, 2014). By 2008 Portugal had a landfill deposition rate of 88 %, reducing to 53 % by 2013, 52 % by 2014, increasing to 57 % by 2017, as seen in Figure 1.1 (Marçal *et al.*, 2014; Marçal and Teixeira, 2017).

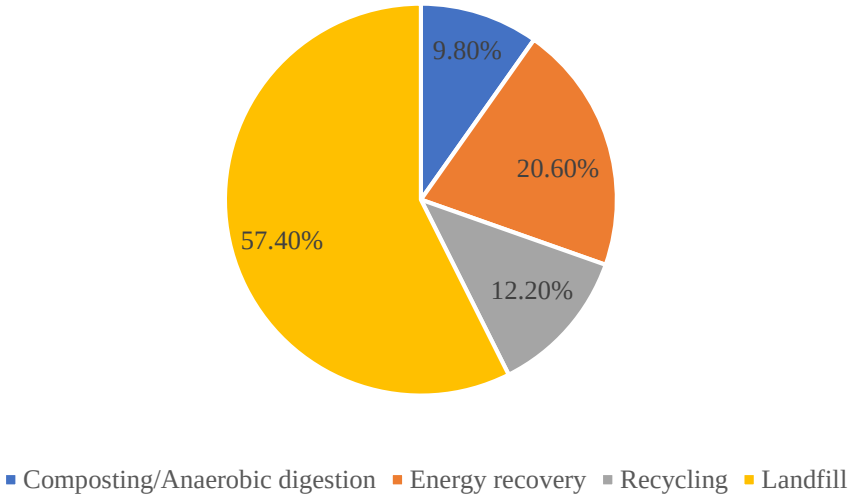

Figure 1.1: Final destinations of MSW in 2017 (Marçal and Teixeira, 2017).

On the 2nd of December 2015, the European Commission approved an action package for circular economy in which the Directive 2008/98/EC was amended. This revised legislative proposal entails a set of common goals for all EU countries until 2030 regarding wastes. It sets clear targets for reducing waste production and it also sets an ambitious and credible route to long-term management and recycling. To ensure its effective implementation, the waste reduction targets contained in the new proposal are accompanied by actual measures to overcome the obstacles *in situ* and the different situations in different Member States (European Union, 2015):

- Re-use and recycle 65 % of municipal waste by 2030;
- Increase re-use and recycling for packaging waste up to 75 % by 2030;
- Binding goal for the limitation of waste landfilling to 10 % by 2030;
- Prohibition of landfilling wastes subjected to selective collection;
- Promotion of economic instruments to discourage landfill deposition;
- Harmonize and simplify the legal framework on by-products and end-of-waste status.

In Portugal, the Action Plan for Circular Economy ("Plano de Ação para a Economia Circular") was discussed and approved by the Council of Ministers Resolution n.º190-A/2017, in November 2017 (Council of Ministers Presidency, 2017).

Re-use and recycling represent effective material recovery. For those waste streams that cannot be efficiently recycled, energy recovery presents itself as the evident solution in order to prevent excessive landfill volumes and save fossil fuel resources. Therefore, a single waste management practice cannot handle the complete range of waste types while simultaneously satisfying the European criteria of an integrated and sustainable management system (Arena and Di Gregorio, 2014; Teixeira *et al.*, 2014).

The production of waste derived fuels such as Refuse Derived Fuel (RDF) or Solid Recovered Fuel (SRF), represents an efficient way to recover energy from wastes (Białowiec *et al.*, 2017). Nevertheless, these fuels often present high heterogeneity which results in less positive physical and chemical properties such as low calorific values, high moisture, ash and chlorine contents. These features can limit their application in thermochemical conversion processes (Edo *et al.*, 2017). Fuels with high chlorine and ash contents are known to cause several operational issues and environmental impacts such as slagging and fouling phenomena, boiler corrosion (Silva *et al.*, 2014) and cause problematic emissions such

as HCl and dioxins/difurans (PCDD/Fs) (Chyang *et al.*, 2010). Moreover, this material can have a significant polymeric fraction that lowers its grindability and can cause problems regarding the feeding systems of boilers or gasifiers. All these factors correlate negatively with its proper use for energy purposes.

Torrefaction, carbonization and hydrothermal carbonization are thermal conversion technologies that may enhance some of the RDF fuel characteristics, by modification of its composition and heating value.

These thermal processes have been applied to lignocellulosic materials resulting in homogeneous chars with lower moisture content, higher calorific values, lower O/C ratios, higher hydrophobicity and enhanced grindability when compared with the original feedstock (Chen *et al.*, 2015b; da Silva *et al.*, 2017; Hwang and Kawamoto, 2010; Manyà *et al.*, 2015; Wang *et al.*, 2018a). According to Vassilev *et al.* (1999) the use of waste derived char as an alternative fuel can bring several advantages when compared with raw waste or RDF, mainly because of its higher quality as a substitute in existing coal-fired power plants, or for its application in gasifiers for syngas production.

Different thermochemical pre-treatments have different operating conditions and process requirements, resulting in the formation of a final product with different physical and chemical characteristics. It is very important to characterize the resulting chars, because their properties will be determinant for their application in the industry.

A careful selection of optimal treatment conditions may allow to upgrade RDF, yielding chars with higher heating value, lower moisture content, higher density and lower chlorine content for fuel applications, such as gasification. Furthermore, the RDF chars may also be used as carbon adsorbents or as activated carbon precursors, applications for which fuel properties, such as ash content, are not as relevant.

Finally, even when the obtained RDF chars are not adequate for energetic or material valorization, thermochemical upgrading will promote an increase in density that is advantageous for the landfill solution, by reducing land use and environmental impacts.

1.2. Research goals

This work intends to give a contribution in implementing solutions for the fuel and material upgrading of RDF, whilst studying the potential applications of an upgraded product. More specifically, this PhD thesis assesses the potential of torrefaction, carbonization and hydrothermal carbonization, as pretreatment steps for RDF, in order to obtain a char with enhanced fuel properties such as homogeneity, carbon content and high heating value. Characterization of the produced chars indicates which thermochemical technology yields chars with better fuel properties. Furthermore, to validate energy applications of the RDF chars, the chars produced via torrefaction were used as feedstock in gasification. Material valorization was also studied by using RDF chars as low-cost adsorbents, and in order to give alternatives for the application of RDF chars.

1.3. Thesis outline

- **Chapter 1 – General introduction**

This chapter describes the relevance of the current thesis in its field of study, as well as the main objectives and the thesis outline.

- **Chapter 2 – State-of-the-art**

This chapter exposes the current issues of waste management, namely RDF production, RDF fuel properties and energy recovery from RDF through different thermal treatment technologies. This chapter also discloses the status of RDF production in Portugal and the need for RDF upgrading technologies. The following book chapter was based on this chapter:

Nobre C., Gonçalves M., Vilarinho C. 2019. A brief assessment on the application of torrefaction and carbonization for Refuse Derived Fuel upgrading. *Lecture Notes in Electrical Engineering*. 505:633–640. doi:10.1007/978-3-319-91334-6_86.

- **Chapter 3 - Upgrading industrial RDF through torrefaction an carbonization: Evaluation of RDF char fuel properties**

Chapter 3 describes the application of the torrefaction and carbonization processes to industrial RDF samples. RDF samples were tested for torrefaction and carbonization varying the process parameters, namely temperature (200-400 ºC) and residence time (15-60 min). The RDF chars were characterized regarding their main physical-chemical properties: proximate and ultimate analysis, high heating value, chlorine content, mineral composition and leaching behavior. The following conference proceedings (oral communication) and paper were based on this chapter:

Nobre, C., Gonçalves, M., Vilarinho, C., Mendes, B. (2018). Upgrading of Refuse Derived Fuel through torrefaction: evaluation of RDF char fuel properties. *Proceedings of ECOS 2018 - the 31st International Conference on Efficiency, Cost, Optimization, Simulation and Environmental Impact of Energy Systems*, 17-22 Junho, Guimarães, Portugal. ISBN: 978-972-99596-4-6.

Nobre C., Vilarinho C., Alves O., Mendes, B., Gonçalves M. 2019. Upgrading of refuse derived fuel through torrefaction and carbonization: Evaluation of RDF char fuel properties. *Energy, 18*. doi: 10.1016/j.energy.2019.05.105.

- **Chapter 4 – Torrefaction and carbonization of RDF: Char characterization and evaluation of gaseous and liquid emissions**

In Chapter 4, RDF torrefaction (300ºC for 30 minutes) and carbonization (400ºC for 30 minutes) were scaled-up in a pre-pilot scale pyrolysis furnace. These tests entailed the chemical and physical characterization of the produced RDF chars, as well as the evaluation and characterization of the liquid and gaseous (permanent gases and condensates) emissions associated with the thermal conversion processes. The following conference proceedings (oral communication) and paper were based on this chapter:

Longo, A., Nobre C., Gonçalves, M., Vilarinho, C., Araújo, J., Mendes, B. (2015). Upgrading of industrial RDF using torrefaction. *3rd International Conference: WASTES: Solutions, Treatments and Opportunities*, pp. 258, 14-16 September, Viana do Castelo, Portugal. ISSN:21830568.

Nobre C., Alves O., Longo A., Vilarinho C., Gonçalves M. 2019. Torrefaction and carbonization of Refuse Derived Fuel: Char characterization and evaluation of gaseous and liquid emissions. *Bioresource Technology,* 285 (121325). doi:https://doi.org/10.1016/j.biortech.2019.121325.

- **Chapter 5 – Hydrothermal carbonization of RDF**

In this chapter, the effect of process variables, such as temperature (250-300 ºC), RDF-to-water ratio (1:5 and 1:15) and reaction time (30 and 120 minutes), in hydrothermal carbonization (HTC) were studied for an industrial RDF sample. HTC tests were conducted in batch mode. The hydrochars were characterized for their fuel properties and the process waters were also characterized in order to evaluated their possible applications or remediation techniques. The following conference proceedings (oral communication) was based on this chapter:

Nobre C., Alves O., Durão, L., Vilarinho C., Gonçalves, M. 2019. Hydrothermal carbonization of Refuse Derived Fuel. *EUBCE 2019 – 27th European Biomass Conference & Exhibition*, Lisbon, 27-30 May. doi: 10.5071/27thEUBCE2019-3CO.15.1

- **Chapter 6 - Gasification of pine waste pellets with incorporation of RDF char**

To validate the energetic valorization of the RDF chars, gasification was chosen as the thermochemical conversion process to convert the obtained chars into a gaseous fuel.

The RDF char was pelletized in different formulations with reference pine wastes. The pellets were characterized for their fuel properties and were gasified varying two very important parameters in gasification: temperature and equivalence ratio. The yield and composition of the producer gas was assessed, as well as the organic composition of the formed tars. The following conference proceedings (oral communications) were based on this chapter:

Nobre, C., Longo, A., Gonçalves, M., Vilarinho, C., Mendes, B. (2016). Gasification of mixtures of lignocellulosic wastes and refuse derived fuel char. *2nd International Conference on Green Chemistry and Sustainable Engineering*, pp.415, 20-22 July, Rome, Itália. ISBN: 978-84-944311-6-6.

Nobre, C., Gonçalves, M., Longo, A., Vilarinho, C., Mendes, B. (2018). Gasification of pellets produced from blends of biomass wastes and refuse derived fuel char. *Proceedings of ECOS 2018 - the 31st International Conference on Efficiency, Cost, Optimization, Simulation and Environmental Impact of Energy Systems*, 17-22 June, Guimarães, Portugal. ISBN: 978-972-99596-4-6.

- **Chapter 7 – Material valorization of Refuse Derived Fuel char – Use as low-cost adsorbent**

This chapter corresponds to the material application of RDF chars. This work consisted in batch and fixed column adsorption experiments for effluent remediation. These tests were performed with model contaminants such as methylene blue and chromium. The potential for enhancing the adsorption capacity of the RDF chars was also studied by testing different decontamination procedures. The following book chapters were based on this chapter:

Nobre C., Gonçalves M., Resende D., Vilarinho C., Mendes B. Removal of chromium and aluminum from aqueous solution using refuse derived char. 2016. *Technological Innovation for Cyber-Physical*

Systems IFIP Advances in Information and Communication Technology, AICT-470; 515-522. doi:10.1007/978-3-319-31165-4_48.

Nobre C., Vilarinho, C., Gonçalves M. Refuse Derived Fuel char as a low-cost adsorbent for the cationic dye methylene blue. 2019. *WASTES: Solutions, Treatments and Opportunities 3rd International Conference,* Caparica, Portugal, 4-6 September (submitted).

- **Chapter 8 – General conclusions**

Chapter 8 includes the main conclusions that were drawn from this PhD work as well as suggestions for future work in the studied area of expertise.

Chapter 2

State-of-the-art

2.1. Introduction

Refuse Derived Fuel (RDF) is the broad designation for fuels obtained from waste not obeying specific technical characteristics and is generally associated with low quality fuels (Nasrullah *et al.*, 2015). This designation was first used by Dr. Jerome Collins, in 1973, to name the secondary fuel produced from processed municipal solid wastes (MSW) (Phillips, 1998). More recently, new regulation and accompanying standards have given rise to a new term, Solid Recovered Fuel (SRF) (Rada and Andreottola, 2012). To provide RDF of a classification based on specific technical criteria, the European Commission has drawn up a set of standards for this fuel and named it as SRF (European Union, 2015).

According to the technical specification CEN/TS 15359:2006, SRF is a solid fuel prepared from non-hazardous waste to be used for energy recovery from incineration and co-incineration facilities. This solid fuel complies with the specifications required by the previously mentioned technical specification and it is processed, homogenized and has an improved quality that allows its trade between producers and consumers (Vieira *et al.*, 2011).

These fuels can originate in several waste streams such as MSW, regular industrial waste (RIW), construction and demolition waste (CDW) or sludge produced from potable water supply and sanitation in treatment plants (Rada and Andreottola, 2012). Only fuels derived from non-hazardous wastes may be classified as RDF or SRF. CEN/TS 15359:2006 also states that solid biofuels and untreated urban wastes are excluded from the SRF definition (Dias *et al.*, 2006).

Moreover, RDF and SRF are considered partly renewable because of their high biogenic content (Dunnu *et al.*, 2010). SRF is classified as a residue with the code "19 12 10" from the European Waste List (EWL) (European Comission, 2014; Vieira et al., 2011). Some countries had a classification and specification system in place before the introduction of these European standards, as such, in these countries, the term RDF and SRF are synonymous. The consequence is that only SRF can be classified as EWL 19 12 10, all the other fractions deriving from a Mechanical and Biological Treatment plant (MBT plant), albeit having suitable fuel properties, must be classified as EWL 19 12 12 (European Comission, 2014).

In the United Kingdom, both EWL 19 12 10 (Combustible waste – Refuse Derived Fuel) and EWL 19 12 12 are used for RDF and rejects from Materials Recycling Facilitiy (MRF) operations, but also for SRF. The exported RDF in Ireland is classified as EWL 20 03 01 (Mixed Municipal Waste), because most RDF producers state that they undertook the minimum level of treatment to allow their waste to be legally exported (Ciceri and Martignon, 2015).

The SRF classification system is based on different indicators, namely economic (lower calorific value), technical (chlorine content) and environmental (mercury content), emphasizing the importance of these three aspects in SRF production and use. This system is based on limit values for the three parameters, using the following data presentation:

- Lower heating value (LHV) - arithmetic average (as received);
- Chlorine content - arithmetic average (dry basis);

- Mercury content – median and 80 percentile values (as received).

The highest of statistical values (median and 80 percentile) in a series of mercury data, determines its classification. Each parameter is divided into five classes and is associated with a scale of 1 to 5 for each parameter. The class code is a combination of three classifications, since the three parameters have equal importance. Table 2.1 shows the classification system for SRF/RDF (Dias *et al.*, 2006).

Table 2.1: Classification system used for solid recovered fuels (Dias *et al.*, 2006).

Parameter	Statistical measure	Units	Class				
			1	2	3	4	5
Lower Heating Value (LHV)	Average	$MJ.kg^{-1}$ (ar)	≥ 25	≥ 20	≥ 15	≥ 10	≥ 3
Chlorine Content (Cl)	Average	% (db)	≤ 0.2	≤ 0.6	≤ 1.0	≤ 1.5	≤ 3
Mercury Content (Hg)	Median	$mg.MJ^{-1}$ (ar)	≤ 0.02	≤ 0.03	≤ 0.08	≤ 0.15	≤ 0.50
	80 percentile	$mg.MJ^{-1}$ (ar)	≤ 0.04	≤ 0.06	≤ 0.16	≤ 0.30	≤ 1.00

This classification is supported by the same technical specification mentioned above (which in Portugal translates to the Portuguese Standard NP 4486:2008).

The shift in definition, classification and specification parameters of RDF for the requirements of the final user, mostly represents an effort to improve the marketability of waste derived fuels (Di Lonardo *et al.*, 2016). Other standards regarding SRF are also available under CEN/TC 343 (Dias *et al.*, 2006), such as the estimation of the biogenic fraction of SRF through the determination of biomass content under the standard EN 15440:2006 (Séverin *et al.*, 2010).

RDF characteristics vary greatly depending on their source and production line scheme and that is why it is important to evaluate the physical and chemical properties of this fuel and the performance of the thermal treatment that the fuel will undergo (Hernandez-Atonal *et al.*, 2007). The distribution of proximate analysis parameters (moisture, ash, volatile matter and fixed carbon) will influence the performance of the burning bed and the heat distribution along the conversion system. Table 2.2 presents typical values for RDF fuel characterization.

Table 2.2: Proximate analysis results for different samples of RDF from different sources.

Sample	Moisture (%, wb[a])	Ash (%, db[b])	Volatile matter (%, db)	Fixed carbon (%, db)	HHV ($MJ.kg^{-1}$)	Waste stream	Reference
RDF 1	8.33	0.37	71.11	20.19	14.04	---	(Duan *et al.*, 2013)
RDF 1	0.99	10.04	79.10	9.60	23.90	MSW	(Grammelis *et al.*, 2009)
RDF 2	1.30	16.10	71.90	10.70	22.35		
RDF 1	3.70	18.90	67.60	9.80	22.30	MSW	(Hernandez-Atonal *et al.*, 2007)
RDF 2	1.70	17.70	73.60	7.00	24.60		
RDF 3	19.70	20.40	49.10	10.80	13.90		
SRF	28.11	9.65	55.99	6.36	14.79	MSW	(Agraniotis *et al.*, 2010)

[a] *wb, wet basis;* [b] *db, dry basis*.

SRF/RDF produced from MSW generally presents larger ranges in each analytical parameter due to its highly heterogeneous composition.

Another characteristic of RDF that impacts the chosen conversion method is its mineral composition. The mineralogical composition determines the predisposal of the fuel for ash fusibility, which leads to fouling and slagging phenomena. It represents one of the most problematic features of waste derived fuels, mainly because these ash related phenomena have a negative impact on the reactor efficiency. Table 2.3 shows the major elements present in two different RDF samples, from different sources.

Table 2.3: Typical metal concentrations in the ash of RDF from different sources (adapted from Rocca *et al.*, 2012 and Baciocchi *et al.*, 2010).

Element	Concentration ($mg.g_{ash}^{-1}$)	Concentration ($mg.g_{ash}^{-1}$)
Al	63.5	66.1
Zn	4.2	2.2
Pb	0.9	1.3
Ni	0.1	0.1
Mn	0.5	2.4
K	4.2	5.4
Cu	3.8	6.2
Cr	0.3	0.4
Cd	-	0.01
Ca	258.4	262.0
Mg	19.1	20.5
Na	54.2	27.7
Cl^-	48.7	36.0

Unlike coal ashes, major elements found in waste derived fuel ashes are not of geological origin. They are mostly derived from refined products that constitute the fuel (Dunnu *et al.*, 2010).

Current regulations are setting high quality standards for waste derived fuels, so that they can be readily accepted as substitutes or auxiliary fuels in most combustion systems with minor modifications (Caputo and Pelagagge, 2002).

Fuels produced from wastes are distinctly cheaper comparing with primary fuels (sometimes they are even offered with additional payment for the consumer) and this causes the willingness to use them in energy intensive branches of industry such as clinker production in the cement industry (Wasielewski *et al.*, 2011).

Waste derived fuels with the right specifications require technologically advanced production lines. The SRF/RDF production process consists in a sequence of organized unit processes aiming to separate the various components of a heterogeneous mixture, using different technologies. The process parameters differ from producer to producer, a consequence of the different strategies with regard to production of this fuel, depending on the degree of quality to be achieved. The line composition will also vary according with specific site conditions and the source of the raw material (Caputo and Pelagagge, 2002; Dias *et al.*, 2006). Collection and treatment of the waste fraction with higher calorific value can be done in two different ways (Ekholm, 2005):

- Separation at the source: Through collection in different bags and containers or simple preparation in two instalments (moist and dry) in two bags of different colors, usually transparent, which are then optically separated on the RDF preparation installation;
- Separation in plants from mixed waste: Mechanical separation through physical processes like shredding, screening, magnetic separation, Eddy Current separation, wind separation, ballistic separation, etc.

In Europe, mechanical treatment (MT) or mechanical biological treatment (MBT) are mixed waste plants that produce SRF/RDF. MBT technologies were developed around 1995 in Germany and Italy, and over the last 20 years, a considerable capacity of MBT has been installed in Europe. These plants are designed for material flow management. They use integrated mechanical processing and biological reactors to convert and separate residual waste into streams of suitable quality, like biostabilized material, dry recyclate or waste-derived fuels. Because of the biological treatments (composting or anaerobic digestion) that handle the organic and putrescible fractions, the MBT system is more suitable for MSW, (Velis *et al.*, 2010).

In MT plants the various unit operations or sorting techniques, aim at separating unwanted components and conditioning the combustible matter in order to obtain an SRF/RDF of predetermined characteristics, following the desired quality standards (Nasrullah *et al.*, 2014). Figure 2.1 shows examples of general procedures and unit operations that can take place in MBT and MT plants.

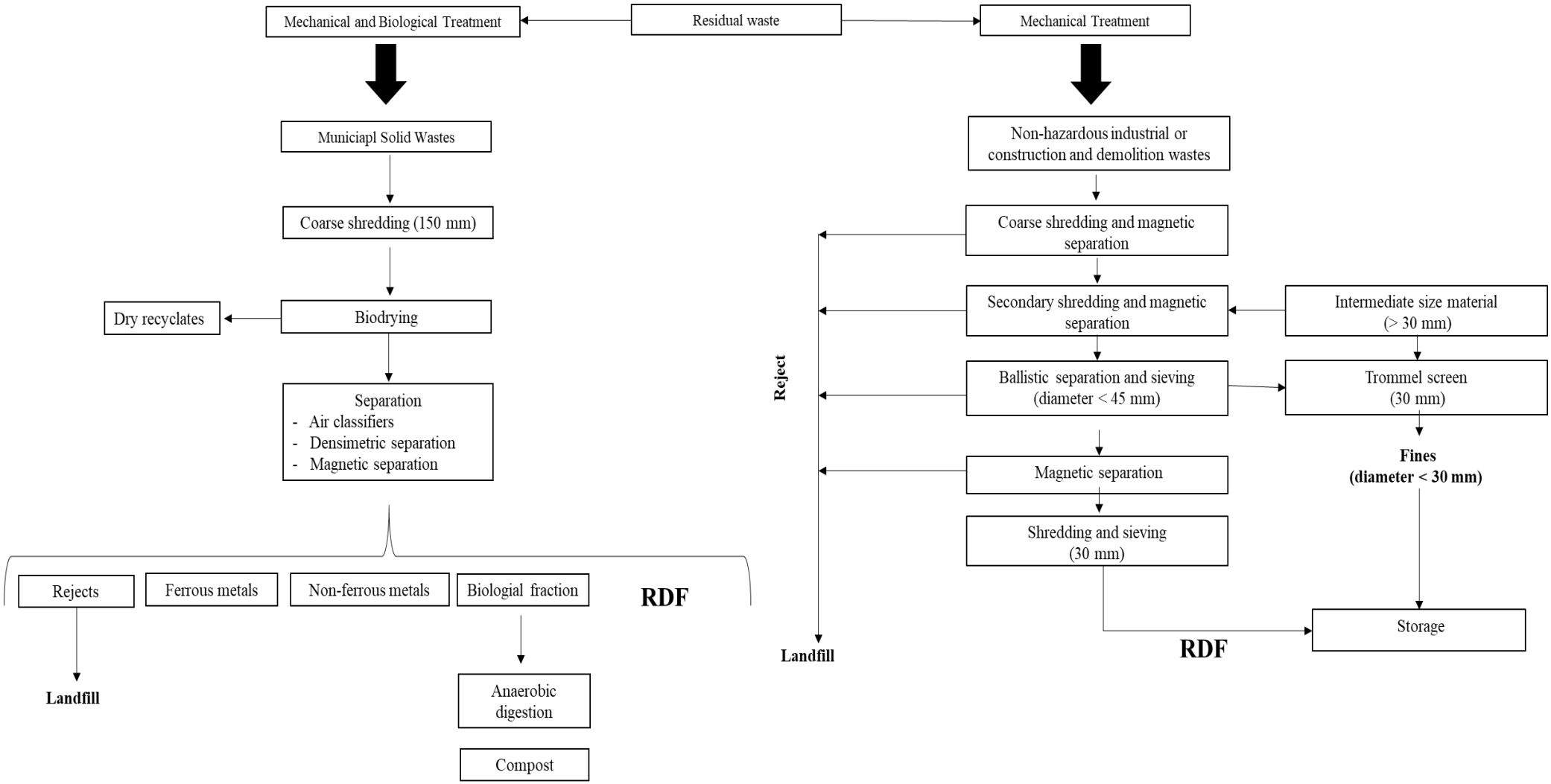

Figure 2.1: Example of process flow schematics for the production lines of MBT and MT plants (adapted from Cimpan and Wenzel, 2013; Cook *et al.*, 2015; Pinto, 2009; Sarc and Lorber, 2013).

MT and MBT plants create opportunities to recover additional resources and increase the spectrum of possible energy recovery applications, including high efficiency industrial processes. Nevertheless, they also increase system complexity, they add inherent system losses and induce additional energy consumption (Cimpan and Wenzel, 2013). Mechanical separation of wastes reduces the concentration of hazardous substances contained in the waste through the concentration of these substances in other streams of the process, not leading up to fuel production (Rotter *et al.*, 2004). The quality of the SRF/RDF is improved through this process due to an increase in the heating value by reducing moisture and ash content of the fuel.

The final stage of SRF/RDF production corresponds to packaging and storage. These final steps require extra safety measures because this fuel can go into spontaneous ignition causing explosions in the storage facilities and surroundings. In 2003 two people died in an explosion caused by the spontaneous ignition of SRF/RDF stored in a cylindrical silo. Chemical oxidation is one of the mechanisms involved in the auto-ignition of SRF/RDF. The fuel is exposed to the air absorbing the oxygen and consequently forming peroxides (this can occur through light exposure, heat or micro-organisms) (Yasuhara *et al.*, 2010).

SRF/RDF typologies can vary depending on their original source or on their shape (Figure 2.2). According to the latter, this fuel can be presented in the forms of:

- Fluff: Loose, low-density material, with dimensions from 10 to 100 mm and can be transported by air;
- Pellets: Produced through densification of the loose material, having dimensions < 25 mm (in diameter or equivalent). The pelletization process enhances the density of the fuel, giving it more energy per volume than regular fluff. It also improves the bulk density of the waste, thus improving its handling, transportation and storage (Marsh *et al.*, 2007).
- Briquette: This typology corresponds to a block or cylinder produced by agglomeration of the fluff with dimensions from 40 to 200 mm.

Figure 2.2: RDF typologies: (a) Fluff SRF (*Source: http://www.itrimpianti.com*); (b) Pellet SRF (*Source: http://www.suxe.co.uk*); (c) Briquette SRF (*Source: http://www.wxteneng.com*).

According to the source, there are many typologies of SRF/RDF. They are generally applied when these fuels are produced from a very specific waste flow, like industrial wastes (PDF – plastic derived fuel or PPF – paper and plastic fuel, for example). Different typologies do not apply for SRF/RDF produced from MSW (Dias *et al.*, 2006).

2.2. RDF production in Portugal

In Portugal, although RDF can be produced from different waste streams, the guidelines for this fuel are directly connected to MSW. The strategic plan for MSW ("Plano Estratégico para os Resíduos Sólidos Urbanos" - PERSU II 2007-2016) promoted the diversification of technical solutions and MSW treatment facilities. These treatment facilities increased the capacity of organic valorization through MT or MBT, maximizing the amount of wastes susceptible to valorization (Agência Portuguesa do Ambiente, 2014).

The strategy for waste derived fuels ("Estratégia para os Combustíveis Derivados de Resíduos") was approved through the Decree n. º 21295/2009 of August 26th by the Ministry of Environment. This strategy followed and complemented PERSU II, presenting a set of acting measures for production, use and marketability of RDF. Some of the measures in this strategy regarded the optimization of the production process, limitations and prohibitions in landfill deposition, establishing RDF production units and sensitization and promotion for the RDF end-users. The strategy covers the period between 2009 and 2020, is binding only on mainland Portugal and represents an investment between 550 and 730 million euros (Agência Portuguesa do Ambiente, 2014).

In 2014, PERSU II was reviewed mostly because the specified goals were not being achieved and a new plan designated PERSU 2020 was approved by the Administrative Rule nº.187-A/2014 of September 17th. This new plan redefined the urban waste management strategy in Portugal for the period of 2014-2020. However, in the assessment of the situation in 2017, it was verified that preparation for reuse and recycling had a value of 38 %, with the target for 2020 being 50 %. The deposition of biodegradable MSW in landfills was 43 % (based on the 1995 value) and the maximum MSW deposition target for 2020 was 35 %. Thus, despite the efforts that have been made by the sector, there was a concern that the 2020 targets still represented a challenge. In that sense, a new document "PERSU 2020+" was recently put to public discussion. This new plan addresses RDF, recognizing the large amounts that are produced and landfilled. The value of RDF landfill deposition of 10 % by 2035 established by the Landfill Directive still seems very ambitious, and the document itself still presents some uncertainties regarding this particular subject (Work Group for the preparation of PERSU 2020+, 2018).

Moreover, the Energy Strategy 2020 ("Estratégia para a Energia - ENE 2020"), approved by the Council of Ministers Resolution n.º 29/2010 of April 15th establishes the "Axis 2 - Bet on renewable energy" ("Eixo 2 – Aposta nas energias renováveis"), in the biogas and waste areas, giving support to RDF potential use and special attention to energy recovery from waste and effluents (Agência Portuguesa do Ambiente, 2014).

The potential of MSW for RDF production was estimated between 950,000 and 1.2 million tons in 2013. It was assumed that the waste management sector, in a perspective of self-sufficiency, was likely to ensure the disposal of a significant part of the RDF produced from MSW in centralized units and that the remaining RDF would be forwarded to other economic activity sectors (Agência Portuguesa do Ambiente, 2014). But the last report on MSW (2017) showed that these expectations were not met (Table 2.4).

Table 2.4: RDF production or production of raw material for RDF (ton) from MSW, in Portugal between 2011 and 2017 (adapted from Marçal *et al.*, 2014; Marçal and Teixeira, 2017).

Year	2011	2012	2013	2014	2015	2016	2017
Triage	---	---	120	757	1308	0	0
MT	---	5709	11484	69996	33750	21042	0
MBT	5412	27153	20498	34190	72564	467	379
RDF production units	---	---	---	---	6943	0	0
Total	5412	32862	32102	104951	114566	21509	379

According to the Portuguese Agency for the Environment (APA), 2011 marked the first time RDF was produced from MSW in Portugal. The amount of RDF increased significantly in 2012 and had a slight decrease in 2013, followed by a significant increase in 2014 and 2015. The waste management companies TRATOLIXO and RESITEJO were the main contributors to the large increase in RDF production verified in 2014 (Marçal *et al.*, 2014). Nevertheless, the decrease that followed, from 2016 on, was very significant. This situation was justified by the unavailability of the waste management operations to receive the produced RDF arguing that it did not comply with the minimum requirements for its use (Marçal and Teixeira, 2017). In 2015, 2.5 % of the produced RDF was stored for future applications, 1.7 % was used by the cement industry, and 96 % was landfilled (Work Group for the preparation of PERSU 2020+, 2018).

The processing and shipment of RDF evidences a stagnation in the market by the clear difficulty in their disposal. According to the Work Group for the preparation of PERSU 2020+ (2018) significant investments should be made regarding preparation and drying of RDF. High moisture and large granulometry were two problems that were assessed in the RDF that is currently being produced in Portugal, and these issues severely hinder fuel applications for RDF. Since the portuguese RDF does not present enough quality to be used by its prime consumer (cement production), RDF entering Portugal by transboundary movements reached 75,909 ton in 2016, and this value represented an increase of 130 % over the value of 2014. The United Kingdom is responsible for 75 % of the RDF shipped to Portugal.

From these facts, it is seen that RDF production needs to be improved in order for the final product to meet the quality standards that are needed for its use. This improvement in quality could be achieved by investigating the possibility of upgrading RDF through thermochemical conversion processes, assessing product characteristics as well as scalability and sustainability of those processes.

2.3. Thermochemical conversion technologies applied to RDF

Thermal conversion processes are fundamental for waste management systems in order to reduce the mass of waste and to recover the energy content (thermal and electric) from unrecyclable materials.

The thermal treatment technologies used for energy recovery from RDF are very similar to current technologies used for fossil fuels so, theoretically, the existing technologies for combustion could be used in RDF valorization. However, because of the different physical and chemical characteristics of the RDF, there may be technical barriers to their application in energy recovery units designed for fossil fuels.

Combustion, co-combustion, gasification, pyrolysis and carbonization represent the five main types of technology used in RDF valorization (Dias *et al.*, 2006). Each technology has its specific requirements regarding calorific value and granulometry of the RDF. Combustion and co-combustion are very mature technologies for waste conversion, whereas gasification, pyrolysis and carbonization in spite of the environmental advantages over combustion, still have technical issues to overcome in order to fully be established as mature and easily scalable technologies.

2.3.1. Combustion

RDF can be used in specifically designed power plants that only incinerate these waste derived fuels. These plants function either for the sole purpose of producing electricity or as combined heat and power (CHP). It is in most part for the use in these facilities that the quality criteria for RDF needed to become more severe. Previous RDF had a non-homogeneous distribution of certain elements like chlorine, cadmium and mercury leading to high concentrations and dangerous emissions, as well as corrosiveness of the ash deposits (Nasrullah *et al.*, 2015). On the other hand, RDF can also be used as a substitute fuel in pre-existing plants or production units with heavy energy demands.

Combustion can be simply defined as a reaction between oxygen and a fuel, meaning, the exothermal oxidation of a fuel. Co-combustion or co-processing is a concept that implies that the energy recovery will be promoted in facilities with a different primary purpose other than the same energy recovery, such as thermoelectric plants or the cement industry. These co-combustion systems using SRF/RDF are already established throughout Europe. One of them is the co-combustion of SRF in a lignite fired power plant in Weisweiler (Germany). This power plant has a pulverized fuel firing system and two boilers of 600 MW. The co-combustion trials were done to investigate fuel handling and feeding system, combustion behavior, emissions and ash properties and lasted for two weeks in March 2005 (Grammelis, 2013).

Cement production plants seem to be the most suitable option for SRF/RDF co-combustion, mainly because these production plants are wide-ranging regarding SRF classes and because of the reduced greenhouse gas (GHG) emissions compared to traditional fuels used in cement kilns (Di Lonardo *et al.*, 2016). Cement manufacturing plants also assure high temperature conditions offering an appropriate guarantee for the thermal destruction of residuals without aggressive environmental impacts (Dias *et al.*, 2006; Genon and Brizio, 2008). Each metric ton of cement corresponds to 60-120 kg of fuel oil or an equivalent mass in other fuels amounting to 3000-5000 $kJ.kg^{-1}$ of produced clinker (Genon and Brizio, 2008; Grammelis, 2013). This energy consumption contributes to 4 % of the world's CO_2 emissions (Grammelis, 2013). Every 10 % decrease in the cement CO_2 intensity by 2050 could save around 0.4 Gt CO_2 (Kara, 2012).

The volumes of waste and biomass that are used in cement production have quadrupled in 15 years (1990 – 2005). The German cement industry, for example, used about 2 million tons of SRF/RDF per year (Grammelis, 2013).

A significant example of fossil fuel reduction in the cement production process is the Portuguese company Cibra-Pataias (CMP). This company has since 2006 replaced traditional fuels with alternative fuels like tires, vegetable waste, animal waste and RDF, although this substitution only takes place when producing grey clinker. Despite the inherent advantages in fuel substitution, the growing increase in fuel substitution rate results in lower energy yields leading to an increase in heat consumption. In 2011, the heat consumption per ton of grey clinker increased from 832 $kcal.kg^{-1}$ to 857 $kcal.kg^{-1}$. This upsurge results in a higher fuel consumption, that rose from 43.1 % to 45.4 % (CMP-Cimentos Maceira e Pataias, 2011).

The research on combustion and co-combustion using refuse derived fuels is well developed and there are several authors dedicated to the study of combustion systems in order to better understand the relation between this thermal treatment and fuel composition, combustion system design, pollutant emissions and ash management.

Hernandez-Atonal *et al.* (2007) investigated RDF combustion characteristics and associated pollutant emissions in a fluidized bed combustor. The results showed that the combustion efficiency of the system was enhanced when secondary air jets were used. Between 2.6 % and 4.3 % of the potential nitrogen present in the fuel was converted to NOx. Also, the authors indicated that there was a small decrease in NOx concentration upon injection of secondary air. The captured fractions of N, Cl and trace elements in the fly ash were also evaluated and the ratios of Ca/(S+0.5Cl) were found between 1.6 and 2.2 proving that the fly ash was very efficient in capturing Cl.

Weber *et al.* (2009) used an experimental furnace to issue jet flames of a pure refuse derived fuel. This work intended to compare the properties of RDF flames with those of pulverized coal flames. The authors demonstrated that there are important differences between the coal flames and RDF flames. For instance, pulverized coals ignited in the close vicinity of the burner with completion of the combustion in the first 300 ms. On the other hand, RDF, in spite of its high volatile content, had its combustion extended far into the furnace with only 94 % burnout after 1.8 s. There were significant amounts of oily tars in the RDF flames albeit temperatures being higher than 1300 ºC. Tars highly affect the slagging

tendency of RDF. This work gave strong indications that the use of even a small quantity of RDF can decrease boiler efficiency and increase slagging and fouling problems.

Duan *et al.* (2013) studied combustion of RDF and sawdust in a pilot scale vortexing fluidized bed combustor (VFBC), employing flue gas recirculation (FGR). For sawdust combustion, CO emissions decreased with bed temperature, excess oxygen ratio and in-bed stoichiometric oxygen ratio. The NOx emissions showed an inversed tendency. Combustion using sawdust as the fuel had difficulty meeting the CO emissions regulation requirement. The CO and NOx emissions of RDF combustion showed a similar trend, but RDF combustion decreased the CO emissions mostly due to its distinct pellet structure and burning pattern.

The thermal characteristics and co-combustion efficiency of two RDF samples were investigated by Akdag *et al.* (2016). The RDF samples were combusted alone and co-combusted with coal and petroleum coke using percentages of 3 %, 5 %, 10 %, 20 % and 30 % on an energy basis. The authors found that the calorific values of RDF samples were similar to those of coal and a little lower than petroleum coke. When RDF in the mixture was higher than 10 %, there was an increase in CO concentration in the flue gas, leading to a decrease in combustion efficiency. The presence of RDF also decreased SO_2 emissions while showing no change in the NOx emission profile. Moreover, the XRF analysis indicated that slagging and fouling potential of the RDF samples was a function of the amount of RDF in the fuel mixtures since the slagging and fouling indices were higher when the RDF was combusted alone.

In spite of being the most mature technology for Waste-to-Energy (WtE) purposes, combustion has very significant environmental impacts, directly related with the produced emissions and hazardous by-products. Moreover, RDF combustion still presents significant challenges mostly regarding combustion efficiency or ash related problems, which are directly associated with RDF chemical and physical properties. There is still a need to study, optimize and test more reactor configurations, combustion conditions, fuel upgrading (thermal pre-treatments) and other parameters in order to efficiently produce energy through RDF.

2.3.2. Gasification

Gasification technology has been around since the 1850s. Back then, the city of London was almost entirely illuminated by “town gas”, which was produced through the gasification of coal (Belgiorno *et al.*, 2003). Nowadays, waste gasification represents one of the most recent and challenging additions to WtE technologies. This thermochemical conversion process basically converts solid wastes into a “producer gas” or “syngas” ($CO+H_2$) (Materazzi *et al.*, 2016), by means of high temperature and an oxidizing agent below stochiometric needs (air, steam, nitrogen, carbon dioxide, oxygen or a combination of the referenced gases) (Kumar *et al.*, 2009). The gasification agent allows the feedstock to be quickly converted into gas through different heterogeneous reactions and the producer gas contains mainly CO_2, CO, H_2, CH_4, H_2O and in smaller amounts higher hydrocarbons, inert gases present in the gasification agent and contaminants like small char particles, ash and tars (Belgiorno *et al.*, 2003). The series of different phenomena occurring during gasification, particularly biomass gasification, entail drying, pyrolysis, oxidation and reduction (Ramos *et al.*, 2018). According to Kumar *et al.* (2009), the overall gasification reaction in an air and/or steam gasifier can be represented by equation 2.1, followed by multiple reactions and pathways. The main reactions that occur during gasification are represented in Table 2.5.

Table 2.5: Main reactions occurring during gasification (adapted from Kumar *et al.*, 2009; Ramos *et al.*, 2018).

Equation	Number
$CH_xO_y(feedstock) + O_2(21\%\ of\ air) + H_2O\ (steam) \rightarrow CH_4 + CO + CO_2 + H_2 + H_2O\ (unreacted\ steam) + C\ (char) + tar$ (overall gasification reaction)	2.1
$2C + O_2 \rightarrow 2CO$ (partial oxidation)	2.2
$C + O_2 \rightarrow CO_2$ (complete oxidation)	2.3
$C + 2H_2 \rightarrow CH_4$ (methanation reaction)	2.4
$CO + H_2O \rightarrow CO_2 + H_2$ (water gas shift reaction)	2.5
$CH_4 + H_2O \rightarrow CO + 3H_2$ (steam reforming reaction)	2.6
$C + H_2O \rightarrow CO + H_2$ (water gas reaction)	2.7
$C + CO_2 \rightarrow 2CO$ (Boudouard reaction)	2.8

The inorganic ash is all that remains after gasification and oxidation of the carbon in the char. After cleaning, the syngas can be further used to produce liquid fuels, used as feedstock for producing hydrogen, methanol, ammonia or it can be used to produce green electricity (Dalai *et al.*, 2009; Materazzi *et al.*, 2016).

In order to have satisfying energy efficiencies, gasification needs fuels with a certain degree of homogeneity and, as such, RDF is often subjected to several preparation pre-treatments before it is used in a gasifier (Belgiorno *et al.*, 2003).

In spite of being associated with lower power production, a higher degree of complexity and to higher implementation costs, gasification of solid wastes accounts for around a hundred of operating plants, with capacities between 10.10^3 and 250.10^3 tons per year (Barba *et al.*, 2016). One example of a successful gasification technology using waste derived fuels, is the power plant in Lahti (Finland), which is an integrated gasification/coal-firing power plant. Gasification with secondary fuels is an alternative thermal use of RDF. The product gas is cleaned and then it is burned in the coal-fired plant. This plant is in use since 1998 and has a capacity of 20 $ton_{SRF}.h^{-1}$. The efficiency of the coal power plant was improved by 11 % with the integration of the gasification process (Grammelis, 2013). Table 2.6 presents other gasification demonstrations and efforts in Europe for RDF/SRF.

Table 2.6: Examples of gasification technologies for energy production from RDF/SRF *(*adapted from Dunnu *et al.*, 2012).

Name	Technology	Specifications	Status	Country	Reference
Corenso	Bubbling fluidized bed gasifier	40 MW_{th}	Demonstration plant was operating for 1400 h during tests	Finland	(Wilén, 2004)
TPS – Termiska AB	Fluidized bed gasifier with dolomite bed	30 MW_{th} input of RDF	Shifted to biomass	Sweden	(Kwant and Knoef, 2004)
Värnamo	Pressurized air gasification	8 MW_e – Combined heat and power	Operated with RDF for short periods of time	Sweden	(Kwant and Knoef, 2004)
Grève-en-Chianti	2 x Circulating fluidized bed gasifiers	15 MW of fuel capacity per gasifier	Processes $100t/day_{RDF\ pellets}$	Italy	(Dias *et al.*, 2006)

Gasification has received increased attention mostly due to the growing environmental concerns based on the use of non-fossil fuels and chemical feedstocks, as well as energy provision and reduction

of fossil fuel dependency (Arena and Di Gregorio, 2014). This process has very desirable pollution minimization effects, as well as a higher recovery efficiency than incineration (Galvagno *et al.*, 2009).

Moreover, gasification presents other advantages over traditional combustion of solid wastes. It offers the possibility of combining operating conditions, such as temperature (1000-1700 K), pressure (1-30 bar), equivalence ratio, gasifying agent (air, O_2 or steam) or combining the features of the specific reactor (fixed bed, fluidized bed, entrained bed, vertical shaft, moving grate furnace, rotary kiln, plasma reactor), in order to produce a syngas with different characteristics for use in diverse applications (Arena, 2012; Molino *et al.*, 2013).

According to different authors, fluidized bed reactors represent the most promising technology, mainly because of the enhanced flow mixing, operation flexibility and closely constant temperature (Arena, 2012, 2011; Barba *et al.*, 2016). This set of characteristics makes it possible to vary raw materials in this type of reactor, ranging from biomass to solid wastes. Fluidized bed gasifiers represent more than 30 commercial units worldwide, and due to the aforementioned characteristics, they are frequently employed as RDF conversion technologies (Materazzi *et al.*, 2015).

Arena and Di Gregorio (2016) studied the technical feasibility of the air gasification of three SRF samples in a pilot scale bubbling fluidized bed reactor. The samples were co-products of a recycling process of post-consumer absorbent hygiene products. Gasification operations occurred under conditions of thermal and chemical steady state, with equivalence ratios (ER) from 0.24 to 0.39. This study obtained carbon conversion efficiencies higher than 93 % and up to 98 %, for an ER higher than 0.3, having cold gas efficiencies up to 67 %. The application of this gasification process on these samples of SRF seemed technically feasible, yielding a syngas of valuable quality for energy applications (CO concentrations between 4.5-9.5 %, H_2 concentrations between 5.9-12.8 %, and LHV_{syngas} between 4.9-7.4 $MJ.Nm^{-3}$) . The authors also found that the high contents of tar and dust may indicate that the syngas could be sent directly to a gas burner (after a pre-cleaning stage) and consequently to heat recovery and steam generation. The authors confirm the flexibility of the fluidized bed gasifier, claiming that this technology is preferable for different kinds of SRF, even in co-gasification mode.

Laboratory scale fluidized bed gasification was studied by Recari *et al.* (2017). The authors assessed the influence of different feedstocks (two SRF samples), different bed material and different gasifying agent on the gasification performance and on the quality of the syngas. Both samples presented similar product yields. The increase in gasification temperature resulted in higher gas yields, and lower tar and char yields. The preferred sand material and gasifying agent were dolomite and O_2/H_2O, which promoted the increase of gas yield comparing with the use of sand and air. Results indicated that the presence of minor contaminants was largely influenced by feedstock composition, composition of the ashes and bed material. The authors claim that the obtained results represent important data in order to assess suitable conditions for SRF gasification.

Tar generation and ash disposal are the most difficult barriers to overcome in the use of stand-alone fluidized bed gasifiers in syngas production from waste. In order to prevent agglomeration and sintering of ashes and bed material, fluidized bed gasifiers use relatively low temperatures. And, as a consequence, the produced gas has tars and other condensable organics which are difficult and expensive to remove (Materazzi *et al.*, 2016). There are combined gasification processes that can overturn these issues. These processes rely on external heat sources, like a separate combustion chamber or a plasma torch in order to pyrolyze and crack the input material (Materazzi *et al.*, 2016, 2015).

Plasma gasification is an allothermal process, using a plasma torch as the external heat source. Plasma acts as a reforming agent for the gas phase by breaking down unwanted complex hydrocarbons in the syngas. The reforming aspect of plasma can also be applied on the solid phase depending on the configuration. This process is done by melting the inorganic fraction and converting it into a vitrified slag, that is dense, inert and non-leachable (Agon *et al.*, 2016).

Agon *et al.* (2016) evaluated the performance of experiments on a single-stage plasma gasification system for the treatment of RDF produced from excavated waste. The tests were conducted using four different combinations of gasifying agents, to a total of seven cases. The composition of the produced syngas was compared with its theoretical composition and the performance of the different cases was assessed based on process yields and energy efficiencies. All cases yielded a medium calorific value syngas with a lower heating value up to 10.9 $MJ.Nm^{-3}$, with low levels of tar, high levels of CO and H_2. The measured syngas composition was relatively close to the theoretical composition, indicating thermodynamic equilibrium inside the reactor during the plasma gasification process. Carbon conversion efficiency ranged from 80 % to 100 %, maximum cold gas efficiency was 56 % and mechanical gasification efficiency was 95 %. The authors state that the treatment of RDF proved to be less performant than that of biomass in the same system and that the syngas produced from the single-stage reactor showed more favorable characteristics than a two-stage plasma gasification system. The recovery of the solid residue as a vitrified slag presents itself as a major advantage of the two-stage set-up .

A novel two stage fluidized bed gasification–plasma converter technology to transform solid waste into clean syngas, at a commercial scale was studied by Materazzi *et al.* (2016). The authors intended to study the process performance while focusing on syngas composition, carbon and energy conversion efficiencies. This work showed that the two-stage gasification system significantly reduces the concentration of condensable tars in the syngas, improving the gas yield of the system and the carbon conversion efficiency which is crucial in other single stage systems. The combination of high temperature, turbulence and residence time reached in the plasma converter enabled near zero values when testing slag samples for organic parameters. The two RDF samples used in this work yielded carbon efficiencies higher than 96 %, which seemed to be independent of the feed type. This work also showed that the energy efficiency of the two-stage process is significantly affected when increasing the oxidant inlet at the second stage, proving that energy efficiency is favored when an external heat source is used.

From the large array of gasification technologies, plasma technology is seen as one of the best alternative approaches to produce syngas with high purity and high calorific value. Plasma gasification methods present several advantages regarding their use with MSW and waste derived fuels, namely because of the high temperatures that are reached. The technical and economic feasibility of this technology has been demonstrated for a large range of hazardous wastes, which is still not the case for its application with MSW. Nevertheless, plasma gasification represents a growing market, having projects and operational plants planned worldwide, meaning that this particular technology will play a significant role in energy conversion from wastes (Fabry *et al.*, 2013).

2.3.3. Pyrolysis

Pyrolysis is a thermochemical conversion process that takes place in the absence of oxygen and results on the decomposition of matter by reducing and cracking higher molecular weight compounds. There are different types of pyrolysis depending on the temperature, reaction time, heating rate and the presence of catalysts, namely, mild, high temperature, conventional, fast, flash, thermal and catalytic pyrolysis (Miskolczi *et al.*, 2010).

The control of the reaction parameters (temperature, pressure, residence time and heating rate), allows for the variation in quantity and composition of the final pyrolysis products, which are char, oxygenated oil and combustible gas (Chen *et al.*, 2014). All three products have potential as fuels, either directly or after an upgrade, in transport, power generation or combined heat and power, for example (Hossain and Davies, 2013).

In order to design and implement large-scale pyrolysis units, the understanding of the process for different raw materials is crucial. There is substantial work done regarding pyrolysis of biomass over the last few years (Abdullah *et al.*, 2007; Jeguirim and Trouvé, 2009; Junming *et al.*, 2009; Lima *et al.*,

2004; Van de Velden *et al.*, 2010). There are also several published papers describing the use of wastes, such as industrial wastes (plastics, tires, waste oils) and MSW (Chen *et al.*, 2014; Domeño and Nerín, 2003; Kim and Kim, 2000; Manyà *et al.*, 2015; Murugan *et al.*, 2008; Nerín *et al.*, 2000; Sharma *et al.*, 2014).

In spite of the lignocellulosic material present in RDF, there are significant differences between RDF and biomass physical and chemical properties and consequently, these two feedstocks have different thermal degradation characteristics (Zhou and Yang, 2015).

According to Whyte *et al.* (2015), during the pyrolysis of RDF, the heavy molecular tar fraction will condense and solidify causing the formation of substances similar to waxes along the condenser, leading to obstructions. On the other hand, the liquid product from the RDF pyrolysis, bio-oil, will be heavily oxygenated and will have a low heating value, high viscosity, corrosiveness and thermal instability. These undesirable characteristics are limiting to its valorization as a fuel.

One of the most important aspects in RDF pyrolysis is kinetic modelling, mainly because kinetic data may affect the reactor selection, optimization of the reactor design and operating conditions at the step of design and implementation (Çepeliogullar *et al.*, 2016).

Grammelis *et al.* (2009) investigated pyrolysis and combustion behaviors of Tetra Pack, RDF and fractions of each waste for a detailed comparison. The study consisted on devolatilization experiments using a heating rate of 20 ºC.min^{-1} until 1000 ºC in an inert atmosphere, applying an independent first-order reaction model to the obtained data. The RDF pyrolysis mechanism was modelled through four independent reactions with first order, corresponding to the devolatilization of cellulose, hemicellulose, lignin and plastics. The authors found that the higher plastic share in RDF resulted in lowered char yield and reduced reactivity caused by the thermal stability of the plastics. Also, the wastes decomposed at lower temperatures than their single components while the presence of paper or plastic accelerated RDF pyrolysis.

Another central aspect of pyrolysis is the characterization of the obtained products. Hwang *et al.* (2014) used three types of wastes as raw materials for pyrolysis and steam gasification in the temperature range of 500–900 ºC, and one of those wastes was RDF. The composition of the gas, liquid, and solid products was analyzed as well as the carbon conversion of the raw materials to products. The quantity of liquid products significantly depended on temperature rather than the type of thermal conversion. The composition of the liquid products varied depending on the raw materials used at 500 ºC, but polycyclic aromatic hydrocarbons (PAHs) became the major compounds at 900 ºC regardless of the raw material. Almost all of the fixed carbon of the raw materials remained as solid products under pyrolysis conditions whereas under steam gasification conditions it started to decompose at 700 ºC. From the results of the carbon balance for RDF, it was confirmed that carbon conversion to liquid products noticeably increased as the amount of plastic increased in the raw material.

Efika *et al.* (2015) studied the pyrolysis of RDF in a horizontal tubular reactor, varying reaction parameters like heating rate and final pyrolysis temperature of the sample, in order to assess the effects of these parameters on product yields and compositions. The authors found that there was volatile degradation at two temperature zones, that were similar to the degradation temperatures of cellulosic and plastic content. Thus, the biomass and plastic contents of RDF could be roughly estimated by the analysis of volatiles degradation in its TGA and dTG thermograms. The increase in heating rate and final temperature yielded more gas (with increased heating value), while the liquid and solid products were reduced. The liquid from rapid pyrolysis was found to contain mostly aromatic compounds and the liquid from slow pyrolysis was found to contain mostly alkanes, alkenes and oxygenated compounds. The solid product from slow pyrolysis presented a slightly higher calorific value than the one from rapid pyrolysis. In this work, the optimal RDF pyrolysis conditions for gas production corresponded to a rapid pyrolysis at 800 ºC with a long residence time. These conditions yielded a gas with a calorific value of

24.8 $MJ.m^{-3}$. The authors concluded that these optimal conditions are easy to achieve through a fluidized bed reactor with small and closely uniform RDF feed sizes, due to high heat transfer rates and good mixing properties of this reactor, as well as better heat transfer properties of smaller sized particles.

The application of pyrolysis technology to MSW is quite promising and in some demand, as the energy content of MSW can be extracted in the form of primary pyrolysis products including solids, liquid and gas. Known and reported pyrolysis reactors include fixed-bed, rotary kiln, fluidized-bed and tubular reactors, but only rotary kilns and tubular reactors are applied in scale-up facilities (Chen *et al.*, 2014; Efika *et al.*, 2015). The yield and composition of the pyrolysis products are greatly affected by the feedstock and, due to its chemical and physical characteristics, RDF is a better feedstock for this thermal conversion process than MSW. MSW or RDF pyrolysis generally have very complex liquid products that are oxygenated, needing upgrade before being considered an end-product. The produced char usually presents a significant calorific value as well as the product gas. Pyrolysis presents the possibility of adjusting product yield and composition through its reaction parameters. Moreover, pyrolysis presents itself as an effective WtE conversion process, perhaps being the most versatile regarding the flexibility of obtaining primary products.

2.3.4. Torrefaction and carbonization

Torrefaction, also known as mild-pyrolysis, corresponds to a thermal treatment that takes place at operating temperatures of typically 200 to 300 °C in the absence of oxygen (Recari *et al.*, 2017). This process can greatly improve the physical, chemical and energy characteristics of different raw materials, contributing to their homogenization, increasing their grindability, density, hydrophobic character and gross calorific value while significantly reducing its volume (Chew and Doshi, 2011; Verhoeff *et al.*, 2011). Figure 2.3 shows the significant increase in homogeneity and volume reduction after submitting an industrial RDF to torrefaction at 300 ºC for 30 minutes.

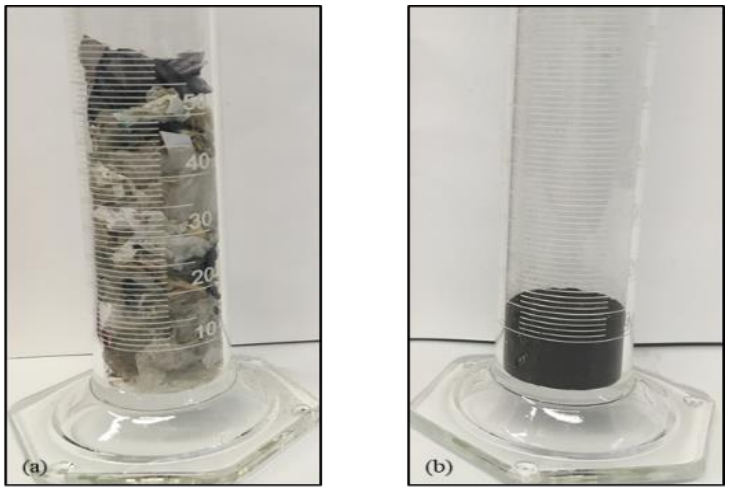

Figure 2.3: Impact of torrefaction in homogeneity and volume reduction. (a) RDF as received, (b) RDF after torrefaction.

Carbonization is another thermal process used to upgrade solid fuels, that also occurs in an inert atmosphere but at a higher temperature range than torrefaction (300– 500 °C), yielding a solid product commonly designated by char (Qi *et al.*, 2018). Although energy valorization is a major application of carbonization char, this thermal process can also be seen as a pre-treatment before landfilling since the carbonized RDF represents less environmental impacts related with the composition of landfill leachates

(I H Hwang *et al.*, 2007). Char consists mostly of carbon and inert material and presents an interesting alternative to other carbonaceous materials and fossil fuels (Hwang and Kawamoto, 2010). Moreover, char can also be used as an adsorbent or as a soil conditioner (Haykırı-Açma *et al.*, 2017; Hwang and Kawamoto, 2010; I H Hwang *et al.*, 2007).

Chosen torrefaction or carbonization conditions (temperature and residence time) are pivotal for the characteristics of the final product. Typically, temperatures above 300 °C yield chars with substantial ash content, they favor volatilization of a larger proportion of carbon and the formation of PCDD/Fs. At low temperatures (around 200 °C) there are no significant physical changes of the raw material regarding density or homogeneity. But between 200–300 °C, water is volatilized and functional groups at the surface of the raw material are eliminated, causing permanent changes in the structure and properties of the torrefied materials (Nobre et al., 2019a). The decrease in the O/C ratio, increase in the hydrophobic character, enhanced heating value and increase in density are relevant modifications for the storage and final use of these fuels (Prins *et al.*, 2006a; Schipfer *et al.*, 2017; Stelte, 2012).

Furthermore, a characteristic mass and energy balance for torrefaction (of lignocellulosic biomass) is that 70 % of the mass is retained as char, containing 90 % of the initial energy content. And the other 30 % of the mass is converted into torrefaction gas, which contains around 10 % of the biomass energy (van der Stelt *et al.*, 2011). A typical mass and energy balance for the torrefaction process of willow wood is presented in Figure 2.4 (Clausen, 2014).

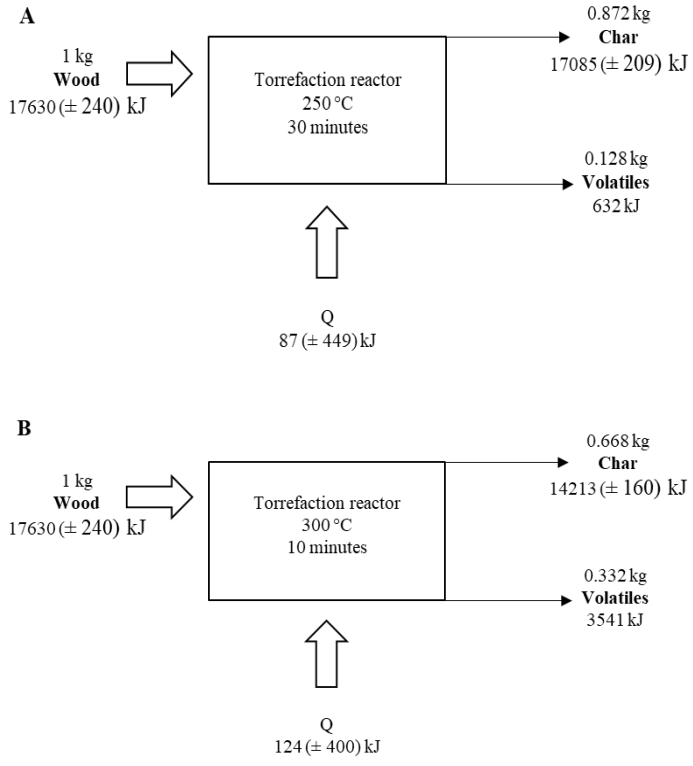

Figure 2.4: Mass and energy balances for the torrefaction of willow wood at different conditions: A – 250 ºC for 30 minutes; B – 300ºC for 10 minutes (adapted from Clausen (2014)).

Waste derived char is being studied as an alternative fuel mainly because of its higher quality and better fit as a substitute in existing coal-fired power plants, presenting itself as an interesting alternative to other carbonaceous materials and fossil fuels (Hwang and Kawamoto, 2010; Vassilev *et al.*, 1999).

Research on RDF torrefaction or carbonization is mainly focused on RDF char characterization or fuel upgrading for application in advanced thermal conversion processes, such as gasification.

Białowiec *et al.* (2017) tested RDF torrefaction at different temperatures and found that the process could reduce moisture content about 21.5 %, consequently increasing the lower heating value (LHV) by 22.5 %. The authors concluded that this method could increase the attractiveness of RDF as a fuel while homogenizing RDF characteristics for market purposes.

Torrefaction as a way to improve SRF properties in order to optimize its use in gasification was studied by Recari *et al.* (2017). The authors applied torrefaction temperatures of 290 and 320 °C and verified that torrefied SRF showed improved gasification parameters, such as lower tar, higher carbon conversion and higher H_2/CO ratio. Moreover, torrefaction reduced the chlorine content in SRF leading to lower HCl concentrations in the producer gas.

Evaluation of toxic emissions is a major concern in the evaluation of waste derived fuels. As such, Edo *et al.* (2017) assessed the emissions of the torrefaction process in different wastes, including RDF. This work showed that the chars had reduced chlorine concentrations, which implied a reduction in the potential for PCDD/Fs formation, and this was experimentally demonstrated by combustion of the torrefaction gas. This study reinforces the concept that applying the torrefaction process to waste fuels can significantly reduce the environmental impacts of their energetic valorization.

The properties of RDF char obtained through carbonization were investigated by Haykırı-Açma *et al.* (2017). Carbonization was carried out in a temperature range of 400–900 ºC. According to the results, effective devolatilization of RDF requires carbonization temperatures not lower than 500 ºC. The increase in carbonization temperatures not only leads to a decrease in volatile content, but also to a loss in calorific value. The ash content also increases very significantly with temperature, exceeding the increase in fixed carbon. Conversely, the burning reactivity of the chars decreased when compared to raw RDF and as such, the ignition and burning temperatures reached considerably high values. The authors concluded that RDF carbonization should not be done in temperatures above 400 ºC. At this temperature, around half of the oxygen content can be removed, there is a significant increase in fixed carbon and the calorific value of the RDF chars reached their maximum value.

The study of RDF torrefaction was performed by Stępień and Białowiec (2018). The authors used RDF derived from MSW in order to determine its torrefaction kinetic parameters and to assess the effect of temperature and residence time on the fuel properties of the produced char. Their tests were conducted in the temperature range of 200 to 300°C, and residence times were 20, 40 and 60 minutes for each temperature. The authors calculated activation energy (200-300°C) around 3.71 $kJ.mol^{-1}$. Also, they state that the torrefaction process had a positive effect on reducing moisture content of the RDF from 17 % to 1 %, describing that as the temperature and retention time of the torrefaction process increased, the material degassed significantly, resulting in an increase in the ash content of the product. Best HHV for RDF char was obtained at 260 ºC for 20 minutes with a value of 26.22 $MJ.kg^{-1}$.

Besides RDF char production for energy purposes, these chars are also used for other applications, namely their use activated carbon precursors for adsorption applications.

Nakagawa *et al.* (2002) prepared activated carbons from carbonized RDF at 773 K (cRDF) by steam-activation. This work encompassed testing different heating rate conditions for the carbonization and also different pre-treatments for the cRDF such as treatment with nitric acid or hydrogen chloride. The prepared activated carbons showed significant surface areas and the authors found that these carbons were effective for a practical use.

Buah and Williams (2010) produced RDF char through pyrolysis and activated the produced char via steam gasification at 900 ° C for 3 h, giving 73 wt.% yield in activated carbon. The produced activated carbon had a surface area of 500 $m^2.g^{-1}$ and a total pore volume of 0.19 $cm^3.g^{-1}$. Gold adsorption capacity was found to be 32.1 $mg.g^{-1}$ and was comparable to commercial activated carbon used in the

gold industry. The authors further demineralized the RDF activated char which resulted in improved textural properties but also in a reduction of adsorption capacity.

The application of RDF char (carbonized at 600 ºC and steam activated at 900 ºC) as an adsorbent for dioxins and furans (PCDD/F) was studied by Hajizadeh and Williams (2013). These experiments were conducted under flue gas stream at 275 ºC using standard fly ash as a source of PCDD/F. The results showed a reduction of 85 % and 43 % on PCDD and PCDF concentrations in the flue gas, and the obtained values were comparable with commercial activated carbon.

Another work regarding activation of RDF char was executed by Wu *et al.* (2014). The authors produced porous activated carbons from RDF through NaOH activation, giving surface areas of 898 and 1461 $m^2.g^{-1}$ for NaOH/char weight ratios of 1 (RDFN1) and 2 (RDFN2), respectively. The chars were tested for their adsorption capacities regarding 4-chlorophenol, acid blue and MB. The authors found the pseudo-second-order equation best described adsorption of 4-chlorophenol and acid blue onto RDFN2, whereas Elovich equation fitted the adsorption of three adsorbates onto RDFN1.

The use of RDF char as an adsorbent without activation processes is not very well documented. Nevertheless, the use of biomass wastes or biochars as low-cost adsorbents is thoroughly represented in the literature, namely, biomass wastes such as wheat shells (Bulut and Ayd, 2006), almond-gum (Bouaziz *et al.*, 2015), waste seeds (Postai *et al.*, 2016), lotus leaf (Han *et al.*, 2011), prickly pear (Barka *et al.*, 2013) or garlic straw (Kallel *et al.*, 2016). Regarding biochars as adsorbents there are reports on different waste materials (Lonappan *et al.*, 2016), sewage-sludge (Fan *et al.*, 2017) or seeds (Bharti *et al.*, 2019).

Laboratory scale studies for removal of coloring material from wastewater using RDF (without thermal pre-treatment) as an adsorbent were performed by Vanjara (1998). The results showed that RDF has considerable potential over a wide range of concentrations of methylene blue (MB). The author studied the effect of different system variables on the adsorption of MB onto RDF and found that increasing the rate of agitation increased dye adsorption rate, while larger particle size decreased adsorption rate. Furthermore, the adsorption of MB onto RDF did not seem to be affect by pH variations, since it was around 98 % for the tested pH range. Higher adsorption capacities were found at 50 ºC with 109 $mg.g^{-1}$, and the author states that the adsorption process was predominantly ruled by the intraparticle diffusion mechanism and that equilibrium time was very low.

Other applications of char produced from RDF found in the literature are its use in carbon fuel cells, or its application in restoring seaweed forests.

Ahn *et al.* (2013) investigated RDF and RPF (refuse plastic/paper fuel) for their electrochemical characteristics, in order to evaluate these fuels as energy sources for a direct carbon fuel cell system. The authors observed that the power density of the used refuse fuels reached values up to 43-62 % when compared to the coals used for comparison. These results were important given that the refused fuels presented significantly low carbon and a substantial volatile matter content.

Togashi *et al.* (2007) developed carbonized RDF (CRDF) and found that the new material was rich in nitrogen, phosphoric acid and potassium and that it presented a large surface area (140 $m^2.g^{-1}$) revealing that CRDF had potential as fertilizer as well as an adsorbent. The authors tested the possibility of using CRDF to restore damaged seaweed forests. During the tests it was confirmed that there was no leaching of toxic substances from CRDF and that the growth of a species of marine green algae (*Derbesia tenuissima* (Moris et De Notaris) Crouan) was accelerated by this material. Furthermore, the results showed that CRDF could supply nitrogen to seawater in the form of nitrate. The authors state that this work had two main advantages: the recovery of biodiversity in coastal ecosystems by restoring seaweed forests and also the reduction of atmospheric CO_2 released to the atmosphere through waste incineration.

Both torrefaction and carbonization carried out in optimal conditions represent a way to produce upgraded RDF chars that have a significant heating value, lower moisture content and high density.

These new characteristics allow this char to be used not only as a solid biofuel but as an adsorbent or as an activated carbon precursor. If the energetic or material valorization pathways are not available for this material, it will also present advantages when landfilled mainly due to its lower volume when compared to the untreated RDF. The choice of the temperature operating range will mainly depend on the RDF initial composition, being that torrefaction can be more adequate for RDF with high contents of lignocellulosic materials while carbonization leads to better results for RDF with a large polymeric fraction (Nobre *et al.*, 2019a).

2.3.5. Hydrothermal carbonization

In order to achieve a good conversion in torrefaction or carbonization (dry processes), the raw material should have a low moisture content, which usually involves a previous drying step. Drying the feedstock is generally very energy demanding. For raw materials with significant moisture content, hydrothermal carbonization (HTC) represents a more feasible alternative as a conversion process (Matsakas *et al.*, 2017; Wang *et al.*, 2018a).

HTC as an artificial coalification process was first discovered by Bergius in 1913 and has been studied with different feedstocks throughout the years, being referred to by different names, such as wet torrefaction, subcritical water treatment or hydrothermal treatment (Berge *et al.*, 2011; Matsakas *et al.*, 2017; Wang *et al.*, 2018a)

In the HTC process, the feedstock is mixed with water and heated to temperatures above 100 ºC and bellow 374 ºC, during variable residence times (from 30 minutes to several hours) and under autogenous pressure (Lucian *et al.*, 2018; Ayoub Missaoui *et al.*, 2017; Zhai *et al.*, 2017). When the reactor is maintained above water saturation pressure, at the operating temperature, water is kept in the liquid state and is said to be in a subcritical state (Kumar *et al.*, 2018). At these conditions (100 ºC < T < 374 °C and 1 bar < P < 221 bar), subcritical water presents an increased capacity to act as an hydrolytic and oxidation agent, when compared with liquid water (Hwang *et al.*, 2012) (see Figure 2.5).

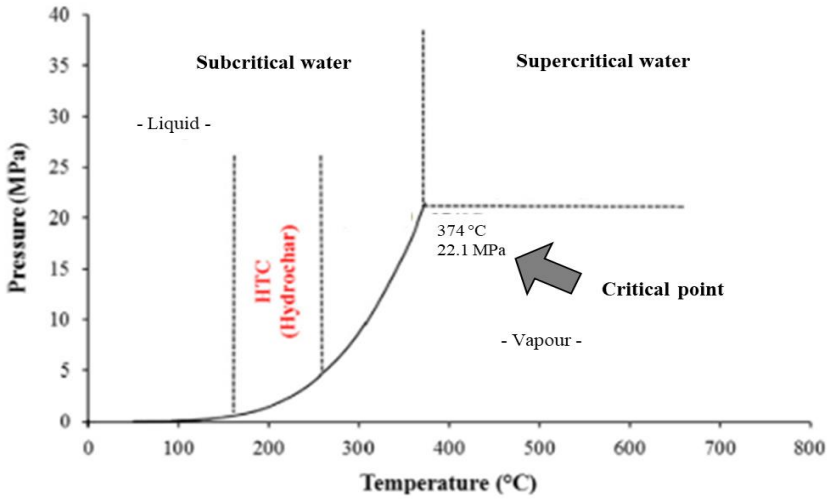

Figure 2.5: Water phase diagram (adapted from Kambo and Dutta, 2015).

Higher reactivity is facilitated by the decrease of water's dielectric constant and density, that occurs in this range of temperatures and pressures and enables a more efficient mixing with organic compounds. Coming closer to the critical point, the dielectric constant becomes similar to that of dichloromethane, and consequently the miscibility of subcritical water with organic liquids increases with increasing

temperature and pressure (Areeprasert *et al.*, 2016). On the other hand, subcritical water is a more efficient catalyst for hydrolysis or oxidation reactions than liquid water also because the concentrations of H_3O^+ and OH^- ions increase with increasing temperature and pressure (Wang *et al.*, 2018a). Thus, during HTC, the feedstock undergoes a series of simultaneous reactions, such as hydrolysis, dehydration, decarboxylation, aromatization and re-condensation (Areeprasert *et al.*, 2016; Berge *et al.*, 2011; Li *et al.*, 2013), as seen in Figure 2.6.

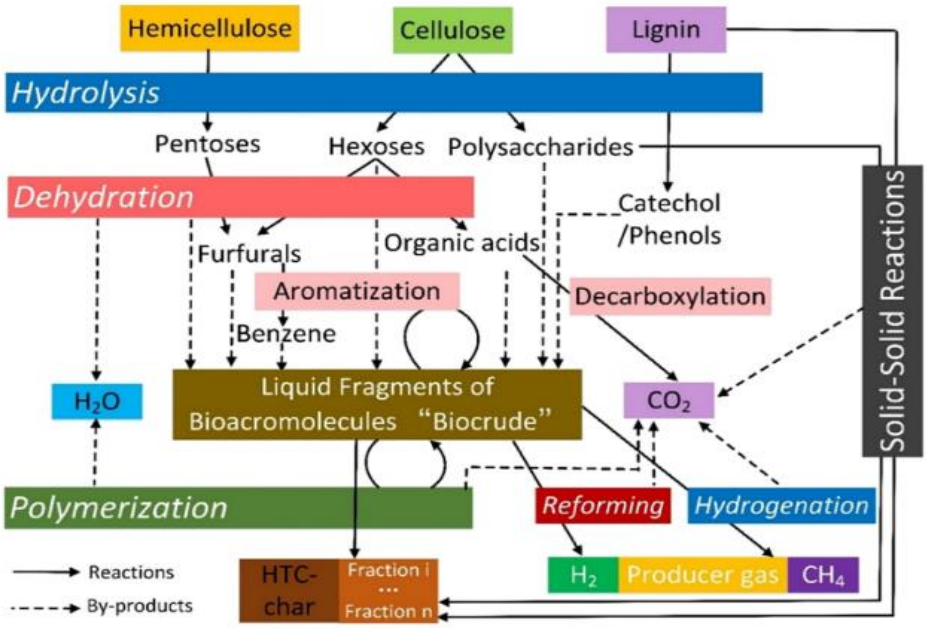

Figure 2.6: Main reaction pathways in biomass hydrothermal carbonization (Shen *et al.*, 2017).

Overall, HTC yields three major products: a solid (hydrochar), process water and, in some cases, gas (mainly CO_2). The process can also lead to byproducts with the potential to be used for power generation and to the recovery of added value compounds or useful nutrients (Kumar *et al.*, 2018).

Hydrochar is generally the major product and it has higher hydrophobic properties and carbon content than the original feedstock. Applications of hydrochar include energy production (Lee *et al.*, 2018; Lin *et al.*, 2015; Mihajlović *et al.*, 2018; Park *et al.*, 2018; Saqib *et al.*, 2018), soil amendment (Puccini *et al.*, 2018; Ren *et al.*, 2017), catalyst (Sun *et al.*, 2008), adsorbent (Li *et al.*, 2018; Qian *et al.*, 2018; Shi *et al.*, 2018; Xue *et al.*, 2012) or activated carbon precursor (Puccini *et al.*, 2017). Regarding the two last described applications, hydrochars contain less aromatic carbon when compared to regular chars produced via carbonization, having an increased cation exchange capacity because of their higher content in surface functional groups containing oxygen and hydrogen (Matsakas *et al.*, 2017).

Over the last few years, a considerable number of works have been conducted regarding HTC of a wide array of feedstocks, such as food wastes, various lignocellulosic wastes, sludges or MSW.

Nakason *et al.* (2018) studied the HTC of cassava rhizome, by assessing the effects of temperature, time and biomass-to-water ratio on the produced hydrochars and liquid fractions. The authors described that the effect of temperature was two-fold since it decreased hydrochar yield between 160 ºC and 180 ºC (from 54 % to 51 %), but between 180 ºC and 200 ºC the hydrochar yield increased up to 58 %. Hydrochars consistently presented lower H/C and O/C, representing better fuel properties. The authors also state that the obtained liquid fractions had various valuable chemical species such as glucose, furan derivatives, acetic acid or levulinic acid, with noteworthy yields (18.5 wt.% for furan derivatives, for example).

HTC of grape pomace was done by Petrovic *et al.* (2016), including the detailed characterization of hydrochar and process water. The study was conducted between 180–220 ºC and it revealed that the hydrochar obtained at 220 ºC exhibited a considerable energetic potential, increased porosity and re-adsorption ability. Furthermore, process temperature increment caused a decrease in antioxidant capacity, anthocyanin and organic acid contents in process water whilst increasing total phenolic and individual organic components content. The authors concluded that the obtained results substantiated the suitability of hydrothermal conversion of grape pomace into highly valuable fuels and versatile products.

Anaerobic granular sludge was used as a raw material in hydrothermal carbonization by Yu *et al.*, (2018), by investigating different temperatures (160 to 240 °C) and assessing the distribution of carbon, nitrogen and phosphorous in the hydrothermal products. The obtained hydrochars showed increased percentages of carbon (from 43.79 % to 49.81 %) with the increase in HTC temperature. Nitrogen showed an opposite trend decreasing from 9.58 % to 5.49 %. The authors also declare that the hydrochars presented increased HHV reaching a maximum of 24 $MJ.kg^{-1}$ at 240 °C. HTC also proved to be effective in immobilizing and recycling phosphorus.

Anthraper *et al.* (2018) did laboratory-scale HTC on MSW in order to study its effect on reducing solid content and recovering value. The authors selected materials like plastics, timber, tires, cardboards, and sanitary items and carried out HTC tests at a temperature range of 240-280 ºC with an initial pressure of 35 bar. The authors verified a substantial solid reduction through the wet oxidation which broke down the physical structure of the waste materials. At 280 ºC, more than 90 % of total suspended solids were reduced and at least 1500 $mg.L^{-1}$ of acetic acid was produced for each individual material. The authors also tested a mixture of materials in order to represent a non-recyclable municipal solid waste stream, and this feedstock produced around 2930 $mg.L^{-1}$ of acetic acid.

Food waste, due to some of its properties, like significant moisture content, is a very promising feedstock for HTC. It is a highly energetic biomass that has very expensive and long recycling and disposal processes. As such, Tradler *et al.*, (2018) studied the feasibility of a decentralized, small-scale HTC plant using food waste. Restaurant food waste was thermally treated at 200 ºC for 6 h, yielding a hydrochar with high-quality that had fuel properties similar to those of lignite with the potential to be used for co-combustion. Also, the authors successfully treated the liquid phase with ultraviolet radiation minimizing the total organic carbon and chemical oxygen demand which will facilitate conventional disposal. The authors claim that this type of HTC plant would pay for itself, and start generating profit within eight years.

HTC was used as a mean to process MSW and reclaim aluminum by Mu'min *et al.* (2017). The authors used a 2.5 L reactor at temperatures below 200 °C. The processed mixed waste was converted into two different products: a mushy organic part and a bulky plastic part. Through mechanical separation, the two products were separated and the separated plastic fraction showed a calorific value of approximately 44 $MJ.kg^{-1}$, which can justify its use as an alternative fuel. The authors also assessed that, by using an additional acetic acid concentration of 3 %, the non-recyclable plastic fraction of laminated aluminum was delaminated and separated from its aluminum counterpart at a temperature of 170 °C leaving less than 25 % of the plastic content in the aluminum part. Plastic products from both samples had high heating values of more than 30 $MJ.kg^{-1}$, which is sufficient to be converted and used as a fuel.

Lokahita *et al.* (2017) proposed the application of the HTC process in Tetra Pak recycling by producing a solid fuel and recovering the aluminum and polyethylene composites. The experiment was conducted at the three different residence times (from 0 to 60 min) and temperatures between 200 and 240 °C. The results showed that HTC could effectively produce hydrochar, that was comparable to sub-bituminous coal after removal of the aluminum, and the process could also yield well-formed aluminum and polyethylene composites. Residence time and temperature had a positive influence on several product characteristics, such as carbon content and HHV, that had significant increases, and ash content that decreased accordingly. The authors found the highest calorific value for the transformed Tetra Pak at an

operating temperature of 240 °C and residence time of 60 min (25.22 $MJ.kg^{-1}$), while the aluminum yield was as much as 37 %.

Kim *et al.* (2017) studied the hydrothermal conversion of model MSW to hydrochars and observed that the properties of the feedstocks were significantly improved by the process, yielding coal-like fuel products. The authors state that the hydrothermal treatment increased calorific value, fixed carbon and carbon contents and the obtained hydrochars had compositions and fuel properties similar to lignite or sub-bituminous coal.

Hydrothermal treatment of a model MSW with subcritical water at 234 or 295 °C, and using a solid-to-water ratio of 1:3 (m/v) produced hydrochars with improved fuel properties and was conducted by Hwang *et al.* (2012). The model MSW (mixture of paper, dog food, wood wastes, mixed plastic film, polyethylene, polypropylene, polystyrene) was added with controlled amounts of polyvinyl chloride or sodium chloride to test the behavior of organic and inorganic chlorine during the process. The authors assessed that around 75 % of the carbon content of the organic fraction was recovered as hydrochar under both conditions, but the polymeric fraction was not fully degraded. Calorific values of the hydrochars were enhanced comparatively to the MSW feedstock, achieving values comparable to those of brown coal and lignite. Nevertheless, more than 70 % of the chlorine present in the raw materials, remained in the hydrochars after the process either for organic chlorine added as PVC or inorganic chlorine added as sodium chloride. Washing the hydrochars with distilled water at a 1:10 (m/v) ratio caused the release of a fraction of the char-adsorbed chlorine but the process had different efficiencies for organic and inorganic chlorine. When chlorine was added as sodium chlorine, the recovery efficiency of the water washing process was between 92 and 100 %, regardless of HTC process temperature. Organic chlorine added as PVC was differently retained in the hydrochars, depending on the temperature of the HTC process: for the hydrochars produced at 234 ºC, water leaching allowed the recovery of 10 to 53 % of the retained chlorine while for the hydrochars obtained at 295 ºC, chlorine recoveries from 89 to 100 % were obtained.

Berge *et al.* (2011) performed hydrothermal carbonization of different feedstocks, including mixed MSW and evaluated physical, chemical, and thermal properties of the produced hydrochars. The authors indicate that around 49 to 75 % of the initial carbon was retained in the hydrochar, 20 to 37 % was transferred to the process water and 2 to11 % transitioned to the gas phase. The authors determined the composition of the hydrochars and concluded that dehydration and decarboxylation were the governing reactions during the HTC process yielding hydrochars with a significant degree of aromaticity.

Polyvinyl chloride (PVC) was subjected to hydrothermal carbonization in subcritical water at 180–260 °C by Poerschmann *et al.* (2015). The authors assessed that dehydrochlorination increased with increasing reaction temperature and that chlorine release was almost quantitative above 235 °C. The organic carbon recovered in the produced hydrochar decreased with increasing operating temperature from 93 % at 180 °C to 75 % at 250 °C. Regarding the process water, the authors detected a significant variety of PAHs, but their combined concentration was only 140 $\mu g.g^{-1}$ at 240 ºC. Chlorinated hydrocarbons, which included chlorophenols, could only be identified at trace levels and PCDD/Fs could not be detected. This work provided evidence that the application of HTC to household organic wastes is an environmentally sound process regarding formation of toxic organic products.

The work of Poerschmann *et al.* (2015) leads to one of the most important features of the HTC process. It can enable the release of organic chlorine up to 235 ºC. In energetic applications this is a very important characteristic, since it relates directly with the potential for reducing corrosion phenomena and dioxin formation (Hwang *et al.*, 2012; Singh Kambo and Dutta, 2015).

HTC process water contains a large array of dissolved organic compounds and inorganic salts resulting from the degradation of the feedstock during the process. Generally, HTC process water has very substantial chemical oxygen demand (COD), biochemical oxygen demand (BOD) and total organic carbon (TOC) values and an acidic pH (Berge *et al.*, 2011).

For lignocellulosic biomass, the inorganic component of HTC process water comprehends the typical mineral components of biomass, namely alkali and alkali-earth metals, phosphorous, sulfur and iron (Kambo *et al.*, 2017; Kambo and Dutta, 2015). The presence of these metals in the process water indicates a reduced ash content in the hydrochar comparing to the original feedstock. In the HTC process, the formation of acetic acid in the liquid by-product stream, leads to an acid solvation mechanism that can solubilize and leach out the inorganic components of the feedstock, reducing the overall ash content of the solid product, which is a clear advantage over regular torrefaction or carbonization (Singh Kambo and Dutta, 2015).

HTC process water mostly contains phenolics, organic acids or furan derivative compounds. Of course, the existence and distribution of these compounds depends on the process conditions and on the type of feedstock. Some of the most interesting compounds found in HTC process water are acetic acid, formic acid, glycolic acid, levulinic acid and 2,5-hydroxymethylfurfural (HMF) (Kambo and Dutta, 2015). Depending on the concentration of these compounds, their recovery and subsequent valorization can be a sustainable approach on managing HTC process water.

The amount of process water is seen as a major drawback of this process, and many authors have suggested solutions regarding its utilization or remediation. Kambo *et al.* (2017), Catalkopru *et al.* (2017) and Mäkelä *et al.* (2018) suggested process water recirculation as a way to manage this contaminated effluent. The experiments show that the mass and energy yields of the hydrochar increased as well as the hydrochar high heating value. Nevertheless, the process water reaches very high organic loads with successive utilizations, eventually affecting the quality of the hydrochar.

Anaerobic digestion is also presented as a solution for HTC process water, fitting perfectly in a circular economy concept. Wirth and Mumme (2013) investigated anaerobic digestion of HTC process water using maize silage. The conducted experiment showed COD and TOC degradability up to 75 and 54 %, respectively. The authors also stated that the degradation was relatively fast when compared to the digestion of conventional organic wastes and that there was no inhibition except for volatile fatty acids.

Lu *et al.* (2014) suggested the use of different moisture sources in the HTC process in order to improve process sustainability. The authors studied the application of liquid waste streams, for instance, landfill leachate, and they evaluated how changes in pH, ionic strength, and organic carbon content of the initial process water influenced cellulose carbonization. The obtained results indicated that changes in initial water quality do influence time-dependent carbonization product composition and yields, suggesting that using municipal and industrial wastewaters, with the exception of streams with high $CaCl_2$ concentrations, may impart little influence on final carbonization products.

Given the simplicity of the process, the elimination of a drying step, the production of an energy dense hydrochar and recoverable compounds in the aqueous phase, HTC has been considered as the most promising and effective thermochemical upgrading technology for biomass wastes, as well as for MSW (Lin *et al.*, 2017). In spite of all the benefits of this thermochemical conversion process, the scale-up of an HTC process could be challenging. There are certain issues, such as the operating pressures, continuous feeding against pressure, efficient heat recovery and the process water management that can turn the scale-up step into a very complex, dangerous and expensive operation (Singh Kambo and Dutta, 2015).

2.4 Final considerations

Production of waste derived fuels represents an opportunity to use the energy contained in wastes. This can be done not only in energy intense industry branches like cement production but also in co-incineration and specialized installations.

Production potential as well as utilization of waste derived fuels in Europe has been quickly rising, bringing assessable economic and environmental outcomes such as a significant reduction in CO_2 emissions and fossil fuel savings. Thus, and according to the European guidelines concerning waste management, production of RDF or SRF should be one of the basic elements of the integrated waste management system.

Currently these solid fuels have to comply with the tough quality standards from CEN/TC 343, nonetheless, they are still regarded as wastes and it is still difficult to acknowledge the difference between different designations of waste derived fuels such as RDF or SRF. This label limits the interest from the power sector and giving the reduction and restrictions in landfill depositions, there is an urge to classify SRF/RDF as a product. This could be achieved by introducing proper economic incentives for users and producers.

As for RDF energy recovery, combustion is the most well-established thermal conversion process for waste and waste derived fuels and is already steadily used throughout Europe. Gasification seems to be the most promising advanced thermal application for RDF, being that this fuel can produce good quality syngas. Nevertheless, the thermal applications using RDF still have room for improvement and many of the research focuses on different reactor conformations, different RDF typologies and compositions, kinetics or reaction conditions in order to optimize processes and yield better quality products. Improving RDF physical and chemical properties in order to optimize its application as fuel is being further investigated and torrefaction, carbonization, pyrolysis and hydrothermal carbonization present significant potential as thermal upgrading tools for raw materials with a high degree of complexity such as RDF. Furthermore, improving energy recovery whilst adding material value to RDF is also an expanding area, where the char produced from the upgrading pre-treatments can also be used for soil amendment or as an adsorbent to extract valuable compounds and for remediation purposes, by removing heavy metals or dyes.

Thermochemical conversion processes for RDF upgrading can represent a whole new perspective for these waste derived fuels. Problems like compositional variability, high moisture content and low calorific value, that make RDF less attractive for energy production, could be overcome by applying a thermal pre-treatment. These pre-treatments would avoid large amounts of RDF being landfilled and justify RDF production and its utilization.

Chapter 3

Upgrading of RDF through torrefaction and carbonization: evaluation of RDF char fuel properties

Abstract

Refuse derived fuel (RDF) is produced in large amounts but its heterogeneous nature and low calorific value reduce the potential for energetic valorization of this material. In this work, the torrefaction and carbonization of RDF was studied in a temperature range of 200 to 400 ºC and residence times from 15 to 60 min, yielding chars with increased density, high heating value (HHV), carbon content, ash content and fixed carbon. Leaching experiments showed that some inorganic components like calcium or chlorine could be removed from the RDF char, upgrading its fuel quality. For temperatures in the torrefaction range (200 ºC and 250 ºC), energy yields were higher than 96.3 % and process energy efficiencies were higher than 85 %, but the HHV of the RDF chars were lower than 19.4 $MJ.kg^{-1}$. In the carbonization range (300 ºC to 400 ºC) it was possible to obtain RDF chars with HHV in the range of 20.1 to 26.2 $MJ.kg^{-1}$, with energy yields from 84.5 to 91.7 % and process energy efficiencies from 70.8 to 79.2 %. The obtained results showed that thermochemical processing can be used to upgrade RDF, thus promoting sustainable solutions for its management and valorization.

Keywords: RDF; Torrefaction; Carbonization; RDF char; Leaching behavior.

3.1. Introduction

As established in Chapter 2, RDF contains a large diversity of components, from cardboard to textiles and non-recyclable plastics, as well as several unidentifiable materials (Brás *et al.*, 2017). This heterogeneity can negatively influence the properties of RDF, decreasing density and calorific value and increasing moisture, ash and chlorine contents, thus limiting their application in thermochemical conversion processes (Edo *et al.*, 2017). Fuels with high chlorine and ash contents are known to cause slagging and fouling phenomena as well as boiler corrosion (Silva *et al.*, 2014). High chlorine contents are also associated with problematic emissions such as HCl and PCDD/Fs (Chyang *et al.*, 2010).

Torrefaction or carbonization are thermal conversion technologies that may enhance some of the RDF fuel characteristics, by modifying its composition and heating value. In these processes, organic matter is heated in a non-oxidizing atmosphere, usually at atmospheric pressure, in temperature ranges from 200 ºC to 300 ºC for torrefaction and from 300 ºC to 500 ºC for carbonization (Qi *et al.*, 2018; Wang *et al.*, 2017). The solid product obtained in these processes (char or biochar) contains most of the carbonaceous and mineral components of the raw materials, while the gaseous products are mainly composed of water, CO_2, CO and several organic compounds, formed and released during the process (Bach *et al.*, 2017; Hwang and Kawamoto, 2010; Stępień and Białowiec, 2018). Generally, torrefaction biochar presents around 70 wt.% of the original mass and can retain up to 90 % of the initial energy content from the feedstock properties that account for their higher energy density (van der Stelt *et al.*, 2011).

The efficiency of these processes and the characteristics of their final products are affected by several parameters, such as temperature, residence time, heating rate, atmosphere composition, and reactor configuration (Ribeiro *et al.*, 2018). In particular, temperature and residence time strongly impact feedstock decomposition and reorganization of its physical structure. According to Prins *et al.* (2006a, 2006b), temperature is crucial for the kinetics of the torrefaction reaction, whereas residence time is more important for process characteristics, albeit only for certain temperature ranges. Overall, the characteristics of the final products are more affected by temperature than by residence time.

In biomass feedstocks, hemicelluloses are extensively volatilized between 250 ºC and 260 ºC, while cellulose and lignin decompose at temperatures above 300 ºC (Eseyin *et al.*, 2015; Tumuluru *et al.*, 2011; van der Stelt *et al.*, 2011). For the particular case of RDF torrefaction or carbonization, the plastic component also has to be considered. Polymers such as polyethylene terephthalate (PET), polypropylene (PP), polystyrene (PS) or polyvinyl chloride (PVC) are some of the most commonly found in RDF (Cozzani *et al.*, 1995; Lin *et al.*, 1999). When considering blends of plastics and biomass, there are synergistic effects to be taken into account (Han *et al.*, 2014; Oyedun *et al.*, 2014). Plastic material pyrolytic decomposition occurs at different temperature ranges depending on the type of polymer, for instance PVC decomposes between 250 ºC and 320 ºC (Lopez-Urionabarrenechea *et al.*, 2012), whereas PET, PP and PS begin their decomposition above 350 ºC (López *et al.*, 2011).

Torrefaction has been largely applied to lignocellulosic materials yielding homogeneous biochars with lower moisture content, higher calorific values, lower O/C ratios, higher hydrophobicity and enhanced grindability when compared with the original biomass (Chen *et al.*, 2015b; da Silva *et al.*, 2017; Qi *et al.*, 2018; Yuan *et al.*, 2015).

Throughout the years, few research groups have investigated, specifically, torrefaction or carbonization of RDF, but some examples can be found in the literature namely, evaluation of carbonization as a pre-treatment before landfilling (Hwang and Matsuto, 2008), characterization of the waste derived chars (Hwang *et al.*, 2007), determination of kinetic parameters of RDF torrefaction (Stępień and Białowiec, 2018), use of carbonized RDF for soil amendment (Tagoe *et al.*, 2008), valorization of waste derived char as precursor for activated carbon production (Buah and Williams, 2010; Hajizadeh and Williams, 2013; Nakagawa *et al.*, 2004), determination of the effect of torrefaction temperature on the properties of RDF chars (Białowiec *et al.*, 2017), evaluation of toxic emissions (heavy metals and organic pollutants) resulting from RDF torrefaction (Edo *et al.*, 2017) or other applications (Togashi *et al.*, 2007).

The main goal of this chapter was to test torrefaction and carbonization of RDF produced from non-hazardous industrial wastes, at different temperatures and residence times, in order to define which conditions yield RDF chars with enhanced fuel properties. The energy yield and energy efficiency of the torrefaction and carbonization processes were also evaluated in order to determine their sustainability as RDF pre-treatment technologies.

3.2. Materials and methods

3.2.1. Raw material

A sample of industrial refuse derived fuel (RDF) was supplied by CITRI, S.A., a waste management company located in Setúbal, Portugal. This company collects industrial wastes, recycles the fractions that can be valorized as raw materials and converts the remaining fractions into RDF in a mechanical treatment (MT) plant. RDF production in this MT unit consisted on a series of unit operations for separation and size reduction until reaching a final product with an average size $\leq$ 30 mm. A schematic representation of the RDF production line is represented in Figure 3.1.

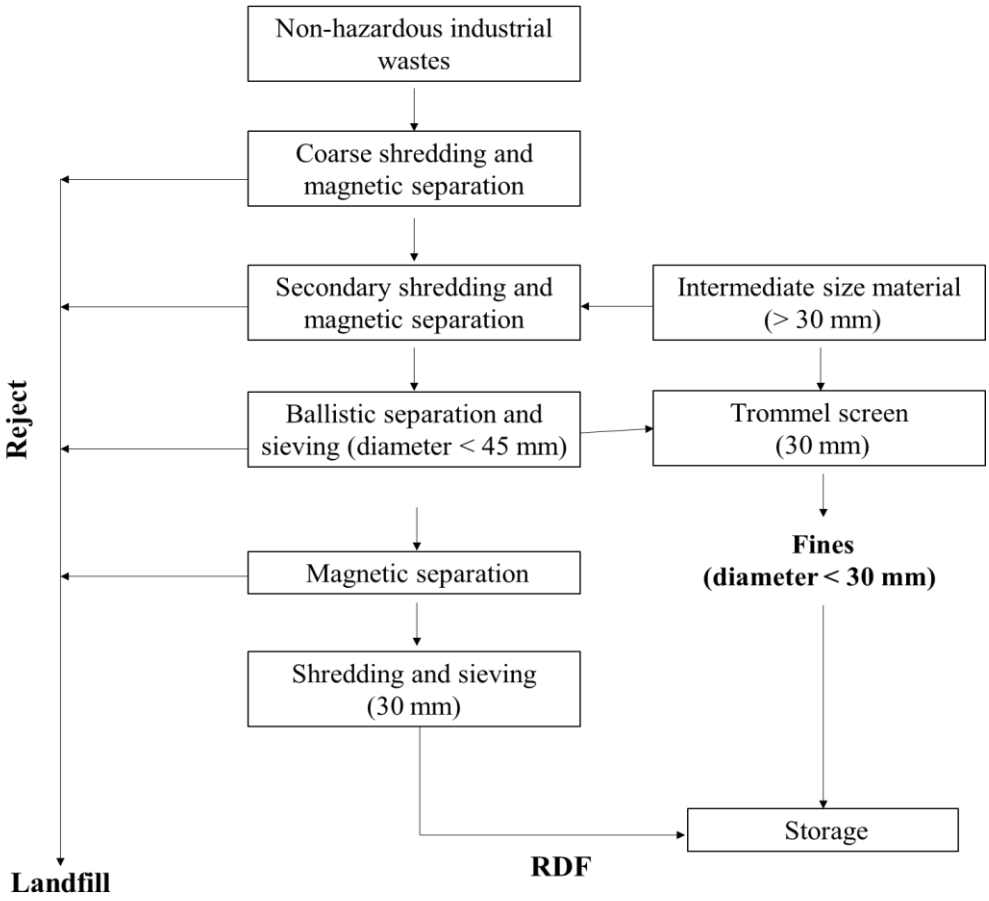

Figure 3.1: Flow chart for the production line of the RDF used in this work.

For sampling purposes, the quartering technique was used to reduce sample size at the RDF storage unit. Initial RDF lot mass was 400 kg and quartering was repeated until the gross sample reached 50 kg. The RDF sample had a very heterogeneous composition, as seen in Figure 3.2.

Figure 3.2: RDF sample used in this work, as received.

The different materials composing this RDF lot and consequent gross sample were assessed through manual sorting. Briefly, three sub-samples of 1 kg were manually separated in their components. The distribution of different components is detailed in Table 3.1.

Table 3.1: Identification of different RDF components through manual sorting. Average values are expressed as weight percentage, as received.

RDF component	Amount (wt.%, ar[a])
Plastics	22.2
Lignocellulosic wastes	29.5
Paper and cardboard	12.6
Textiles	9.9
Hard rubber and cigarette buds	0.6
Miscellaneous particles > 500 µm	22.5
Miscellaneous particles < 500 µm	2.7

[a]*ar, as received basis.*

3.2.2. Torrefaction and carbonization experiments

Temperature and residence time are determining process parameters regarding the characteristics of the final product. As such, for the experimental design, three temperatures were chosen in order to represent torrefaction (200, 250 and 300 ºC) and higher temperatures (350 and 400 ºC) accounting for carbonization.

Torrefaction and carbonization tests were performed based on the works conducted by Wilk *et al.* (2016) and Correia *et al.* (2017). Briefly, thermal conversion was carried out in covered porcelain crucibles under oxygen deficient conditions using a muffle furnace (Nabertherm® L3/1106). Prior to each experiment, the muffle was equilibrated at the target torrefaction temperature. Firstly, the crucibles and lids were fired empty at the chosen temperatures and cooled to room temperature in a desiccator and weighed. In each experiment, approximately 10 g of RDF were further milled into a fluff form (DeLonghi mill), transferred to the 50 mL porcelain crucibles, covered with their corresponding lids and heated at the target temperatures for the designated residence times. After each test, the crucibles were left to cool to room temperature in a desiccator and weighed.

For each combination of temperature and residence time, the torrefaction or carbonization assays were repeated ten times and the char samples obtained for each condition were combined, milled, sieved with a 500 µm screen (Retsch) and stored in dry conditions until further analysis.

The RDF char samples were coded with "CT/t" where "T" represents operating temperature and "t" represents residence time. For example, sample "C200/15" represents the RDF char produced at 200 ºC for 15 min.

3.2.3. RDF and RDF char characterization

Moisture, volatile matter and ash contents were determined gravimetrically according to the procedures described in ASTM 949-88, 897-88 and 830-87, respectively. Fixed carbon was determined by difference, on a dry basis (db).

Elemental analysis (CHNS) was performed using an elemental analyzer (Thermo Finnigan – CE Instruments Model Flash EA 112 CHNS series). Oxygen content was obtained by difference, on a dry ash free basis (daf).

Apparent density (g.cm^{-3}) of the RDF and RDF chars was determined gravimetrically.

High heating values (HHV) of the raw RDF and the RDF chars were calculated using a correlation established by Nhuchhen and Afzal (2017) based on ultimate composition data:

$$HHV(MJ.kg^{-1}, db) = 32.7934 + 0.0053C^2 - 0.5321C - 2.8769H + 0.0608CH - 0.2401N \quad \text{Equation 3.1}$$

where, C, H and N are the carbon, hydrogen and nitrogen contents, expressed in wt. %, db. Lower heating value (LHV) was determined according to the equation 3.2:

$$LHV\ (MJ.kg^{-1}, db) = HHV - 2.26\frac{9H}{100} \quad \text{Equation 3.2}$$

where 2.26 MJ.kg^{-1} represents the latent heat of water evaporation.

Mineral composition of the RDF and RDF chars was determined by X-Ray fluorescence (Nilton XL 3T Gold++).

Base-to-acid ratio (B/A), and fouling ratio (Fu), were used as slagging and fouling potential indexes, respectively. These parameters were determined according to the empirical relations described by Akdag *et al.* (2016) and Park and Jang (2011), as follows:

$$B/A = \frac{Fe_2O_3+CaO+MgO+K_2O+Na_2O}{SiO_2+TiO_2+Al_2O_3} \quad \text{Equation 3.3}$$

$$Fu = B/A \times (Na_2O + K_2O) \quad \text{Equation 3.4}$$

Leaching tests were carried out according to EN 12457-2: 2002. After the leaching tests, the leachates were analyzed for their conductivity (MC226 Conductivity meter Mettler Toledo) and pH (Crimson MicropH 2001 meter). Their mineral composition was evaluated through ICP-AES (Inductively Couple Plasma – Atomic Emission Spectrometer Horiba Jobin-Yvon, Ultima) and their chlorine content was determined by titration according to the methodology described in EPA-SW-948 test method 9253.

All the characterization analyses were conducted with replicates, and the presented results correspond to average values (variation coefficient ≤ 10 %).

3.2.4. Process performance

The mass and energy yields of the RDF chars produced at all the tested conditions were calculated using equations 3.5 and 3.6, respectively:

$$Mass\ yield\ (\%) = \frac{m_{char}}{m_{RDF}} \times 100 \quad \text{Equation 3.5}$$

$$Energy\ yield\ (\%) = Mass\ yield \times \frac{HHV_{char}}{HHV_{RDF}} \quad \text{Equation 3.6}$$

where m_{char} and HHV_{char} are the mass (kg) and high heating value of RDF char (MJ.kg^{-1}); m_{RDF} and HHV_{RDF} are the mass and high heating value of raw RDF.

Process energy efficiency (PEE) establishes a comparison between the energy contained in the torrefaction and carbonization products and the sum of the energy contained in the original raw material with the energy inputs required by the thermal conversion process. This parameter was calculated through equation 3.7:

$$PEE\ (\%) = \frac{m_{char}HHV_{char}}{m_{RDF}HHV_{RDF}+Q_{input}} \times 100 \quad \text{Equation 3.7}$$

where Q_{input} is the total energy requirements of the torrefaction or carbonization processes, in MJ. Q_{input} was determined as the sum of the different energy requirements of the process, as follows:

$$Q_{input} = Q_1 + Q_2 + Q_3 + Q_4 + Q_5 \quad \text{Equation 3.8}$$

$$Q_1 = m_{RDF} C_p^{RDF} \Delta T \quad \text{Equation 3.9}$$

$$Q_2 = m_{H_2O} C_p^{H2O} \Delta T \quad \text{Equation 3.10}$$

$$Q_3 = m_{H_2O} \times L \quad \text{Equation 3.11}$$

Where Q_1 represents the energy needed to heat the feedstock from room temperature to the temperature of the process (ΔT). The specific heat of the RDF sample (C_p^{RDF}) was calculated taking into account its biogenic and polymeric fractions, which were measured by the selective dissolution method, as described in CEN/TS 15440:2006. A value of 1.70×10^{-3} MJ.kg^{-1}.K^{-1} was considered for the specific heat of the biogenic component (Collazo *et al.*, 2012). For the specific heat of the plastic component it was assumed that this fraction was composed of polyethylene terephthalate and polypropylene in equal proportions (PET, C_p^{PET} = 1.05×10^{-3} MJ.kg^{-1}.K^{-1}; PP, C_p^{pp} = 1.95×10^{-3} MJ.kg^{-1}.K^{-1}) (Osswald and Hernández-Ortiz, 2006).

Q_2 represents the energy needed for heating the water present in the system (m_{H2O}) from room temperature to 100 ºC (ΔT), considering the specific heat of water (C_p^{H2O} = 4.178×10^{-3} MJ.kg.$^{-1}$.K^{-1}).

Q_3 corresponds to the energy needed for water evaporation at 100 ºC, considering the latent heat of water vaporization (L = 2.26 MJ.kg^{-1}).

Q_4 corresponds to the heat of reaction for the torrefaction process itself. This parameter was estimated by linear regression of the values obtained by Ohliger *et al.* (2013), for the different temperatures and residence times (See Appendix, Figure A.1). Considering the higher difficulty in degrading the plastic fraction and also its poor conduction properties (Lin *et al.*, 1999), 45 % of the final value was added to Q_4

Q_5 are the thermal losses related to heat loss from the char and produced gas exiting the reactor, and diffusion losses through the reactor walls. These thermal losses were assumed to be 25 % at 200 ºC 15 min, 55 % at 400 ºC 60 min and interpolated values for all the other combinations of temperature and residence time were used (See Appendix, Table A.1).

3.3. Results and discussion

3.3.1. RDF and RDF char characterization

The appearance of the RDF chars obtained by torrefaction and carbonization of the RDF sample, at different temperatures and residence times is shown in Figure 3.3.

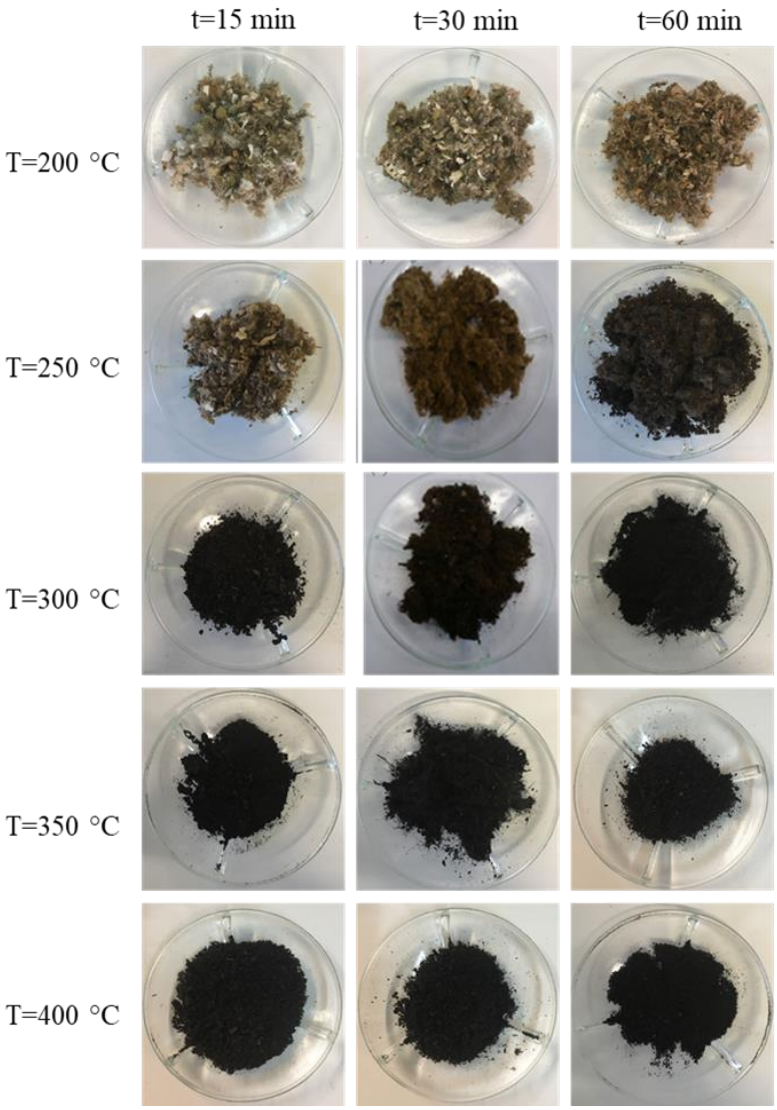

Figure 3.3: RDF chars produced by torrefaction and carbonization at 200, 250, 300, 350 and 400 ºC and residence times of 15, 30 and 60 min.

The products obtained at 200 ºC had an appearance similar to the raw RDF (Figure 3.2), suggesting that, at such mild conditions, the torrefaction process produced only minor changes of the RDF composition and structure, namely loss of water and volatile matter. Visual changes of color and texture were evident for chars obtained at 250 ºC and residence times of 30 to 60 min and for chars obtained at higher temperatures (300, 350 and 400 °C). Increasing process temperature had a larger impact on RDF char color than increasing residence time, thus indicating that the degree of decomposition and molecular rearrangement of the raw RDF is mainly influenced by the temperature of the thermochemical treatment.

The RDF chars could be hand-milled using a mortar, while the homogenization and particle size reduction of the raw RDF or of the chars obtained at 200 ºC could only be done using a mechanical mill, which is a qualitative indication of the positive effect of torrefaction and carbonization on grindability, for temperatures of 250 ºC or higher. According to Yuan *et al.* (2015) this characteristic could enable the use of these chars in different types of furnaces and feeding systems, since it reduces the problems of clogging associated with the presence of polymeric fractions in RDF.

The proximate compositions of the raw RDF and the RDF chars produced at different temperatures and residence times are presented in Figure 3.4.

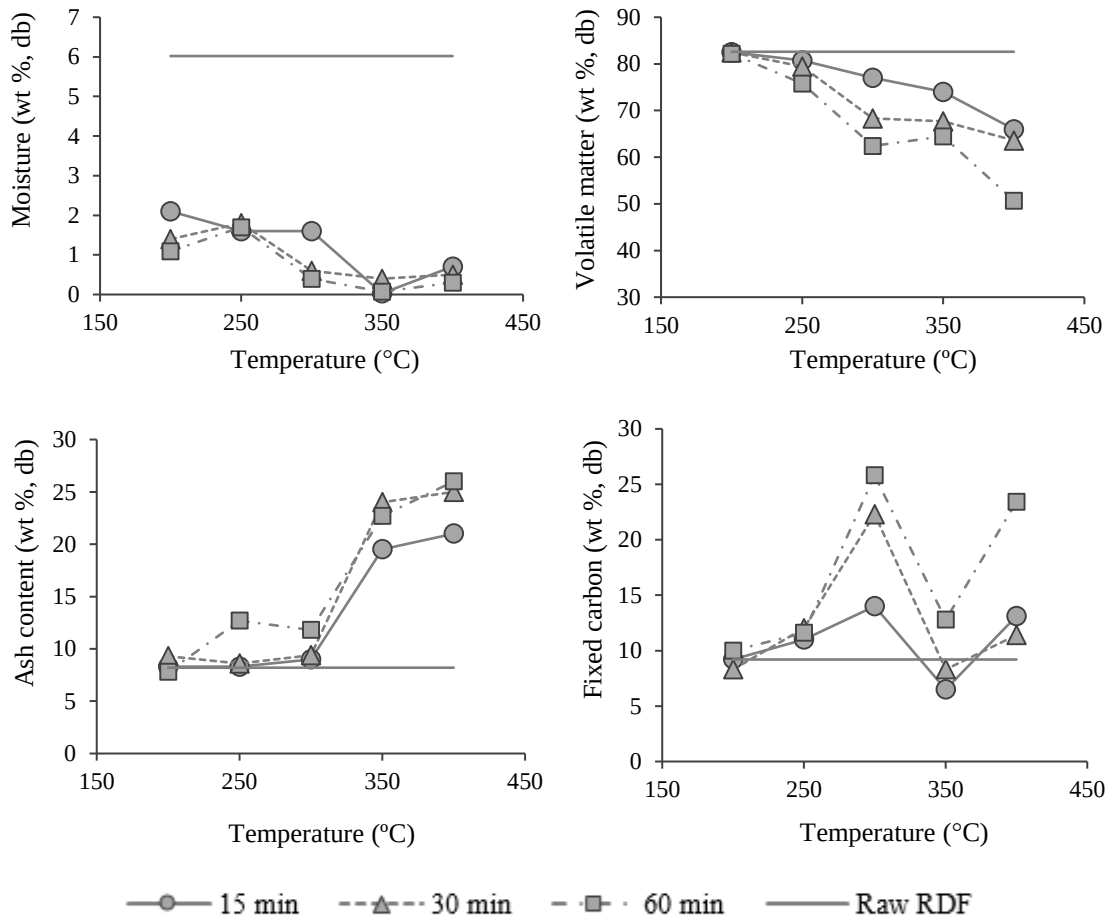

Figure 3.4: Proximate composition of the raw RDF and the RDF chars produced at 200, 250, 300, 350 and 400 ºC and residence times of 15, 30 and 60 min.

The moisture content of raw RDF was already low (6.0 wt.%), because this material was collected in September, after several dry and hot months. This parameter is negatively correlated with the fuel lower heating value and with the potential for biological degradation during storage. Also, RDF with higher moisture levels is more prone to self-ignition at room temperature (Yasuhara *et al.*, 2010). The RDF chars had residual moisture contents between 0.3 and 2.1 wt.%, due to some atmospheric moisture adsorption during char cooling to room temperature. The chars produced at the higher temperatures (350 and 400 ºC) had the lowest moisture contents probably due to their higher hydrophobicity (Zornoza *et al.*, 2016).

Volatile matter also decreased with increasing temperature and residence time, but at higher rate for temperatures in the torrefaction range (200 to 300 ºC) than for temperatures in the carbonization range (300 to 400 ºC). This indicates that the decrease in volatiles can be related to the decomposition of the biomass fraction in RDF, namely hemicellulose, cellulose and lignin, that occurs in a temperature range of 250 to 400 ºC (Qi *et al.*, 2018), but also to the pyrolytic decomposition of some polymer components, especially the ones with smaller monomer units, higher degree of unsaturation and higher chlorine content, such as PVC or PS. RDF thermochemical decomposition begins at 230 ºC, following different stages as temperature increases, according to a pattern dependent of its polymer composition (Haykiri-Acma *et al.*, 2017). PS, PP and PET are thermally degraded between 350 and 500 ºC (López *et al.*, 2011), justifying the larger decrease in volatile content observed for the char produced at 400 ºC.

The ash content of the RDF chars increased with increasing temperature but also at different rates: in the torrefaction range (200 to 300 ºC) ash content increased from 8.2 to 12.7 wt.% while in the carbonization range (300 to 400 ºC) the ash content reached 26.0 wt.%. Białowiec *et al.* (2017) observed an increase of ash content from 14.2 to 23.8 wt.% for the torrefaction of RDF at 300 ºC and 60 min, using a furnace purged with CO_2, thus promoting tar removal. Excluding the RDF chars obtained at 300 ºC, the ash content of the RDF chars had a strong linear correlation (ρ= 0.970) with the RDF mass loss that varied from 3.2 to 41.7 %, for the different conditions that were used. A similar increase of the char ash content as the severity of the process increased was also observed for torrefaction and carbonization of biomass wastes (Yue *et al.*, 2017), SRF (Recari *et al.*, 2017), MSW (Yuan *et al.*, 2015) or RDF (Białowiec *et al.*, 2017; Stępień and Białowiec, 2018). The ash content of the chars obtained at 300 ºC was similar to those obtained at 250 ºC, although different RDF mass losses were observed at these two temperatures (3.7 to 10.0 % at 250 ºC and 19.4 to 27.6 % at 300 ºC). This anomaly in the linear correlation between ash content and RDF mass loss may result from ash dissolution and entrainment by the tars formed during the process, and occurs at this specific temperature because of unbalanced rates of tar formation and volatilization. This effect is probably reduced in torrefaction systems with continuous purging of the volatiles with an inert gas but that is not always the case for torrefaction or carbonization systems at an industrial scale, because the use of a modified atmosphere increases the economic and energetic requirements of the process (Sarvaramini and Larachi, 2014). The ash content of the RDF chars was less influenced by residence time than by temperature, as observed for their moisture and volatile matter.

Fixed carbon had a non-regular variation over the temperature range because of its dependence on volatile matter and ash contents, that are inversely correlated with the temperature of the process. Fixed carbon values higher than 20.0 wt.%, were obtained for the chars produced at 300 ºC for 30 and 60 min and at 400 ºC for 60 min.

Ultimate analysis and heating values (HHV and LHV) of the raw RDF and produced RDF chars are presented in Table 3.2.

Table 3.2: Ultimate composition and heating values of the raw RDF and the RDF chars obtained at the different temperatures and residence times.

Sample	Ultimate composition (wt.%, daf)					HHV ($MJ.kg^{-1}$, db)	LHV ($MJ.kg^{-1}$, db)
	C	H	N	S	O		
RDF	36.7	4.1	1.3	0.6	57.4	18.0	17.8
C200/15	43.4	6.1	0.7	0.3	49.5	17.6	17.5
C200/30	48.0	6.7	0.4	0.3	44.7	18.4	18.3
C200/60	47.5	6.4	0.7	0.3	45.1	18.6	18.5
C250/15	41.1	5.5	0.9	0.4	52.2	17.5	17.4
C250/30	47.8	5.9	1.3	0.3	44.6	18.8	18.5
C250/60	53.3	6.0	0.7	0.3	39.7	19.4	19.3
C300/15	53.5	6.0	1.0	0.2	39.3	20.1	19.9
C300/30	56.7	5.4	0.9	0.3	36.7	20.8	20.7
C300/60	59.5	5.1	1.0	0.3	34.1	21.1	20.9
C350/15	63.7	6.0	1.2	0.5	28.6	20.8	20.6
C350/30	71.3	5.5	1.2	0.4	21.5	21.5	21.3
C350/60	71.7	6.5	1.2	0.3	20.2	22.3	22.1
C400/15	67.7	6.7	0.9	0.3	24.3	21.7	21.5
C400/30	77.5	7.3	1.0	0.3	13.9	23.5	23.4
C400/60	84.9	8.2	1.1	0.4	5.4	26.2	26.0

Carbon content and heating value of the RDF chars were improved relatively to the raw RDF, showing the fuel upgrading effect that results from the preferential elimination of oxygen from the raw materials during torrefaction or carbonization. This deoxygenation effect is more evident for temperatures in the carbonization range (300 to 400 ºC), that produced chars with carbon contents from 53.5 to 84.9 wt.% and oxygen contents from 39.5 to 5.8 wt.%, departing from an RDF sample with 36.7 wt.% carbon and 57.4 wt.% oxygen. The concentration of hydrogen was relatively constant for the different treatment conditions, showing the highest values for the RDF chars produced at 400 ºC for 30 min and 60 min (7.3 and 8.2 wt.%) indicating some degree of preservation of the C-H bonds in the carbonaceous structure. Both nitrogen and sulphur contents showed small decreases in concentration throughout the tested temperatures and residence times, which may be related with the fact that C-S and C-N polar covalent bonds are easier to break than the non-polar C-C bonds that are relatively stable up to 400 ºC (Vollhardt and Schore, 2007).

As a consequence of the composition changes associated with the torrefaction and carbonization processes, the HHV of raw RDF (18.0 $MJ.kg^{-1}$, db) was upgraded to 20.1 $MJ.kg^{-1}$ for the char produced at 300 ºC 30 min, and to 26.2 $MJ.kg^{-1}$for the char produced at 400 ºC, 60 min. Similar improvements in carbon content and HHV were observed for the torrefaction of almond shells (Chiou *et al.*, 2016), wood biomass (Wilk *et al.*, 2016) and MSW (Yuan *et al.*, 2015).

Changes in mass, volume and density are very important parameters regarding torrefaction plant design (Basu *et al.*, 2013), including transport and storage of the raw materials and the produced chars. The apparent density of the RDF chars increased relatively to the density of the raw RDF (0.12 $g.cm^{-3}$), at a rate that was proportional to the temperature and residence time of the thermochemical process. RDF chars produced with a residence time of 30 min had apparent densities that ranged from 0.13 to 0.27 $g.cm^{-3}$, when the process temperature increased from 200 ºC to 400 ºC. Also, increasing residence time from 15 min to 60 min, at 300 ºC, caused an increase of the apparent density of the produced chars from 0.19 to 0.21 $g.cm^{-3}$. This density increase implies savings in land use and material transport, which are relevant parameters for RDF management. The density increase is one of the torrefaction outputs

that must be optimized by adaptation of operating conditions to initial RDF composition, and thus achieve the ideal balance between mass loss and volume reduction (Basu *et al.*, 2013).

The H/C and O/C ratios of the RDF chars and the raw RDF, are presented in a van Krevelen diagram and compared to those of fossil fuels and biomass wastes (Figure 3.5).

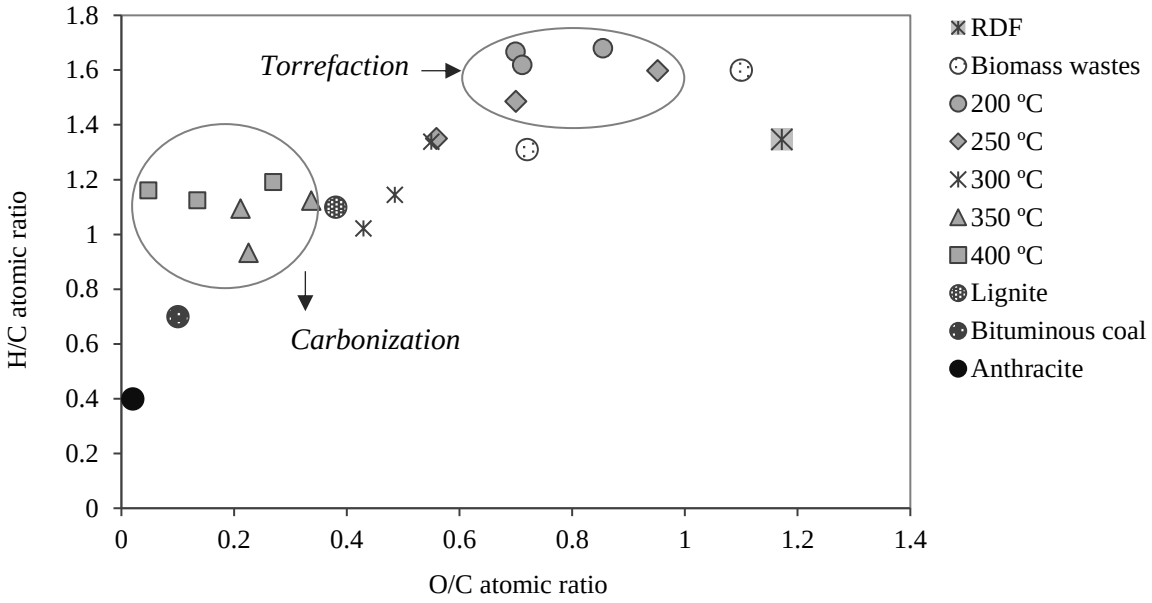

Figure 3.5: van Krevelen diagram for raw RDF and the RDF chars obtained in this work and comparison with different fossil fuels (Vassilev *et al.*, 2010) and biomass wastes (Cardona *et al.*, 2019; Wilk *et al.*, 2016).

The torrefaction process strongly reduced the O/C ratio of the RDF, to yield a char with an elemental composition close to lignite, while the raw RDF shows a composition analogous to non-treated ligno-cellulosic biomass, thus depicting a clear fuel upgrading effect. The O/C ratio of the raw RDF is even higher than those of different types of biomass wastes due to the presence of cellulose-rich materials such as paper, cotton fabrics or cardboard.

The effect of torrefaction and carbonization on the ash mineral composition of the RDF and RDF chars is presented in Table 3.3.

Table 3.3: Ash mineral composition, chlorine content and slagging and fouling indexes for the raw RDF and produced RDF chars.

Parameter	RDF	Process conditions						
		t=30 min					T= 300 ºC	
		200 ºC	250 ºC	300 ºC	350 ºC	400 ºC	15 min	60 min
Mineral composition (mg.kg^{-1}, db)								
Ca	72904.4	92133.2	105066.9	64165.0	131186.3	112436.3	89575.3	118721.5
Si	22867.4	9664.2	7184.5	6724.7	8909.2	8907.8	6733.2	8659.3
Fe	8598.5	5077.7	4267.3	3016.7	3411.0	3049.2	3439.3	3733.2
Na	6299.9	4329.0	2838.0	6700.5	6275.4	3803.1	5926.4	6183.7
K	4590.6	2839.7	4106.5	3430.0	2576.9	2552.4	2430.5	2255.0
Al	2980.1	4379.9	4908.8	3120.2	5878.9	5167.2	4355.6	5572.8
Ti	2907.6	1849.2	2094.1	4709.1	4964.0	3330.0	1926.9	2709.6
Mg	1740.0	1081.1	1482.3	1330.1	1030.2	989.7	942.4	884.4
Mn	1451.7	452.8	364.4	184.8	169.6	382.8	191.9	234.1
Zn	870.4	520.5	545.3	268.3	845.2	724.5	493.5	536.4
Cu	358.9	1072.5	264.6	406.1	281.4	271.9	152.7	645.1
Pb	337.9	125.9	162.7	178.7	158.3	120.3	133.6	135.6
Sn	285.1	70.0	92.9	69.4	99.2	67.5	83.4	94.1
Sc	209.3	276.1	334.9	205.6	362.8	351.3	276.5	381.1
Cr	163.4	159.1	124.9	19.6	152.5	108.4	91.5	234.4
Sr	90.6	57.4	62.3	61.2	78.8	52.4	45.8	64.3
Ba	83.8	0.0	0.0	0.0	59.3	36.5	0.0	0.0
Bi	65.7	27.1	27.6	0.0	39.2	9.4	35.7	110.1
Rb	60.8	32.2	35.0	8.4	49.0	14.5	44.2	127.8
Zr	57.0	28.9	26.7	40.6	28.5	26.7	24.3	33.6
Cl (wt.%, db)	0.7	1.4	0.7	2.3	3.1	1.3	1.4	1.6
B/A	2.4	4.8	6.0	4.2	5.5	5.1	5.8	5.7
Fu	5.3	7.2	7.5	9.3	10.9	6.8	11.0	11.1

The thermochemical processes caused an increase of total ash of the RDF chars but affected differently the concentrations of individual ash components. Calcium is the element with the most remarkable concentration increase, when compared with the raw RDF. This element presented its higher concentration for the RDF char produced at 350 ºC, with 131186.3 mg.kg^{-1}. The concentrations of other mineral components such as potassium silicon, iron, magnesium or manganese decreased with the thermochemical treatment, showing values consistently lower for the RDF chars than for raw RDF. Finally, another group of inorganic components had a miscellaneous behavior, increasing or decreasing in the RDF chars depending on the conditions of temperature and residence time at which those chars were produced. Kuzmina *et al.* (2016), suggested that the interactions between condensates and chars, which occur in reactors without a modified atmosphere, contribute to a reduction of the organic matter content of condensates, through the adsorption of more hydrophobic components on the surface and porous structure of the chars, thus increasing solid yield. These interactions may have the opposite effect on the ash

content of the chars by partial dissolution of the mineral fraction of the chars in the condensates, a behavior similar to that observed during hydrothermal carbonization (Reza *et al.*, 2013). As seen in Table 3.3, there is a positive trend regarding heavy metals, since in general, these elements show lower concentrations in the RDF chars relatively to the raw RDF.

Regarding slagging and fouling indexes, all the studied samples presented potential for these ash related problems. The raw RDF already had a B/A value above 1, indicating a high slagging tendency when compared to limit values, where B/A< 0.5 represents low slagging tendency, 0.5 < B/A < 1 corresponds to a moderate slagging tendency and B/A > 1 represents a high slagging tendency (Akdag *et al.*, 2016). B/A values for the RDF chars increased even further, reaching a maximum value of 6.0 for the RDF char produced at 250 ºC for 30 min. The same behavior is verified for the fouling index. This parameter was 5.3 for the raw RDF and reached its highest value (11.1) for the RDF char produced at 300 ºC for 60 min. These values are directly related with the concentrations of alkali metal oxides which present significant concentrations in the ashes of both raw RDF and RDF chars. Furthermore, chlorine content increased in the RDF chars samples, and it is also a strong indicator of potential slagging problems (Nutalapati *et al.*, 2007). The determined slagging and fouling indexes for the studied samples are significantly high comparing with other RDF samples (Akdag *et al.*, 2016) or coals (Park and Jang, 2011).

The leaching of inorganic components from the raw RDF and the RDF chars was evaluated in comparable conditions to assess the stability of those materials during landfill storage and evaluate the efficiency of such treatment in the removal of chlorine and other ash-forming species from the RDF chars. The leachates were characterized for their pH, conductivity, chlorine content and concentrations of main mineral components (Table 3.4).

Table 3.4: Concentrations of chlorine and other mineral components removed by the leaching procedures of raw RDF and the RDF chars produced at different temperatures and residence times (expressed in wt.% for chlorine and $mg.kg^{-1}$ for the other elements) and properties of the leachates obtained for each sample.

Parameter	RDF	Process conditions						
		t=30 min					T= 300 ºC	
		200 ºC	250 ºC	300 ºC	350 ºC	400 ºC	15 min	60 min
pH	7.3	7.6	7.5	7.0	7.5	7.6	7.1	7.3
Conductivity ($mS.cm^{-1}$)	1.6	1.6	2.8	4.4	4.4	4.4	3.0	4.3
Cl (wt.%, db)	0.1	0.2	0.2	0.5	0.8	0.7	0.5	0.8
Metals ($mg.kg^{-1}$, db)								
Ca	737.0	819.6	906.8	1896.8	6888.1	3731.3	2383.2	3994.0
K	229.1	244.2	169.1	171.2	166.5	110.9	338.8	115.7
Mg	67.2	70.4	48.4	103.3	86.4	34.6	86.8	48.8
Na	87.9	63.8	39.6	26.6	52.8	33.5	79.2	46.2
Si	14.2	18.7	6.2	5.6	7.0	6.0	12.6	7.4
Al	11.1	7.4	11.1	8.0	6.7	3.9	10.3	5.4
Zn	4.7	2.2	2.1	2.1	9.9	1.4	3.4	2.4
Fe	5.8	1.7	1.3	1.8	1.7	0.9	2.5	2.8
Mn	1.1	0.5	0.6	4.5	2.3	0.7	2.5	1.8
Cu	2.6	3.8	0.7	5.0	4.9	0	0	1.6
Ti	0.8	0	0	0	0	0	0	0
Pb	0.7	0	0	0	0	0	0	0
Cr	0.3	0	0	0	0	0	0	0

The leachates presented comparable pH values in the neutral range, which can be related with decreased metal concentrations, according to Hwang *et al.* (2007). The conductivity of the leachates was higher for those obtained from the RDF chars, reflecting the higher concentration but also the higher mobility of ionic species in these samples. Torrefaction and carbonization can alter the surface properties of the raw materials depending on temperature an residence time (Weber and Quicker, 2018) and these structural alterations lead to molecular rearrangements responsible for the retention or release of the different elements, depending on several factors, such as volatility or water solubility.

Calcium was readily released by the RDF chars when compared with the raw RDF, presenting a maximum leaching concentration for the char produced at 350 ºC 30 min (6.9 $g.kg^{-1}$). The increase of calcium and potassium concentrations in the leachates from the RDF chars had strong positive correlations ($\rho = 0.734$ and $\rho = 0.898$, respectively) with the temperature used for char production while magnesium and sodium leaching from the RDF chars showed strong positive correlations ($\rho = 0.806$ and $\rho = 0.890$, respectively) with the residence time of the thermal treatments (correlations are reported in the Appendix, Figures A.2 and A.3 and Table A.2).

Alkali and alkali-earth metals do not add to leachate toxicity, and generally leachates from waste-derived chars present high concentrations of these elements when compared with the leachates from the original wastes (Hwang and Matsuto, 2008).

Metals lead, chromium and titanium, although present in the RDF chars at concentrations higher than 100 $mg.kg^{-1}$, db, were not detected in the corresponding leachates suggesting a stable retention of these elements in the char matrix, by electrostatic interactions or pore adsorption.

According to Vassilev *et al.* (1999) chlorine in refuse-derived char is distributed among organic and inorganic forms that may be adsorbed in the char surface or pores. As such, chlorine release during the leaching assays of the RDF chars would mostly result from dissolution of inorganic chlorine. Comparing with the raw RDF, all the RDF chars showed a higher chlorine release, particularly the chars produced at 300, 350 and 400 ºC (0.5-0.8 wt.%). From the fuel perspective, water leaching can be seen as way to remove chlorine from the RDF chars, to yield upgraded fuels. For further chlorine removal, sequential washing, the use of temperature or carbonation could be applied (Hwang *et al.*, 2006). Overall, the characteristics of the obtained leachates were in compliance with limit-values established by the EU landfill regulation regarding pH, chlorine and the tested heavy metals (OJEC, 2003).

3.3.2. Process performance

Mass and energy yields as well process energy efficiency can be useful indicators of the torrefaction and carbonization processes performance (Zhang *et al.*, 2018). The results for the process performance calculations for all the tested torrefaction and carbonization conditions are depicted in Table 3.5.

Table 3.5: Mass yield, energy yield, energy requirements and process energy efficiency for the torrefaction and carbonization of RDF.

Process conditions		Mass yield (%)	Energy yield (%)	Energy requirements[a]						PEE (%)
T (ºC)	t (min)			Q_1 (MJ)	Q_2 (MJ)	Q_3 (MJ)	Q_4 (MJ)	Q_5 (MJ)	Q_{input} (MJ)	
200	15	96.8	94.6	0.26	0.03	0.21	0.94	0.36	1.81	86.0
	30	95.9	97.6	0.26	0.03	0.21	0.86	0.41	1.77	88.8
	60	94.5	97.7	0.26	0.03	0.21	0.70	0.42	1.63	89.6
250	15	96.3	93.6	0.34	0.03	0.22	0.81	0.42	1.82	85.0
	30	94.4	98.3	0.34	0.04	0.26	0.74	0.48	1.85	89.1
	60	90.0	96.9	0.34	0.04	0.30	0.59	0.51	1.77	88.2
300	15	80.6	90.0	0.41	0.08	0.57	0.77	0.64	2.49	79.1
	30	75.0	86.7	0.41	0.10	0.70	0.70	0.76	2.68	75.5
	6	72.4	84.7	0.41	0.11	0.76	0.55	0.82	2.65	73.9
350	15	78.7	91.0	0.49	0.09	0.62	0.74	0.77	2.70	79.2
	30	72.7	86.8	0.49	0.10	0.75	0.66	0.90	2.91	74.7
	60	68.3	84.5	0.49	0.12	0.85	0.52	0.99	2.96	72.6
400	15	76.3	91.7	0.56	0.09	0.67	0.70	0.91	2.94	78.9
	30	69.3	90.4	0.56	0.11	0.83	0.63	1.07	3.20	76.8
	60	58.3	84.7	0.56	0.15	1.08	0.48	1.25	3.52	70.8

[a] *Q_1, energy needed to heat the feedstock; Q_2, energy needed for heating water to 100 ºC; Q_3, energy needed for water evaporation at 100 ºC; Q_4, heat of reaction for the torrefaction process; Q_5, thermal losses.*

As expected, mass yields of the RDF chars decreased with increasing temperature and residence time, reaching 58.3 % at 400 ºC 60 min. Overall, high mass yields indicate that most of the fixed carbon fraction was recovered in the char and mass losses were restricted to light components, such as water and volatile components, but it may also be associated to a limited deoxygenation of the RDF sample, such as observed at 200 ºC. At 350 ºC and 400 ºC the polymeric fraction of the RDF also decomposes, contributing to mass loss along with the lignocellulosic materials, justifying the lower mass yields obtained at these most severe process conditions (Silva *et al.*, 2015). The elemental compositions of the raw RDF and the RDF chars, as presented in Table 3.2, confirm that mass loss is positively correlated with the reduction of the O/C ratio, an upgrading effect intended by these thermochemical processes. The RDF char mass yields obtained in this work are higher than those obtained by Białowiec *et al.* (2017) for RDF torrefaction (200-300ºC, 60 min) and those reported by Yuan *et al.* (2015) for MSW thermal treatment (250-450 ºC, 30 min). These differences may be attributed to a higher deposition of hydrophobic organic components in the char surface due to a higher contact between condensates and chars, that is possible when a purging inert gas is not used (Kuzmina *et al.*, 2016). The specific composition of the used raw material also has an important role in the outcome of the thermochemical processes, both in yield and char properties.

Energy yield represents the amount of energy of the raw material that was retained in the solid product, and reached its highest value (98.3 %), at 250 ºC and 30 min. Chars produced by torrefaction of different biomass wastes, such as spent coffee grounds, forest residues and MSW at 300 ºC, had energy yields that ranged from 80 to 90 % (Bach *et al.*, 2017; Samad *et al.*, 2017; Zhang *et al.*, 2018).

According to Sermyagina *et al.* (2015) determination of the heat requirements in torrefaction is quite challenging because there are significant variations in the specific heat of raw materials and also in the

heat of reaction and in the magnitude of thermal losses, depending on the dimensions and configurations of the used reactors.

For the determination of the heat requirements for the tested torrefaction and carbonization conditions, Q_1 (energy required for feedstock heating) was evaluated considering the RDF sample as received with its initial moisture content (6.0 wt.%) and without including drying of the feedstock since moisture value was below 10 wt.% and drying was not performed (Sermyagina *et al.*, 2015). To evaluate the specific heat of the RDF (C_p^{RDF}), the composition of the RDF sample as evaluated by the selective dissolution method (64.1 wt.% biogenic component, 27.7 wt.% non-biogenic component and 8.2 wt.% ash), was taken into account. As detailed earlier in Section 3.2.4, the specific heat of the biomass component was obtained from Collazo *et al.* (2012) and the plastic fraction was assumed to contain equivalent amounts of PET and PP with specific heat values obtained from Osswald and Hernández-Ortiz (2006) . The specific heat of the RDF (C_p^{RDF}) was determined as 1.5×10^{-3} MJ.kg^{-1}.K^{-1}.

As expected, Q_1 (energy required for feedstock heating), increased with process temperature as seen in Table 3.5. Q_2 and Q_3, which are energy requirements regarding heating and evaporation of the water present in the system, also increased with temperature and residence time because those parameters influenced the condensate yield. Q_4 was evaluated taking into account the heats of torrefaction determined by Ohliger *et al.* (2013), for the torrefaction of beechwood. The increase of temperature and residence time were negatively correlated with the heat of reaction because increasing the severity of the processes also increased the extent of exothermic reactions (Ohliger *et al.*, 2013). Thermal losses Q_5, increased with the process temperature and residence time. The calculated Q_{input} values were similar to values found in various literature references regarding the torrefaction and pyrolysis of different biomass wastes from 0.392 to 2.935 MJ.kg^{-1} with the exception of the values calculated for the most severe carbonization conditions (400 ºC, 30 and 60 min) (Ábrego *et al.*, 2018; Cardona *et al.*, 2019; Granados *et al.*, 2014; Guo *et al.*, 2017).

The relations between the process energy efficiency (PEE), and two relevant performance parameters (HHV of the produced chars and energy yield) are presented in Figure 3.6.

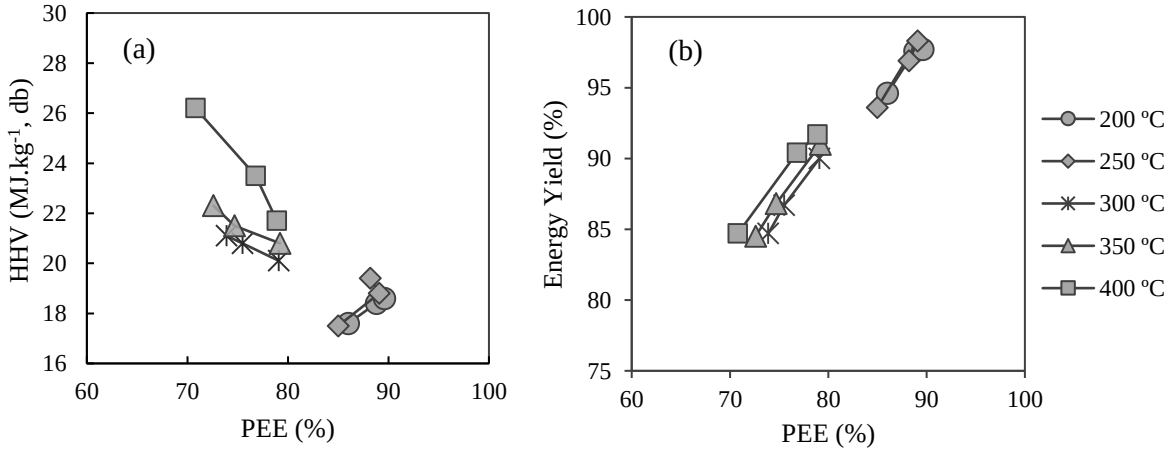

Figure 3.6: Relations between the process energy efficiency (PEE) and: (a) heating value of RDF chars (HHV) and (b) energy yield.

At torrefaction conditions (200 ºC and 250 ºC), PEE and energy yield were high, mostly due to the reduced mass loss, but the HHV of the chars was low as a result of their high O/C ratio. On the other hand, at 300, 350 and 400 ºC lower PEE values and lower energy yields were obtained but corresponding to RDF chars that had a higher calorific value and therefore better fuel quality.

3.4. Conclusions

RDF is a waste material with a strong polymeric component and variable composition, which are challenging trends for the development of energy recovery applications. Low density, low grindability and high chlorine contents are other characteristics that hinder the efficiency of RDF combustion and increase associated emissions.

Torrefaction and carbonization of an industrial RDF allowed to obtain chars with improved fixed carbon, heating value and carbon content, that presented O/C ratios similar to lignite or bituminous coal, in the carbonization range. The concentrations of ash and chlorine also increased with the thermal treatments, probably due to interactions between chars and condensates, but leaching with water allowed significant reductions of the inorganic fraction of the RDF chars.

RDF torrefaction or carbonization is also interesting from the landfill management perspective since it allowed significant density increase and reduced the mobility of some heavy metals such as lead or chromium.

Carbonization conditions offered a good compromise between fuel properties and process efficiency, allowing the production of chars with HHV between 20.1 and 26.2 $MJ.kg^{-1}$ with process energy efficiencies from 70.8 to 79.2 %.

Thus, the thermochemical conversion of RDF between 300-400 ºC appears to be a useful pre-treatment for RDF, both for energetic applications or landfill storage, contributing to improve its fuel quality and reduce its environmental impact.

Chapter 4

Torrefaction and carbonization of RDF: Char characterization and evaluation of gaseous and liquid emissions

Abstract

RDF containing non-hazardous industrial wastes was subjected to torrefaction and carbonization in a rotary pyrolysis furnace. The RDF samples were heated at 300 °C and 400 °C, for 30 min, yielding solid products (chars) as well as gases and liquids. Proximate and ultimate composition, mineral composition, chlorine content and high heating value were determined for the original sample and the produced chars. Thermal treatment produced RDF chars with carbon contents of 61.6 and 80.2 wt. %, and high heating values of 19.9 and 23.5 $MJ.kg^{-1}$, that could be further upgraded by washing with water to reduce ash and chlorine concentrations and improve calorific value. Gas products were composed of carbon dioxide and carbon monoxide with minor amounts of hydrogen. Methane was only detected in the gas produced at 400 ºC. The process generated liquid products rich in organic compounds that represent potential in further energy or material recovery.

Keywords: Scale up; Torrefaction; Carbonization; Gas products; Condensates.

4.1. Introduction

As seen in the previous chapter, the main product of torrefaction and carbonization is a char that presents a homogeneous carbon structure and contains some inert mineral components. In addition to the char, gas products (primarily carbon dioxide, carbon monoxide and methane) and a condensable liquid (water, acetic acid and other oxygenated compounds) are also produced (Tumuluru *et al.*, 2011). The amount of each product is dependent on the process main parameters, namely temperature, heating rate or residence time, as well as on the characteristics of the feedstock (Tumuluru *et al.*, 2011; van der Stelt *et al.*, 2011; Volpe *et al.*, 2015). Biomass is by far the most used raw material in torrefaction and carbonization applications. There are less studies focused on the torrefaction or carbonization of other waste streams, such as MSW or RDF, and the majority of those is dedicated to the characterization of the main product (char) and does not include the characterization of the corresponding emissions (gas product and condensates). The characterization of the emissions associated with torrefaction or carbonization is necessary to develop appropriate strategies to treat or reduce emissions and therefore improve the sustainability of those processes at an industrial scale. Detailed description of gaseous and/or liquid emissions associated with these thermal conversion processes has been done mostly for biomass feedstocks, such as rice husk (Chen *et al.*, 2018b), bamboo (Chen *et al.*, 2015a) or sorghum (Yue *et al.*, 2017).

Most literature reports on RDF torrefaction or carbonization were performed in the sub-kilogram scale (Białowiec *et al.*, 2017; Edo *et al.*, 2017; Haykiri-Acma *et al.*, 2017), but given the heterogeneity of RDF the evaluation of these treatments in a larger scale could probably provide more representative

information on product composition. Recari *et al.* (2017) studied torrefaction of SRF in a continuous reactor, at a 13kg.h^{-1} rate, processing around 3.3 kg of material in each test, but did not study the associated emissions.

In this chapter, the thermochemical upgrading of an industrial refuse derived fuel (RDF) containing comparable amounts of lignocellulosic and polymeric components, was studied at temperatures corresponding to the higher limit of the torrefaction range (300 ºC) and an average temperature in the carbonization range (400 ºC). For temperatures lower than 300 ºC, a poor decomposition of the polymeric fraction is expected while for temperatures above 400 ºC, substantial loss of fixed carbon may hinder mass and energy yields (Haykiri-Acma *et al.*, 2017). The tests were performed at a pre-pilot scale (5 kg samples), in order to achieve a representative evaluation of the conversion process and associated emissions. The RDF chars as well as the co-produced gases and condensates were characterized and the mass and energy yields were evaluated in order to discuss the process performance and the possible pathways for valorization or remediation of the secondary products.

4.2. Materials and methods

4.2.1. Raw material

The RDF sample used in this work was produced from non-hazardous industrial wastes and was supplied by CITRI S.A.. Sampling of the RDF was performed as described in Chapter 3. Main components of the sample were determined by manual sorting, through three sub-samples of 1 kg, as represented in Figure 4.1.

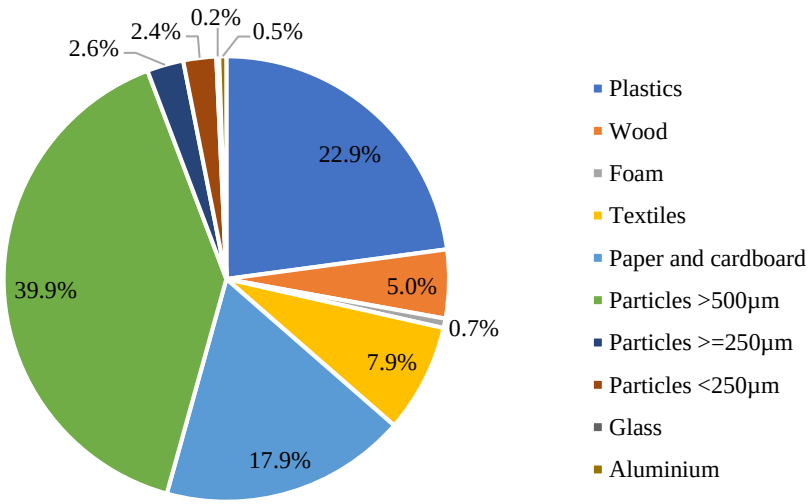

Figure 4.1: Morphological composition of the RDF sample, obtained through manual sorting. Presented results correspond to average values.

4.2.2. Torrefaction and carbonization tests

RDF was subjected to torrefaction and carbonization at the temperatures of 300 ºC and 400 ºC, respectively, using an industrial rotary furnace (MJ Amaral, model FR 100), equipped with an emission collection system schematically represented in Figure 4.2.

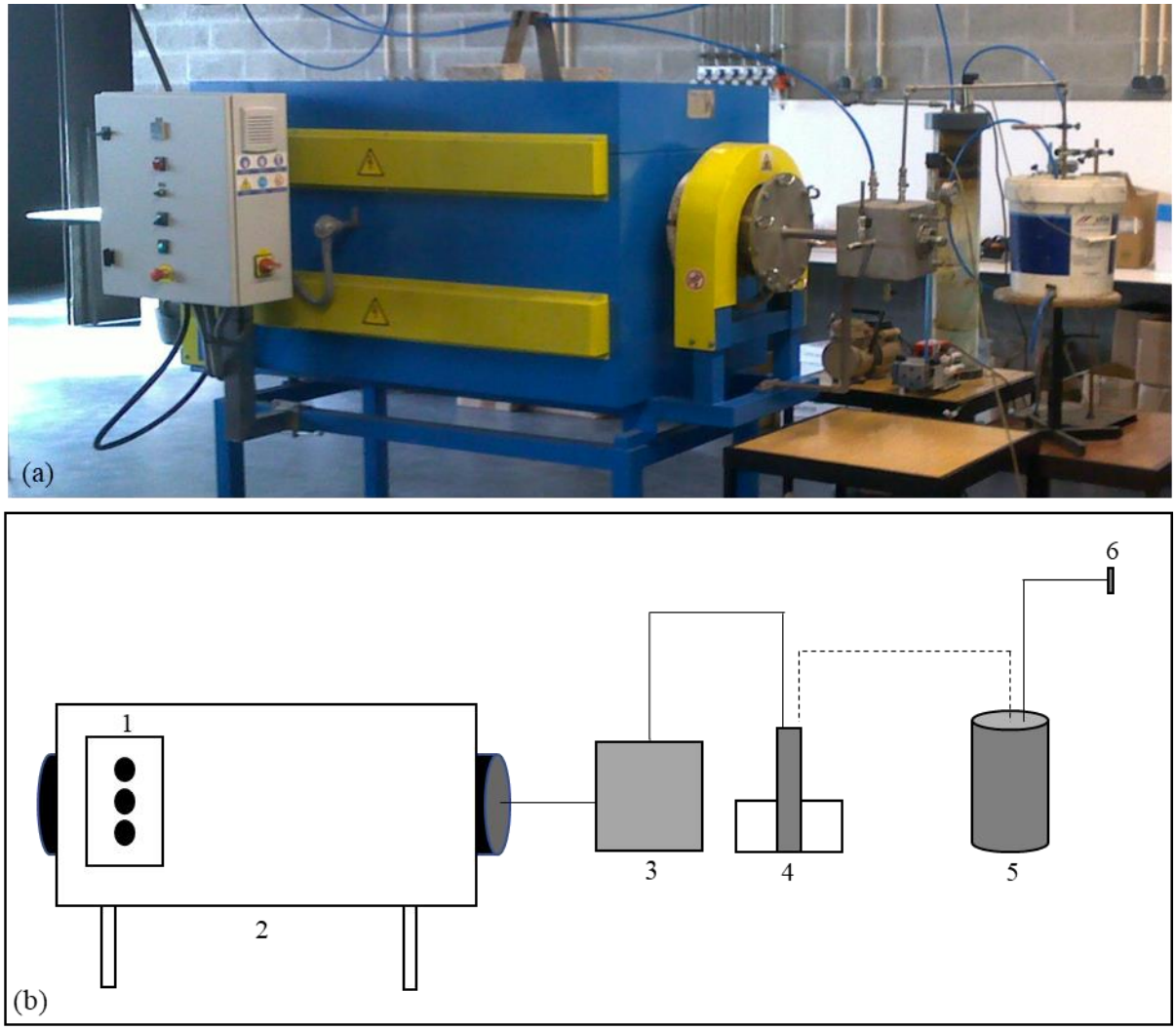

Figure 4.2: (a) Photographic representation of the rotary pyrolysis furnace; (b) Schematic diagram of the experimental setup used in the torrefaction and carbonization tests: 1 – Control panel; 2 – Rotary pyrolysis furnace; 3 – Condensation chamber (1st collection point); 4 – Condensation chamber (2nd collection point); 5 – Water column; 6 – Permanent gas collection.

For each run, approximately 5 kg of RDF (as received) were placed in the furnace, the air was removed using a vacuum pump (in order to reduce oxygen availability), and the rotation movement was initiated at a rate of 1 rpm. The furnace was then heated to 200 ºC for 15 min, to allow for temperature equilibration with the furnace walls and reduction of the RDF sample moisture. Afterwards, temperature was risen to 300 ºC or 400 ºC, at 4 ºC.min^{-1} and held at those values for 30 minutes. During this period pressure increased as gas products were continuously formed and released through two condensation chambers and a water scrubbing column before being vented to the atmosphere. The condensed phases collected in the condensation chambers (1st and 2nd collection points) were recovered in the end of each test and kept at 4 ºC until analysis. Non-condensable gases were collected in 5 L Tedlar bags for later characterization.

4.2.3. RDF and RDF char characterization

Before analytical characterization, the RDF gross sample was air-dried for 15 days, and homogenized using a mechanical mill (DeLonghi mill). The homogenized RDF samples were stored in plastic containers until analysis. The RDF char samples obtained in each test were milled and sieved to a particle diameter < 500 µm (Retsch sieve) and stored in glass containers until analysis. All analytical determinations were done with replicates and results are presented as average values (variation coefficient ≤ 10 %).

Moisture, volatile matter and ash contents were determined according to CEN/TS 15414-3:2010, EN 15402:2011 and EN 15403:2011, respectively. Fixed carbon content was obtained by difference, on a dry basis (db). Ultimate analysis (CHNS) was performed using an elemental analyzer (Thermo Finnigan – CE Instruments Model Flash EA 112 CHNS series). Oxygen content was calculated by difference, on a dry ash-free basis (daf).

High heating values (HHV) of the RDF and the RDF char samples were determined with a calorimeter bomb (IKA C200), in isoperibolic mode at 25 °C, using benzoic acid as a calibration standard.

The mass and energy yields of RDF chars (on a dry basis) were calculated based on equations 3.5 and 3.6, respectively (from Chapter 3).

Mineral composition of ash from RDF and RDF char samples was determined through X-Ray fluorescence (Niton XL 3T Gold++). Chlorine content was determined through an adaptation of ASTM D4208-02, using a bomb calorimeter (IKA C200) with Na_2CO_3 absorbing solution used during the combustion step and a chloride selective electrode (Hanna HI 4007) connected to a potentiometer (Hanna HI 98185).

4.2.4. Leaching tests

Upgrading of the RDF chars by removal of water-soluble species was evaluated by two leaching tests: extraction with distilled water at room temperature and Soxhlet extraction also with distilled water. For the room temperature leaching test, an adaptation of EN 12457-2: 2002 was used. Briefly, the RDF char samples were mixed with distilled water in closed glass flasks, at an L/S ratio of 10 $L.kg^{-1}$ and constant temperature of 20 ± 2 °C. The flasks were shaken at 10 rpm (Heidolph), for a period of 24 ± 0.5 h. For the Soxhlet extraction, the same L/S ratio was used, as well as the same contact time. After both extraction procedures, the RDF char samples were filtered and oven dried (Memmert) at 105 ± 2 ºC for 12 h. Chlorine content, HHV and ash content were measured in the decontaminated chars as described in Section 4.2.3.

4.2.5. Characterization of gaseous products

Torrefaction and carbonization gas products were analyzed by GC-TCD (Thermo Trace GC Ultra) for quantification of oxygen, carbon dioxide, carbon monoxide, hydrogen and methane. Total volatile organic compounds (VOCs) were determined using a total hydrocarbon analyzer (Signal, Model 3010), based on flame ionization detection and using propane as a calibration standard. The yield of the gaseous products was determined by difference between 100 % and the sum of char mass yield and liquid fraction mass yield.

4.2.6. Characterization of liquid products

Liquid fraction mass yield was obtained by applying equation 3.5 and using the mass of collected condensate ($m_{condensates}$) instead of the mass of char.

The water content in the condensed phase was analyzed according to ASTM D95, using *o*-xylene and a Dean-Stark apparatus. Chemical oxygen demand (COD) was determined after open vessel digestion using the potassium dichromate methodology, as described in method 5220B from Standard Methods for the Examination of Water and Wastewater. Density was determined gravimetrically and the pH was measured with a pH meter (Crimson MicropH 2001).

Characterization of the organic fraction present in the condensed phase was performed by solvent extraction followed by GC-MS. The condensate samples (5 mL) were acidified until pH=2 (H_2SO_4, 97 %, Panreac), to ensure protonation of weak acid species and extracted three times with $CHCl_3$ (Fisher Scientific), 2 mL each extraction. The combined extracts were dried with anhydrous sodium sulphate, filtered and derivatized with BSA (N,O-Bis(trimethylsilyl)acetamide, Sigma), to convert the carboxylic functional groups into their trimethylsilyl derivatives. The chromatographic analysis of the extracts was performed using a GC-MS analyzer (Focus GC, Polaris Q - Thermo) equipped with a DB-5 capillary column (30 m length, 0.25 mm inner diameter and 0.25 μm film thickness). The extracts were injected in split mode, at 250 °C and the GC temperature was programmed as follows: initial temperature of 35 °C, held for 5 min, increased to 260 °C at a rate of 5°C/min, and held for 1 min. The transfer line and ion source temperatures were 260 °C and 200 °C, respectively. The organic compounds present in the chloroform extracts were identified by comparing their mass spectra with those in NIST and WILEY databases and with the retention time and mass spectra of corresponding standards (Organic acid profile can be found in the Appendix, Figure A.4).

4.3. Results and Discussion

4.3.1. Characterization of raw material and produced chars

The thermochemical upgrading process converted the raw RDF sample to RDF chars with a darker color and a more homogeneous appearance. In the char produced at 300 ºC, it was still possible to detect particle color gradients corresponding to different materials, whereas the char produced at 400 ºC had a uniform black color (Figure 4.3).

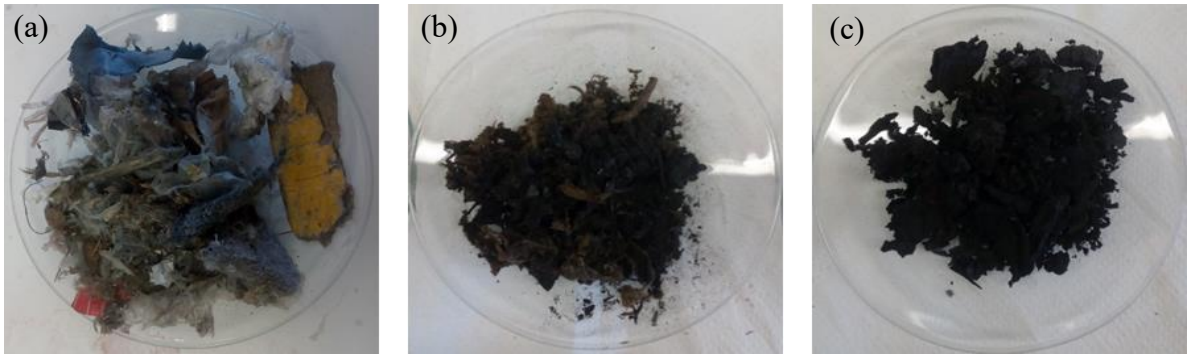

Figure 4.3: (a) Raw RDF, as received; (b) RDF char produced at 300 °C for 30 min and (torrefaction) (c) RDF char produced at 400 ºC for 30 min (carbonization).

The tenacity of the RDF was reduced by thermal processing, since the produced chars were significantly more brittle than the raw RDF, an advantageous characteristic for size reduction operations. According to observations by Verhoeff *et al.* (2011), raw RDF is difficult to mill, whereas after torrefaction, the produced char is easily milled at room temperature.

The main product of torrefaction or carbonization of the raw RDF was the solid char (62.9 and 82.0 wt.%), but variable amounts of liquid and gas products were also formed during these processes, in proportions that were dependent on the process temperature (in Figure 4.4).

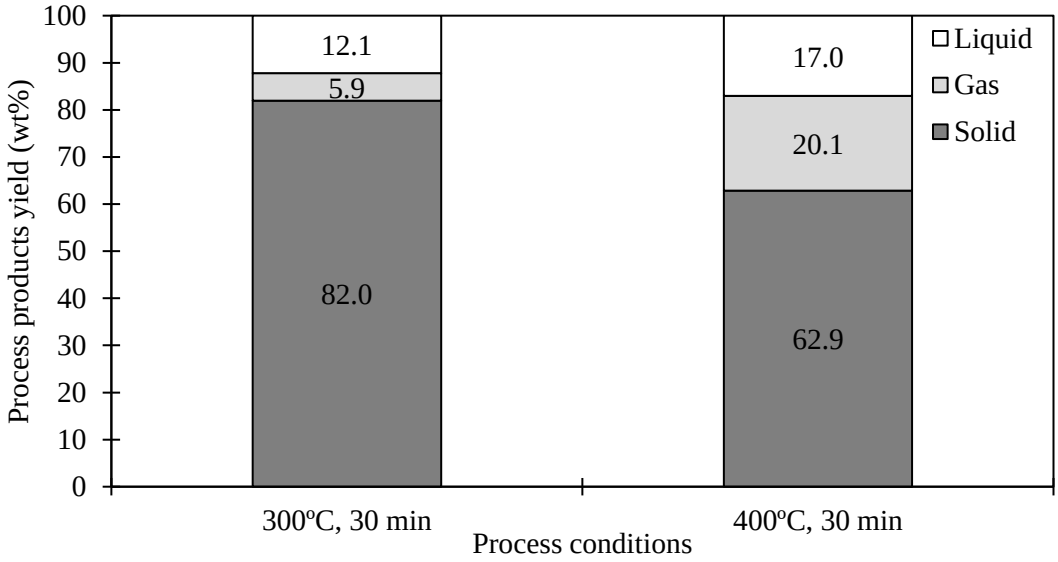

Figure 4.4: Solid, liquid and gaseous products distribution (wt.%) obtained with RDF torrefaction (300 ºC) and carbonization (400 ºC).

As expected, raising the temperature from 300 ºC to 400 ºC increased liquid and gas yields from 12.1 to 17.0 wt.% and from 5.9 to 20.1 wt.%, respectively. The reduction of the RDF mass during thermal treatment is due to the vaporization of water and volatile components and to the thermochemical decomposition of RDF to yield low to medium molecular weight products, a process that occurs at a larger extent for higher temperatures.

The chemical compositions of the raw RDF and of the corresponding chars showed noticeable differences, as detailed in Table 4.1.

Table 4.1: Chemical properties of raw RDF and produced RDF chars, expressed as average values.

Parameter	Unit	RDF	RDF char (300 ºC, 30 min)	RDF char (400 ºC, 30 min)
Proximate analysis				
Moisture	wt.%, ar[a]	10.5	1.3	0.4
Volatile matter	wt.%, db[b]	74.9	56.3	47.6
Ash		16.9	22.8	28.8
Fixed carbon		8.2	20.9	23.6
Ultimate analysis				
C	wt.%, daf[c]	41.1	61.0	80.2
N		2.5	1.3	1.9
H		5.6	6.2	8.4
S		0.4	0.3	0.3
O		50.4	31.2	9.2
Ash mineral composition				
Ca	wt.%, db	50.6	34.1	36.8
Fe		3.1	13.9	12.2
Ti		5.5	8.6	9.0
Cu		0.4	6.3	4.9
Zn		2.9	6.8	7.0
K		6.0	4.0	3.8
Si		21.6	16.3	16.1
Al		7.9	4.4	4.7
Mg		-	-	-
P		-	1.3	0.5
Others		2.0	4.0	5.0
Cl	wt.%, db	0.7	1.8	1.9
HHV	$MJ.kg^{-1}$, db	16.4	19.9	23.5
Energy yield	%, db	-	98.3	85.6

[a]ar, as received basis; [b]db, dry basis; [c]daf , dry ash free basis.

While the raw RDF sample had a moisture content of around 10 wt.%, the RDF chars presented residual moisture contents (below 1.5 wt.%) which is an advantage regarding storage and transportation, since high moisture contents are related to low calorific values and microbial degradation(Samad *et al.*, 2017).

Significant devolatilization was observed at both temperatures, leading to a decrease in volatile matter of the chars formed at 300 ºC and 400 ºC (56.3 and 47.6 wt.%, respectively) when compared to the volatile matter of raw RDF (74.9 wt.%). The RDF mass loss observed at 300 ºC can be mainly attributed to the decomposition of lignocellulosic materials, since hemicellulose, cellulose and lignin, are susceptible to thermal decomposition in the temperature range of 225-500 ºC (Prins *et al.*, 2006a; Qi *et al.*, 2018). At 400 ºC, both fractions are susceptible to thermal decomposition, as most polymeric materials decompose at higher temperatures, in the range of 350 to 550 ºC, due to the high stability of the C-C bonds, that support their polymeric structures (Haykiri-Acma *et al.*, 2017; López *et al.*, 2011; Park *et al.*, 2012).

As moisture and volatile matter are eliminated from the RDF, the non-volatile components (fixed carbon and ash) are concentrated in the RDF char. Ash content reached values of 22.8 and 28.8 wt.%, for the chars produced at 300 ºC and 400 ºC. These values represent an increment of 5.8 and 11.9 %, respectively, relatively to the ash content of the raw RDF. On the other hand, fixed carbon also increased from 8.3 wt.% for raw RDF to 20.9 wt.% and 23.5 wt.% for the RDF chars produced at 300 ºC and 400 ºC, respectively. This outcome is a common feature of these thermochemical processes and has been described by other authors using RDF and MSW and biomass (Białowiec *et al.*, 2017; Recari *et al.*, 2017; Samad *et al.*, 2017). As these two parameters (ash and fixed carbon) have opposite effects on the

fuel heating value, the thermochemical conditions should be chosen in order to maximize this fuel property.

High ash chars have limited application as fuels in combustion or gasification because there are several related operational issues such as excessive ash deposition or slagging and fouling phenomena (Akdag *et al.*, 2016). The co-combustion of high-ash chars with less problematic fuels, such as biomass or coal can still enable their energetic valorization with lower operational drawbacks (Casado *et al.*, 2016). In alternative to fuel applications, RDF chars may be explored for their material valorization as activated carbon precursors (Gopu *et al.*, 2018; Hajizadeh and Williams, 2013).

The quality of solid fuels is not only influenced by ash content but also by ash composition, therefore that was a parameter determined for raw RDF and the RDF chars (Table 4.1). Ash composition determines its melting point thus affecting the fuel tendency to form solid deposits inside boilers or gasifiers. The main components detected in the raw RDF and in the RDF char ash were calcium and silica (> 15 wt.%). Aluminum, potassium, zinc, titanium, iron and copper were present at concentrations lower than 15 wt.% and phosphorus was only detected in the RDF chars. A group of minor components with concentrations lower than 1 wt.% was not presented individually but as a sum of other mineral components (Table 4.1). The torrefaction and carbonization processes caused an increase in the concentration of all mineral components relatively to the raw RDF, except for calcium, silica, potassium and aluminum. Also, the concentrations of iron, copper, potassium silica and phosphorus did not increase with the severity of the thermochemical process, when the temperature was increase from 300 ºC to 400 ºC, regardless of the decrease in char yield. This indicates that another process besides the concentration effect of RDF mass loss is influencing the concentration of the non-volatile inorganic fraction. A possible explanation is the dissolution or entrainment of the more abundant mineral components by the process condensates, that are mainly composed of water. This phenomenon is analogous to the dissolution of inorganic components during hydrothermal carbonization (Reza *et al.*, 2013) and may occur especially during the cooling phase of condensates and chars. A similar process explains the deposition of tar components in the carbonaceous structure of the char, during torrefaction or carbonization of biomass fuels (Kuzmina *et al.*, 2016).

Bond breaking during torrefaction or carbonization favors the elimination of more electronegative elements such as oxygen or nitrogen relatively to carbon or hydrogen (Vollhardt and Schore, 2007), a tendency that will influence the elemental composition of the formed chars. Ultimate analysis showed that carbon content increased from 41.1 wt.% to 61.0 wt.% and 80.2 wt.%, for the RDF chars produced at 300 ºC and 400 ºC, respectively. Hydrogen content also increased with process temperature although in a less pronounced way, reaching the highest value at 400 ºC (8.4 wt.%). On the other hand, oxygen content that was relatively high for the raw RDF (50.4 wt.%) due to the presence of the lignocellulosic materials, decreased to 31.2 and 9.2 wt. % for the RDF chars produced at 300 ºC and 400 ºC, respectively. The release of volatile oxygenated compounds during decomposition of hemicellulose, cellulose and lignin from the RDF biomass component is the possible mechanism by which carbon is concentrated in the RDF chars (Yue *et al.*, 2017). Nitrogen and sulphur in RDF are also partially eliminated during torrefaction or carbonization because their polar covalent bonds with carbon atoms are easier to break than the non-polar C-C bonds that are relatively stable up to 400 ºC. As a consequence, the RDF chars presented lower concentrations of nitrogen and sulphur than the raw RDF, a positive characteristic regarding harmful NOx and SOx emissions during combustion.

The relation between H/C ratio and O/C ratio for the raw RDF and resulting RDF chars is compared in Figure 4.5 with similar data reported in the literature for different biofuels and fossil fuels showed for comparison.

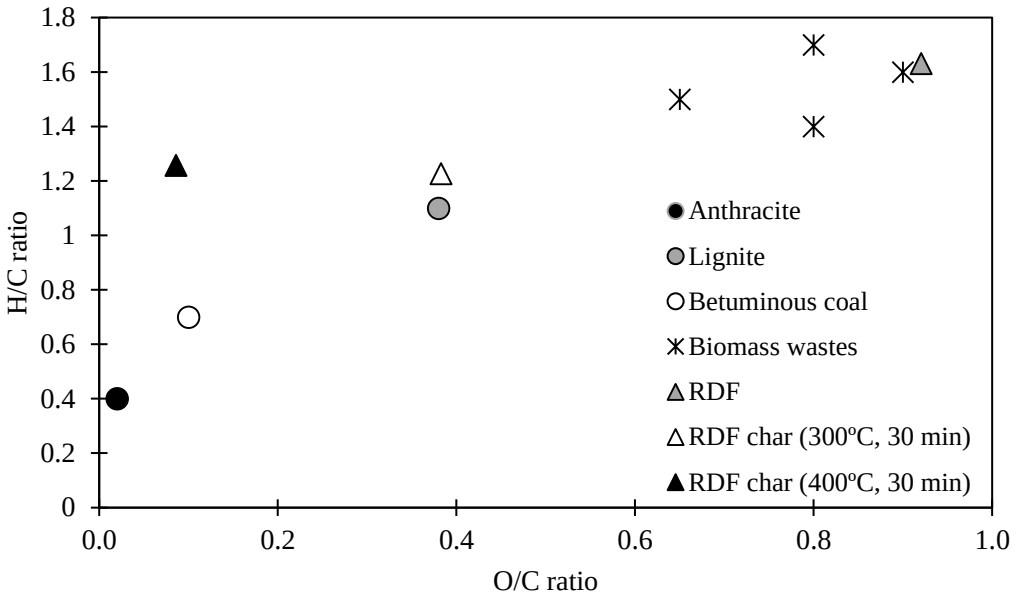

Figure 4.5: van Krevelen diagram for the RDF and RDF chars produced at 300 ºC and 400 ºC. Fossil fuels and biomass wastes are shown for comparison (van der Stelt *et al.*, 2011).

While raw RDF had a composition comparable to biomass wastes, the RDF chars presented much lower O/C ratios, similar to lignite (RDF char produced at 300 °C) or to bituminous coal (RDF char produced at 400 °C). The H/C ratio of both chars is lower than the raw RDF, but higher than bituminous coal or lignite reflecting a lower degree of aromatization of the RDF chars when compared with these fossil fuels. The elemental composition differences observed between raw RDF and the RDF chars clearly depicts a fuel upgrading effect brought by torrefaction and carbonization, regarding water removal and oxygen elimination in the form of oxygenated volatile compounds through decarboxylation, decarbonylation and dehydration reactions (Yue *et al.*, 2017) occurring in both processes but more extensively in the carbonization range.

Oxygen reduction and carbon increase are also the primary reasons for the increase in HHV of the RDF chars (Table 4.1). The char obtained at 300 ºC had a HHV of 19.9 $MJ.kg^{-1}$ while the char produced at 400 ºC had a HHV of 23.5 $MJ.kg^{-1}$, values that are respectively, 21 and 43 % higher than the HHV of the raw RDF (16.4 $MJ.kg^{-1}$).

Energy yield was 98.3 % and 85.6 %, for the processes at 300 ºC and 400 ºC, respectively, although the RDF char obtained at 400 ºC had a higher HHV than the one obtained at 300 ºC. At 400 ºC a higher fraction of the RDF carbon was lost to the vapor phase, reducing mass yield to an extent that overcomes the influence of the RDF char heating value on the energy yield. According to van der Stelt *et al.* (2011), although there is a 30 wt.% mass loss during torrefaction, the torrefied product can retain up to 90 % of the energy content, which is in accordance with the mass and energy yields obtained in the present work. This increase in energy density after both thermochemical treatments, is of high relevance for the adaptation of these processes to an industrial scale because of the consequences at the levels of product quality, transportation and logistics (Recari *et al.*, 2017; van der Stelt *et al.*, 2011).

Chlorine content in the produced RDF chars was higher when compared to the raw RDF, and increased with the treatment temperature, reaching values of 1.8 and 1.9 wt.%, at 300 ºC and 400 ºC, respectively (Table 4.1). According to Hwang *et al.* (2007) these chlorine values are high enough to cause problems during combustion, with the potential to damage several components of the thermal conversion system due to high temperature corrosion. Contrary to the results obtained in this work, several authors report a decrease in chlorine content for RDF or MSW after torrefaction or carbonization (Edo *et al.*, 2017; Recari *et al.*, 2017; Yuan *et al.*, 2015). The chlorine content, due to its volatility, is reduced after the carbonization process, transitioning to the condensable and non-condensable gas phase (Edo *et al.*, 2017). The increase in chlorine content may be associated with chlorine re-condensation on the RDF char surface, or chlorine adsorbed onto the organic and mineral phases of the RDF char (Vassilev *et al.*, 1999). Additionally, chlorine from the plastic component (PVC) of RDF is almost completely released under 400 ºC, but there are also potential for the formation of inorganic salts such as potassium or calcium chloride, which have boiling points significantly above 400 ºC (Hwang *et al.*, 2006; S. V. Vassilev *et al.*, 1999). This behavior can be expected for the torrefaction or carbonization of chlorine-containing polymers in industrial units that are not usually equipped with gas purging systems by injection of an inert gas, because the continuous injection of a purging gas during the torrefaction or carbonization process increases costs and energy requirements of the processes by introducing another material input and potentially lowering the operating temperature (Sarvaramini and Larachi, 2014).

To evaluate the potential of water leaching in the upgrading of the RDF chars by chorine dissolution, the RDF char was subject to leaching experiments, with water at room temperature and with water close to its boiling point, using a Soxhlet apparatus (Figure 4.6). These experiments aimed to evaluate whether chlorine was chemically bonded to the char structure or simply adsorbed on its surface or pores and therefore accessible to water solvation.

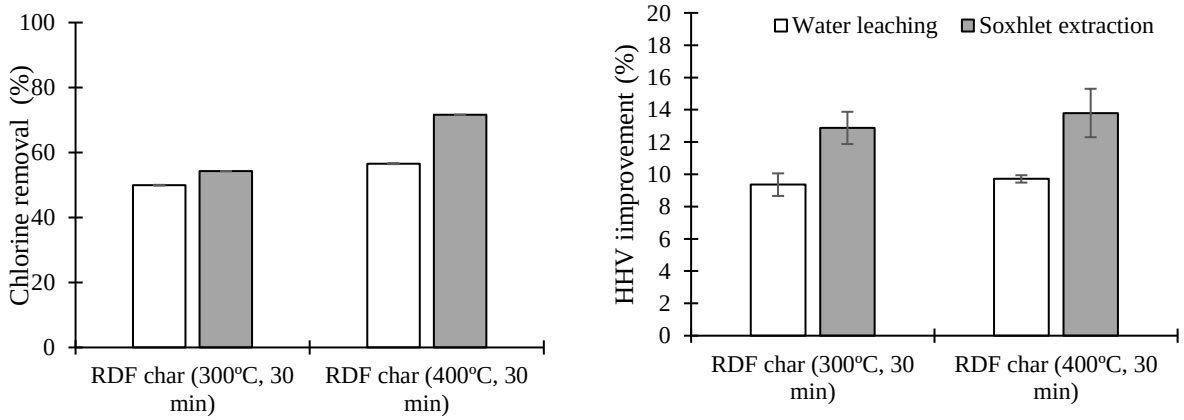

Figure 4.6: Chlorine removal efficiency (%) and high heating value (HHV) improvement (%) for the RDF chars produced at 300 ºC and 400 ºC, after water leaching and Soxhlet extraction.

Both water leaching tests caused a reduction of chlorine content in the RDF chars, indicating that this element is present in the form water-soluble chlorine compounds, that were formed during the torrefaction and carbonization experiments. The decrease was more accentuated in the RDF char produced at 400 ºC with Soxhlet extraction, reaching a chlorine concentration of 0.544 wt.%, which is below the chlorine concentration of the raw RDF. Although carbonization at 400 ºC is expected to lead to a higher dechlorination degree than torrefaction at 300 ºC, the chlorine content of the char obtained at 300 ºC was lower. This observation suggests that the char produced at 400 ºC may have a more organized structure with a higher porosity that is more favorable to chlorine adsorption. Other mineral components

were also removed by the leaching processes since the ash content in the RDF chars decreased around 1 % for both chars after water leaching at room temperature and around 3 % after Soxhlet extraction, which is beneficial to the RDF chars fuel properties. In particular, HHV of both chars was increased by the washing treatments, reaching values of 22.5 and 26.7 $MJ.kg^{-1}$ for the chars produced at 300 and 400 ºC, respectively, after the Soxhlet extraction with water. Nevertheless, this final treatment with hot water must be optimized to minimize water use, by recycling the water through an ion exchange unit, and the associated energy consumption must be considered in the process energetic balances.

4.3.2. Characterization of gaseous products

The release of gaseous products during torrefaction or carbonization occurs either by evaporation or thermal decomposition of the raw materials. The amount of produced torrefaction emissions depends on the composition of raw material, heating rate, temperature and residence time (Stelte, 2012).

The concentrations of the main gas products from torrefaction and carbonization of RDF are presented in Figure 4.7.

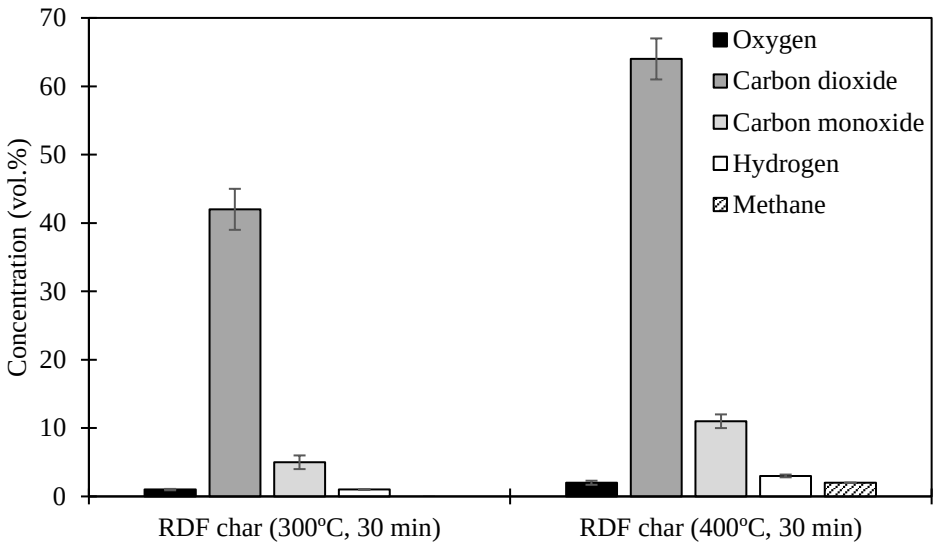

Figure 4.7: Composition of the gas products for RDF torrefaction (300 ºC) and carbonization (400 ºC).

Excluding water, the major gas products from RDF torrefaction and carbonization were carbon dioxide and carbon monoxide, which is expected from the thermal decomposition in an oxygen deficient atmosphere. Carbon dioxide, carbon monoxide and water are formed by decarboxylation, decarbonylation and dehydration reactions, that occur during the thermal decomposition of lignocellulosic materials (White and Dietenberger, 2001). There were also traces of hydrogen, with higher concentrations at 400 ºC, while methane could only be detected at 400 ºC. According to Wahid *et al.* (2017), at higher temperatures, methane may be formed through methanation (reaction of carbon monoxide with hydrogen to yield methane and water). Both process conditions yielded a concentration of volatile organic compounds (VOCs) of 1280 ppm (expressed in total carbon). The composition of the gas products obtained in this work are in line with other studies using different raw materials, such as willow, starch, straw and larch (Prins *et al.*, 2006b) or RDF and Stabilat (Stelte, 2012).

4.3.3. Characterization of liquid products

Condensates from the torrefaction and carbonization of RDF included liquid formed and collected in two condensation chambers (1st and 2nd collection points), as previously described (Section 4.2.2.). Liquid fractions from the torrefaction process presented a lighter color than the ones produced at 400 ºC, a sign of the more extensive decomposition occurring at the higher temperature. Moreover, condensates collected in the 1st collection point had a darker color and appeared to have particulate matter in suspension, probably corresponding to heavy non-polar products. The condensates collected in the 2nd collection point, had a lighter color and presented an oily upper layer, composed of water-insoluble liquid products (Figure 4.8).

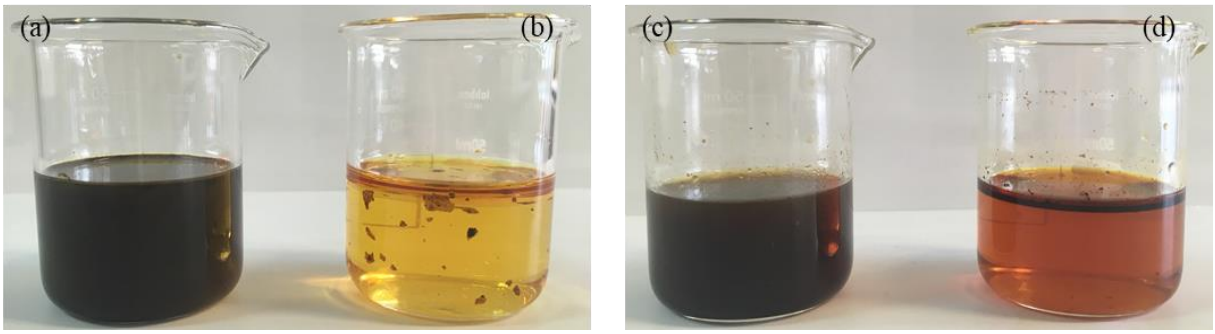

Figure 4.8: Condensates originating from RDF torrefaction (300 ºC) and carbonization (400 ºC): (a) 300 ºC, 1st collection point; (b) 300 ºC, 2nd collection point; (c) 400 ºC, 1st collection point; (d) 400 ºC, 2nd collection point.

As shown in Figure 4.4, condensate yield was 12.1 wt.% at 300 ºC (635 mL) and 17.0 wt.% at 400 ºC (992 mL), reflecting the influence of temperature increase on the thermochemical decomposition of the raw RDF. At both collection points, the condensates had water contents of 95 % and 90 % for 300 ºC and 400 ºC, respectively (Table 4.2). A lower water content (45-56 %) was found in the condensates produced during the torrefaction of bamboo between 250 and 350 ºC (Chen *et al.*, 2015a).

Table 4.2: Characterization of RDF torrefaction and carbonization liquid products. Results presented as average values.

Parameters	Unit	Process temperature			
		300 ºC		400 ºC	
		1st collection point	2nd collection point	1st collection point	2nd collection point
Density	$g.cm^{-3}$	0.99	0.98	1.00	1.00
Water content	wt.%	95	95	90	90
COD	$g\ O_2.L^{-1}$	13.5	36.5	39.2	69.3
pH		3	4	3	2

Chemical oxygen demand (COD) of the condensates recovered at the 2nd collection point, was higher than COD of the condensates recovered from the 1st collection point, suggesting that volatile organic components only recovered in the second condensation chamber contribute to this higher value. Chemical oxygen demand also increased with the process temperature, reaching a value of 69.3 g $O_2.L^{-1}$, for the condensate collected in the 2nd collection point, after carbonization at 400 ºC. The obtained values indicate that these liquid phases have very significant amounts of suspended and dissolved solids that must be removed before discharging this effluent. Nevertheless, these COD values are inferior to those

measured by Fagërnas *et al.* (2015) for condensates from the torrefaction of spruce and bamboo, at temperatures of 240-300 ºC. The higher water contents and the lower COD values of the condensates obtained in this work relatively to those reported (Chen *et al.*, 2015a; Fagërnas *et al.*, 2015) concerning torrefaction of lignocellulosic materials, may be related with RDF composition, since the polymeric fraction is less susceptible to thermal degradation than the lignocellulosic biomass, but also with the possible adsorption of tar components on the char's surface. This process is avoided in torrefaction systems with injection of a purging inert gas, but has the advantage of promoting a higher retention of carbonaceous species from the condensates in the char products, therefore increasing their yield (Kuzmina *et al.*, 2016).

The pH of all condensate samples was acidic, reflecting the presence of organic acids, which are typical products of lignocellulosic biomass degradation (Chen *et al.*, 2015a; Tumuluru *et al.*, 2011).

The identification of the major organic compounds found in the chloroform extracts of the condensates and their relative chromatographic peak areas are presented in Table 4.3. Figure 4.9 represents the major chemical species present in the extracts. A representative chromatogram with corresponding identifications can be found in the Appendix (Figure A.5 and Table A.3).

Table 4.3: GC-MS relative peak areas of the main organic compounds found in the chloroform extracts from the condensates obtained in RDF torrefaction (300 ºC) and carbonization (400 ºC) experiments.

Compounds	Molecular formula	CAS number	Relative peak area (%)			
			300 ºC		400 ºC	
			1st collection point	2nd collection point	1st collection point	2nd collection point
Acids						
Acetic acid	$C_2H_4O_2$	64-19-7	6.87	0.55	1.17	2.16
Oxalic acid	$C_2H_4O_4$	144-62-7	-	-	-	11.97
Propionic acid	$C_3H_6O_2$	79-09-4	2.59	0.58	2.52	1.48
Butyric acid	$C_4H_8O_2$	107-92-6	2.14	-	0.62	-
2-Methyl-2-furoic acid	$C_6H_6O_3$	4412-96-8	0.76	-	0.74	-
Benzoic acid	$C_7H_6O_2$	65-05-0	21.40	0.35	21.80	1.06
Aldehydes						
4,4-Dimethyl-2-pentynal	$C_7H_{10}O$	2579-21-7	-	1.75	0.87	0.37
Ketones						
2-Ethylcyclopentanone	$C_7H_{12}O$	4971-18-0	-	-	4.02	0.48
Dihydroxyacetophenone	$C_8H_8O_3$	1075-06-5	0.73	-	0.77	0.40
Guaiacylacetone	$C_{10}H_{12}O_3$	2503-46-0	-	-	1.22	0.16
3-Hidroxy-2-methyl-4H-pyran-4-one	$C_6H_6O_3$	118-71-8	1.06	1.33	2.68	1.75
Alcohols						
Butanol	$C_4H_{10}O$	71-36-3	0.95	3.28	1.29	1.81
2-Chloroethanol	ClC_2H_5O	107-07-3	1.93	2.59	1.33	1.57
Octanol	$C_8H_{18}O$	111-87-5	-	1.36	-	1.38
Esters						
Hydroxyethylbenzoate	$C_9H_{10}O_3$	94-33-7	-	-	3.04	-
Ethers						
2,4,6-Trimethyl-(2α,4α,6α)-1,3-dioxane	$C_6H_6O_3$	19145-91-6	-	-	0.53	< 0.10
Furans						
Furfural	$C_5H_4O_2$	98-01-1	17.4	50.31	13.82	7.22
2,4-Dimethyl-furan	C_6H_8O	3710-43-8	0.22	-	0.59	-
Acetylfuran	$C_6H_6O_2$	1192-62-7	0.97	0.85	1.69	0.76
5-Methylfurfural	$C_6H_6O_2$	620-02-0	7.40	10.30	8.18	4.28
Aromatic Hydrocarbons						
1,1-Biphenyl	$(C_6H_5)_2$	92-52-4	0.64	0.30	-	0.56
Benzonitrile	C_6H_5CN	100-47-0	-	0.94	0.67	0.42
Ethylbenzene	C_8H_{10}	100-41-4	-	-	-	0.28
Xylene	C_8H_{10}	1330-20-7	-	-	-	0.31
Styrene	C_8H_8	100-42-5	-	-	-	1.65
2-Propenylbenzene	C_9H_{10}	300-57-2	-	-	-	0.47
1-Ethyl-2-methylbenzene	C_9H_{12}	611-14-3	-	-	-	0.35
Cumene	C_9H_{12}	98-82-8	-	0.49	-	0.16
Naphtalene	$C_{10}H_8$	91-20-3	-	-	-	0.32
Phenatrene	$C_{14}H_{10}$	85-01-8	-	-	-	0.46
Phenols						
Phenol	C_6H_6O	108-95-2	4.27	1.98	9.01	2.22
4-Methoxyphenol	$C_7H_8O_2$	150-76-5	-	-	1.59	-
2-Methoxy-4-methylphenol	$C_8H_{10}O_2$	95-51-6	-	-	0.60	-
2,6-Dimethoxyphenol	$C_8H_{10}O_3$	91-10-1	0.42	-	1.15	-
3,4-Dimethoxyphenol	$C_8H_{10}O_3$	2033-89-8	-	-	0.84	-
Hydroquinone	$C_6H_6O_2$	123-31-9	0.88	-	0.50	-
Terpenes						
3-carene	$C_{10}H_{16}$	13466-78-9	0.26	0.47	-	0.51
Total identified peaks (% peak area)			**70.89**	**77.43**	**77.22**	**44.08**

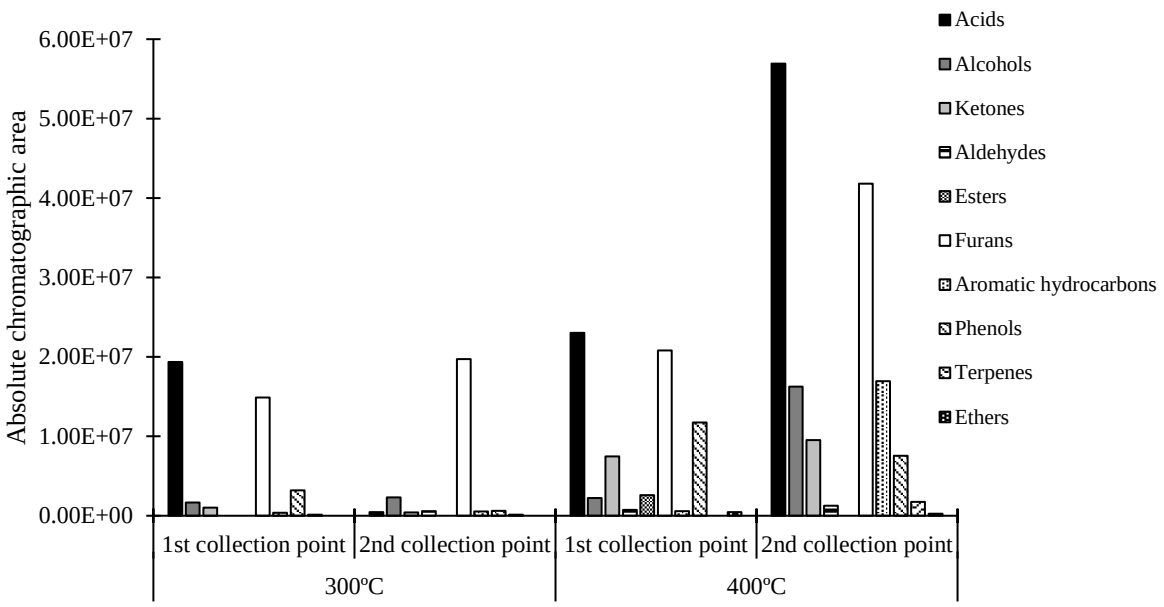

Figure 4.9: Major chemical species present in the liquid phase of RDF torrefaction (300 ºC) and carbonization (400 ºC) at different collection points, expressed in absolute peak area.

At 400 ºC, in both collection points, it was possible to identify a larger number of compounds, as well as heavier compounds, evidencing a higher degree of tar formation at this temperature. Increasing process temperature yielded a higher number of phenols and carbonyl derivatives, which could be the result of a more extensive decomposition of lignin from the RDF biomass component (Chua *et al.*, 2017). Also, more aromatic hydrocarbon molecules were identified at 400 ºC, including two polycyclic aromatic hydrocarbons (naphthalene and phenanthrene), which is expected because higher temperatures favor condensation of aromatic compounds to form polycyclic structures (Richter and Howard, 2000). Furans, alcohols and monocyclic aromatic hydrocarbons were consistently more abundant in the 2nd collection point as a consequence of the relatively high volatility of those components, relatively to condensed aromatic hydrocarbons or phenols.

A higher presence of phenolic compounds at 400 ºC was also detected. Furfural and 5-methylfurfural presented the largest peak areas within the furan group, similarly to biomass torrefaction tars in which these compounds are abundant as the result of direct ring-opening and rearrangement reactions of cellulose molecules (Shen and Gu, 2009). The abundance of oxygenated compounds in the condensates from RDF torrefaction or carbonization is an evidence of the deoxygenation of the original raw material, justifying the low oxygen content of the chars formed at both process temperatures (Chen *et al.*, 2018a).

The volume and complex composition of the condensates collected during these processes represents one of the main issues that must be addressed when scaling up the torrefaction process. The recirculation of torrefaction condensates through the raw materials prior to the thermal conversion process to retain organic molecules (Chen *et al.*, 2017), the separation of different organic compounds with added value (acetic acid, furfural, phenol) (Fagërnas *et al.*, 2015) or the use of these tars as additives in biomass pelletizing processes (Stelte, 2012), are some of the processes proposed in literature to minimize the environmental impact of these condensates and recover some of their organic content.

4.4. Conclusions

Torrefaction (300 ºC) and carbonization (400 ºC), converted RDF to chars with higher carbon content and calorific value, thus upgrading the composition and properties of this waste derived fuel. Ash and

chlorine concentrations increased with process temperature, but could be reduced by subsequent washing with hot water, yielding chars with even higher calorific values. Gaseous emissions were mainly composed of carbon dioxide and carbon monoxide, with smaller amounts of methane and hydrogen. Liquid emissions presented very high COD values and were mostly composed by water and organic oxygenated compounds such as acids, furans and phenols.

Chapter 5

Hydrothermal carbonization of RDF

Abstract

In this chapter, hydrothermal carbonization (HTC) was employed as an upgrading thermochemical conversion process for Refuse Derived Fuel (RDF). The effect of process temperature (250 ºC, 275 ºC and 300 ºC), residence time (30 min and 120 min) and solid-to-water ratio (1:15 and 1:5) on the main characteristics of the produced hydrochars and process waters, was assessed. Results illustrated that the HTC process yielded hydrochars with upgraded characteristics such as reduced ash contents and increased high heating values when compared to the original feedstock. The lower ash content was obtained for the hydrochar produced at 300 ºC for 120 min (3.3 wt.%, db), whereas the higher high heating value was found for the hydrochar obtained at 275 ºC for 120 min (28.1 $MJ.kg^{-1}$, db). Hydrochars also presented reduced chlorine contents, with the process reaching 55 % dechlorination efficiency at 300 ºC for 120 minutes. Furthermore, the obtained hydrochars presented significantly reduced oxygen and hydrogen contents, increasing their similarities with O/C and H/C profiles of fossil fuels. However, process waters in all the conducted tests presented an acidic pH, high COD (maximum 27.2 $gO_2.L^{-1}$) and significant concentrations of total phenolics and total reducing sugars. Various organic compounds were identified in the process waters, mainly organic acids, alcohols, furan derivatives, phenolic compounds and aromatic hydrocarbons, and the process water obtained at the most severe process conditions presented the higher number of identified compounds, highlighting the more extensive degradation occurring at those conditions. Process performance was evaluated and the conditions of 275 ºC, 30 minutes, solid-to-water ratio of 1:5 were selected as optimal, since they presented the lower energy requirements to operate (5.6 MJ), exhibited a positive net energy (8.5 MJ) and also presented the highest process energy efficiency (52.6 %).

Keywords: Refuse Derived Fuel; Hydrothermal carbonization; Alternative solid fuel; Hydrochar; Process water.

5.1. Introduction

Hydrothermal carbonization (HTC) has been considered one of the most promising and effective thermochemical upgrading technologies for feedstocks with a high degree of heterogeneity and high moisture or ash contents (Erdogan *et al.*, 2015; Lin *et al.*, 2017; Mihajlović *et al.*, 2018; Reza *et al.*, 2013).

The hydrochar is the process product with higher potential for power generation, presenting high hydrophobicity, high energy content as well as good grindability when compared with other chars produced by different thermal processes namely torrefaction or carbonization (Acharya *et al.*, 2015; Kumar *et al.*, 2018). Besides their potential as solid fuels, hydrochars have also shown potential as catalysts, soil ameliorants or adsorbents (Saha *et al.*, 2018).

Lately, a considerable amount of research has been conducted on HTC as a treatment and upgrading process for different waste feedstocks such as food waste (Saqib *et al.*, 2018; Wang *et al.*, 2018b), agricultural wastes (Ayoub Missaoui *et al.*, 2017; Nakason *et al.*, 2018; Pala *et al.*, 2014), biomass wastes (Gao *et al.*, 2016; Mäkelä *et al.*, 2015; Wu *et al.*, 2017), algae (Lee *et al.*, 2018; Park *et al.*, 2018; Smith and Ross, 2016), packaging and plastics (Lokahita *et al.*, 2017; Yao and Ma, 2018) or sludges (Wilk *et al.*, 2019; Xu and Jiang, 2017). The HTC process allowed the conversion of all these feedstocks into hydrochars with higher carbon content, lower ash content and higher calorific values than the corresponding raw materials.

MSW has also been used in different studies as raw material for HTC (Berge *et al.*, 2011; Hwang *et al.*, 2012; Kim *et al.*, 2017; Lu *et al.*, 2011; Mu'min *et al.*, 2017). But, according to Lin *et al.* (2017), due to the inherent variability of this type of waste, further investigation of MSW hydrothermal conversion is necessary to achieve a more-detailed and clear understanding of the underlying reaction mechanisms. Nevertheless, HTC seems to be responsible of yielding hydrochars with reduced chlorine content, which is extremely important in order to use the hydrochars in fuel applications (Poerschmann *et al.*, 2015; Shen *et al.*, 2017; Yao and Ma, 2018).

In spite of the positive features of the HTC process regarding hydrochar properties, the management and valorization of the process water is one of the challenges that should be addressed to enable sustainable application of this process at industrial scale. This effluent contains high amounts of dissolved organic and inorganic compounds that hinder its treatment. Furthermore, this effluent is produced at large volumes because most processes are effective at solid-to-water ratios higher than 1:5 (m/v).

Characterization of HTC process water is necessary in order to define adequate treatment or valorization pathways that are fundamental components of a sustainable HTC process. Recirculation of the process water after hydrochar filtration was studied by Stemann *et al.* (2013) and Catalkopru *et al.* (2017) and both works showed that this approach can increase hydrochar mass and energy yields. Moreover, Catalkopru *et al.* (2017) also showed that the number of recirculations decreases the leaching of inorganic components, affecting the ash content of the hydrochars, and that the high heating value of the chars is almost unchaged with the recirculation process.

Biomethane production through anaerobic digestion is also a solution for HTC process water, due to the considerable amount of hydrolyzed sugars and organic acids that are present in this water (Erdogan *et al.*, 2015; Wirth and Mumme, 2013).

Since HTC process water is a highly contaminated effluent, remediation technologies, such as adsorption or chemical precipitation could also represent a solution. Adsorption is a widespread wastewater remediation technology because it is easily implemented and entails lower costs than other technologies, like for example, reverse osmosis (Khadhri *et al.*, 2019). According to Yorgun *et al.* (2009) activated carbon is predominantly an amorphous solid with a large internal surface area and pore volume, consisting of a basic structural unit building up of condensed aromatic rings. The pores in the carbon contribute to increase its surface area and textural properties. These characteristics are responsible for its superior ability to remove of a wide variety of organic and inorganic pollutants from liquid or gaseous media. Activated carbon is the most employed adsorbent in wastewater treatment, but besides of this adsorbent there are several other materials that present adsorptive potential with lower associated production costs, particularly if they derive from wastes. Hydrochars can also present strong sorption capacities for both polar and non-polar organic contaminants due to their diverse surface functionalities (Fang *et al.*, 2018). Manyuchi *et al.* (2018) used char produced at 300 ºC for 30 min, from municipal organic waste, to treat municipal wastewater, and obtained removal efficiencies of 90 %, 89 %, 64 % and 78 %, for COD, total suspended solids, Kjehldal nitrogen, and total phosphorous, respectively.

Chemical precipitation is another technique that is extensively applied in wastewater treatment. During this process, dissolved and suspended matter are converted via chemical reactions to an insoluble

solid that precipitates. Precipitation has been used for the removal of non-biodegradable organic compounds in highly contaminated wastewaters such as landfill leachates. A number of chemical agents such as CaO, hydrated lime ($Ca(OH)_2$) or struvite ($Mg\text{-}NH_3\text{-}PO_4$), have been used as precipitating agents (Kurniawan *et al.*, 2006). For example, lime precipitation is applied for underground or surface water treatment, because lime is capable of removing high molecular organic compounds (like humic and fulvic acids) through complexation of Ca^{2+} with these compounds. These organic species are refractory anionic macromolecules containing both aromatic and aliphatic compounds with phenolic and carboxylic functional groups (Renou *et al.*, 2009).

The main goal of this chapter was the evaluation of the hydrothermal carbonization of RDF, by varying process parameters and characterizing the two major products of this process: hydrochar and process water. HTC tests were conducted by varying temperature, residence time and solid-to-water ratio. The obtained products were subjected to different characterization analyses, in order to evaluate the impact of process parameters and their potential applications. Furthermore, process performance was calculated, which is very important information to evaluate the energetic viability of this process and for planning and modelling scaled-up facilities.

Some preliminary tests of process water treatment through precipitation and adsorption were also performed to provide some insight on treatment alternatives for this effluent.

5.2. Materials and methods

5.2.1. Raw material

The RDF sample used in this chapter was supplied by CITRI, S.A. RDF production scheme and sampling has been performed as described in Chapter 3.

5.2.2. HTC experiments

HTC experiments were carried out using a 1 L stainless steel autoclave reactor (Parr Pressure Reactor) coupled with an electric heater and a controller (Parr 4848 Reactor controller), under autogenic pressure (Figure 5.1).

Figure 5.1: Stainless steel autoclave reactor used in the HTC experiments.

For each experiment, a given mass of the RDF (as received) was placed in the reactor and tap water was added at a solid-to-water ratio of 1:15 or 1:5 (m/v). After sealing and removing air with a vacuum pump, the reactor was heated to the desired carbonization temperature (250, 275 or 300 ºC), kept at that

temperature for a given residence time (30 and 120 min) and cooled to room temperature using an internal refrigeration coil, fed with tap water. When at room temperature, any residual gas products were vented. The hydrochars and liquid products were separated by filtration through a pre-weighted qualitative filter paper. The hydrochars were washed with 1 L of deionized water, air-dried for 12 h and oven-dried at 105 ± 2 ºC for 12 h. Afterwards, the hydrochar samples were equilibrated to room temperature in a desiccator, weighted for yield determination and stored in air-tight containers until subsequent analysis. The liquid product (process water) was stored at 4 ºC until further analysis.

The hydrochar samples were coded with "H-T-t/R" where "T" represents operating temperature, "t" represents residence time and "R" represents the solid-to-water ratio. For example, the code "H-275-30/5" represents the hydrochar produced at 275 ºC for 30 min with a solid-to-water ratio of 1:5. For the process water samples a similar nomenclature was used "W-T-t/R where W stands for water sample and the other symbols correspond to the same codification used for the hydrochars. The operational conditions used in each HTC experiment are described in Table 5.1.

Table 5.1: Experimental layout for HTC experiments.

Temperature (ºC)	Residence time (min)	Generated pressure (bar)	Solid-to-water ratio	Hydrochar code	Process water code
250	30	40	1:15	H-250-30/15	W-250-30/15
275	30	60	1:15	H-275-30/15	W-275-30/15
275	30	60	1:5	H-275-30/5	W-275-30/5
300	30	88	1:15	H-300-30/15	W-300-30/15
250	120	40	1:15	H-250-120/15	W-250-120/15
275	120	60	1:15	H-275-120/15	W-275-120/15
300	120	88	1:15	H-300-120/15	W-300-120/15

5.2.3. RDF and hydrochar characterization

Prior to analysis the hydrochars were milled (DeLongui mill) and sieved (Retsch sieve) to a particle size diameter < 500 µm. All the determinations were conducted with replicates, and the results are presented as average values (variation coefficient ≤ 10%).

Moisture content was determined according to CEN/TS 15414-3:2010. Volatile matter content was carried out according to EN 15402:2011. Ash content was determined in agreement with EN 15403:2011. Fixed carbon content was calculated by difference, on a dry basis (db).

Elemental composition (CHNS) of the RDF and hydrochar samples was determined using an elemental analyzer (Thermo Finnigan – CE Instruments Model Flash EA 112 CHNS series). Oxygen content was obtained by difference, on a dry ash free basis (daf).

Mineral composition of the RDF and hydrochar samples was determined through X-Ray fluorescence (Niton XL 3T Gold++).

High heating values (HHV) of the RDF and hydrochar samples were determined using a calorimeter bomb (IKA C200), using benzoic acid as a calibration standard.

Mass yield, energy density and energy yield of the hydrochars were calculated based on equations 5.1, 5.2, 5.3, respectively:

$$Mass\ yield\ (\%, db) = \left(\frac{m_{hydrochar}}{m_{RDF}}\right) \times 100 \qquad \text{Equation 5.1}$$

$$Energy\ density = \frac{HHV_{hydrochar}}{HHV_{RDF}}$$ Equation 5.2

$$Energy\ yield\ (\%, db) = Mass\ yield\ \times Energy\ density$$ Equation 5.3

where $m_{hydrochar}$ (kg) and $HHV_{hydrochar}$ ($MJ.kg^{-1}$) are the mass and high heating value of hydrochar; m_{RDF} and HHV_{RDF} are the mass and high heating value of RDF.

Chlorine content of the RDF and hydrochars samples was determined through X-Ray fluorescence (Niton XL 3T Gold++). Dechlorination efficiency of RDF was estimated according to the following equation:

$$Dechlorination\ efficiency\ (\%) = \left(\frac{Cl_{RDF} - Cl_{hydrochar}}{Cl_{RDF}}\right) \times 100$$ Equation 5.4

where Cl_{RDF} and $Cl_{hydrochar}$ (wt.%, db) correspond to the chlorine content determined in the RDF and in the hydrochar, respectively.

Thermogravimetric analysis of the RDF and hydrochars was carried out using a thermogravimetric analyzer (TA Instruments, SDT 2960 Simultaneous DSC-TGA), from room temperature to 800 ºC with a heating rate of 10 °C/min, under air atmosphere, with an air flow of 100 mL/min.

Surface morphology was analyzed for RDF and hydrochar samples through scanning electron microscopy - energy dispersive X-ray spectroscopy (NanoSEM, FEI Nova 200 (FEG/SEM)). The acceleration voltage of 15 kV was used, sample distance was ~10 mm and the analyses were carried out with x800 and x2500 magnifications. EDS results are presented in an atomic weigh basis (at.%).

The chemical functional groups on the hydrochars surface were identified by FT-IR. Infrared spectra (4000-650 cm^{-1}) were obtained based on the attenuated total reflectance (ATR) method using a FT-IR Spectrometer (Nicolet iS10, Thermo Scientific) equipped with a diamond ATR attachment by using 128 scans at a resolution of 4 cm^{-1}.

5.2.4. Process water characterization

The liquid fractions obtained in each HTC experiment were characterized for their pH, conductivity, chemical oxygen demand (COD), biochemical oxygen demand (BOD_5), total solids (volatile and fixed solids), Kjeldahl nitrogen, total phosphorous, total phenolic compounds and total reducing sugars.

pH was determined with a pH meter (Crimson MicropH 2001 meter) and electrical conductivity was measured by electrometric method (MC226 Conductivity meter Mettler Toledo). Chlorine content in the process water was determined by titration according to the methodology described in EPA- SW-948 test method 9253. BOD_5 was performed according to the OxiTop® methodology. Total phenolics were measured by the Folin-Ciocalteau method, as described by Singleton *et al.* (1998). Total reducing sugars content was determined by the DNS method, as proposed by Miller (1959). Evaluation of total solids, Kjeldahl nitrogen, total phosphorous and COD was performed according to methods 2540B, 4500N_{org}-C, 4500P-E and 5220B, respectively, from the Standard Methods for Water and Wastewater.

Qualitative analysis of the organic fraction present in the process water was performed by solvent extraction and GC-MS. The process water samples were acidified until pH= 2 using concentrated H_2SO_4 (95 %, Panreac), to ensure protonation of carboxylic acids. Each sample (5 mL) was extracted three times (2 mL) with $CHCl_3$ (Fisher Scientific). The organic extracts were combined and dried with

anhydrous sodium sulphate, and derivatized with BSA (N,O-Bis(trimethylsilyl)acetamide, Sigma). Finally, the extracts were analyzed in a GC-MS system (Focus GC, Polaris Q - Thermo), equipped with a DB-5 capillary column (30 m length, 0.25 mm inner diameter, and 0.25 μm film thickness). The extracts were injected in split mode, at 250 °C and the oven temperature was programmed as follows: initial temperature of 35 °C, held for 4 min, increased to 150 °C at a rate of 4°C.min^{-1}, and increased to 280 ºC at 10°C.min^{-1} held for 5 min. The transfer line and ion source temperatures were 270 °C and 200 °C, respectively. The organic compounds present in the chloroform extracts were identified by comparison of their mass spectra with those from the NIST and WILEY databases.

5.2.5. Process water remediation

Preliminary process water remediation (total phenolic compounds and COD) was tested through precipitation (batch mode) and adsorption (batch and column modes). For the batch tests, precipitation was tested with biomass bottom ash, and adsorption was tested using powdered activated charcoal (PAC, Panreac), hydrochar sample H-300-120/15, and RDF char sample produced at 300 ºC for 30 minutes (Chapter 3). Briefly, a designated amount of precipitant or adsorbent was put into contact with a mixture of the process waters obtained in this chapter (in equal proportions), under magnetic stirring, for 20 minutes. The layout of the batch tests is described in Table 5.2:

Table 5.2: Experimental layout of the batch precipitation/adsorption tests for HTC water remediation.

Test	Material	Dose (g/L)	Contact time (min)	Temperature (ºC)
B1	Biomass bottom ash	40	20	25
B2	PAC	20		
B3	HTC-300-30	20		
B4	RDF char	20		
B5	PAC	10		
B6	PAC	4		
B7	PAC	2		

After the established contact time, the mixtures were filtered, properly diluted, and total phenolic compounds and COD were measured as described in Section 5.2.4. Removal efficiency, R (%), of the HTC process water mixture was determined according to equation 5.5:

$$R(\%) = \frac{(C_0 - C_f)}{C_0} \times 100 \qquad \text{Equation 5.5}$$

where C_0 and C_f are the initial and final concentrations of total phenolics or COD, respectively.

For the adsorption column tests, glass columns (1 cm diameter and 14 cm height), were packed with 250 and 500 mg of PAC (Tests C1 and C2, respectively). Before adsorption the column was conditioned with distilled water and the tests were conducted at room temperature. The mixture of HTC process water was pumped in down flow mode at a fixed flow rate using a peristaltic pump (2.5 mL/min). Samples (effluent) were collected at fixed volumes of 10 mL. Breakthrough curves were established by plotting C_t/C_o versus effluent volume (mL), where C_t is the effluent total phenolics concentration or COD value, C_o is influent total phenolics concentration or COD. Breakthrough time corresponded to the

time at which C_t/C_o equals 0.05 and exhaustion time corresponds to C_t/C_o equal to 0.95 (Kumar and Jena, 2016).

5.2.6. Process performance

Mass yield, energy density and energy yield of the hydrochars were calculated, as mentioned above using equations 5.1, 5.2, 5.3.

The energy input (Q_{input}) and the net energy generation (Q_{net}) of the HTC process were estimated according to the works of Mau and Gross (2018) and Yu *et al.* (2018). The energy input during the HTC process (Q_{input}), expressed in MJ, was calculated according to equation 5.6:

$$Q_{input} = \frac{m_w(H_{w,HT} - H_{w,RT}) + m_{RDF} \cdot C_p^{RDF} \cdot \Delta T}{m_{RDF}} \quad \text{Equation 5.6}$$

where m_w (kg) and m_{RDF} (kg) are the amounts of water and RDF fed to the reactor; $H_{w,HT}$ and $H_{w,RT}$ are the enthalpy of water at the final hydrothermal temperature and at room temperature, respectively; C_p^{RDF} is the specific heat capacity of RDF, calculated as described in Chapter 3, using the selective dissolution method to assess the amounts of the biogenic and non-biogenic fractions of RDF and assuming that the non-biogenic fraction is composed by equal amounts of polyethylene terephthalate and polypropylene (biomass, $C_p^{biomass}$ 1.70×10^{-3} $MJ.kg^{-1}.K^{-1}$; PET, C_p^{PET} = 1.05×10^{-3} $MJ.kg^{-1}.K^{-1}$; PP, C_p^{PP} = 1.95×10^{-3} $MJ.kg^{-1}.K^{-1}$) (Collazo *et al.*, 2012; Osswald and Hernández-Ortiz, 2006).

The energy output (Q_{output}), expressed in MJ, corresponds to the energy contained in the hydrochars and was calculated through equation 5.7:

$$Q_{output} = m_{hydrochar} \times HHV_{hydrochar} \quad \text{Equation 5.7}$$

where $m_{hydrochar}$ (kg) is the mass of hydrochar produced from HTC and $HHV_{hydrochar}$ is the hydrochar high heating value, expressed in $MJ.kg^{-1}$.

The net energy generation (Q_{net}), expressed in MJ, corresponds to the balance between energy supplied to the process and the energy recovered in the products and was calculated as follows:

$$Q_{net} = Q_{output} - Q_{input} \quad \text{Equation 5.8}$$

where Q_{input} and Q_{output} are the HTC process outputs and inputs as evaluated by equations 5.6 and 5.7.

The HTC process efficiency (PEE) was calculated by the equation 5.9, similarly to the calculations made in Chapter 3, as follows:

$$PEE\ (\%) = \frac{Q_{output}}{(m_{RDF} \times HHV_{RDF}) + Q_{input}} \times 100 \quad \text{Equation 5.9}$$

where HHV_{RDF} ($MJ.kg^{-1}$) is the high heating value of the RDF sample; m_{RDF} the RDF mass introduced in the reactor (1 kg for all energy calculations). Q_{input} and Q_{output} are the HTC process outputs and inputs as evaluated by equations 5.6 and 5.7.

5.3. Results and discussion

5.3.1. Proximate and elemental analysis of RDF and hydrochars

The HTC process had a clear effect on the visual aspect of the solid products regarding their homogeneity. The process converted RDF into a dark hydrochar composed of uniformly-shaped particles, as shown in Figure 5.2.

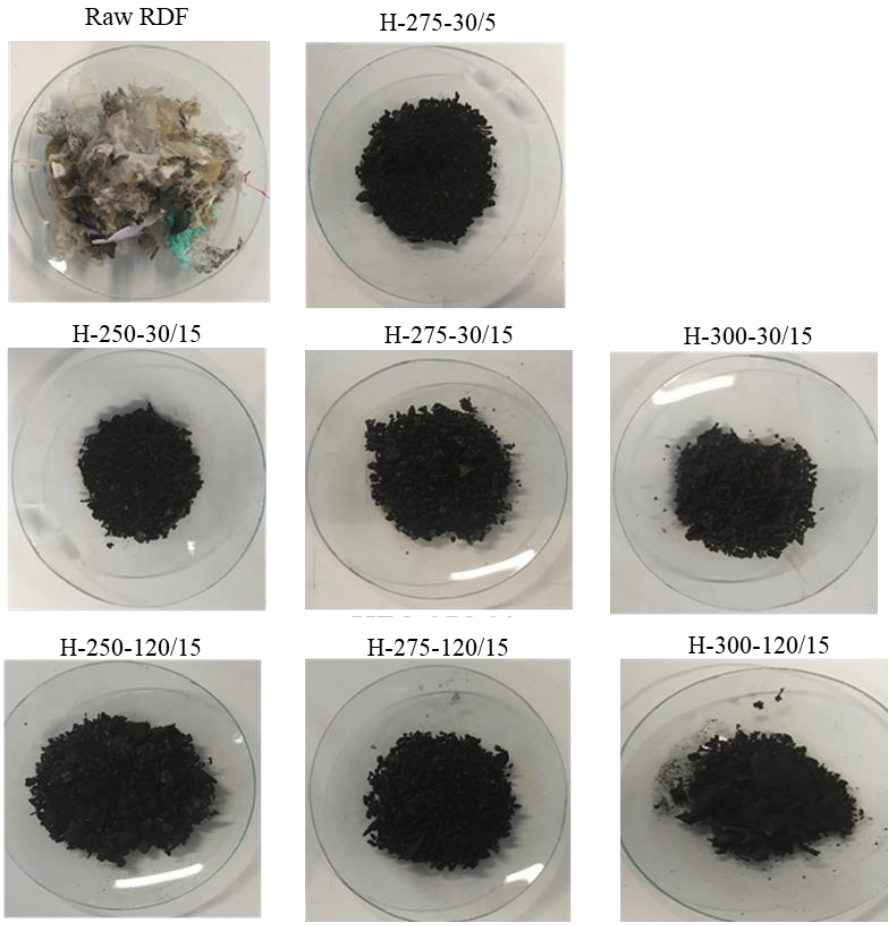

Figure 5.2: Raw RDF and produced hydrochars in different conditions.

The variation of process parameters (temperature, residence time and solid-to-water ratio) did not have a clear correlation with the color of the obtained hydrochars. The appearance of the hydrochars produced at different temperatures, residence times or solid-to-water ratio was relatively uniform, unlike what was observed for the RDF chars obtained by dry carbonization experiments (Chapters 3 and 4).

Furthermore, all the hydrochars were easily grinded by hand milling while the raw RDF could only be homogenized using mechanical mills.

The results obtained for proximate composition, ultimate composition, mineral composition and fuel properties of the raw RDF and of the produced hydrochars are summarized in Table 5.3.

Table 5.3: Chemical characteristics and fuel properties of RDF and RDF hydrochars.

Parameter	Sample							
	RDF	H-250-30/15	H-275-30/15	H-300-30/15	H-275-30/5	H-250-120/15	H-275-120/15	H-300-120/15
Proximate analysis (wt.%, db[a])								
Moisture[b]	6.0	0.5	0.6	0.6	0.5	0.7	0.7	0.7
Volatile matter	85.1	81.8	80.4	82.7	80.4	79.6	80.6	79.8
Ash	10.7	4.8	4.7	3.8	5.3	4.1	4.3	3.3
Fixed carbon	4.2	13.4	14.3	13.5	14.8	16.3	15.1	16.9
Ultimate analysis (wt.%, daf[c])								
C	53.7	61.9	62.6	64.5	64.1	64.8	66.7	62.9
H	8.7	7.9	7.2	8.0	7.3	7.7	7.7	8.0
N	1.5	1.8	1.7	1.9	2.1	2.4	1.7	2.1
S	0.0	0.0	0.0	0.0	0.0	0.0	0.0	0.0
O	36.1	28.4	28.5	25.6	26.5	25.0	23.8	27.1
Mineral composition (mg.kg^{-1}, db)								
Ca	63740.8	6556.3	5258.7	3209.0	8537.9	7334.9	5722.0	9906.6
K	4322.1	2477.3	2020.1	1725.4	1814.8	2232.1	2229.6	1717.6
Fe	16676.7	8875.8	4906.0	5398.2	13140.5	10930.6	7231.5	6673.7
Zn	1105.7	323.0	415.1	960.4	326.8	327.1	95.5	1239.6
Ni	0.0	316.0	440.0	676.4	472.4	354.0	845.7	882.6
Ti	1616.6	7237.2	9314.1	5514.5	4164.0	6525.6	6810.5	5168.1
Pb	171.8	89.8	153.6	187.2	2601.8	193.7	37.5	205.1
Cu	251.8	543.4	829.4	724.2	629.9	767.5	643.2	1006.3
Cr	304.4	521.0	679.9	592.5	2942.0	558.6	807.1	548.5
Si	14943.8	22990.7	21068.0	38617.9	28922.8	32257.7	22493.7	22530.9
Fuel properties								
HHV (MJ.kg^{-1})	21.2	26.1	25.2	27.7	26.3	27.4	28.1	27.2
Mass yield (%, db)	-	49.2	49.3	45.2	53.7	53.6	51.6	47.6
Energy density	-	1.2	1.2	1.3	1.2	1.3	1.3	1.3
Energy yield (%, db)	-	60.4	58.7	59.2	66.5	69.3	68.3	61.0
Cl (wt.%, db)	2.03	1.27	0.91	1.01	1.08	1.06	0.90	0.95
Dichlorination efficiency (%, db)	-	34.1	52.8	49.8	45.3	45.2	54.6	55.0

[a]db, dry basis; [b]Moisture was determined as received; [c]daf, dry ash free basis.

The raw RDF presented a moisture content of 6.0 wt.%, whereas the hydrochars presented values between 0.5 and 1.4 wt.% for the same parameter, after air drying for 12 h, oven-drying for 12 h and re-equilibration with atmospheric moisture. Thermal processing is expected reduce oxygen containing functional groups at which water is adsorbed (Stemann *et al.*, 2013). Also, according to Lu *et al.* (2011), hydrolysis reactions occurring during HTC are responsible for the rupture of water bound to the raw material, having as primary consequence an increase in the hydrophobicity of the hydrochars. This is an important feature regarding fuel storage because fermentation processes that may potentiate self-ignition and degradation due to microbial proliferation are minimized by reducing moisture and increasing the hydrophobic character of the hydrochars (Kambo and Dutta, 2015).

Proximate composition results show that the volatile matter content of the RDF sample (85.1 wt.%) was decreased to a range of 79.6 - 82.7 wt.% for the hydrochars. This reduction is mainly due to dehydration and decarboxylation reactions occurring during the process (Tag *et al.*, 2018), that in the case of

the produced hydrochars were more extensive for 120 min, since sample H-250-120/15 presented the lower volatile matter content (79.6 wt.%).

The hydrochars had ash contents from 3.3 to 5.3 wt.%, values that are 2.0 to 3.2 times lower than the ash content of RDF. That is a specific characteristic of hydrothermal carbonization, that results from a partial dissolution of the mineral components of the raw material in the process water (Broch *et al.*, 2014; Liu *et al.*, 2013; Mihajlović *et al.*, 2018). Increasing temperature and residence time had the effect of reducing the ash contents of the hydrochar samples. Hydrochars obtained at 300 ºC and 30 or 120 min, had ash contents of 3.8 wt.% and 3.3 wt.% respectively, while hydrochars produced at 30 min and 250 ºC or 300 ºC, had ash contents of 4.8 wt.% and 3.8 wt.%, respectively. This behavior can be attributed to the dissolution of ash components in subcritical water, that is favored by the increase in process temperature or residence time, and has also been reported by other authors using similar temperature ranges (200-300 ºC). For example, maximum ash content reductions of 20.4 % were observed by Pala *et al.*, (2014) for grape pomace hydrochars, and of 33.0 % by Mihajlović *et al.* (2018) for hydrochars produced from *Miscanthus x giganteus* biomass. Smith *et al.* (2016) performed HTC of various biomass samples (willow, *Miscanthus x giganteus*, oak, greenhouse waste, food waste, secondary sewage sludge, anaerobic digestion press cake, macroalgae and microalgae), at 200 - 250 ºC, using a solid-to-water ratio of 1:10, and also observed a decrease in the ash content of hydrochars relatively to the starting materials. Nevertheless, although ash content reduction is a consistent feature of the HTC process, the concentration of individual ash components is not always reduced in the hydrochars, since ash components have distinct solubilities in the process water. Therefore, the feedstock specific ash chemistry may lead to the concentration of individual ash components in the hydrochar, regardless of an overall of ash decrease effect being also observed (Smith *et al.*, 2016).

The ash contents of the hydrochars were also influenced by the solid-to-water ratio, presenting values of 5.3 wt.% and 4.7 wt.% for the hydrochars produced at 275 ºC and 30 min, using solid-to-water ratios of 1:5 and 1:15, respectively. The influence of this parameter is relatively straightforward, since the extension of ash dissolution is expected to increase as the volume of water available for that process also increases.

The produced hydrochars presented increased fixed carbon contents, particularly the hydrochars produced at the longer residence times. For example, the fixed carbon contents of the hydrochars produced at 300 ºC and 30 min or 120 min were 3.2 to 4.0 times higher than the fixed carbon content of the raw RDF sample. Fixed carbon is determined by difference from all the other proximate analysis parameters, therefore, the obtained values are directly related with the decrease in volatile matter and in ash content, as well as aromatization and repolymerization reactions occurring during the process (Lin *et al.*, 2017).

Regarding the ultimate composition of the raw RDF and the corresponding hydrochars, the increase in carbon content was an evident consequence of the HTC process. Carbon content of the hydrochars was found to be between 15.3 - 24.2 % higher than that of the RDF, reaching the highest carbon increment for the sample H-275-120/15. The increase of carbon concentration may be directly related with the elimination of other elements, such as oxygen or hydrogen, by devolatilization or dissolution in subcritical water and was generally favored by the increase of temperature or residence time (Liu *et al.*, 2013). Nevertheless, increasing residence time from 30 min to 120 min, at 300 ºC caused a decrease of carbon content from 64.5 to 62.9 wt.%. Also, increasing temperature from 250 ºC to 300 ºC, for a residence time of 120 min, caused a decrease in carbon content from 64.8 to 62.9 wt.%. Thus, at higher temperatures and residence times, carbon loss by devolatilization or dissolution may start to overcome the elimination of oxygen and hydrogen that occurred at milder conditions, contributing to the observed decrease of carbon concentration in the hydrochars.

Hydrogen and oxygen contents showed lower values for the hydrochars than for the RDF, indicating that aromatization of the carbon structure and deoxygenation are processes taking place during HTC (Kambo and Dutta, 2015; Lin *et al.*, 2017; Nizamuddin *et al.*, 2017).

Nitrogen concentration increased with the HTC process, indicating that this element was retained in the structure of the hydrochars. At both residence times (30 and 120 min) the nitrogen concentration in the hydrochars increased when temperature was raised from 250 ºC to 275 ºC and decreased when temperature was raised from 275 ºC to 300 ºC. This non-regular variation of nitrogen concentration in the hydrochars produced at different operational conditions indicates that this element is not efficiently removed from the raw RDF by the HTC process and variations of its concentration in the hydrochars may be related to the dilution or concentration effects that result from the mobility of other elements. Changing the solid-to-water ratio from 1:15 to 1:5 increased nitrogen concentration in the hydrochars from 1.7 to 2.1 wt.%, an indication that reducing the volume of subcritical water available for dissolution of nitrogenous organic compounds, further increased their retention in the hydrochar structure. According to Wang *et al.* (2018) higher nitrogen concentrations in hydrochars from food waste can be attributed to polymerization reactions occurring at high temperatures and also to absorption of nitrogen containing substances present in the reactive medium.

Sulphur was not detected in the raw RDF or any of the RDF hydrochars.

The relative variations in hydrogen, oxygen and carbon contents of the produced hydrochars can be further assessed by analyzing changes in the corresponding O/C and H/C atomic ratios. These ratios can be related to the coalification degree of RDF after HTC, as well as with the reaction pathways involved in the process (Zhuang *et al.*, 2018), and are represented in the van Krevelen diagram (Figure 5.3).

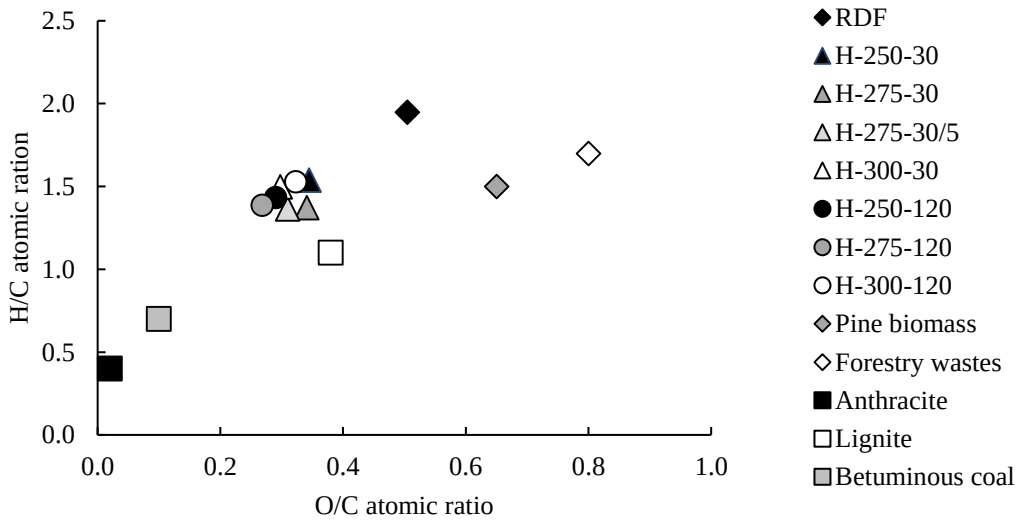

Figure 5.3: van Krevelen diagram comparing the produced hydrochars, RDF, biomass wastes and fossil fuels (van der Stelt *et al.*, 2011).

The RDF sample had an O/C ratio lower than pine biomass or forestry wastes and an H/C ratio higher than those biomass wastes, reflecting the presence of polymeric materials with high carbon and hydrogen contents such as polyethylene or polypropylene. The O/C ratios of the produced hydrochars were slightly lower than that of lignite while their H/C ratios were comparable to that of pine biomass. Thus, HTC promotes a clear deoxygenation effect while retaining a fraction of the C-H bonds. This effect is mostly related with dehydration and decarboxylation reactions that enhance the coalification degree through the removal of oxygen and hydrogen atoms (Table 5.3), releasing water and carbon dioxide

(Kim *et al.*, 2017; Zhuang *et al.*, 2018). The lowest atomic ratios were observed for sample H-275-120/15, as expected from the proximate and ultimate analysis results. The hydrochars position in the van Krevelen diagram was close to the coal region that begins at O/C of 0.23 and H/C of 0.9 (Minaret and Dutta, 2016).

Mineral composition of the raw RDF and of the produced hydrochars is presented in Table 5.3. Sodium is not detectable by the XRF equipment used and magnesium and cadmium were below the detection limit for all the samples tested, hence these elements were not included in this analysis. The main inorganic components of RDF and of the RDF hydrochars were calcium, iron, and silica. Dissolution in process water was not equivalent for the different mineral components and therefore their concentration increased or decreased in the hydrochars accordingly to their water solubility and to the homogeneity of their distribution in the RDF sample. The concentrations of calcium, potassium and iron were significantly reduced in the hydrochars which is coherent with the relatively high solubility of these elements' salts or oxides in water. On the other hand, the concentrations of elements such as copper, nickel, titanium, chromium and silicon increased in the hydrochars as a result of their poor water solubility and of the elimination of water-soluble components. For some mineral components like zinc or lead a random behavior was observed, suggesting that they may be heterogeneously distributed in the RDF sample and not always available for dissolution in process water. Table 5.4 summarizes the variation of the mineral composition of the hydrochars expressed as element removal efficiency (ERE %). Positive values express effective removal of the element from the RDF and therefore decrease of its concentration in the hydrochars while negative values express element retention in the hydrochar structure.

Table 5.4: Element removal efficiency of the HTC process regarding the different mineral components, evaluated as ERE (%) = $(C_{RDF}-C_{hydrochar})/C_{RDF}).100$, where C_{RDF} is the element concentration in the RDF and $C_{hydrochar}$ represents element concentration in the hydrochars.

Metal	Element removal efficiency (%)						
	H-250-30/15	H-275-30/15	H-300-30/15	H-275-30/5	H-250-120/15	H-275-120/15	H-300-120/15
Ca	89.7	91.7	95.0	86.6	88.5	91.0	84.5
K	42.7	53.3	60.1	58.0	48.4	48.4	60.3
Fe	46.8	70.6	67.6	21.2	34.5	56.6	60.0
Zn	70.8	62.5	13.1	70.4	70.4	91.4	-12.1
Ti	-347.7	-476.2	-241.1	-157.6	-303.7	-321.3	-219.7
Pb	47.7	10.6	-9.0	-1414.3	-12.7	78.2	-19.4
Cu	-115.8	-229.3	-187.6	-150.1	-204.8	-2454.0	-299.6
Cr	-71.1	-123.3	-94.7	-866.5	-83.5	-165.2	-80.2
Si	-53.8	-41.0	-158.4	-93.5	-115.9	-50.5	-50.8

Calcium was the less retained mineral component with reductions up to 95.0 % for the hydrochar H-300-30/15 and exhibiting a positive correlation between temperature and element removal efficiency, for the tests performed at 30 minutes (ρ=0.992, see Appendix, Figure A.9). Potassium concentration was also reduced as temperature increased, (ρ=0.992, see Appendix, Figure A.9), achieving its lower value for the sample H-300-120/15. Decrease of iron concentration was highest for the sample H-275-30/15 and was also positively correlated with temperature (ρ=0.804, see Appendix, Figure A.9). According to Reza *et al.* (2013) inorganics like calcium, magnesium and potassium are easily removed, in a range of 50-90 % only by hot water leaching, as such HTC is usually very effective in removing these inorganic species. Wüst *et al.* (2019) also stated that alkali salts dissolve faster in the reaction medium water resulting in the modification of the organic structure during HTC.

Slagging and fouling phenomena are mostly related with alkali metal reactions (with silica forming alkali silicates or with sulphur to form alkali sulphates). Although silica content is increased, the reduction in potassium (as well as chlorine reduction) can contribute to a reduction in the hydrochar's tendency to exhibit these ash related phenomena (Smith *et al.*, 2016).

Silicon content dominates the mineral fraction of the hydrochars, and its concentration increases significantly for hydrochar sample H-300-30/15, and its removal efficiency is positively correlated with temperature (ρ=0.812, see Appendix, Figure A.10).

Titanium, lead, copper and chromium had negative removal efficiencies, that is, they were concentrated in the hydrochars. This is an undesirable outcome of HTC, since some of these heavy metals will be concentrated in the hydrochar ash after combustion or gasification thus increasing the hazardous character of those ashes (Reza *et al.*, 2013). The observed concentration of heavy metals was not observed for hydrochars obtained from various biomass materials, like corn stover, *Miscanthus x giganteus*, switch grass and rice hull (Reza *et al.*, 2013). These different behaviors may be related to the different concentrations of those elements in the raw materials and also to their chemical state within those matrices, that may strongly influence their mobility to the water phase.

The values obtained for high heating value, energy density, dechlorination efficiency, mass and energy yields, regarding the hydrochars produced in the HTC tests are presented in Table 5.3.

The higher heating values (HHV) of the hydrochars were always higher than that of the raw RDF, therefore confirming the positive effect of HTC in this fuel quality parameter. Residence time seemed to have a significant role in the increase of HHV since the hydrochars produced at 250ºC and 275 ºC, during 120 min presented higher values for this parameter than those produced at the same temperatures, during 30 min. Except for sample H-275-30/15, all the hydrochars presented HHV higher than lignite (25.7 $MJ.kg^{-1}$) (Liu *et al.*, 2013).

The mass yield of the hydrochars decreased with increasing temperature except for the tests performed at 250 ºC and 275 ºC during 30 min, that had comparable mass yields. This behavior may be attributed to a higher extent of devolatilization and water dissolution of the RDF components, since both processes are favored when temperature is increased (Nakason *et al.*, 2018). The mass yield of the hydrochars had a positive correlation with the residence time, indicating that condensation or adsorption phenomena that contribute to an increase of hydrochar mass may occur more extensively as residence time increases. Higher values for hydrochar mass yield with increasing residence time have been reported by other authors using food waste (Zhao *et al.*, 2018) and pine biomass (Wu *et al.*, 2017). As the feedstock decomposes during HTC, it also partially dissolves in the aqueous medium but for longer residence times the dissolved compounds are more likely to undergo polymerization and cross-linking reactions leading to their deposition on the surface of the hydrochar and therefore enhancing its mass yield (Lin *et al.*, 2017; Zhao *et al.*, 2018).

Energy density is the ratio between the heating value of the solid product (hydrochar) and of the raw material (RDF), and therefore, it expresses the upgrading effect of the process in a fuel property, regardless of the corresponding mass yield. For the HTC experiments included in this work, energy density was 1.2 for the experiments performed at 250 ºC and 275 ºC using a residence time of 30 min, and 1.3 for the remaining conditions. Thus, the HTC process enabled the conversion of the RDF to hydrochars with a calorific value 20 – 30 % higher, reflecting the modifications of composition and density of the raw material.

The energy yield combines energy density data with the corresponding mass yield, therefore it measures how much energy of the original raw material is retained in the hydrochar (Nakason *et al.*, 2017). The energy yields of the produced hydrochars followed the same tendency as the mass yields, because the energy density was a fairly constant parameter for the different tested conditions. HTC

conducted at 250 ºC and 275 ºC for 120 minutes, presented the highest energy yield values with 69.3 % and 68.3 %, respectively. This observation is coherent with the influence of operating temperature and residence time in the mass yield. As mentioned above, increasing temperature leads to a higher decomposition and dissolution rate, while longer residence time allows condensation reactions like polymerization of the degraded components of the feedstock and their precipitation onto the hydrochar's surface (Funke and Ziegler, 2010). According to Kambo and Dutta (2015), energy yield also increases because these degraded intermediates from biomass decomposition, have very significant HHV, and as they precipitate they are not only responsible for mass yield increase but also energy yield.

The solid-to-water ratio of 1:5 had a positive impact regarding mass and energy yield. Sample H-275-30/5 had increments of 4 % and 7.8 % on mass and energy yields, respectively, when compared to sample H-275-30/15. This observation is in accordance with the increments of ash content, fixed carbon content and carbon concentration of the hydrochar, found when the solid-to-water ratio was reduced from 1:15 to 1:5.

HTC also reduced the chlorine concentration of the RDF presenting dechlorination efficiencies from 34.1 % (H-250-30/15) to 55 % (H-300-120/15). Different authors also report significant chlorine decrease in hydrochars obtained by HTC of: mixtures of medical wastes and lignocellulosic biomass (Shen *et al.*, 2017), PVC (Poerschmann *et al.*, 2015) or MSW (Prawisudha *et al.*, 2012) and mixtures of bamboo and PVC (Yao and Ma, 2018). This result could reinforce that organic chlorine (present in RDF through PVC residues) could be effectively converted to inorganic chlorine by HTC (Matsakas *et al.*, 2017; Shen *et al.*, 2017) and that higher temperatures, such as 300 ºC, favor higher dechlorination degrees (Poerschmann *et al.*, 2015).

5.3.2. Thermogravimetric analysis

The thermal degradation profile of the RDF and of the produced chars in an oxygen-rich atmosphere was evaluated by their thermogravimetric profiles in air atmosphere, that are represented in Figure 5.4. These results display the TGA and DTG curves of the raw RDF and of the samples H-250-30/15, H-300-30/15 and H-300-120/15, in order the discuss the influence of temperature and residence time on the thermal decomposition behavior of the produced hydrochars, under combustion conditions.

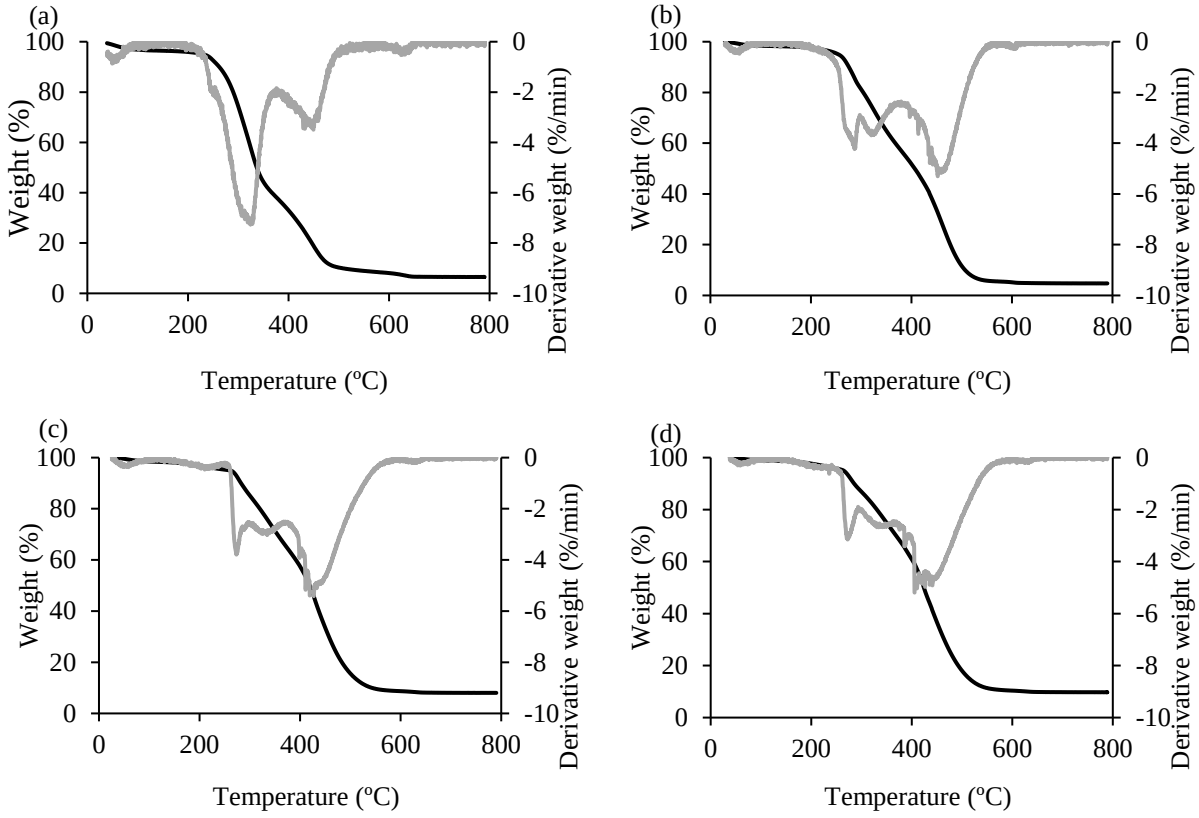

Figure 5.4: TGA and DTG profiles of: (a) RDF; (b) H-250-30/15; (c) H-300-30/15 and (d) H-300-120/15.

The first decomposition step is normally attributed to the loss of moisture and small volatiles and it represented around 4.4 %, 2.9 %, 2.9 % and 2.5 % of mass loss for RDF, H-250-30/15, H-300-30/15 and H-300-120/15, respectively. The DTG peaks in the temperature range between 55-60 ºC of the hydrochars are smaller in comparison with the RDF, and decrease with increasing temperature and residence time, is in accordance with the reduced moisture and volatile matter contents of the hydrochars.

The second thermal decomposition stage that occurs between 220 to 390 ºC corresponded to a higher mass loss for all samples, but in particular for the RDF that reached a value of 49.8 %, with a maximum weight loss rate at 328 ºC. Hydrochars lost significantly less mass during this stage with sample H-250-30/15 losing 43.4 %, H-300-30/15 losing 33.7 % and H-300-120/15 29.5 %. This indicates that a fraction of the lignocellulosic materials present in the raw RDF were converted to more thermally stable carbonaceous structures that were less degraded in this temperature range. Biomass structural components, cellulose (250-350 ºC), hemicellulose (200-300 ºC) and lignin (200-500 ºC) decompose at the indicated temperature ranges, and their conversion to CO_2, H_2O, CO and CH_4 is largely assumed to justify most of the mass loss observed during combustion of lignocellulosic materials (Carrier *et al.*, 2011; Mihajlović *et al.*, 2018). Increasing the temperature and residence time of HTC reduced the mass loss suffered by the corresponding hydrochars at temperatures from 220 to 390 ºC. This result highlights the effect of higher temperatures and residence times in the degree of molecular rearrangement and decomposition caused by the HTC process (Akdag *et al.*, 2016).

The RDF sample presents two more mass loss curves, one from 350 ºC to 510 ºC corresponding to 35.7 % loss, and the other one from 510 ºC to 690 ºC losing 3.3 % of its mass. The mass loss observed in the temperature range of 510 to 690 ºC is consistent with the thermal decomposition of some polymers, for instance, polyethylene that decomposes above 400 ºC (Lokahita *et al.*, 2017). The mass loss

observed at 640 ºC could be attributed to char combustion or reactions between chars and volatiles, or metals such as aluminum (Lokahita *et al.*, 2017).

The hydrochars had the major fraction of their mass loss at temperatures from 390 ºC to 690 ºC, with a maximum weight loss rate varying from 427 ºC to 461 ºC. The differences of thermal decomposition behavior between the RDF and the RDF hydrochars, for temperatures higher than 390 ºC, suggests that the polymeric fraction of RDF was also affected by the HTC treatment. Sample H-300-120/120 presented the highest mass loss with 56.2 % indicating the more extensive decomposition of RDF took place during HTC at these conditions.

5.3.3. Structural properties of RDF and hydrochars

Microscopic observations of the RDF and the produced hydrochars reveal some morphological alterations brought by the HTC process. Figure 5.5. depicts the SEM images of RDF and of samples H-250-30/15, H-300-30/15 and H-300-120/15 obtained at different temperatures and residence times.

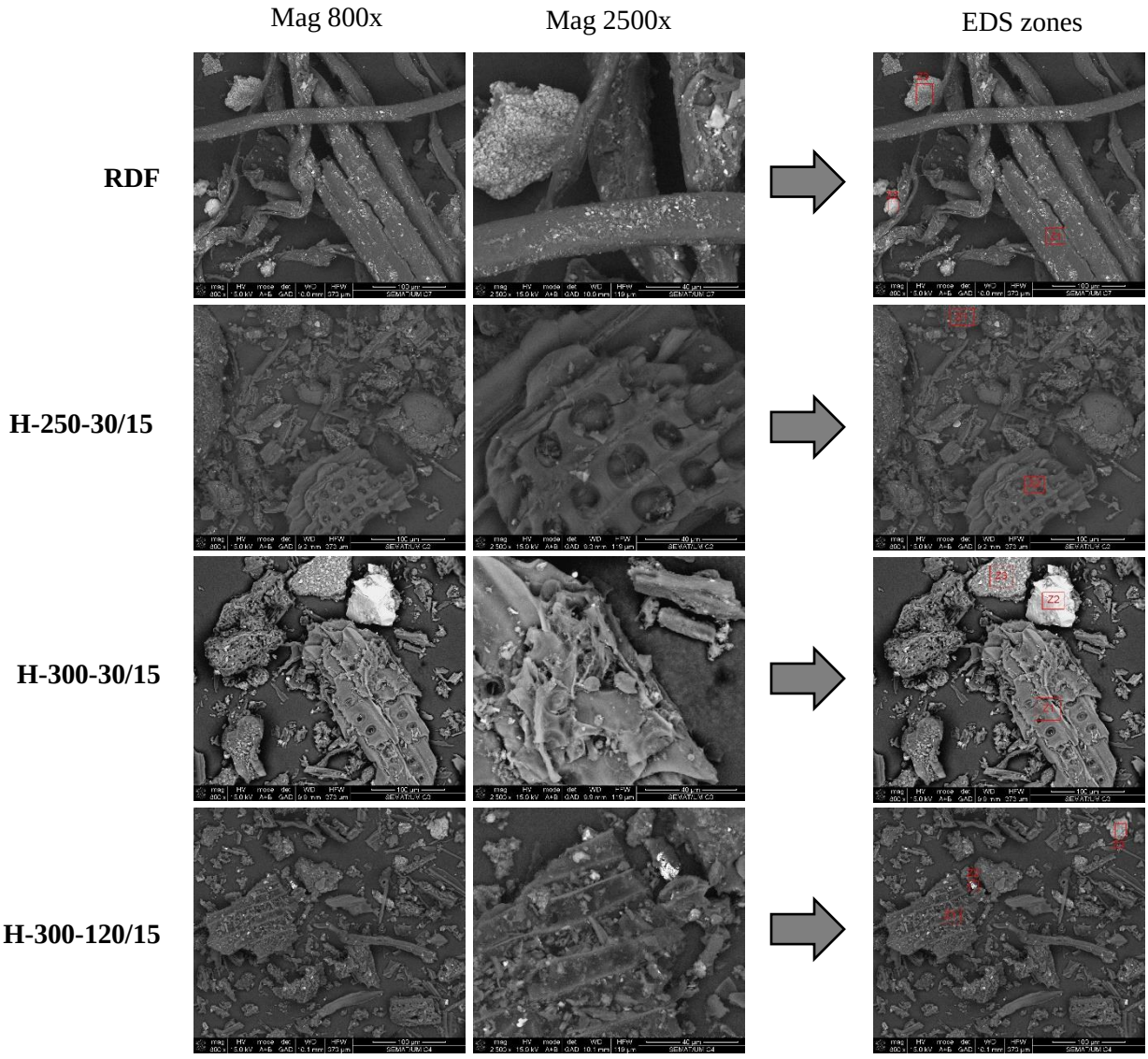

Figure 5.5: SEM images for: (a) RDF, (b) H-250-30/15; (c) H-300-30/15 and (d) H-300-120/15.

The surface morphology of RDF was quite fibrous and smooth, denoting some rigidity. After HTC, substantial changes on the surface morphology could be perceived, in spite of the large heterogeneity inherent to these samples. One of the more evident changes is related to the degradation of the fibrous structure into fragments with groves and holes that could be detected in the three hydrochar samples. Hydrochars presented a more disordered structure, particularly sample H-300-30/15 showing visible cracks that may be related to the release of volatile matter during the thermal process (Ma *et al.*, 2016; Saqib *et al.*, 2018).

Elemental composition of three distinct zones (Z1, Z2 and Z3) for the RDF and hydrochar samples is present in Table 5.5. These zones were selected based on obvious differences assessed through Figure 5.5.

Table 5.5: Localized elemental composition (Z1, Z2 and Z3) in the raw RDF and in three hydrochar samples, obtained through EDS.

Element (at. %)	Sample											
	RDF			H-250-30/15			H-300-30/15			H-300-120/15		
	Z1	Z2	Z3	Z1	Z2	Z3	Z1	Z2	Z3	Z1	Z2	Z3
C Kα	-	-	-	80.65	82.05	-	85.15	34.56	74.64	-	64.72	63.30
O Kα	87.93	28.94	32.36	17.96	17.94	-	14.85	44.64	16.71	86.86	3.54	26.56
Al Kα	1.72	0.90	1.00	0.47	-	-	-	-	3.99	6.76	0.52	3.96
Si Kα	3.22	54.93	2.46	0.93	-	-	-	20.80	4.49	6.39	0.66	4.76
Cl Kα	1.90	-	-	-	-	-	-	-	-	-	-	-
K Kα	1.88	-	-	-	-	-	-	-	-	-	-	0.25
Na Kα	-	-	-	-	-	-	-	-	-	-	-	0.07
Ca Kα	3.34	2.16	63.82	-	-	-	-	-	0.17	-	-	0.20
Mg Kα	-	7.38	-	-	-	-	-	-	-	-	-	0.40
Fe Kα	-	5.68	-	-	-	-	-	-	-	-	30.57	0.52
P Kα	-	-	0.36	-	-	-	-	-	-	-	-	-
Sum	100	100	100	100	100	100	100	100	100	100	100	100

The EDS results highlight the high degree of heterogeneity of these samples, reflected in the presence of different elements with variable concentrations in the selected zones for each sample. Carbon was not detected in any of the selected zones for the RDF sample while the three hydrochars all had significant carbon contents in at least two of the selected areas, reinforcing the already established carbon increase (discussed in Section 5.3.1.). Furthermore, chlorine was only detected for the RDF sample, additionally demonstrating the dechlorination efficiency of the HTC process. Aluminum and silicon were found in the four samples, whereas potassium, sodium, magnesium and iron were detected for the RDF sample and in Z3 for sample H-300-120/15. Sodium and magnesium were below the detection limit using the XRF technique but were detected through EDS, albeit in very low concentrations, and not for all the samples. As already discussed in Section 5.3.1 alkali (Na and K) and alkali-earth metals (Ca and Mg) are easily dissolved in the aqueous phase, and their reduced presence in the hydrochar samples compared with the RDF can indicate reduced potential for ash-related issues in energy applications. This is a clear advantage of HTC over conventional torrefaction or carbonization, which present a concentration effect yielding higher ash contents.

The FT-IR analysis enables further understanding of the structural composition of the raw RDF and the produced hydrochars, and underlines differences in functional groups between the raw RDF and the hydrochars obtained at different temperatures and residence times (Table 5.6).

Table 5.6: FT-IR peak frequencies (cm^{-1}) and corresponding assignments for RDF and hydrochars samples.

Sample								Assignment
RDF	H-250-30/15	H-275-30/15	H-275-30/5	H-300-30/15	H-250-120/15	H-275-120/15	H-300-120/15	
3296	3295	3295	3295	3296	3295	3295	3296	O-H stretching in hydroxyl and carboxyl groups (Yao and Ma, 2018).
2914	2914	2915	2915	2915	2915	2915	2914	C-H stretching in aliphatic methyl, methylene and methine groups (Shen *et al.*, 2017).
2846	2848	2848	2846	-	2847	-	-	
-	1692	1692	1691	1691	1692	1691	1691	C=O stretching in quinone, conjugated ketone, amide or carboxylic acid (Coates, 2000; Wu *et al.*, 2017).
-	1591	1596	1587	1587	1587	1587	1585	C=C stretching in aromatic rings (Catalkopru *et al.*, 2017).
1443	-	-	-	1443	-	1443	1440	C-H bending in methyl group (Coates, 2000).
1264	1254	1251	1263	1263	1257	1264	1264	Aryl-O stretching in aromatic ethers (Stemann *et al.*, 2013).
1206	1201	1206	1202	1202	1206	1206	1206	C-O stretching in phenolic hydroxyl group (Coates, 2000; Yan *et al.*, 2017)
-	1107	1107	1099	1101	1109	1098	1095	C-O stretching in ethers (alkyl substituted or large cyclic ethers) or C-N stretching in primary amines (Coates, 2000).
-	1031	1030	1030	1030	1031	1031	1029	
-	-	781	782	781	-	782	782	C-H out-of-plane bending in aromatic rings (875-650 cm^{-1}) (Saqib *et al.*, 2018; Wu *et al.*, 2017)
663	669	668	668	651	668	669	668	C-Cl stretching in aliphatic chloro compounds (800-600 cm^{-1}) (Shen *et al.*, 2017)

The peaks at 3295 and 3296 cm^{-1}, which are attributable to O-H stretching vibration in hydroxyl or carboxyl groups, although present in all the samples, became weaker as HTC temperature and residence time increased due to dehydration and decarboxylation reactions. This observation is in accordance with the results depicted in the van Krevelen diagram (Figure 5.3) and it can also mean a higher degree of hydrophobicity from the hydrochars, which is a very important feature regarding storage of solid fuels (Liu *et al.*, 2013). According to Stemann *et al.* (2013), process water is chemically bound to the HTC char especially by OH- groups, as such a decrease of this particular functional group can represent better dewaterability, which is important in the application of hydrochar in combustion applications.

C-H stretching of methyl, methylene and methine groups, are reflected in peaks at 2914-2915 cm^{-1} and 2846-2848 cm^{-1}. These groups are present in hemicellulose, cellulose and lignin, and peak intensity decreases for all hydrochar samples, particularly samples H-300-30, H-275-120 and H-300-120, that represent the more severe HTC conditions. This could be related with the more extensive oxidation of the biomass components occurring at these conditions. Peaks presented at 1691-1692 cm^{-1} and 1585-1591 cm^{-1} were not detected in the RDF spectrum. These peaks correspond to C=O and C=C stretching in aromatic rings, and became more intense with increasing temperature and residence time, reflecting an increase in the occurrence of carbonyl derivatives and in the aromaticity of the carbonaceous structure. The hydrochar produced at a higher solid-to-water ratio (1:5) also presented increased peak intensity at these wavenumbers. These results indicate condensation and polymerization reactions may occur

more extensively for longer reaction times or a smaller water volume, a trend also reflected in the higher mass yield obtained for samples H-275-30/5, H-250/120 and H-275/120. Peaks at 781-782 cm^{-1}, that were not detected in the raw RDF indicate that the HTC process involves some degree of aromatization of the carbonaceous structure, since these peaks are assigned to C-H bending in aromatic rings. The presence of these peaks only in the hydrochars produced at 275 ºC and 300 ºC, confirm that higher temperatures favor these aromatization reactions (Saqib *et al.*, 2018).

Peaks corresponding to Aryl-O stretching in aromatic ethers (1248-1264 cm^{-1}) and C-O stretching in the hydroxyl group of phenolic compounds (1202-1206 cm^{-1}), increased with process temperature, being more pronounced in samples H-275-30, H-300-30, and showed a slight decrease for the longer residence time. These peaks correspond to lignin interactions, and as lignin has a more difficult degradation profile, the reduction in intensity is in accordance with the HTC conditions used (Liu *et al.*, 2013).

The decrease in chlorine content can also be related to the FT-IR data, since the peaks at 651-669 cm^{-1} are significantly smaller for the hydrochars when compared to the original RDF sample.

5.3.4. Process performance

Evaluation of energy balance of the HTC process was done by estimation of the energy necessary for the process to occur (Q_{input}) and the energy that is obtained from the process products (Q_{output}). The difference between these two terms is the net energy generation (Q_{net}) that should be zero for an autothermal process (Mau and Gross, 2018; Yu *et al.*, 2018). The energy contained in the raw materials is not considered in this balance because the purpose is to evaluate if the energy recovered in the products is enough to ensure the process energy needs or if further energy inputs are necessary.

In order to estimate the specific heat capacity of the RDF sample (C_p^{RDF}), its composition as determined through the selective dissolution method was taken into account. The RDF sample contained 65.9 % biogenic components (lignocellulosic materials) and 24.2 % non-biogenic components (polymers). The non-biogenic component was considered to be composed of equal amounts of polyethylene terephthalate and polypropylene. The C_p^{RDF} was evaluated as the weighted average of the specific heat capacities of a lignocellulosic material, polyethylene terephthalate and polypropylene, as described in Section 5.2.6.

The heat requirements of the HTC process (Q_{input}), took into account the energy necessary to heat the RDF and the water present in the reactor from room temperature to the operating temperature but did not include a term for water vaporization because unlike what happens during dry carbonization (Chapters 3 and 4), during HTC phase change is avoided due to the autogenous pressure that keeps water in a condensed state (Mau and Gross, 2018). Recirculation of the residual gas phase through the feed may provide the heat needed for drying raw materials or contributed in the drying stage of the hydrochars (Tran, 2018). Furthermore, mechanical dewatering of the hydrochars can be facilitated by the higher hydrophobicity of these products, and it has potential to require lower operating temperatures in the mechanical process (Lin *et al.*, 2017; Stemann and Ziegler, 2011). Evaporation of water from the liquid phase was also not accounted for, since this liquid product may be used as produced, for recirculation in the HTC process, for anaerobic digestion or for irrigation purposes (Kambo *et al.*, 2017; Stemann *et al.*, 2013) .

Furthermore, Q_{output} considers only the energy content of the hydrochar, since the residual heat of the hydrochar products and the energy contained in some residual gas products were assumed to be used for drying raw materials and hydrochar products.

The process energy efficiency takes into account the Q_{input}, Q_{output} and the energy content of the raw RDF, according to equation 5.9 of Section 5.2.6. Results for the energy calculations are presented in Table 5.7.

Table 5.7: Energy balance for HTC of RDF.

Process conditions				Energy calculations				
T (ºC)	Solid-to-water ratio	t (min)	Hydrochar yield (%)	C_p^{RDF} (MJ.kg^{-1}.K^{-1})	Q_{input} (MJ)	Q_{output} (MJ)	Q_{net} (MJ)	PEE (%)
250	1:15	30	49.2		14.45	12.81	-1.64	35.9
275	1:15	30	49.3		16.06	12.43	-3.62	33.4
275	1:5	30	53.7		**5.60**	**14.10**	**8.50**	**52.6**
300	1:15	30	45.2	1.5×10^{-3}	17.67	12.55	-5.11	32.3
250	1:15	120	53.6		**14.45**	**14.70**	**0.24**	**41.2**
275	1:15	120	51.6		16.06	14.48	-1.58	38.9
300	1:15	120	47.6		17.67	12.93	-4.73	33.3

As expected, the energy necessary for heating the process water gives a major contribution to the input energy and is the key energy requirement that is specific to HTC. Increasing the temperature and decreasing the solid-to-water ratio caused significant increases of Q_{input}. For example, the decrease of the solid-to-water ratio from 1:5 to 1:15 caused a 2.9-fold increase of Q_{input}. Increasing the temperature also had a negative effect in Q_{output}, because the associated decrease of the hydrochar mass yield outweighs the increase in the hydrochar calorific value. Thus, in most of the tested conditions Q_{net} was negative, indicating that, in those conditions the HTC process is not autothermal. The only conditions at which the HTC process was exothermic were for the assay performed at 250 ºC, 120 min and a solid-to-water ratio of 1:15 (Q_{net} = 0.24 MJ) and for the assay performed at 275 ºC, 30 min and a solid-to-water ratio of 1:5 (Q_{net} = 8.50 MJ). Missaoui *et al.* (2017) tested the HTC of olive pomace, and also verified that for a biomass-to-water ratio of 1:6, Q_{net} net values were negative (-2.4 MJ.kg^{-1}) whereas for a ratio of 1:5 that parameter was positive (2.2 MJ.kg^{-1}).

When compared with conventional torrefaction and carbonization, HTC showed lower hydrochar yields and higher Q_{input}, which reflected on lower process efficiencies. The highest PEE value was also obtained for the test with 1:5 solid-to-water ratio (52.6 %).

The relation between the energy recovered in the hydrochars (Q_{output}, MJ) and the HTC process energetic efficiency (PEE, %), is represented in Figure 5.6, for all the tested conditions.

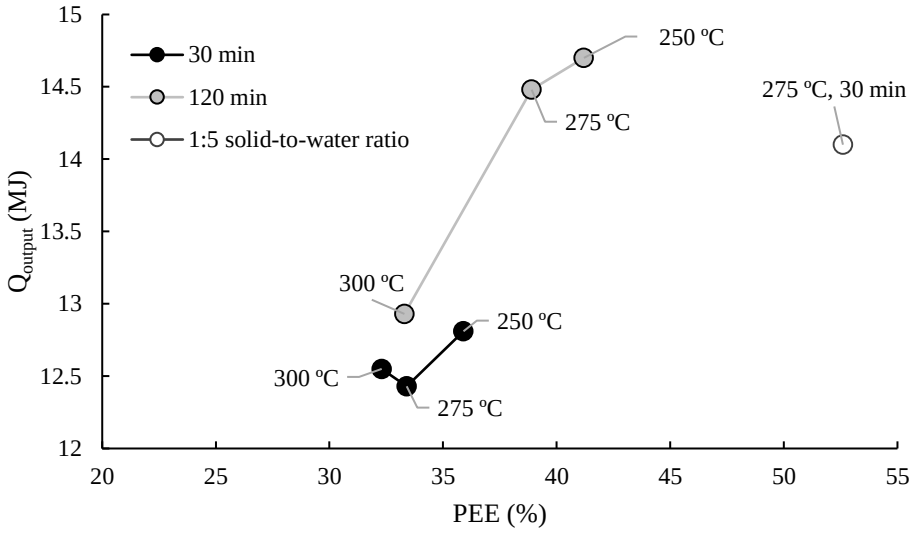

Figure 5.6: Representation of the energy recovered in the hydrochars (Q_{output}, MJ) as a function of the HTC process energy efficiency (PEE, %).

As it can be seen in Figure 5.6, increasing temperature had a negative impact both in Q_{output} and PEE, by the combined effects of reducing the hydrochar mass yield and increasing the process energy requirements (Q_{input}). On the other hand, increasing the residence time had the opposite effect because this condition promotes further condensation reactions favoring mass yield and, for lower temperatures, it also had a beneficial effect in the HHV of the hydrochar as result of a more extensive deoxygenation. As a consequence, increasing the residence time produced a slight increase of PEE and a significant increase of Q_{output}, especially at 250 ºC and 275 ºC. Thus, to maximize Q_{output} and the process efficiency, lower temperatures and longer residence times should be chosen, within the range that also allows other desirable upgrading effects such as reduction of ash and chlorine contents.

Increasing the solid-to-water ratio from 1:15 to 1:5, at 275 ºC and 30 min, caused a clear increase of the process efficiency as a result of the decrease in Q_{input}, as well as in Q_{output}, but this condition yielded the hydrochar with the highest ash content. Also, increasing the solid-to-water ratio from 1:15 to 1:5, at 275 ºC and 30 min, caused an increase of the chlorine content of the hydrochar from 0.91 to 1.08 wt. %. Decreasing the water added to the reactor may also decrease pressure to values lower than the vapor saturation pressure at the process temperature, at which a condensed water phase no longer exists. The presence of condensed water (subcritical water) has an impact in the reactions that occur during the HTC process and especially affects the solvating power towards different components of the raw materials, such as the mineral fraction and non-volatile oxygenated compounds (Funke *et al.*, 2013; Minaret and Dutta, 2016; Yeoh *et al.*, 2018).

These results suggest that HTC applied to RDF should be done with moderate temperatures, longer residence times and with the highest possible solid-to-water ratio, in order to minimize energy expenditure regarding water heating and also in order to obtain higher hydrochar yields (Stemann and Ziegler, 2011).

Nevertheless, increasing the solid-to-water ratio is limited by the need to provide reaction conditions that enable the appropriate reduction of ash and chlorine contents of the RDF, two fundamental parameters for RDF upgrading and hydrochar fuel quality.

5.3.5. Characterization of HTC process water

The HTC process water composition and volume are some of the main drawbacks of this thermal conversion process, due to the relevant amounts of this effluent that are produced and its heavy pollutant charge (Catalkopru *et al.*, 2017; Kambo *et al.*, 2017; Mäkelä *et al.*, 2018; Pala *et al.*, 2014). Increasing the solid-to-water ratio has already been established that may be an advantage for the process energetic balance but is limited by the need to provide an adequate reactional medium for the raw materials. Therefore, determining the composition of the process liquid effluent and evaluating possible pathways for its treatment or valorization are fundamental tasks for a sustainable scale-up of the process to an industrial scale. The process waters generated in each HTC experiment were characterized for critical parameters regarding their treatment or discharge and the results are presented in Table 5.8.

Table 5.8: Chemical characterization of the process waters obtained from the different HTC tests.

Parameter		Unit	Sample						
			W-250-30/15	W-275-30/15	W-275-30/5	W-300-30/15	W-250-120/15	W-275-120/15	W-300-120/15
pH		Sorensen	3.2	3.8	2.8	3.8	3.2	3.8	4.0
Conductivity		$mS.cm^{-1}$	5.0	6.1	9.2	4.1	5.7	6.7	4.0
COD		$gO_2.L^{-1}$	12.2	12.8	27.2	13.8	12.7	14.2	15.5
BOD_5		$mgO_2.L^{-1}$	300	333	450	350	333	393	400
Solids	Total	$g.L^{-1}$	12.2	11.7	23.1	12.5	11.2	10.8	13.5
	Fixed		3.6	3.2	6.7	3.9	3.8	3.4	3.9
	Volatile		8.6	8.6	16.4	8.7	7.4	7.4	9.6
Kjeldahl nitrogen		$mg.L^{-1}$	41.7	42.9	49.2	30.5	41.1	44.8	26.1
Total phosphorous			0.29	0.10	0.31	0.10	0.16	0.09	0.06
Total reducing sugars			6.7	4.2	5.1	5.1	4.7	4.8	4.3
Total phenolics		$g.L^{-1}$	1.6	2.1	2.1	1.7	1.5	1.3	1.5
Chlorine			0.9	1.8	3.2	1.4	1.7	2.6	1.9

Process waters had a low pH, varying between 2.8 and 4.0. Since the added water had a higher pH (5-6) the decrease of this parameter during the HTC process suggests the presence of acidic species such as organic acids that result from sugar decomposition from the biomass fraction of the RDF. Temperature and residence time did not seem to exert significant effects on this parameter, whereas increasing solid-to-water ratio to 1:5 further decreased pH to the lowest value among the different water samples (2.8), because reducing the volume of water introduced in the reactor increased the concentration of pH influencing species. Furthermore, sample W-275-30/5 presented the highest conductivity value (9.2 $mS.cm^{-1}$), reflecting the presence of higher concentrations of ionic or polar species. The highest value of fixed solids (6.7 $g.L^{-1}$) was also obtained for this sample.

Kjeldahl nitrogen presented values between 26.1 $mg.L^{-1}$ and 49.2 $mg.L^{-1}$ showing a tendency to decrease for higher temperatures. At 300 ºC (30 and 120 minutes), nitrogen values in the process water were the lowest indicating that at this temperature nitrogen species were more retained in the hydrochar or transferred to the gas phase. The obtained values regarding nitrogen are higher than the discharge limits imposed by Decree-Law n.º236/98 for the discharge in water bodies (Total nitrogen = 15 $mg.L^{-1}$ N, and Ammonia nitrogen = 10 $mg.L^{-1}$ NH_4) (Ministry of the Environment, 1998).

Although found in very small concentrations in the process water samples, total phosphorous showed a tendency to decrease with increasing temperature and residence time. This decrease may result from

reactions of phosphorous with metallic cations such as calcium, magnesium, aluminum or iron, to yield products that may be deposited in the surface of the hydrochars (Huang *et al.*, 2018; Idowu *et al.*, 2017).

The reducing sugars concentration had a high value at 250 ºC for 30 minutes (6.7 $g.L^{-1}$) but decreased for the subsequent temperatures, and for the tests conducted for 120 minutes. At 275 ºC and 300 ºC (as well as the longer residence time) dehydration and decarboxylation reactions are enhanced and the sugars are converted into intermediate products such as organic acids and CO_2, which justifies this concentration decrease, and is further confirmed by the acidic pH of the process waters (Wang *et al.*, 2018b). Also, reducing sugars are known to participate in condensation reactions with amine groups, from compounds such as proteins or amino acids, in the so-called Maillard reactions, that yield condensation products that may adsorb to the hydrochar surface (Wang *et al.*, 2018b). Although the RDF sample did not have high concentrations of nitrogen, the decrease of reducing sugars and nitrogen in the process water samples obtained at the higher temperatures may be explained by condensation reactions between these two species.

COD and BOD_5 values of the water samples were influenced by all tested HTC process variables: temperature, residence time and solid-to-water ratio. These parameters had a positive correlation with temperature, residence time and solid-to-water ratio. COD values varied in the range from 12.2 $gO_2.L^{-1}$ (W-250-30/15) to 27.2 $gO_2.L^{-1}$ (W-275-30/5), which are significantly higher that the discharge limit for water bodies (150 $mgO_2.L^{-1}$) and also for municipal collectors (Ministry of the Environment, 1998; Municipality of Lisbon, 1991). Higher temperature and longer residence time increased the degradation of the RDF, and the dissolution of organic and inorganic compounds in the water phase, while a reduced amount of water in the reactor will, as previously described, lead to a concentration effect and thus a higher COD value of 27.2 $gO_2.L^{-1}$. On the other hand, BOD_5 measured after 5 days presented values between 300 and 450 $mgO_2.L^{-1}$ (the discharge value is 40 $mgO_2.L^{-1}$ in water bodies) (Ministry of the Environment, 1998). For HTC process waters, these values are very low indicating that biodegradation was inhibited. COD and BOD_5 values of the water samples analyzed in this work were significantly lower than values found for HTC of mixed MSW with a solid-to-ratio of 1:4 (Berge *et al.*, 2011). This was probably due to the solid-to-water ratios that were used (1:15 and 1:5). Wilk *et al.* (2019) had COD values between 19.9 - 30.3 $gO_2.L^{-1}$ using urban sludge and a solid-to-water ratio of 1:8. On the other hand, Anthraper *et al.* (2018) conducted HTC experiments (240-280 ºC) varying solid concentration 1-3 wt.% in a 500 mL vessel reactor. These authors used different raw materials to simulate MSW, and their process waters presented COD values between 493-9580 $mgO_2.L^{-1}$. RDF, as opposed to MSW, represents an already treated solid waste, meaning that during its production the organic and putrescible fraction is separated, leaving mostly lignocellulosic components and plastics, which could also contribute to lower COD and BOD_5 values when compared to MSW. Furthermore, the BOD_5/COD value ranged from 0.02 to 0.03 reinforcing that biological treatment of these process waters would probably not be a viable solution. The BOD_5 of the process waters is not only influenced by process conditions but also by the nature of the raw materials, that influence the release of biodegradable compounds or ecotoxic ones (Berge *et al.*, 2011; Li *et al.*, 2018).

Although inorganic components may also influence the toxicity of the water samples, the influence of the ecotoxicity of organic components present in HTC process waters has been addressed by different authors (Benavente *et al.*, 2017; Berge *et al.*, 2015). As such, in order to evaluate the qualitative composition of the organic fraction present in the process water samples, the organic components were extracted with chloroform and analyzed by GC-MS (Table 5.9).

Table 5.9: Qualitative analysis of the process waters by GC-MS.

Compounds	Molecular formula	CAS number	Relative peak area (%)						
			W-250-30/15	W-275-30/15	W-275-30/5	W-300-30/15	W-250-120/15	W-275-120/15	W-300-120/15
Acetic acid	$C_2H_4O_2$	64-19-7	5.1	2.7	8.4	8.2	9.9	7.7	5.3
Prop-2-enoic acid	$C_3H_4O_2$	79-10-7	-	0.5	-	0.5	-	0.7	0.7
Propionic acid	$C_3H_6O_2$	79-09-4	1.0	0.6	1.5	1.4	1.0	1.7	1.2
Isobutyric acid	$C_4H_8O_2$	107-92-6	-	-	1.8	1.1	-	2.3	1.2
Sorbic acid	$C_6H_8O_2$	110-44-1	1.9	3.2	3.1	4.1	3.9	5.2	3.4
Benzoic acid	$C_7H_6O_2$	65-05-0	-	-	-	1.3	-	-	7.1
3-Methoxybenzoic acid	$C_8H_8O_3$	586-38-9	3.6	1.9	-	1.4	3.6	-	-
1,2-Ethanediol	$C_2H_6O_2$	59609-67-5	-	-	-	0.5	-	-	-
Butanol	$C_4H_{10}O$	71-36-3	-	-	1.2	2.7	-	0.7	1.2
Pentanol	$C_5H_{12}O$	71-41-0	-	-	-	-	-	-	2.2
Octanol	$C_8H_{18}O$	111-87-5	-	-	4.7	4.5	-	-	-
3-Furaldehyde	$C_5H_4O_2$	98-01-1	19.8	1.8	4.5	2.2	1.6	4	0.3
2,4-Dimethylfuran	C_6H_8O	3710-43-8	-	0.7	3.9	1.7	-	2.6	2.3
3-Furaldehyde	$C_5H_4O_2$	98-01-1	19.8	1.8	4.5	2.2	1.6	4.0	0.3
2,4-Dimethylfuran	C_6H_8O	3710-43-8	-	0.7	3.9	1.7	-	2.6	2.3
3-Hydroxybut-3-en-2-one	$C_4H_6O_2$	73623-81-1	-	-	-	-	-	-	0.9
2-Methylcyclopent-2-en-1-one	C_6H_8O	1120-73-6	-	-	-	-	-	-	11.3
1-(cyclohexen-1-yl)-ethanone	$C_8H_{12}O$	88449-93-8	-	1.3	-	1.3	-	-	0.4
(2-hydroxyphenyl)-phenylmethanone	$C_{13}H_{10}O_2$	117-99-7	-	1.1	2.8	-	-	1.6	1.9
1-Phenylethanone	C_8H_8O	98-86-2	-	-	-	-	-	-	0.9
1-Phenanthren-9-ylethanone	$C_{16}H_{12}O$	2039-77-2	-	-	-	-	-	-	1.2
3-Methoxybenzaldehyde	$C_8H_8O_2$	591-31-1	-	1.9	3.7	2.2	-	-	0.7
1-Phenoxynaphtalene	$C_{16}H_{12}O$	3402-76-4	8.5	-	1.8	-	8.5	1.2	-
Phenol	C_6H_6O	108-95-2	1.3	15.3	4.3	2.8	6.9	5.4	4.8
Benzene-1,4-diol	$C_6H_6O_2$	123-31-9	-	-	1.8	-	-	-	0.9
4-Methylphenol	C_7H_8O	106-44-5	1.9	1.6	-	1.4	1.9	4.5	2.0
2-Methylphenol	C_7H_8O	95-48-7	1.8	-	-	-	1.8	1.8	0.6
2-Methoxyphenol	$C_7H_8O_2$	90-05-1	-	0.8	-	-	-	-	3.1
2,6-Dimethoxyphenol	$C_8H_{10}O_3$	91-10-1	-	-	3.7	-	-	-	1.0
1,3,5-Trimethoxy-2-methylbenzene	$C_{10}H_{14}O_3$	14107-97-2	-	-	-	-	-	1.2	1.0
2-Ethenyl-1,3,4,5-tetramethoxybenzene	$C_{12}H_{16}O_4$	n.d.	-	-	-	-	-	-	1.0
2-Benzylphenol	$C_{13}H_{12}O$	1322-51-6	-	-	-	12	-	1.4	1.2
1-Benzyl-2,4-dimethylbenzene	$C_{15}H_{16}$	28122-28-3	-	-	-	-	-	-	0.6
1-Ethyl-2-methylphenanthrene	$C_{17}H_{16}$	61983-53-7	-	-	-	-	-	-	0.5
4-[1-(3,4-dimethylphenyl)ethyl]-1,2-dimethylbenzene	$C_{18}H_{22}$	1742-14-9	-	0.8	-	-	-	-	1.3
2,2,7,7-Tetramethyloctane	$C_{12}H_{26}$	1071-31-4	-	-	1.2	0.8	-	1.2	0.5
Total identified peaks			**44.9**	**34.2**	**48.4**	**50.1**	**39.1**	**43.2**	**60.7**

The HTC process water samples obtained at the higher temperature (300 ºC), for both residence times (30 and 120 min) presented the largest number of identifiable compounds, due to the more extensive

thermal degradation occurring at this temperature. Several acids, alcohols, ketones, aromatic hydrocarbons and phenolic compounds were identified with a cut-off value for relative peak area of 0.5 %.

Acetic, propionic and sorbic acids, as well as 3-furaldehyde (3-furfural) and phenol were present in all the samples, varying their relative percentage for the different operational conditions used in the experiments. The products of thermal decomposition may have a high variability both at qualitative and quantitative level because their formation is influenced by the raw materials composition and also by the specific operating conditions that will determine the formation of primary and secondary products (Mihajlović *et al.,* 2018). But regardless of that variability, the main functional groups found in these process waters, namely organic acids, furanic aldehydes, aromatic compounds and phenolic compounds, have been consistently described in the literature in the process waters from the HTC process (Berge *et al.*, 2011; Mihajlović *et al.*, 2018).

The wide variety of aromatic compounds found in these process waters is consistent with other reports on RDF thermal conversion. According to Efika *et al.* (2015), there was a predominance of aromatic compounds in oil from RDF pyrolysis at 350 ºC, because their forming reactions (conversion of alkanes to alkenes and subsequent Diels-Alder reactions) are favored by high temperature and long residence times. The presence of aromatic compounds is an indicator of the toxicity of these process waters (Mihajlović *et al.*, 2018), and corroborates the low biodegradability expressed through the BOD_5/COD values.

Given the chemical characteristics of these samples, a detailed study of different solutions for the management or valorization of HTC process water is required. Anaerobic digestion, which is the most common valorization process suggested for these effluents (De la Rubia *et al.*, 2018; Weide *et al.*, 2019; Wirth and Mumme, 2013) may be difficult to implement due to the low biodegradability presented by these samples. Nevertheless, process water recirculation, or extraction of certain organic compounds (with added-value) are re-utilization solutions that could be further studied and validated in order to increase the sustainability of the RDF HTC process.

5.3.6. Remediation of HTC process water

Some preliminary tests of remediation of the HTC process water, using precipitation and adsorption techniques were performed. The remediation tests were performed using one precipitating agent B1 (biomass ash, a mineral waste produced in a ceramic furnace for brick production) and three adsorption agents: B2 (powdered activated carbon), B3 (an hydrochar obtained from hydrothermal carbonization of RDF at 300 ºC and 30 min), B4 (a char obtained by torrefaction of RDF at 300 ºC and 30 min).

The composition of the biomass bottom ash mineral used as precipitating agent is given in Table 5.10.

Table 5.10: Biomass bottom ash mineral composition.

Mineral composition	Concentration (wt.%, db)
Al_2O_3	3.97
BaO	0.16
CaO	65.90
Cl	11.50
Cr_2O_3	0.07
CuO	0.06
Fe_2O_3	2.28
K_2O	1.18
MgO	3.16
MnO	0.17
Na_2O	0.56
P_2O_5	0.77
SO_3	0.92
SiO_2	6.59
SrO	0.09
TiO_2	2.52
ZnO	0.09

Ash composition can be variable, depending on its origin but is usually rich in silicon, aluminum, iron, calcium and magnesium oxides, which are known for their precipitating capacity (Wang and Wu, 2006). The biomass ash used in this work has as main components calcium oxide, chlorine, silicon oxide, aluminum oxide and magnesium oxide thus, it may represent a viable and alternative to the typical chemical precipitants.

The hydrochar produced in this chapter (sample H-300-30/15) and char produced by torrefaction of RDF at 300 ºC for 30 min (Chapter 3), were also tested as alternative adsorbents, in comparison with powdered activated carbon (PAC).

The removal efficiencies of total phenolic compounds and COD were evaluated in batch experiments and the results are given in Figure 5.7.

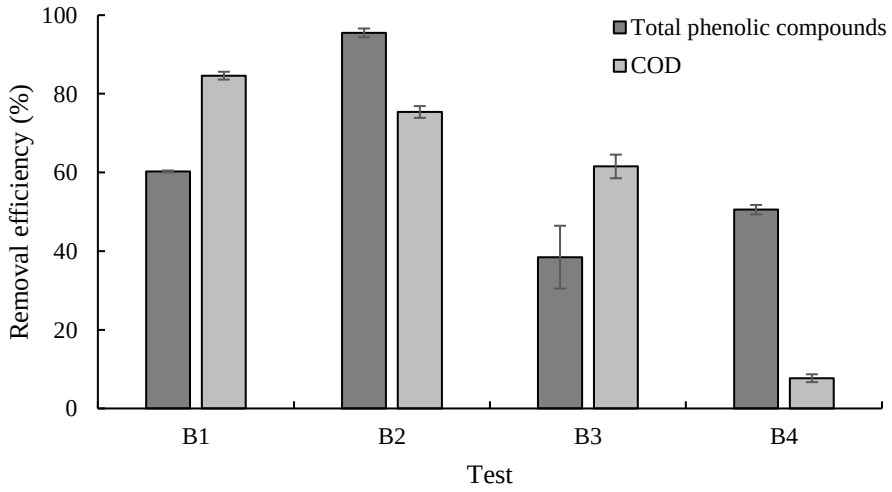

Figure 5.7: Removal efficiencies of total phenolic compounds and COD after batch adsorption tests with different adsorbents B1 (biomass ash), B2 (PAC), B3 (HTC-300-30), B4 (RDF char).

The HTC process water sample used in these experiments was a mixture of water samples obtained in the different hydrothermal carbonization experiments described in this chapter. This composite water sample presented a total phenolic compounds concentration of 1.6 $g.L^{-1}$, a COD value of 12.4 $gO_2.L^{-1}$, and a pH value of 3.8.

The higher removal efficiency towards phenolic compounds (95.5 %) was obtained for activated carbon (B2), followed by the biomass ash, B1 (60.3 %) and the RDF char, B4 (50.5 %). The RDF hydrochar, B3, presented the lowest removal efficiency (38.5 %), indicating that this was the adsorbent with less surface-active groups or porous structure that could enable adsorption of phenolic compounds. At the solution pH (3.8) most phenolic compounds do not present a net charge that could increase electrostatic interactions, thus the availability of a porous structure such as the existing in the activated carbon facilitates adsorption of these phenolic species. In the experiment where the biomass ash was used, a fraction of the ash components was dissolved in the water sample, changing the solution pH from 3.8 to 11, which contributes positively to the formation of complexes between metallic ions and phenolic compounds (which are weak acids). The deprotonated phenolic compounds may have a larger ability to form complexes with inorganic cations such as Ca^{2+}, Mg^{2+} or Al^{3+}, that exist in the biomass ash, and that have lower water solubility leading to precipitation. According to Tantemsapya (2004), the removal efficiencies presented in test B1 can be attributed to the precipitation of high molecular weight compounds with Ca^{2+} ions, available by CaO dissolution. Furthermore, products of lignin decomposition are used as chelating agents for the removal of divalent metal ions (Cu^{2+}, Mg^{2+}, Pb^{2+}), in industrial plants of pulp and paper production (Garcia-Valls and Hatton, 2003)

The precipitation with biomass ash (B1) had the highest removal efficiency regarding COD (84.6 %), followed by the activated carbon, B2 (75.4 %) and the RDF hydrochar, B3 (61.5 %). In this case, the adsorbent with lowest performance was the RDF char, that had a COD removal efficiency of 7.7 %. Chemical precipitation is easily implemented and represents a relatively low investment, but generates sludges that must be adequately valorized or disposed of, to reduce environmental impacts (Kurniawan *et al.*, 2006).

Experiments B3 and B4, that used non-activated waste derived chars presented the lowest removal efficiency values for both parameters which may be explained by the absence of an activated porous structure that may efficiently retain organic and inorganic species. Nevertheless, the RDF char (B4) could remove more than 50 % of the phenolic compounds while the RDF hydrochar (B3) was able to reduce COD by more than 60 %, thus a combination of these waste derived materials could be used as a pre-treatment of these aqueous effluents, contributing to reduce the use of a high cost adsorbent such as the activated carbon. Furthermore, the adsorption properties of the RDF chars or hydrochar may be improved by chemical or physical activation processes that can develop a significant pore structure and increase their surface area.

To evaluate the relation between removal efficiency and adsorbent dose, further batch tests were performed using PAC at doses from 2-20 $g.L^{-1}$. The results are shown in Figure 5.8.

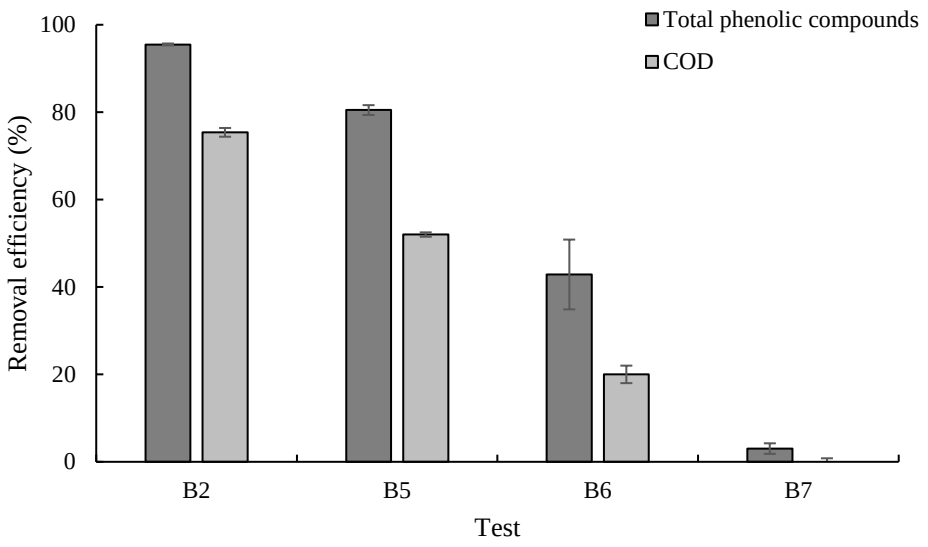

Figure 5.8: Removal efficiencies of total phenolic compounds and COD after batch adsorption tests with PAC at different doses, B2 (20 $g.L^{-1}$), B5 (10 $g.L^{-1}$), B6 (4 $g.L^{-1}$), B7 (2 $g.L^{-1}$).

As seen in Figure 5.8, a PAC dose of 20 $g.L^{-1}$ yields better results for both COD and total phenolic compounds. These results are similar with the ones reported by Devi and Dahiya (2006), that using a dose of 40 $g.L^{-1}$ obtained a removal of around 89 % for COD (20 min and with 600 rpm agitation). This indicates that, although PAC has good removal efficiencies, the HTC process water contains a diverse array of compounds, at concentrations that can easily saturate the char, when using lower doses. Given that PAC is an expensive adsorbent, difficult to regenerate, these results suggest that its use in process water decontamination may have prohibitive costs if implemented in a large scale (Shehzad *et al.*, 2015).

The removal of process water components was also evaluated in column adsorption experiments in order to determine breakthrough volumes relative to phenolic compounds or COD (Fig 5.9).

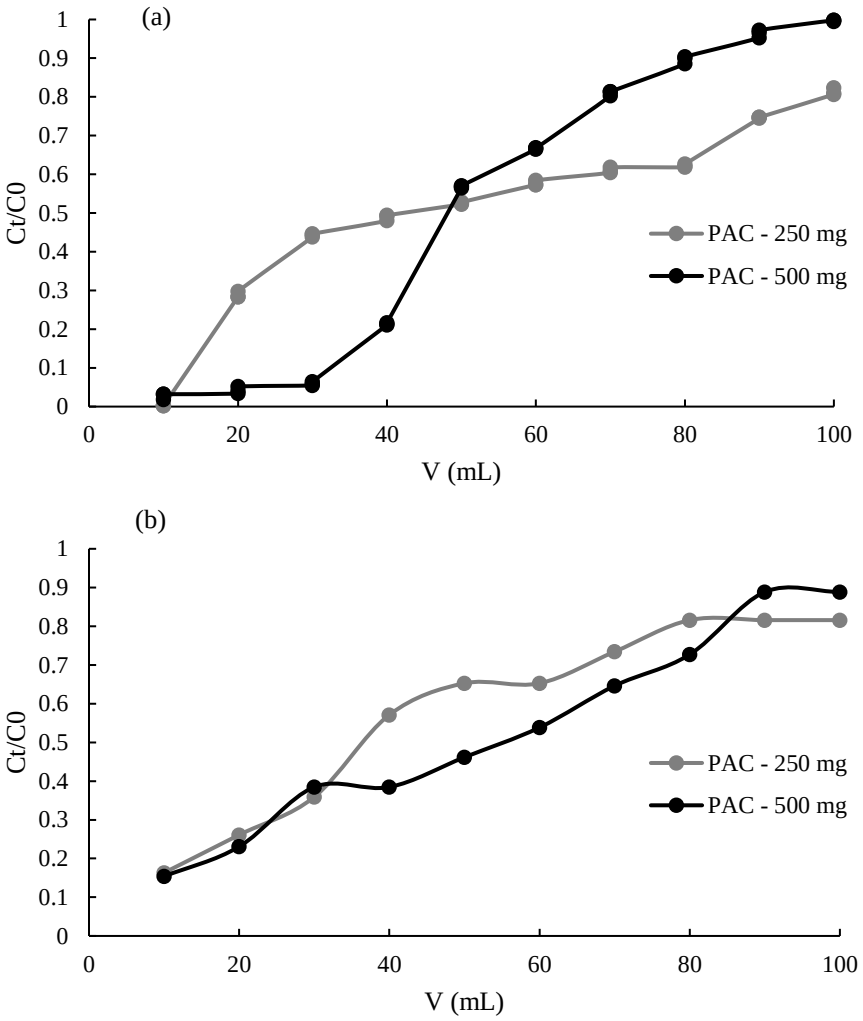

Figure 5.9: Column adsorption tests with PAC at different doses (a) Total phenolic compounds and (b) COD.

The results for all the tests show an early breakthrough followed by a quick rise in the relative concentrations of COD and total phenolics of the effluent (C_t/C_0). Also, for both parameters, a larger amount of PAC showed better removals (as assessed in the batch experiments). With 500 mg of adsorbent in the column, breakthrough for total phenolics occurred very soon (12 min), after passing only 30 mL of the HTC process water mixture. Increasing bed height (adsorbent mass) or reducing flow rate could yield better adsorption results. Moreover, a combined treatment comprising chemical precipitation with biomass bottom ash followed by adsorption, could give positive results, since the larger anionic molecules would precipitate, which could enable a more efficient adsorption process.

5.4. Conclusions

Hydrothermal carbonization of RDF in the temperature range between 250 ºC and 300 ºC, with residence times of 30 min and 120 min, and solid-to-water ratios of 1:15 and 1:5, can be an effective mean to upgrade this very heterogeneous waste derived fuel. Increase in reaction temperature (up to 275 ºC) and time (120 min), led to higher reaction severity, resulting in an increase of RDF degradation, but also of a higher polymerization and condensation of dissolved products with subsequent higher mass yield. The produced hydrochars presented upgraded fuel properties, namely reduced volatile matter and ash contents and increased fixed carbon and HHV reaching a value of 28.1 $MJ.kg^{-1}$ for the hydrochar

produced at 275 ºC for 120 minutes. The hydrochars showed similarities with fossil fuels such as lignite regarding the reduced oxygen and hydrogen contents. These new-found characteristics illustrate their potential as alternative solid fuels.

Although RDF hydrochars presented very enhanced fuel characteristics, the HTC process uses high amounts of water and higher temperatures, which are characteristics that increase the energy requirements of this process. The experiment conducted at 275 ºC and 30 min and solid-to-waster ratio of 1:5, which also presented the highest hydrochar yield, presented a Q_{net} value of 8.50 MJ and a process efficiency of 52.6 %. Increasing the residence time at temperatures from 250 ºC and 275 ºC increased significantly the Q_{output}, reflecting higher yields or calorific values of the hydrochars.

The process waters from all the HTC tests presented acidic pH and significant COD, total phenolic and total reducing sugars values, as well as the presence of various organic species, namely organic acids, alcohols, furan derivatives, phenolic compounds and aromatic hydrocarbons. Owning to their composition, these process waters need to be treated with adequate methods, to reduced their organic and inorganic charge and therefore increase the sustainability of the HTC process.

Remediation of the HTC process water was attempted through chemical precipitation and through adsorption. The results showed that chemical precipitation is effective in COD removal, but has the disadvantage of sludge formation. On the other, although activated carbon showed promising removal efficiencies for COD and total phenolic compounds, the amount of adsorbent needed hinders large scale applications. RDF hydrochar and conventional RDF char also show potential as adsorbents, and in spite of lower removal efficiencies, they present the clear advantage of being produced from wastes, which translates into lower production costs. Moreover, both waste derived chars may be subjected to chemical of physical activation, to enhance their adsorption properties.

Chapter 6

Gasification of pine waste pellets with incorporation of RDF char

Abstract

RDF was carbonized at 300 °C for 30 minutes and the resulting RDF char was used as additive for biomass pellets. Pine waste pellets with 0 %, 5 % and 10 % incorporation of RDF char were prepared and characterized. RDF char incorporation caused an increase in fixed carbon and ash contents of the supplemented pellets. The produced pellets were subjected to gasification in a 1 $kg.h^{-1}$ bubbling-fluidized-bed gasifier at different temperatures (800 and 850 ºC) and equivalence ratios (0.25 and 0.30). The producer gas yield varied from 1.5 to 2.5 $m^3.kg^{-1}$ and was higher for an equivalence ratio of 0.25. Carbon conversion efficiency and cold gas efficiency were in the range of 60.4 to 96.1 % and 42.2 to 73.5 %, respectively.

The pellets with RDF char incorporation had a best gasification performance at 850 ºC and ER 0.25. Concentrations of CO_2, CO, H_2 and CH_4, ethane, ethylene, benzene and toluene were determined in the producer gas. The tars produced during gasification contained mainly aromatic hydrocarbons and phenols. RDF char incorporation increased the concentrations of heavy PAHs in the gasification tars. The RDF char can be used as a gasification additive at moderate incorporation ratios.

Keywords: RDF char; Pine wastes; Blended pellets; Gasification; BFBG; Tars.

6.1. Introduction

Gasification is an attractive alternative to combustion as a thermochemical technology for energy recovery from solid wastes and has been proposed as core technology for numerous WtE applications. The gasification process has the potential of providing alternative pathways for sustainable waste management whilst promoting non-fossil fuels and chemical feedstocks, thus reducing fossil fuel dependency (Arena *et al.*, 2010; Arena and Di Gregorio, 2014).

Different feedstocks, such as solid wastes, may be converted into a "producer gas" or "syngas" ($CO+H_2$), by means of gasification at high temperature and in the presence of an oxidizing agent at limited concentration (Materazzi *et al.*, 2016).

Gasification presents several advantages over traditional combustion of solid wastes, like desirable pollution minimization effects, higher recovery efficiency and higher operational flexibility (Galvagno *et al.*, 2009). Among the different reactor configurations used in gasification, the bubbling fluidized bed gasifier (BFBG) is a frequent choice since it can handle a large array of solid fuels such as biomass, agricultural and forestry wastes or RDF (Corella *et al.*, 2008; George *et al.*, 2018; Monteiro *et al.*, 2018; G. Xue *et al.*, 2014). Nevertheless, fuels with a low degree of homogeneity and calorific value, such as MSW or RDF, may benefit from various upgrading pre-treatments, in order to improve those properties and the energy efficiency of the process (Belgiorno *et al.*, 2003; Ramos *et al.*, 2018). The fuel applications of RDF are also limited by their high content of polymeric materials that can cause clogging in feeding systems and can contribute to an increase of solid and gaseous emissions associated with

incomplete combustion or gasification. In particular, the polymeric fraction of RDF is the source of organic chlorine that leads to the formation of HCl and organochlorine derivatives during gasification (Ma *et al.*, 2010). In this sense, torrefaction and carbonization, as shown in Chapters 3 and 4, can contribute to the enhancement of some of these problematic features.

The advantages of gasifying raw materials that were previously torrefied have been reported by different authors. The torrefaction of SRF has been studied by Recari *et al.* (2017) in the perspective of its application as feedstock in gasification. The authors conducted the torrefaction pre-treatment in the range of 290–320 °C, and concluded that the use of torrefied SRF improved the gasification performance, increasing carbon conversion and H_2/CO ratio while reducing tar formation. Gang Xue *et al.* (2014) studied the torrefaction of *Miscanthus x giganteus* biomass as a pre-treatment to reduce moisture, hemicellulose content and O/C ratio, thus obtaining a material that presented more adequate properties for gasification.

Moreover, according to Pinto *et al.* (2014) a strategy to reduce problems associated with RDF gasification is the co-gasification with less problematic materials, such as biomass, enabling the dilution of the RDF's negative characteristics.

In this chapter, the gasification of lignocellulosic pellets, composed of pine biomass wastes and RDF char was studied. The incorporation of RDF char was evaluated at the concentrations of 0 %, 5 % and 10 %, using different temperatures and equivalence ratios, in order to validate the application of RDF char in energy applications. These lignocellulosic wastes and the RDF char may be considered raw materials with low carbon footprint because they are by-products of other industrial activities, and therefore their use in the production of syngas may improve process sustainability and constitute a recovery pathway for these wastes.

6.2. Materials and methods

6.2.1. Raw materials

Pine waste biomass (PW) and industrial RDF were supplied by CITRI S.A. The PW sample was composed of end-of-life pine materials. The RDF sample was the same that was used in Chapter 4.

The RDF was subjected to torrefaction at 300 ºC for 30 minutes, in a rotary pyrolysis furnace (MJ Amaral, model FR 100), to obtain the RDF char (as described in Chapter 4). PW and RDF char were milled to a particle size below 1 mm and used to prepare pellets in an axial 400 $kg.h^{-1}$ maximum capacity small-scale pelletizer unit with 6 mm diameter holes.

The produced pellet formulations were: 100 % PW (sample 1), 95 % PW + 5 % RDF char (sample 2) and 90 % PW + 10 % RDF char (sample 3).

6.2.2. Pellet characterization

Before characterization, the pellets and the RDF char were milled and sieved (Retsch sieve) to a < 500 µm particle size diameter, as seen in Figure 6.1.

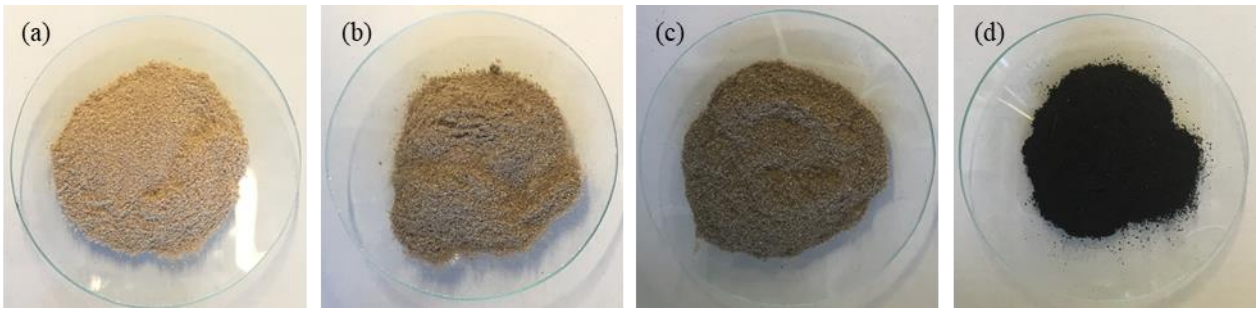

Figure 6.1: Materials used in the preparation of the tested pellets: (a) Sample 1 - 100% PW; (b) Sample 2 - 95% PW + 5% RDF char; (c) Sample 3 - 90% PW + 10% RDF char; (d) RDF char.

The proximate and ultimate composition, chlorine content, mineral composition and high heating value were determined for the pellet samples and the original raw materials. Moisture content, was determined according to BS EN 14774-1:2009 on an as received basis (ar). Volatile matter and ash contents were determined gravimetrically according to standards BS EN 15148:2009 and BS EN 14775:2009, respectively, on a dry basis (db). Fixed carbon was calculated by difference (db).

Ultimate analysis (CHNS) was performed using an elemental analyzer (Thermo Finnigan - CE Instruments, Model 112 CHNS Flash EA series). Oxygen was determined by difference, in a dry ash free basis (daf).

The high heating values (HHV) of the samples were determined through bomb calorimetry (Leco AC500 Automatic Calorimeter) using benzoic acid as reference (British Chemical Standard, HHV= 26439.7 J/g). Low heating values (LHV) were calculated according to equation 3.2 (from Chapter 3):

Chlorine content was determined according to CEN/TS 15289:2006. Mineral composition was determined using flame atomic absorption spectroscopy (EAA Solaar M Series/Unicam Solaar System spectrometer), after ashing and acid digestion of the samples.

The analytical procedures were conducted with replicates, and the results are presented as average values (variation coefficient ≤ 10 %).

6.2.3. Gasification tests

The pellet samples were submitted to a Retsch mill with a 6 mm sieve before being admitted to the gasifier. The gasification experiments were conducted in a 1 $kg.h^{-1}$ bubbling-fluidized-bed gasifier (WOB) at the ECN installations (Energy Research Centre of the Netherlands). The gasifier is electrically heated and has an internal diameter of 74 mm in the bubbling fluidized bed section, increasing to 108 mm in the freeboard section at a height of 500 mm, as described by G. Xue *et al.* (2014). In the producer gas outlet, a small cyclone is positioned for removal of the bulk of the ash leaving the gasifier. Samples were fed into the gasifier through a previously calibrated feeding screw. The photographic representation and schematics for the WOB gasifier are represented in Figure 6.2.

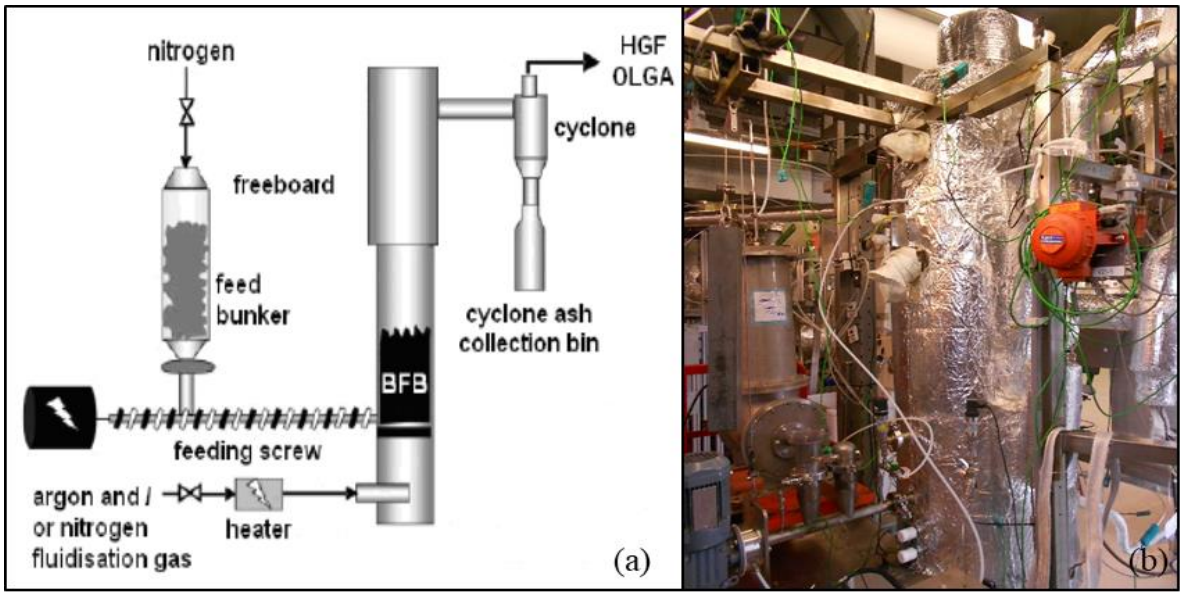

Figure 6.2: Bubbling-fluidised-bed gasifier (WOB) schematics (Zwart *et al.*, 2010) (a) and photographic representation (b).

In the beginning of each experiment, the gasifier was charged with ~1068 g of sand as bed material, sieved to a particle size range of 0.25-0.50 mm. The feeding rate of the samples was approximately 409 ± 46 $g.h^{-1}$ (daf). The experiments were carried out in air and at different temperatures as well as different equivalence ratios completing a total of 12 tests (see Table 6.1).

Table 6.1: Experimental layout for the gasification of each sample.

Code	Sample composition	Experimental conditions		Duration of each test (min)
		Temperature (ºC)	Equivalence ratio (ER)	
Sample 1	100 % PW	800	0.25	60-140
			0.30	
		850	0.25	
			0.30	
Sample 2	95 % PW + 5 % RDF char	800	0.25	
			0.30	
		850	0.25	
			0.30	
Sample 3	90 % PW + 10 % RDF char	800	0.25	
			0.30	
		850	0.25	
			0.30	

Producer gas composition (CO, CO_2, CH_4, H_2, C_2H_4, C_2H_6, benzene and toluene) was measured on-line every minute with gas monitors and a micro-GC (Varian, CP4900).

6.2.4. Gasification performance

Producer gas LHV was calculated according to equation 6.1 taking into account the concentrations of carbon monoxide, hydrogen, methane and ethylene and the LHV of each gas component taken from Waldheim and Nilsson (2001):

$$LHV_{producer\ gas}(MJ.m^{-3}) = 12.6\ [CO] + 10.8[H_2] + 35.8[CH_4] + 59.0[C_2H_4] \quad \text{Equation 6.1}$$

Producer gas yield (PGY) was determined according to equation 6.2, as a relation of the flow rate of dry producer gas ($m^3.h^{-1}$) to the mass flow rate of the samples ($kg.h^{-1}$, daf) (Basu, 2010):

$$PGY\ (m^3.kg^{-1}) = \frac{Flow\ rate_{dry\ producer\ gas}}{Comsumption\ rate_{sample}} \quad \text{Equation 6.2}$$

Carbon conversion efficiency (CCE) was estimated as the fraction of carbon in sample feed that was converted into producer gas (equation 6.3), considering the volumetric percentages of carbon monoxide, carbon dioxide, methane and ethylene in the producer gas and the mass percentage of carbon in the samples ($\%C_{sample}$) (George *et al.*, 2018):

$$CCE\ (\%) = \frac{PGY \times 12 \times [(\%CO + \%CO_2 + \%CH_4) + (2 \times C_2H_4)]}{22.4 \times \%C_{sample}} \quad \text{Equation 6.3}$$

Cold gas efficiency (CGE) was calculated as the ratio between the chemical energy contained in the producer gas ($LHV_{producer\ gas}$) and the input energy of the sample (LHV_{sample}) (Gu *et al.*, 2018), according to equation 6.4:

$$CGE(\%) = PGY \times \frac{LHV_{producer\ gas}}{LHV_{sample}} \times 100 \quad \text{Equation 6.4}$$

6.2.5. Tar analysis

Two tar samples per gasification test were taken using the SPA (solid phase adsorption) method with a LC-NH2 column, as described by Grootjes (2012) and Osipovs (2013). SPA samples were extracted with chloroform and tar composition (polycyclic aromatic hydrocarbons – PAHs) was determined with a GC-MS analyzer (Focus GC, Polaris Q-Thermo) equipped with a DB-5 capillary column (30 m length, 0.25 mm inner diameter, and 0.25 μm film thickness). Helium was used as a carrier gas at 1.0 $mL.min^{-1}$. Injection temperature was 240 ºC in splitless mode with 1 min of splitless time and 30 $mL.min^{-1}$ of split flow. The interface and ion source were set at 230 ºC. The oven temperature was held at 40 °C for 1 min, increased to 260 °C at a rate of 4 $°C.min^{-1}$, and then held at 260 °C for 5 min. The mass spectrometer was operated in the full scan mode from 50 to 600 mass units. Identification of tar components was carried out by comparison of mass spectra with reference libraries (NIST, WILEY). Determination of PAHs was performed by comparison of retention time and mass spectra with a PAHs mix standard solution (Chem Service) analyzed in similar conditions (PAHs standard profile can be found in the Appendix, Figure A.13).

6.3. Results and discussion

6.3.1. Characterization of raw materials

Proximate, ultimate and mineral compositions, chlorine content and heating values of the samples used in the gasification tests, as well as of the RDF char used as an additive are presented in Table 6.2.

Table 6.2: Main chemical properties of the tested samples (Sample 1 – 100 % PW, Sample 2 – 95 % PW+5 % RDF char, Sample 3 – 90 % PW and RDF char).

Parameter	Units	Sample 1	Sample 2	Sample 3	RDF char
Moisture	wt.%, ar[a]	8.9	10.8	7.6	1.3
Volatile matter		84.8	82.2	81.7	56.3
Ash	wt.%, db[b]	0.8	1.6	2.4	22.8
Fixed carbon		14.4	16.1	15.9	20.9
C		50.0	50.5	51.3	61.0
N		0.1	0.1	0.2	1.3
H	wt.%, daf[c]	6.1	6.0	6.1	6.2
S		0	0	0	0.2
O		43.7	43.4	42.5	31.2
Al		177.7	446.3	685.4	4324.5
Zn		25.6	188.8	380.6	4557.2
Pb		25.0	37.2	48.8	265.7
Ni		11.7	26.9	33.7	209.2
Mn		59.4	61.3	68.1	110.3
Cu		5.2	132.5	270.6	2425.3
Fe	$mg.kg^{-1}$, db	< 1.0	166.8	556.2	4745.0
Cr		2.5	13.0	26.3	231.9
Cd		1.3	1.3	1.5	2.0
Ca		993.8	2871.9	7291.9	29504.0
Mg		529.3	676.2	1101.8	2900.3
Na		973.4	915.7	638.0	6845.0
K		943.6	774.5	788.4	3021.3
Chlorine	wt.%, db	0.03	0.26	0.14	1.1
HHV	$MJ.kg^{-1}$, db	18.4	18.8	18.8	19.3
LHV	$MJ.kg^{-1}$, db	17.1	17.5	17.5	18.2

[a]ar - as received basis; [b]db - dry basis; [c]daf - dry ash free basis.

The RDF char had a higher carbon content (61.0 wt.%) than PW (50.0 wt.%), therefore its incorporation in samples 2 and 3 improved their carbon concentrations. The same effect was observed for ash content and for the concentrations of most mineral components. Parameters such as volatile matter and oxygen contents, that had lower values for the RDF char than for PW suffered a dilution effect, therefore decreased for samples 2 and 3 relatively to sample 1.

The inorganic elements with concentrations higher than 1 $g.kg^{-1}$ in the RDF char (Ca, Mg, Al, Zn, Cu and Fe) were also the main mineral components of samples 2 and 3. The same was not observed for Na and K, regardless of their high concentrations in the RDF char, respectively 6.8 $g.kg^{-1}$ and 3.0 $g.kg^{-1}$. This behavior suggests that Na and K may be partially dissolved in tars, during the carbonization process, and heterogeneously distributed in the RDF char. The ash concentration in the gasification bed after the tests involving samples 1, 2 and 3 were respectively 1.36 %, 2.92 % and 5.26 %, reflecting the ash contents of those samples.

There was a moderate increase of the chlorine content to 0.26 wt.% in sample 2 and 0.14 wt.% in sample 3 when compared to the pine biomass pellets (0.03 wt.%). Elevated chlorine content is one of the main drawbacks of raw RDF utilization because it can lead to very harmful emissions and operational issues (Silva *et al.*, 2014) . The torrefaction process has proven useful to reduce the chlorine content of RDF, MSW or waste wood samples (Edo *et al.*, 2017; Recari *et al.*, 2017).

RDF char had a LHV of 18.2 MJ.kg^{-1}, slightly higher than the LHV of PW (17.1 MJ.kg^{-1}) thus char incorporation had a small positive effect on the calorific value of samples 2 and 3 (17.5 MJ.kg^{-1}).

6.3.2. Gasification performance

The performance of the gasification process was evaluated at different temperatures and equivalence ratios, by the determination of carbon conversion efficiency (CCE), cold gas efficiency (CGE), producer gas yield (PGY) and producer gas lower heating value (Table 6.3).

Table 6.3: Effect of temperature and equivalence ratio on gasification performance LHV of the producer gas, producer gas yield (PGY), carbon conversion efficiency (CCE) and cold gas efficiency (CGE).

Sample	Gasification conditions	$LHV_{producer\ gas}$ (MJ.m^{-3})	PGY (m^3.kg^{-1})	CCE (%)	CGE (%)
1	800 ºC - ER 0.25	5.4	2.3	96.1	72.8
	800 ºC - ER 0.30	4.6	1.6	60.6	42.2
	850 ºC - ER 0.25	5.4	2.1	81.8	65.7
	850 ºC - ER 0.30	5.4	1.5	60.4	46.8
2	800 ºC - ER 0.25	4.9	2.3	86.5	65.7
	800 ºC - ER 0.30	4.5	1.7	62.3	43.5
	850 ºC - ER 0.25	5.0	2.4	89.7	68.9
	850 ºC - ER 0.30	4.5	1.7	62.5	44.3
3	800 ºC - ER 0.25	5.2	2.4	88.7	69.7
	800 ºC - ER 0.30	4.7	1.7	64.3	46.8
	850 ºC - ER 0.25	5.3	2.5	92.3	73.5
	850 ºC - ER 0.30	4.5	1.7	62.2	45.0

According to Arena and Di Gregorio (2014), ER defines the availability of the oxidation agent, it influences the extension of the oxidative decomposition of biomass in the pyrolysis zone and the extension of the gas oxidation reactions. On the other hand, gasification is an endothermic process and as such, the extent of the gasification reactions and therefore the producer gas composition are affected by temperature changes (Olufemi, 2017).

Gas yield, carbon conversion efficiency and cold gas efficiency were higher for the lower ER (0.25), at both tested temperatures. High equivalence ratios may cause the excessive formation of complete combustion products thus reducing its performance, as seen for the lower LHV values obtained at ER 0.30. The LHV of the producer gas did not show a correlation with the incorporation of RDF char: samples 1 and 3 present comparable LHV values while sample 2 presents overall slightly lower values. The obtained calorific values are in the range of different studies using coir pith (Dillibabu and Natarajan, 2014), miscanthus (G. Xue *et al.*, 2014), SRF (Arena and Di Gregorio, 2014; Recari *et al.*, 2016), Stabilat (Dunnu *et al.*, 2012) or olive bagasse (Almeida *et al.*, 2019).

Increasing the gasification temperature from 800 ºC to 850 ºC, at ER 0.25, caused an increase of PGY, CCE and CGE for samples 2 and 3 but had the inverse effect for sample 1. This behavior reflects the higher thermal stability of the RDF char components, that is expectable since it is a material already subjected to a thermochemical pre-treatment. According to Almeida *et al.* (2019) the producer gas yield represents the fraction of sample particles that were converted to producer gas and therefore it is a parameter that directly impacts the gasification performance. At higher temperatures the rates of pyrolysis and devolatilization may be enhanced, which would reflect in high CCE values. Moreover, an increased CCE can be related to a lower formation of heavy tars (Arena and Di Gregorio, 2014).

6.3.3. Producer gas composition

The composition of the producer gas is presented in Table 6.4, for the different temperatures and equivalence ratios used in the experiments.

Table 6.4: Effect of temperature and equivalence ratio on the composition of the producer gas.

Sample	Test conditions		N_2	CO	CO_2	H_2	CH_4
	T (ºC)	ER	vol. %, dry				
1	800	0.25	55.2	17.4	13.9	6.5	4.5
		0.30	61.3	16.1	13.9	4.9	3.9
	850	0.25	57.9	15.3	14.7	11.1	4.4
		0.30	62.8	16.7	14.7	10.3	4.4
2	800	0.25	53.9	14.2	13.5	7.0	3.9
		0.30	57.8	14.1	14.0	5.5	3.5
	850	0.25	52.8	13.5	14.2	8.3	3.9
		0.30	57.5	13.3	14.5	6.4	3.6
3	800	0.25	54.1	15.0	13.1	6.6	4.1
		0.30	57.7	14.9	13.5	5.0	3.7
	850	0.25	53.4	14.4	13.8	7.9	4.2
		0.30	57.9	13.6	14.0	5.6	3.6

Increasing ER from 0.25 to 0.30 increased the concentration of N_2 in the producer gas and reduced the concentrations of other components, in almost all conditions tested, because of the dilution effect resulting from the higher air flow (G. Xue *et al.*, 2014). The decrease of H_2, CO and CH_4 concentrations and the increase of CO_2 concentration in the producer gas when ER increases, may also be related to the higher availability of oxidizing agent and the consequent improvement of carbon conversion, as observed by different authors (Arena and Di Gregorio, 2014; G. Xue *et al.*, 2014).

Since the main reactions in the gasification process are endothermic, they are favored by high temperatures, that are necessary to promote the pyrolytic decomposition of the feed and formation of low molecular weight species (Almeida *et al.*, 2019; George *et al.*, 2018; Ramos *et al.*, 2018). Increasing the temperature at ER 0.25, decreased CO concentration and increased H_2 and CO_2 concentrations in the producer gas, for all samples, indicating that hydrocarbon cracking, reforming reactions and carbon oxidation are favored by the temperature increase (Pinto *et al.*, 2014).

At comparable conditions of temperature and equivalence ratio, samples 2 and 3 showed lower CO and CO_2 concentrations than sample 1, which indicates that the RDF char is a less reactive raw material, and its incorporation in the feed should be compensated by an increase in the efficiency of the oxidizing agent, for example, by increasing the oxygen concentration in the gasifier (Gu *et al.*, 2018).

The concentrations of other light hydrocarbons such as ethane, ethylene, benzene and toluene, present in the producer gas were also evaluated for the different gasification tests (Figure 6.3).

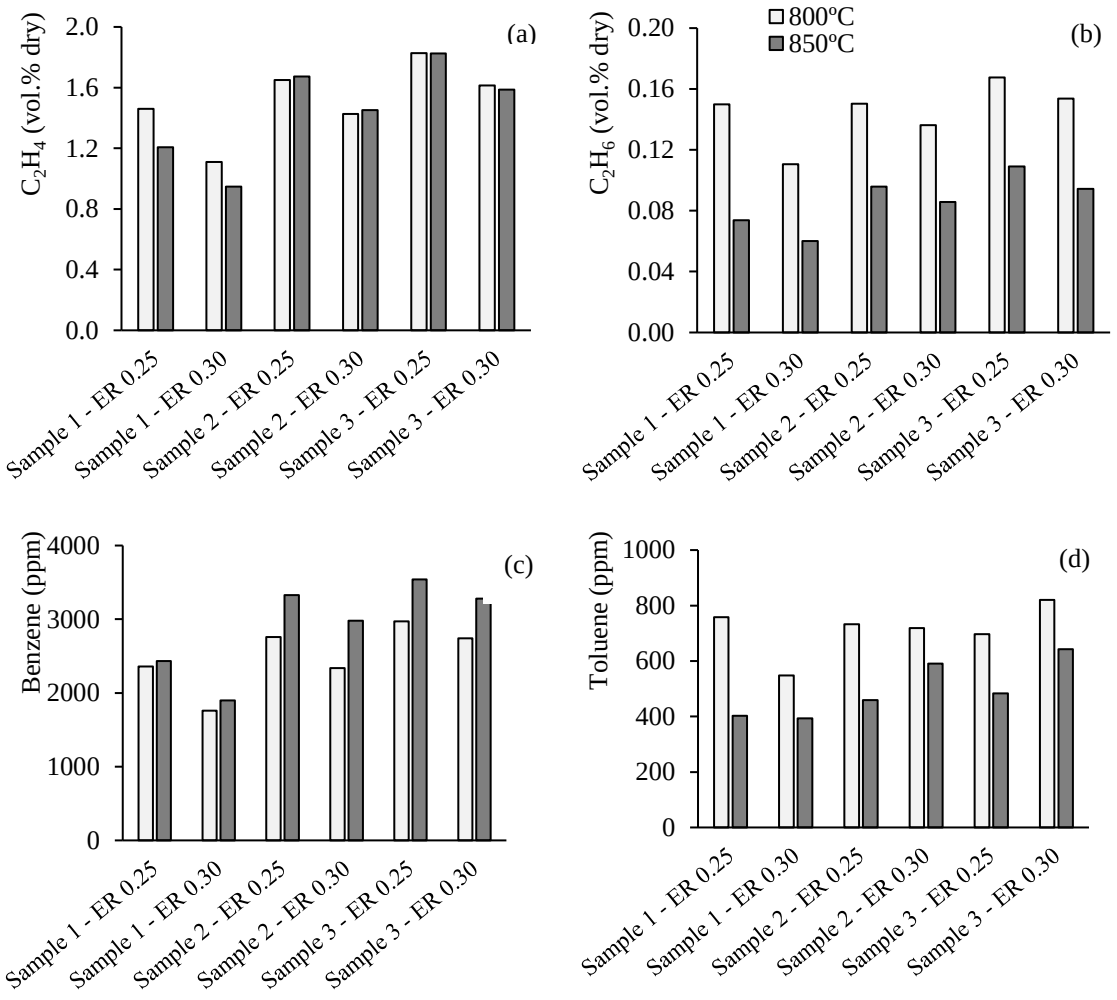

Figure 6.3: Effect of temperature and equivalence ratio on light hydrocarbons. (a) Ethylene; (b) Ethane; (c) Benzene; (d) Toluene.

Some of these light hydrocarbons are liquid at room temperature (benzene, toluene) but they are entrained by the gas components, and are present in small concentrations in the vapor phase. The concentrations of light hydrocarbons were negatively affected by the increase of ER, because higher O_2 availability favored their oxidation to CO or CO_2. These hydrocarbon gases and light aromatic hydrocarbons showed higher concentrations for samples 2 and 3 (Figs. 6.3a to 6.3d), confirming the higher stability of the RDF char matrix.

Increasing the temperature from 800 ºC to 850 ºC promoted the decomposition of ethane and toluene (Figs. 6.3b and 6.3d), had little effect in the concentration of ethylene and increased the concentration of benzene (Figs. 6.3a and 6.3b). These results reflect the specific degradation reactions involving these species and the other hydrocarbon components of the producer gas. For example, the observed increase in the concentration of benzene may result from the degradation of toluene by loss of the methyl group.

Although present at concentrations lower than 2 vol.% or in the range of ppm, since these hydrocarbon components have carbon numbers from 2 to 6, their heating values are much higher than those of the gas producer main hydrocarbon components (CO or CH_4).

Taking into account the producer gas composition and absolute yield, it is possible to evaluate the volume yield of each gas component relatively to feed mass (Figure 6.4).

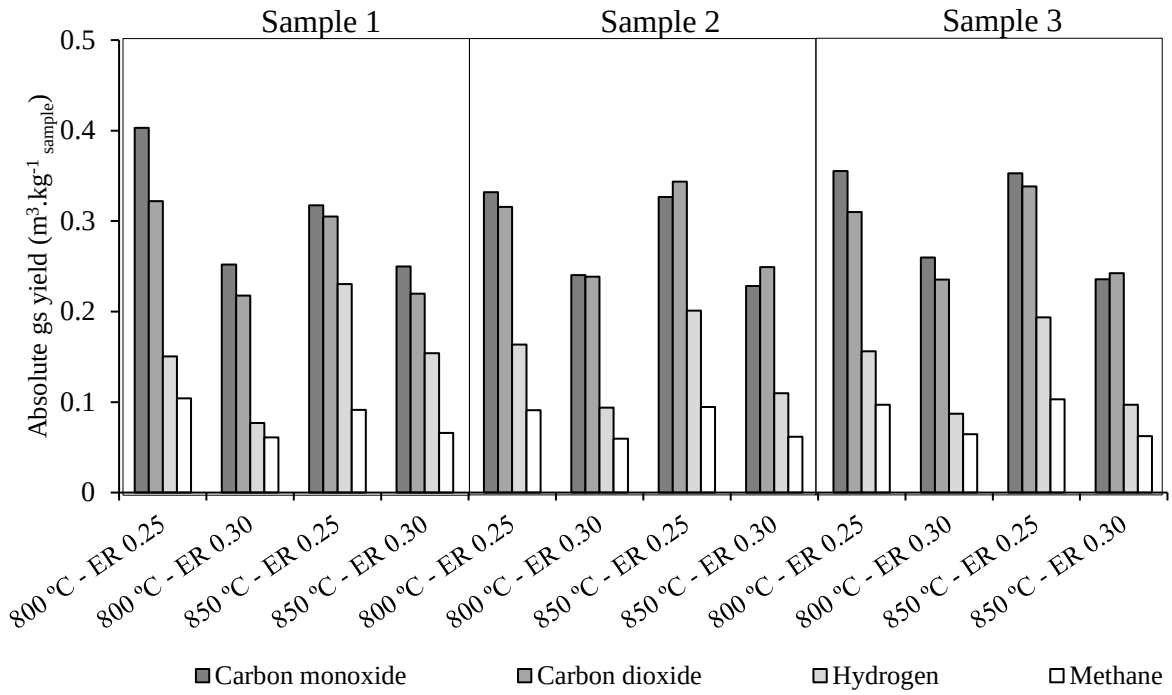

Figure 6.4: Effect of temperature and equivalence ratio on the yield of producer gas main components.

The best yields of CO and CH_4 were obtained for an equivalence ratio of 0.25, for sample 1 at 800 ºC, while for samples 2 and 3 there were no significant differences in the concentrations of those components at both temperatures. H_2 concentration increased at 850 ºC, for the three samples tested indicating that reforming reactions were favored by this temperature increase. Increasing ER did not have a positive effect on the yields of combustible gases for any of the samples, indicating that the dilution effect of the inlet nitrogen may have a shielding effect in the reactive species.

6.3.4. Tar analysis

Tar formation during biomass or waste gasification is not a desired reaction because it generates secondary products, it can result in operational difficulties and in a decrease in the producer gas quality (Sikarwar *et al.*, 2016). Characterization of tar composition allows the definition of adequate pathways for its valorization or treatment in order improve the sustainability of the gasification process and reduce the environmental impact of these secondary products.

The collected tar samples contained mainly aromatic compounds with one to four rings, including *o*-xylene, styrene, benzofuran, phenol, indene, methylnaphthalene, biphenyl and a group of twelve PAHs. The chromatographic profile of the tar extract obtained for sample 1 at 850 ºC and ER 0.25, is presented in Figure 6.5.

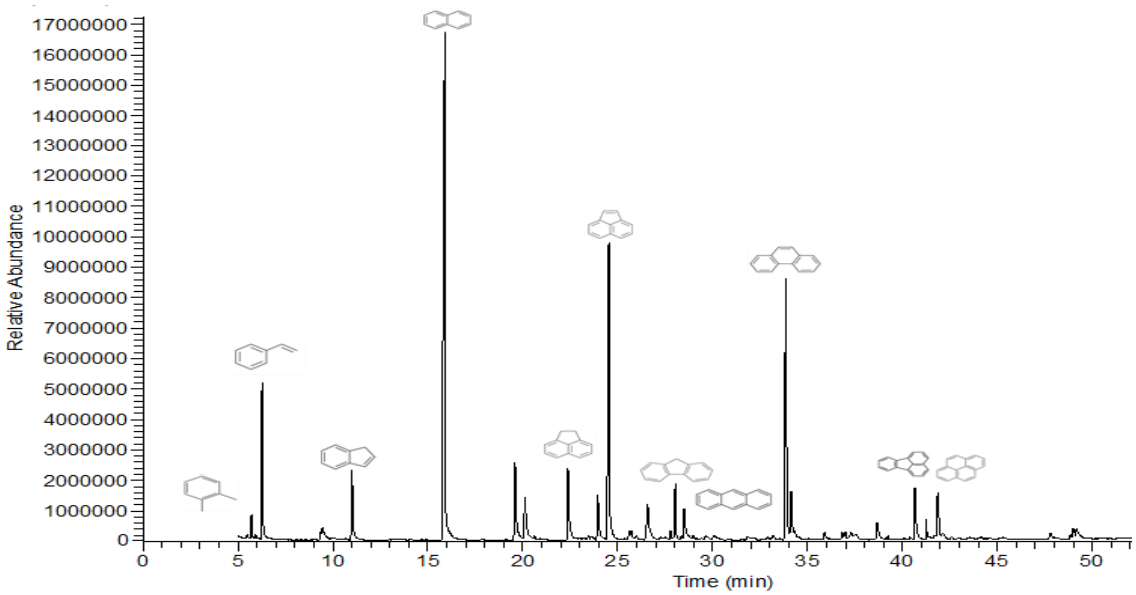

Figure 6.5: GC-MS profile of tar extract from Sample 1 (850 ºC, ER 0.25).

Tar composition and normalized relative abundance of each identified compounds were evaluated for each gasification test (Figure 6.6 and Figure 6.7). At all the tested conditions, naphthalene, acenaphtylene and phenanthrene were the main tar components, as reported in other studies regarding the composition of tars produced by gasification biomass or wastes (Blanco *et al.*, 2012; Huang *et al.*, 2015; Rabou, 2005).

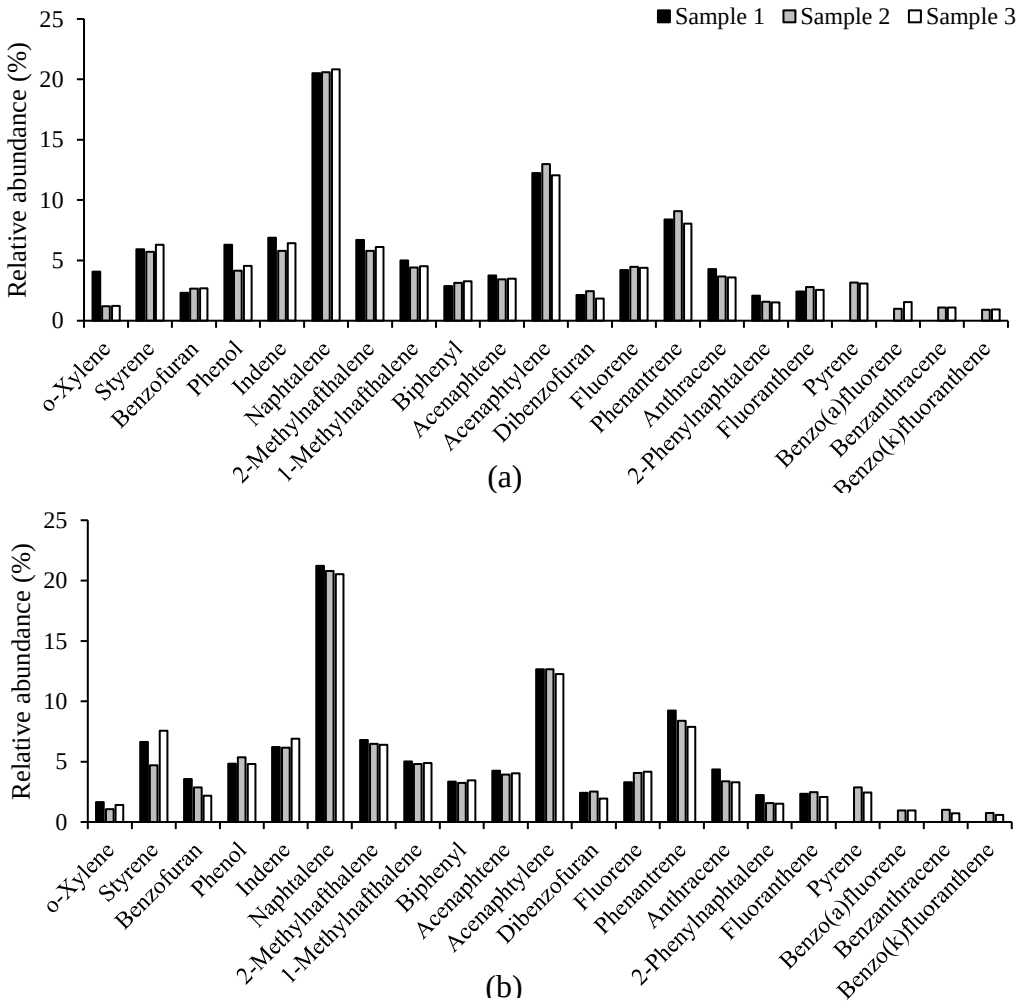

Figure 6.6: Relative abundance of tar components for the gasification tests performed at 800 ºC and ER 0.25 (a) or ER 0.30 (b).

For the tars obtained at 800 ºC, the ER increase had little effect in tar composition, an expected behavior since the main tar components are polyaromatic hydrocarbons and the only oxygenated compounds detected in the samples (phenol, benzofuran and dibenzofuran) were present in very low percentages. The incorporation of RDF char had the effect of increasing the formation of heavier PAHs (pyrene, benzo(a)fluorene, benzanthracene and benzo(k)fluoranthene) in the tars obtained from the gasification of samples 2 and 3, at 800 ºC, while these compounds were not detected in the tars obtained from sample 1, at the same temperature. The production of PAHs with higher molecular weight increases the ecotoxicity of the tars because these PAHs are hydrophobic, persistent and genotoxic (Kanaly and Harayama, 2000).

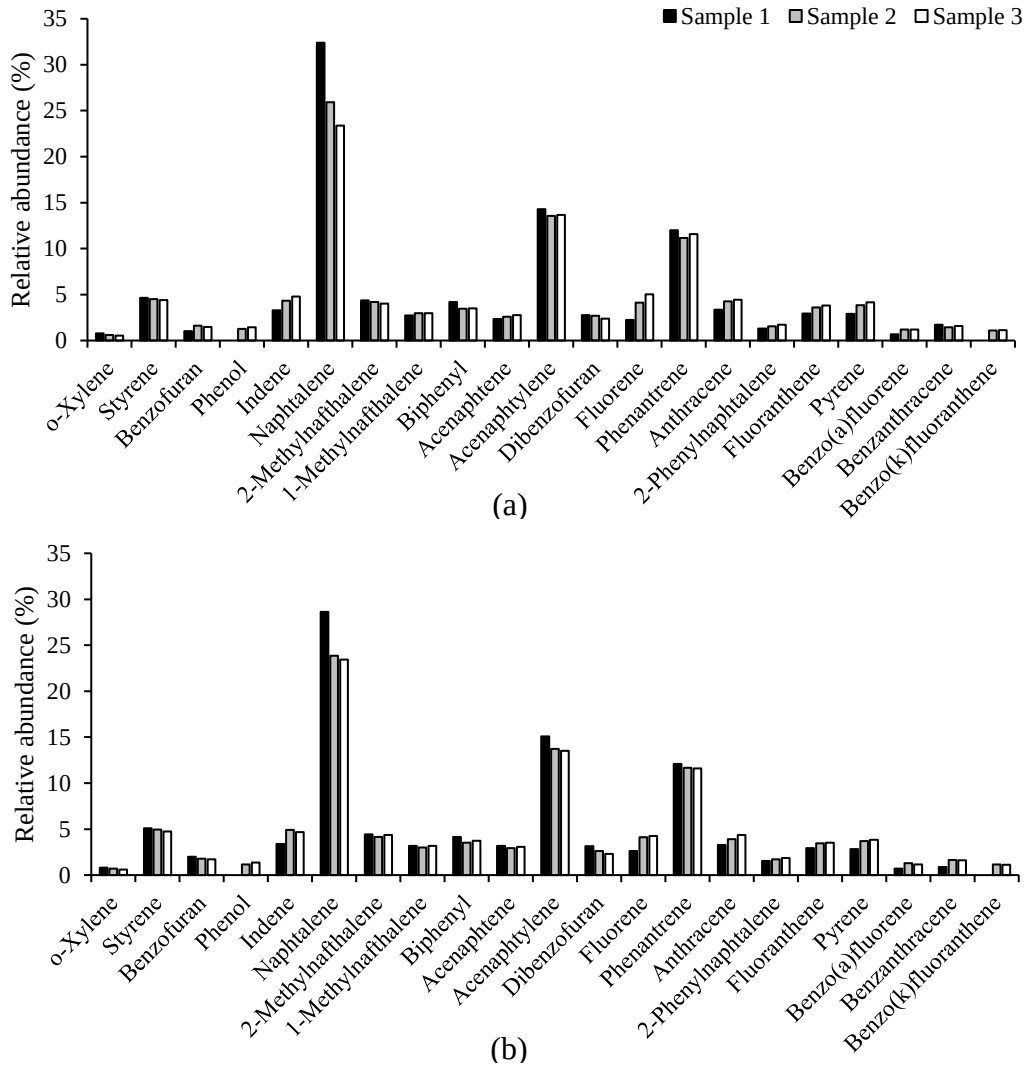

Figure 6.7: Relative abundance of tar components for the gasification tests performed at 850 ºC and ER 0.25 (a) or ER 0.30 (b).

For the tests performed at 850 ºC, the equivalence ratio did not have a clear impact in tar composition. According to Mastellone *et al.* (2010), ER has a significant effect in tar concentration but this was not observed in the present work. The heavier PAHs were detected in all tars obtained at 850 ºC, including those obtained from sample 1.

The relative abundance of naphthalene is higher for the tars obtained at 850 ºC than for the ones obtained at 800 ºC indicating that at higher temperatures the formation of more complex structures is not favored or some of the formed heavier tar components suffered secondary thermal decomposition to yield lighter PAHs and in particular naphthalene. Most of the compounds present in these tars are well known carcinogens, that pose a serious threat to the health and the well-being of humans (Abdel-Shafy and Mansour, 2016; Huang *et al.*, 2015).

6.4. Conclusions

This chapter focused on the gasification of biomass wastes pellets supplemented with RDF char. The obtained results indicated that the incorporation of RDF char in biomass pellets can be a viable pathway for the energetic valorization of this industrial waste while improving the sustainability of the solid biofuels sector. RDF torrefaction is recommended as opposed to the direct incorporation of the RDF in the biomass pellets. Torrefaction has positive effects on carbon content, calorific value, grindability and particle distribution size, which are of great importance for the subsequent gasification step. Furthermore, mixing RDF char with biomass fuels dilutes some of the more negative fuel characteristics of the RDF char (ash and chlorine contents, recalcitrant carbonaceous structure), enabling its energetic valorization in existing gasification facilities.

Overall, cold gas efficiency and producer gas lower heating values were higher for 850 ºC and a lower ER value (0.25) for the pellets with RDF char incorporation. Pellets produced only with pine waste biomass showed an opposite trend regarding temperature. Nevertheless, cold gas efficiency presented values between 42.2 and 73.5 % and producer gas lower heating values were found to be between 4.5 and 5.4 $MJ.m^{-3}$.

The increased formation of aromatic hydrocarbons associated with the RDF incorporation, indicates that more efficient gasification conditions may still improve the conversion of the fortified pellets. This could be achieved by an additional temperature increase or a supplementation of the inlet air with oxygen.

Chapter 7

Material valorization of RDF char – Use as low-cost adsorbent

Abstract

This chapter addresses the valorization of RDF char as a low-cost adsorbent for cationic species. Methylene blue (MB) was chosen as a model analyte to evaluate the removal capacity towards cationic species, in batch and column experiments. The RDF chars were tested as produced and after a pre-treatment with an alkali solution.

The characterization of the RDF char adsorbents was performed by N_2 adsorption/desorption, FT-IR, proximate and ultimate analysis as well as pH at the point of zero charge. Kinetic studies revealed that the used adsorbent followed a pseudo-second-order kinetic model. Between 3 min and 48 h, RDF char-KOH reached MB removal efficiencies in an interval of 79.5-99.9 %, whereas RDF char showed values of 10.1-88.1 %. Adsorption isotherms showed differences in the possible adsorption mechanisms of the two studied chars. Using an initial MB concentration of 800 $mg.L^{-1}$, at 293.15 K, RDF char-KOH presented a removal efficiency of 86.9% and RDF char removed 39.3 %. Furthermore, thermodynamic studies showed that the adsorption of MB onto RDF chars is spontaneous and endothermic. The capacity of the RDF char-KOH to remove the heavy metal chromium (VI) from an aqueous effluent was also evaluated in the fixed-bed column experiments. Best results were obtained for a Cr (VI) concentration of 10 $mg.L^{-1}$, reaching a removal of 47.9 % for a total effluent volume of 690 mL. Dynamic tests indicated that bed height is highly influential in the adsorption process, and the Thomas model fitted moderately onto the experimental data. This work highlighted that RDF chars may also be valorized as low-cost adsorbents, both prior to energetic applications or as an alternative application.

Keywords: RDF, char, adsorption, methylene blue, batch, fixed-bed column, chromium.

7.1. Introduction

Water pollution due to organic and inorganic compounds, such as heavy metals or dyes, is rapidly increasing mainly because of uncontrolled discharge of untreated industrial effluents into the environment (Rangabhashiyam and Balasubramanian, 2018). For instance, it has been estimated that more than 280,000 ton of untreated synthetic dyes are discharged into water bodies globally (Bharti *et al.*, 2019). Most dyes are not biodegradable and usually suppress photosynthetic activities in aquatic environments by preventing sunlight penetration. Furthermore, dyes are toxic when ingested or inhaled, they can cause skin and eye irritation and some dyes have been proven carcinogenic (Gupta and Suhas, 2009). Methylene blue (MB) is a one of the most used dyes for coloring paper, cotton, wood or silk (Manna *et al.*, 2017). It is a thiazine cationic dye and it causes some harmful effects, such as increased heart rate, cyanosis and tissue necrosis on human beings (Setiabudi *et al.*, 2016). Due to the complex structures and synthetic origin of dyes, effluents containing them are very hard to treat through conventional processes, which are costly and not always efficient towards all the dyes present in these wastewaters (López-Cervantes *et al.*, 2018).

On the other hand, heavy metals are highly persistent, and exposure to them can cause long-term health risks for humans and ecosystems (Karnib *et al.*, 2014). Chromium is one of the toxic heavy metals faced as a priority pollutant, since it is listed on the top 20 contaminants under the category of hazardous materials (Rangabhashiyam and Balasubramanian, 2018; Zhang *et al.*, 2012). Several industries like electroplating, metal polishing, leather tanning, wood preserving or chemical production generate significant amounts of wastewaters containing Cr (VI) (Chen *et al.*, 2012; Rangabhashiyam and Balasubramanian, 2018).

In recent decades, diverse techniques, such as electrochemical processes, membrane separation, coagulation or flocculation, chemical oxidation and adsorption have been employed for the remediation of wastewaters containing dyes, heavy metals or both. Adsorption has gained increased attention as a treatment because it is a very efficient technique, that operates at ambient temperature and pressure, whilst generating low amounts of residues. Adsorption is a physical–chemical treatment in which the dissolved molecule binds to an adsorbent surface by means of physical and chemical properties. Depending on the nature of the adsorbent and the origin of the dyes, different interactions may occur, such as electrostatic interactions and van der Waals forces (Postai *et al.*, 2016). Some types of adsorbent allow regeneration, a characteristic that increases the sustainability of the treatment process (Reza and Ahmaruzzaman, 2015).

Activated carbon is the most applied adsorbent in wastewater remediation of dyes and heavy metals. This adsorbent, although extremely effective, has significant drawbacks, namely its high cost that represents an economical problem. Also, most activated carbons cannot be regenerated because pore adsorption is essentially irreversible. Removal of adsorbed analytes from activated carbon can be done only by processes equivalent to the activation process itself, that are not sustainable and are more expensive than the use of virgin activated carbon and disposal of the used activated carbon as a solid waste (Gupta and Suhas, 2009).

Therefore, there is a need for the development of low cost and easily available materials to be used as adsorbents. These low-cost adsorbents should derive from locally available materials, preferably wastes with minimum processing, in order to grant economic and environmental sustainability as well as the capacity to use them in large-scale systems (Chang *et al.*, 2016; Rafatullah *et al.*, 2010).

RDF is produced in very significant amounts and not always used for its intended purpose, mostly because its fuel properties tend to be affected by the composition of the waste streams used in its production. In particular, low apparent density, low calorific value, high ash content and high chlorine content are characteristics frequently found in RDF that do not favor its energetic valorization. As such, torrefaction of this fuel has been proposed as an upgrading treatment in order to homogenize and improve its physical and chemical characteristics, enabling it to be used as a fuel or in different material applications (Białowiec *et al.*, 2017; Nobre *et al.*, 2019b, 2016).

As seen in Chapters 3 and 4, torrefaction and carbonization notoriously had a negative effect on the ash content. The mineral composition does not alter during these processes, but the yield of solid product decreases, leading to a concentration of the mineral component on the char. High ash contents can hinder energetic applications because they are related with several operational problems such as difficult disposal of the ashes or slagging and fouling phenomena in the boilers (Niu *et al.*, 2016). Due to this limitation, chars with high ash content could be regarded as potential low-cost adsorbents, as described by Correia *et al.* (2017).

Typically, torrefaction does not yield chars with high surface area, because at the operating temperatures a partial biomass decomposition occurs, but a porous structure is not developed (Mohan *et al.*, 2014). On the other hand, chars produced at moderate temperatures tend to preserve stable oxygenated functional groups, being suitable for the adsorption of organic contaminants (Ahmad *et al.*, 2014).

As detailed in Chapter 2, some works report the use of RDF char produced at temperatures higher than 500 ºC, and subjected to some kind of activation process or the use of RDF without any treatment in adsorption tests.

This chapter studied the adsorption capacity of RDF char produced at 300 ºC for 30 min, using MB and Cr (VI) as model adsorbates. The treatment of the RDF char by Soxhlet extraction with acetone and by extraction with concentrated KOH was also performed and the capacity of the treated RDF chars to remove MB was evaluated and compared with that of non-treated RDF char.

Batch adsorption experiments using non-treated RDF char and RDF char treated with KOH were applied to MB solutions and included batch equilibrium experiments with variable adsorbent dose, solution pH, contact time, MB initial concentrations and temperature. The adsorption of MB and Cr (VI) in RDF char treated with KOH, was also studied in fixed-bed column experiments, varying the adsorbent mass.

7.2. Materials and methods

7.2.1. Chemicals

Stock solutions of MB (Labchem) (Figure 7.1) and chromium VI ($K_2Cr_2O_4$, Panreac) with 1000 $mg.L^{-1}$ concentration, were prepared by dissolving an appropriate amount of each compound in distilled water. The working solutions were obtained by dilution of the stock solutions with distilled water. Fresh dilutions were performed for the study on each adsorption process. All the chemicals used in this chapter were of analytical grade.

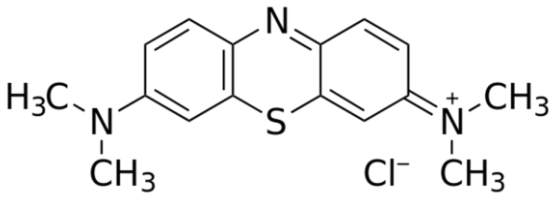

Figure 7.1: Chemical structure of methylene blue (MB).

7.2.2. Raw material

The industrial RDF sample used in this chapter (Figure 7.2) was supplied by CITRI, S.A. The RDF production process and RDF sampling procedure were identical to the detailed description given in Chapter 3.

Figure 7.2: RDF sample used in this chapter, before particle size reduction.

7.2.3. RDF char production and treatment

Lab-scale torrefaction was carried out in covered porcelain crucibles under oxygen-limited conditions using a muffle furnace (Nabertherm® L3/1106), as described in Chapter 3, for a fixed temperature of 300 ºC and a fixed residence time of 30 minutes. After torrefaction, the RDF char was milled (DeLonghi mill) and sieved to a particle diameter < 500 µm (Retsch sieve).

The produced RDF char was chemically treated in order to assess the potential of the treatments in enhancing adsorption capacity. Two treatments were applied:

1) Soxhlet extraction with acetone for a 12 h period, after which the RDF char (RDF char – Soxhlet) was air dried for 12 h, and oven dried (Memmert) at 105 ± 2 ºC for 12 h.
2) Extraction with a concentrated KOH aqueous solution was performed through an adaptation of the method described by Regmi *et al.* (2012). Briefly, 4 g of RDF char were mixed with 500 mL of 2 M KOH solution and stirred for 1 h. This mixture was filtered and the RDF char (RDF char-KOH) was recovered on qualitative filter paper. The RDF char-KOH was then mixed with distilled water and the solution pH was adjusted to 7 with HCl 1 M. Finally, the mixture was filtered and RDF char-KOH was recovered and oven dried (Memmert), at 105 ± 2 ºC, overnight.

Non-treated RDF char, RDF char-Soxhlet and RDF char-KOH were tested for their MB removal efficiency, in order to select the most effective treatment. MB removal was evaluated through an adaptation of the fast adsorption test described by Correia *et al.* (2017). Briefly, 50 mg of each char sample (in triplicate) were placed in centrifuge tubes and 10 mL of MB aqueous solution (100 $mg.L^{-1}$) was added. The tubes were shaken for 60 min (Heidolph) and after the contact time, the mixture was centrifuged at 3000 rpm for 5 min (Hettich EBA 20). The supernatant was removed by decantation and the concentration of MB dye was determined by UV–vis spectrophotometry (Pharmacia LKB-Novaspec II) at 664 nm. MB concentrations were determined using a calibration curve, constructed with several dilutions from the MB stock solution (Appendix, Figure A.14).

7.2.4. RDF char characterization

Moisture, volatile matter and ash contents were determined gravimetrically according to the procedures described in ASTM 949-88, 897-88 and 830-87, respectively. Fixed carbon (FC) was determined by difference, on a dry basis (db).

Ultimate analysis (CHNS) was performed using an elemental analyzer (Thermo Finnigan – CE Instruments Model Flash EA 112 CHNS series). Oxygen content was obtained by difference, on a dry ash free basis (daf).

High heating values (HHV) of the chars were measured in a bomb calorimeter (IKA C200), using benzoic acid as a calibration standard.

Point of zero charge pH (pH_{pzc}) was determined through pH drift tests, using a pH meter (Crimson MicropH 2001 meter). This was done by adding 10 mL NaCl solutions (0.01M) with pH values between 2 and 12 (adjusted using either HCl or NaOH, 0.1 M) to 30 mg of RDF char and shaking the mixture in an overhead agitation system (Heidolph) for 24 h at room temperature. The pH_{pzc} value was determined by plotting the final pH of the decanted solutions versus the initial pH of the NaCl solution added and extrapolating the point where $pH_{initial} = pH_{final}$ that corresponds to pH_{pzc} (Faria *et al.*, 2004). These characterization tests were performed with replicates, and the presented results correspond to average values (variation coefficient ≤ 10%).

Porosity assessment was done by nitrogen gas porosimetry (Micromeritics ASAP 2010).

Fourier transform infrared (FT-IR) spectrophotometry was used to characterize the functional groups present on the surface of chars. Solid samples were prepared using KBr pellets and data acquisition was

performed in the range of 4000–400 cm^{-1} using a Perkin-Elmer spectrophotometer (Model spectrum 1000).

7.2.5. Batch equilibrium experiments

A given amount of char was added into centrifuge tubes with 5 mL of aqueous solution of MB dye having a specific concentration and pH value. The pH of the dye solution was adjusted to the required value by adding HCl or NaOH 0.1 M (Panreac). The mixture was stirred at constant speed of 15 rpm (Heidolph), during the contact time of each experiment. The effect of operating parameters such as solution pH, adsorbent dose, contact time, MB dye concentration and temperature on the extent of dye removal have been investigated. In the case of the temperature effect, shaking at constant speed in an over-head shaker was replaced by incubation at room temperature (20ºC) or in ventilated oven (Memmert), for the temperatures of 30 ºC and 40 ºC, with periodic stirring (at each 15 min), during 15 s, using a vortex shaker (REAX top shaker). After reaching the established contact time, samples were centrifuged (Hettich EBA 20) at 3000 rpm for 5 minutes and the supernatant was analyzed using an UV-vis spectrophotometer (Pharmacia LKB-Novaspec II), as described for the fast adsorption tests. All the tests were conducted in triplicate, and the presented results correspond to average values (variation coefficient < 10 %).

- The effect of varying the adsorbent dosage in the removal of MB was tested in a range of 1 to 6 $g.L^{-1}$, for MB solutions with an initial concentration of 100 $mg.L^{-1}$, a contact time of 60 min, at the natural pH of the dye solution (6-6.5), and at room temperature.
- The effect of pH on the adsorption of MB was studied in a range from 2.0 to 10.0, with an initial MB concentration of 100 $mg.L^{-1}$, a contact time of 60 min, an adsorbent dosage of 5 $g.L^{-1}$, and at room temperature.
- The effect of contact time was determined for contact times between 3 minutes and 48 hours, with an initial MB concentration of 100 $mg.L^{-1}$, adsorbent dosage of 5 $g.L^{-1}$, without pH adjustment and at room temperature.
- The effect of the initial dye concentration and temperature were evaluated for MB concentrations of 100, 200, 400 and 800 $mg.L^{-1}$ and for temperatures of 293.15, 303.15 and 313.15 K. Adsorbent doe was 5 $g.L^{-1}$, contact time was 24 h (to ensure equilibrium) and there was no pH adjustment.

The adsorption capacity, q ($mg.g^{-1}$), of the RDF char was calculated according to equation 7.1:

$$q\ (mg.g^{-1}) = \frac{(C_0 - C_f)V}{m} \qquad \text{Equation 7.1}$$

Removal efficiency, R (%), was determined according to equation 7.2:

$$R(\%) = \frac{(C_0 - C_f)}{C_0} \times 100 \qquad \text{Equation 7.2}$$

where C_0 and C_f are the initial and final dye concentrations ($mg.L^{-1}$), respectively, V is the volume of the solution (L), and m is the adsorbent mass (g).

In order to assess the adsorption reaction kinetics, two mathematical models (pseudo-first order and pseudo-second order) were applied to the experimental data. The equations corresponding to these models are the following:

Pseudo-first order: $log(q_e - q_t) = log(q_e) - \frac{k_1 t}{2.303}$ Equation 7.3

where q_e and q_t are the amounts of dye adsorbed ($mg.g^{-1}$) at equilibrium and at time t (min), respectively, and k_1 is the rate constant of adsorption (min^{-1}) (Bulut and Ayd, 2006).

Pseudo-second order: $\frac{t}{qt} = \frac{1}{k_2 q_e^2} + \frac{t}{q_e}$ Equation 7.4

where k_2 represents the second-order constant ($g.mg^{-1}.min^{-1}$), q_e is the amount of dye adsorbed at equilibrium ($mg.g^{-1}$) (Bulut and Ayd, 2006). h_0 is the initial adsorption rate ($mg.g^{-1}.\ min^{-1}$), which was calculated through k_2 and q_e as reported by Tovar-Gómez *et al.* (2012):

$h_0 = k_2 q_e^2$ Equation 7.5

Adsorption isotherms were studied using the data obtained at different MB concentrations and different temperatures. Three isotherm adsorption models (Langmuir, Freundlich, Temkin) were tested in order to elucidate the adsorption mechanisms. The linearized equations corresponding to these isotherms are the following:

Langmuir $\frac{C_e}{q_e} = \frac{C_e}{q_{máx}} + \frac{1}{K_L q_{máx}}$ Equation 7.6

where C_e is the concentration of dye at equilibrium in solution ($mg.L^{-1}$), q_e is the amount of MB adsorbed per unit mass of adsorbent at equilibrium ($mg.g^{-1}$), $q_{máx}$ is the maximum dye uptake, giving the information about adsorption capacity for a complete monolayer (mg/g) and K_L is a constant regarding the energy of adsorption and affinity of the binding sites ($L.mg^{-1}$) (Zhang *et al.*, 2013).

Freundlich $ln(q_e) = ln(K_f) + \frac{1}{n} ln(C_e)$ Equation 7.7

where 1/n is the Freundlich coefficient and K_F is the Freundlich constant ($mg.g^{-1}$) and both parameters give an indication of adsorption intensity and capacity, respectively (Pathania *et al.*, 2017).

Temkin $q_e = \frac{RT}{b} ln(K_T) + \frac{RT}{b} ln(C_e)$ Equation 7.8

where R is the universal gas constant ($8.314\ J.mol^{-1}.K^{-1}$), T is temperature (K), K_T is Temkin isotherm equilibrium binding constant ($L.g^{-1}$) and B_T is a constant related to heat of adsorption ($J.mol^{-1}$) corresponding to $\frac{RT}{b}$, where b corresponds to Temkin isotherm constant (Zhu *et al.*, 2018).

The thermodynamic parameters were determined according to the thermodynamic laws through the following equations (Tran *et al.*, 2016):

$\Delta G = -RTln(K_c)$ Equation 7.9

where ΔG is the Gibbs free energy (J.mol^{-1}) and Kc is a dimensionless constant involving the ratio between q_e in mg.L^{-1} and C_e also in mg.L^{-1}.

$$\Delta G = \Delta H - T\Delta S \quad \text{Equation 7.10}$$

where ΔH represents enthalpy change (J.mol^{-1}) and ΔS represents entropy change (J.mol^{-1}.K). By substituting Equation 7.9 into 7.10, comes the van´t Hoff equation, as follows:

$$ln(K_c) = \frac{-\Delta H}{R} \times \frac{1}{T} + \frac{\Delta S}{R} \quad \text{Equation 7.11}$$

7.2.6. Fixed-bed column adsorption experiments

7.2.6.1. Methylene blue

Continuous adsorption experiments in a fixed-bed column were conducted with the char that exhibited a better performance in the batch studies (RDF char-KOH). Tests were done in a glass column (1 cm diameter and 14 cm height), packed with a known quantity of adsorbent. Before adsorption the column was conditioned with distilled water and the tests were conducted at room temperature. A solution of MB (100 mg.L^{-1}) was pumped in down flow mode at a fixed flow rate using a peristaltic pump (2.5 mL.min^{-1}). Samples were collected at fixed volumes of 20 mL. The effect of bed height (adsorbent mass) was studied. Breakthrough curves were established by plotting C_t/C_o versus effluent volume (mL), where C_t is the effluent MB dye concentration and C_o is MB influent dye concentration. Breakthrough time corresponded to the time at which C_t/C_o equals 0.05 and exhaustion time corresponds to C_t/C_o equal to 0.95(Kumar and Jena, 2016).

Effluent volume, V_{eff} (mL), was calculated from the following equation (Chen *et al.*, 2012):

$$V_{eff} = Q.t_{exhaustion} \quad \text{Equation 7.12}$$

where Q is the flow rate (mL.min^{-1}) and $t_{exhaustion}$ is exhaustion (min).

The total amount of methylene blue retained in the column (mg), was determined using equation 7.13 (Khadhri *et al.*, 2019):

$$q_{total} = \frac{QA}{1000} = \frac{Q}{1000}\int_{t=0}^{t=t_{exhaustion}} C_{ad}dt \quad \text{Equation 7.13}$$

where A is the area above the breakthrough curve, C_{ad} (mg.L^{-1}) is the adsorbed concentration. C_{ad} corresponds to adsorbed dye concentration (mg.L^{-1}) and was calculated by equation 7.14:

$$C_{ad} = C_0 - C_t \quad \text{Equation 7.14}$$

W_{total}, corresponds to the total amount of adsorbate sent to the column (mg) until saturation point, and was calculated by equation 7.15 (Khadhri *et al.*, 2019):

$$W_{total} = \frac{C_0 Q t_{exhaustion}}{1000}$$ Equation 7.15

The equilibrium uptake q_{eq} (mg.g^{-1}) or maximum capacity of the column was calculated by equation 7.16 (Khadhri *et al.*, 2019):

$$q_{eq} = \frac{W_{total}}{m}$$ Equation 7.16

where m is the dry weight of adsorbent in the column (g).

The total amount of dye removed - R (%) was calculated using the following equation (Khadhri *et al.*, 2019):

$$R(\%) = \frac{q_{total}}{W_{total}} \times 100$$ Equation 7.17

According to Chen *et al.* (2012), the flow rate represents the empty bed contact time - EBCT (min) in the column, as seen in equation 7.18:

$$EBCT = \frac{\pi r^2 Z}{Q}$$ Equation 7.18

where $\pi r^2 Z$ represents the volume of the bed and Z is bed height (cm).

The length of the mass transfer zone (cm) (MTZ) was calculate according to equation 7.19 (Fernandez *et al.*, 2014):

$$MTZ = Z\left(1 - \left(\frac{t_{breakthrough}}{t_{exhaustion}}\right)\right)$$ Equation 7.19

where $t_{breakthrough}$ is breakthrough time (min).

Breakthrough curve modelling was done using the Thomas model, in its linearized form, as represented in equation 7.20 (Chen *et al.*, 2012):

$$ln\left(\frac{C_0}{C_t} - 1\right) = \frac{k_{TH} q_0 m}{Q} - k_{TH} C_0 t$$ Equation 7.20

where k_{TH} is the Thomas rate constant (ml.min^{-1}.mg^{-1}).

7.2.6.2. Chromium (VI)

RDF char-KOH was also tested for the adsorption of chromium (VI), using a 10 mg.L^{-1} aqueous solution, prepared from $K_2Cr_2O_4$ (Panreac) and adjusted to pH=2 to avoid metal precipitation.

Chromium adsorption was conducted in a glass column (1 cm diameter and 14 cm height), packed with a specific adsorbent amount (0.500 g). The adsorption procedure was identical to the one described in Section 7.2.6.1. Measurement of Cr (VI) concentrations was done through the standard colorimetric method for Cr (VI) using 1,5- diphenylcarbohidrazide using a UV–vis spectrophotometer (Pharmacia LKB-Novaspec II) at 540 nm (Zhang *et al.*, 2012). Calculations were done through a calibration curve, constructed with several dilutions from the $K_2Cr_2O_4$ stock solution, after being submitted to the same reaction as the samples (Appendix, Figure A.15).

7.3. Results and discussion

7.3.1. Adsorbent selection and characterization

The removal efficiencies of the RDF char and the treated chars (RDF char-Soxhlet and RDF char-KOH) are presented in Figure 7.3, and compared with the removal efficiency of a commercial activated charcoal.

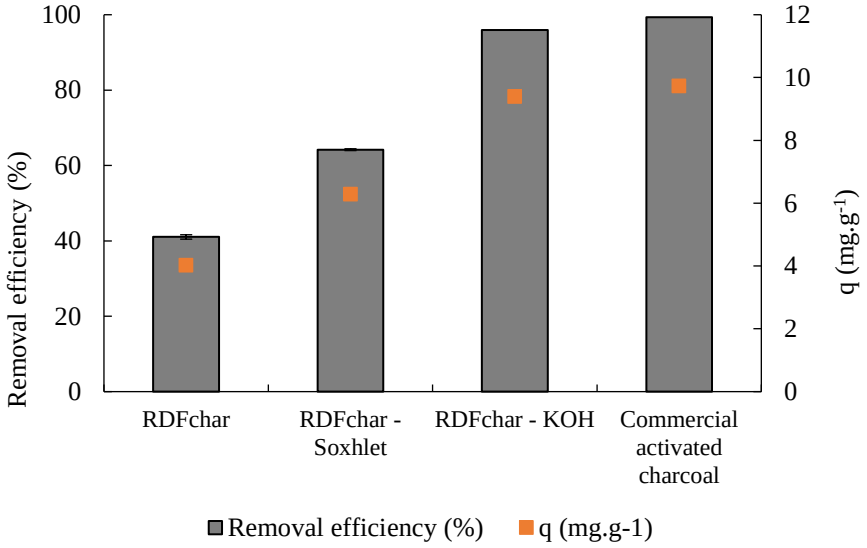

Figure 7.3: Results for the quick adsorption test for adsorbent selection.

Both activation processes had a positive effect in the char removal efficiency towards MB, indicating that the removal of organic and inorganic products adsorbed in the char surface is essential to increase the availability of pores or functional groups for MB adsorption to occur at a greater extension. Nevertheless, only RDF char-KOH was able to present a removal efficiency closer to that of activated carbon, removing around 95.9 % of the dye present in the solution. The basic treatment, when compared with the solvent extraction, removed tars (that were deposited in the surface of the char) more extensively, thus promoting a more pronounce removal of MB molecules. The RDF char with no treatment presented a removal efficiency of only 41.0 %, but the study of its adsorption capacity, is still interesting since production costs and environmental impacts are only related with the torrefaction process, whereas the activated chars have further energy requirements associated with cleaning treatment, that also generates large volumes of contaminated effluents. More detailed char characterization tests and MB adsorption studies were therefore conducted with the RDF char-KOH and the non-treated RDF char.

Results for the characterization of RDF char and RDF char-KOH are shown in Table 7.1.

Table 7.1: Proximate analysis, elemental analysis, high heating value (HHV) and pH_{pzc} results for the RDF char and RDF char-KOH.

Parameter	Unit	RDF	RDF char	RDFchar-KOH
Moisture	wt.%, ar[a]	7.0	1.7	1.2
Volatile matter		76.1	61.1	63.7
Ash	wt.%, db[b]	10.7	21.9	23.5
Fixed carbon		13.2	17.0	12.8
C		38.2	59.7	66.8
H		5.2	6.0	6.5
N	wt.%, daf[c]	2.3	1.1	1.4
S		0.4	0.2	0.0
O		53.9	33.0	25.3
O/C		1.06	0.4	0.3
H/C		1.63	1.2	1.2
HHV	$MJ.kg^{-1}$, db	15.9	17.2	19.6
pHpzc		---	6.5	6.8
Surface $area_{BET}$	$m^2 \cdot g^{-1}$		4.049	4.265

[a]ar, as received basis;[b]db,dry basis; [c]daf, dry ash free basis.

As expected with torrefaction, moisture content decreased significantly from the original RDF to the produced char. Torrefaction is known for enhancing the hydrophobic characteristics of materials, making them more resisting to biological degradation and storage due to water removal (Wilk *et al.*, 2015).

The increase in fixed carbon content is a result of the devolatilization process and hence the decrease in the amount of volatile matter (Weber and Quicker, 2018). As fixed carbon is determined by difference from the other proximate analysis parameters, it increased significantly from the original RDF (13.26 wt.%) to sample RDF char (16.97 wt.%). The treatment with KOH decreased moisture, volatile matter and fixed carbon and increased ash content relatively to the non-treated char. This indicates that the basic treatment probably removed some tars from the surface of the char but some retention of K^+ or OH^- ions by adsorption or reaction may also occur (Regmi *et al.*, 2012).

As seen in Table 7.3 both chars presented ash values above 20 wt.%, a characteristic that is not favorable to their energetic valorization. Nonetheless, high ash is not relevant for adsorption applications and can even contribute to greater efficiencies in pollutant removal (Buah and Williams, 2010).

Carbon and hydrogen contents increased markedly, whereas nitrogen, sulphur and oxygen decreased with the torrefaction treatment. The treatment with KOH further increased the concentration of carbon and hydrogen mainly at the expense of oxygen reduction, indicating that the extraction with aqueous KOH selectively dissolved oxygenated compounds which is expectable since those compounds are more polar than hydrocarbons. The KOH treatment also decreased nitrogen and sulphur concentrations in the RDF char-KOH, a positive effect regarding fuel applications.

Both chars presented low O/C and H/C ratios when compared to the original RDF, and these reductions are mainly caused by water release and partial elimination of oxygen by decarboxylation, decarbonylation and dehydration reactions that occur during the torrefaction process (Bergman *et al.*, 2005). The deoxygenation effect associated with the treatment with KOH is reflected in the decrease of O/C ratio and increase of HHV that was observed for the RDF char-KOH when compared to the non-treated char.

The surface of adsorbents may contain both negatively and positively charged sites, depending on the pH of the medium. According to the pH_{pzc} concept, at $pH > pH_{pzc}$ the surface becomes negatively charged favoring the adsorption of cationic species while adsorption of anionic species will be favored

at pH < pH_{pzc} (Faria *et al.*, 2004). As such it is expected that the adsorption of cationic MB will be favored by electrostatic interactions, for both chars at higher pH (above 6.5), given their pHpzc values.

The specific surface areas of the RDF char and RDF char-KOH were determined based on the nitrogen adsorption at 77 K (Figure 7.4).

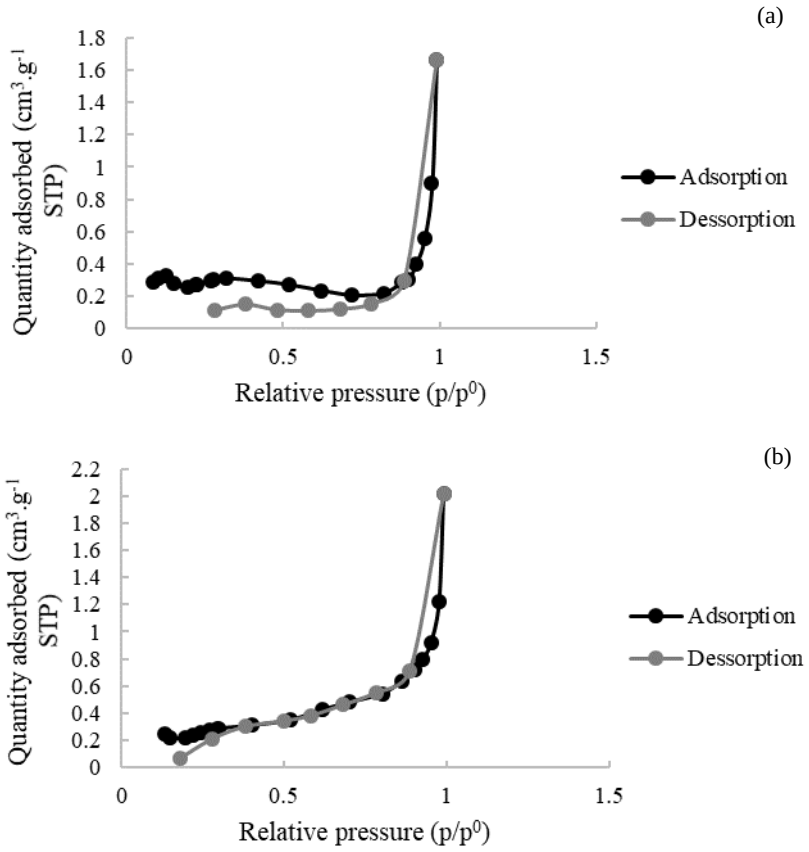

Figure 7.4: N_2 adsorption–desorption isotherms of: (a) RDF char and (b) RDFchar-KOH.

Collected data suggests that these chars present type II isotherms (according to IUPAC classification), characterized by multilayer adsorption, that is typical of non-porous or microporous solids (Thommes *et al.*, 2015). The BET surface area of sample RDF char was 4.049 $m^2.g^{-1}$, whereas sample RDF char-KOH presented a value of 4.265 $m^2.g^{-1}$. These are very low surface area values, corroborating the absence of a porous structure, but the slightly higher value obtained for the RDF char-KOH indicates that there was a slight improvement of adsorption capacity by removal of adsorbed species. Some low-cost adsorbents like lotus leaf (Han *et al.*, 2011) also presented low values for BET surface areas. The BET surface area, evaluated by N_2 adsorption, relates to the capacity of adsorption in porous structures but may not reflect the capacity of adsorbing organic contaminants, such as MB, with much larger molecular size and different dipole moment characteristics (Zhu *et al.*, 2018). Furthermore, the development of a porous structure by thermal/physical activation methods entails expenses and environmental impacts which would hinder the entire concept of sustainable and low-cost adsorbents (Hadjittofi *et al.*, 2014)

FT-IR data can elucidate the nature of the functional groups at the surface of the char which, given the lack of porosity of these chars, may influence their adsorption behavior. The infrared spectra of RDF char and RDF char-KOH is presented in Figure 7.5. Both chars showed a significant number of absorption peaks. These chars are produced from a waste derived fuel comprising significantly different materials and this observation corroborates the complexity of these samples.

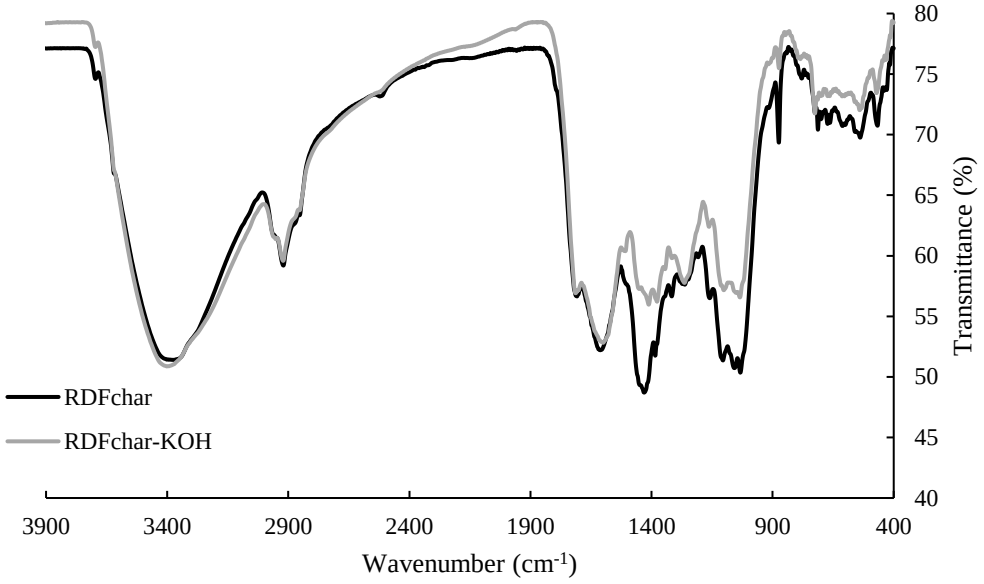

Figure 7.5: FT-IR spectra for the adsorbents used in this work (RDF char, and RDF char-KOH).

There is a broad band located at 3371.18 cm^{-1} (RDF char) and 3401.33 cm^{-1} (RDF char-KOH) attributed the stretch vibration of bonded hydroxyl groups on the surface of chars. The broad absorption peak at 2920.28 cm^{-1} (RDF char) and 2921.01 cm^{-1} (RDF char-KOH) was attributed to the asymmetrical stretch vibration of methyl groups (Coates, 2000). Typical C=O stretching in non-aromatic carboxyl groups was found at 1707.69 cm^{-1} (RDF char) and at 1713.36 cm^{-1} (RDF char-KOH) (Das *et al.*, 2015). Bands around 1600 cm^{-1} were assigned to C=C stretching of aromatic rings, specifically at 1611.80 cm^{-1} for the RDF char and 1600.04 cm^{-1} for RDF char-KOH (Das *et al.*, 2015). These first bands presented approximately the same intensity for both chars.

The peak at 1430.83 cm^{-1} was more intense for the RDF char than it was for the RDF char-KOH and it can be associated with a -COO- asymmetric vibration of carboxylic groups (Bedin *et al.*, 2016). Bands located at 1384.56 cm^{-1} (RDF char) and 1377.22 cm^{-1} (RDF char-KOH) were assigned to O–H bending in phenols or asymmetrical C–H bending in CH_3 groups (Coates, 2000). The band at 1264.11 cm^{-1} exists only in sample RDF char-KOH and is attributed to Aryl–O stretching in aromatic ethers in lignin (Correia *et al.*, 2017). Bands around 1105.24 cm^{-1} and 1033.21 cm^{-1} (RDF char) that were more intense for the char without basic treatment, indicate the presence of C-O single bonds, such as the ones existing in alcohols, phenols, acids, ethers or esters (Bedin *et al.*, 2016).

Lastly, the final bands found between 800 – 700 cm^{-1} were more intense for the sample RDF char, and can be assigned to C-H and $CH=CH_2$ stretching vibrations in aromatic structures (Li *et al.*, 2011). The results of the FT-IR analysis indicated that a large number of carboxylic and hydroxyl groups were included on the surface of both chars, and these groups have the potential to be active sites for interaction with the studied cationic dye.

7.3.2. Batch equilibrium experiments

7.3.2.1. Effect of pH

Effect of solution initial pH on MB adsorption onto RDF char and RDF char-KOH was examined, and the results are illustrated in Figure 7.6.

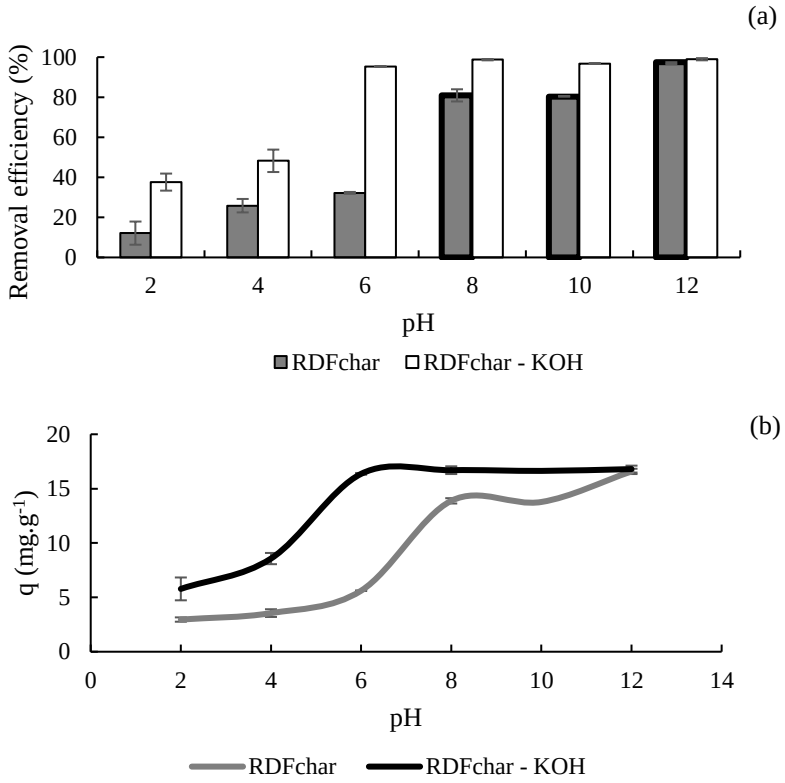

Figure 7.6: Influence of solution initial pH on MB adsorption onto RDF char and RDF char-KOH. (a) Removal efficiency, (b) Amount adsorbed, q. (MB concentration = 100 $mg.L^{-1}$; Contact time = 60 min; Adsorbent dosage = 5 $g.L^{-1}$).

RDF char-KOH shows a high adsorption capacity of MB from pH 6 to pH 12, with removal efficiencies starting at 95.3 % (q=16.4 $mg.g^{-1}$) reaching 99.0 % at pH 12 (q = 16.8 $mg.g^{-1}$). For RDF char, a significant increase in removal efficiency is shown between pH 8 (80.9 %) and pH 12 (97.5 %), and at the highest pH both chars have comparable removal efficiencies (97.5 % for RDF char and 99.0 % for RDF char-KOH).

From pH 6.8 forward, MB solution pH is higher than the pHpzc of both chars, so the chars, when in contact with MB solution at that pH range will be negatively charged, contributing to an increased removal efficiency. Nevertheless, pH adjustments require expenditure of acid or base in order to achieve the desired pH, which can represent an extra cost for the adsorption process. As such, further tests were always performed without pH adjustment.

7.3.2.2. Effect of adsorbent dose

Increasing the adsorbent dosage increased the removal efficiency for both tested chars, as expected by the higher availability of adsorption sites (Figure 7.7).

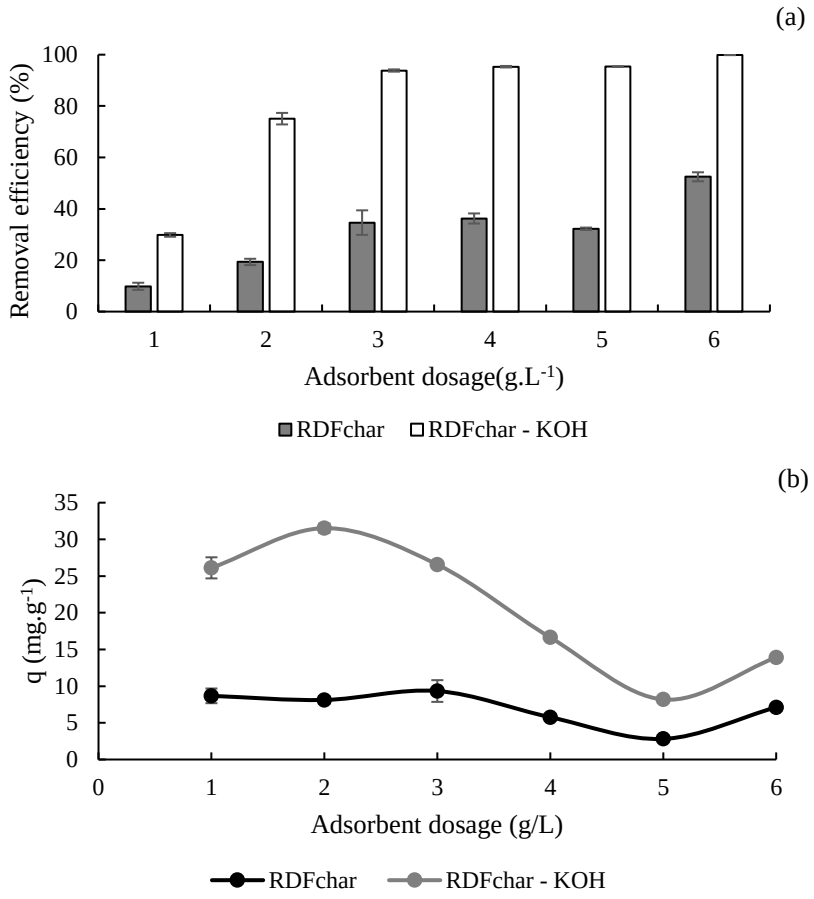

Figure 7.7: Influence of adsorbent dose on MB adsorption onto RDFchar and RDFchar-KOH. (a) Removal efficiency, (b) Amount adsorbed, q. (MB concentration = 100 mg.L^{-1}; no pH adjustment; Contact time = 60 min.).

RDF char-KOH had removal efficiencies higher than 80 % for adsorbent doses higher than 3 g.L^{-1}, while the non-treated RDF char only presented a removal efficiency higher than 50 % for an adsorbent dose of 6 g.L^{-1}. The increase of removal efficiency with the adsorbent mass can be ascribed to the increased surface area and availability of more adsorption sites (Kallel *et al.*, 2016; Mahmoud *et al.*, 2012). But, further increasing the adsorbent dose above a given value may have no improvement effect on the removal efficiency, either because 100 % removal is achieved or because the adsorption mechanism is reversible and desorption starts to occur. Considering the analyte concentration in the char, as can be seen in Figure 7.7b, it decreased for both chars for adsorbent doses higher than 3 g.L^{-1} regardless of the increase of removal efficiency, indicating an incomplete occupation of the adsorption sites. This behavior has also been described by Han *et al.* (2011) using lotus leaf as an adsorbent, and by Reddy *et al.* (2015) using corn cob.

7.3.2.3. Effect of contact time

It can be seen from Figures 7.8a and 7.8b that the removal efficiency, as well as the amount of dye adsorbed, increased with increasing contact time, until reaching a plateau from 4 h to 48 h in the case of the RDF char-KOH and from 24 h to 48 h for the RDF char. This stabilization is related with a state of dynamic equilibrium where the amount of adsorbed dye is in equilibrium with the dye still present in

the solution (Mahamad *et al.*, 2015). Furthermore, RDF char-KOH seemingly reaches equilibrium faster (~ 6 h) than RDF char (~24 h).

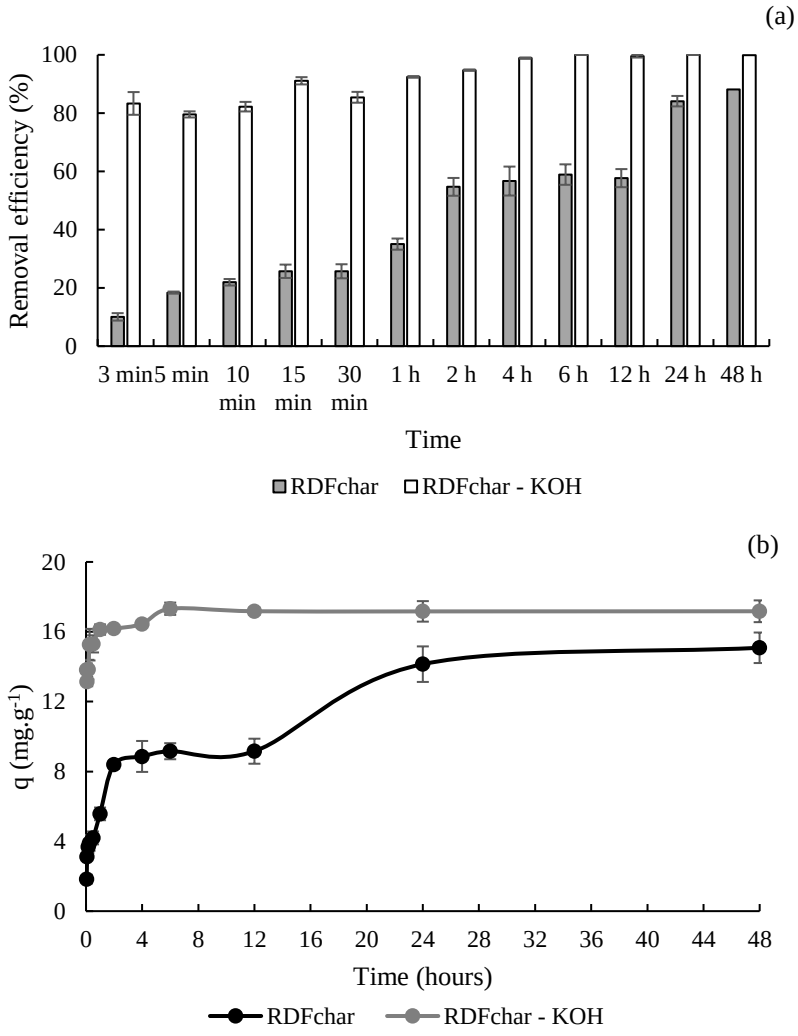

Figure 7.8: Influence of contact time on MB adsorption onto RDF char and RDF char-KOH. (a) Removal efficiency, (b) Amount adsorbed, q. (Adsorbent dosage = 5 $g.L^{-1}$; MB concentration = 100 $mg.L^{-1}$; no pH adjustment; room temperature).

The different MB adsorption capacities of these two RDF chars is clearly elucidated by their behaviors at lower contact times (from 3 min to 1h): the MB removal efficiency varied from 10.1 to 92.4 % for the non-treated RDF char and was in the range of 79.5 to 92.4 % for the RDF char-KOH.

Kinetic study

In order to analyze the adsorption kinetics of MB onto RDF char and RDF char-KOH, the pseudo-first-order (Equation 7.3) and the pseudo-second-order (Equation 7.4) models were applied to the experimental data.

For the pseudo-first-order model, the values of k_1 and q_e were obtained from the slope and intercept, respectively, of plots of log ($q_e - q_t$) versus t (Figure 7.9a). For the pseudo-second-order model k_2 and q_e were calculated from the slope and intercept in the plot of t/qt versus t (Figure 7.9b).

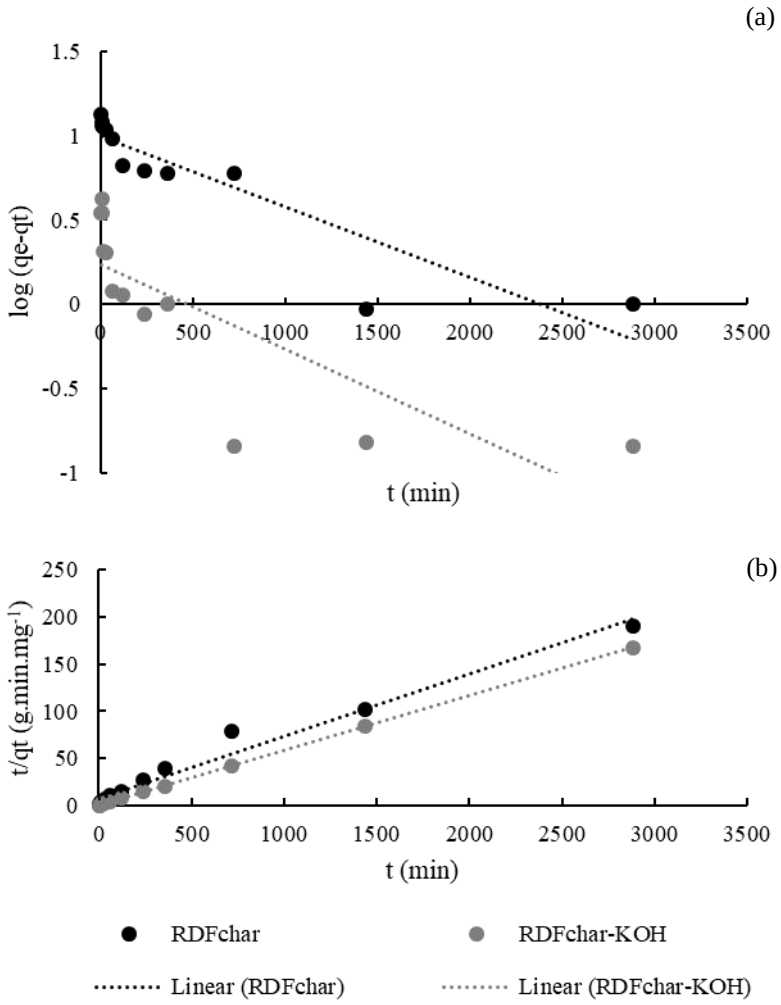

Figure 7.9: Adsorption kinetics of MB onto RDF char and RDF char-KOH: (a) Pseudo-first-order model and (b) Pseudo-second-order model.

As it can be seen from Table 7.2, the pseudo-first-order model cannot adequately describe the adsorption behavior of the RDF chars, since the calculated q_e values did not agree with the experimental ones, and the regression coefficient (R^2) was considered low (0.8309 for RDF char and 0.6362 RDF char-KOH). The pseudo-second-order model fitted the experimental data better, and enabled the calculation of q_e values with differences of 0.6 % comparing with the experimental ones. R^2 values obtained for the pseudo-second-order model were above 0.97 for both tested chars (0.9777 for RDF char and 1.000 for RDF char-KOH) reflecting a good adjustment between calculated values and experimental data. Similar results have been obtained for MB adsorption onto different low-cost adsorbents, like defatted algal biomass (Chandra *et al.*, 2015), date palm leaves (Gouamid *et al.*, 2013), almond gum (Bouaziz *et al.*, 2015), garlic straw (Kallel *et al.*, 2016) or soursop and sugarcane (Meili *et al.*, 2018).

Table 7.2: Kinetic parameters for the adsorption of MB onto RDF char and RDF char-KOH.

Kinetic model	Sample	
	RDFchar	RDFchar-KOH
$q_{e\ (experimental)}$ ($mg.g^{-1}$)	15.08	17.32
Pseudo-first order		
k^1 (min^{-1})	-0.0009	-0.0012
q_e ($mg.g^{-1}$)	2.6988	1.2687
R^2	0.8309	0.6362
Pseudo-second order		
k^2 ($g.mg^{-1}.min$)	0.0006	0.0186
q_e ($mg.g^{-1}$)	15.1745	17.2117
h_0 ($mg.g^{-1}.min$)	0.1307	5.5157
R^2	0.9777	1.0000

According to Ho and McKay (1999), when the adsorption data can be described by a pseudo-second-order model the adsorption mechanism is probably chemisorption involving electrostatic forces or bond forming through partition or exchange of electrons between adsorbent and adsorbate. This affirmation can also be related with the FT-IR data discussed in section 7.3.1., since the FT-IR spectra revealed the existence of several functional groups on the surface of the RDF char adsorbents that have potential to be involved in chemical interactions with ionized dye molecules. The influence of the pH on the removal efficiency is also an indication of charge-related interactions between the analyte (MB) and the RDF chars.

7.3.2.4. Effect of initial dye concentration and temperature

Figures 7.10 and 7.11 show the effect of the initial MB concentrations and temperature on the dye removal efficiency and on the amount of dye adsorbed by RDF char (Figure 7.10a and 7.11a) and RDF char-KOH (Figure 7.10b and 7.11b).

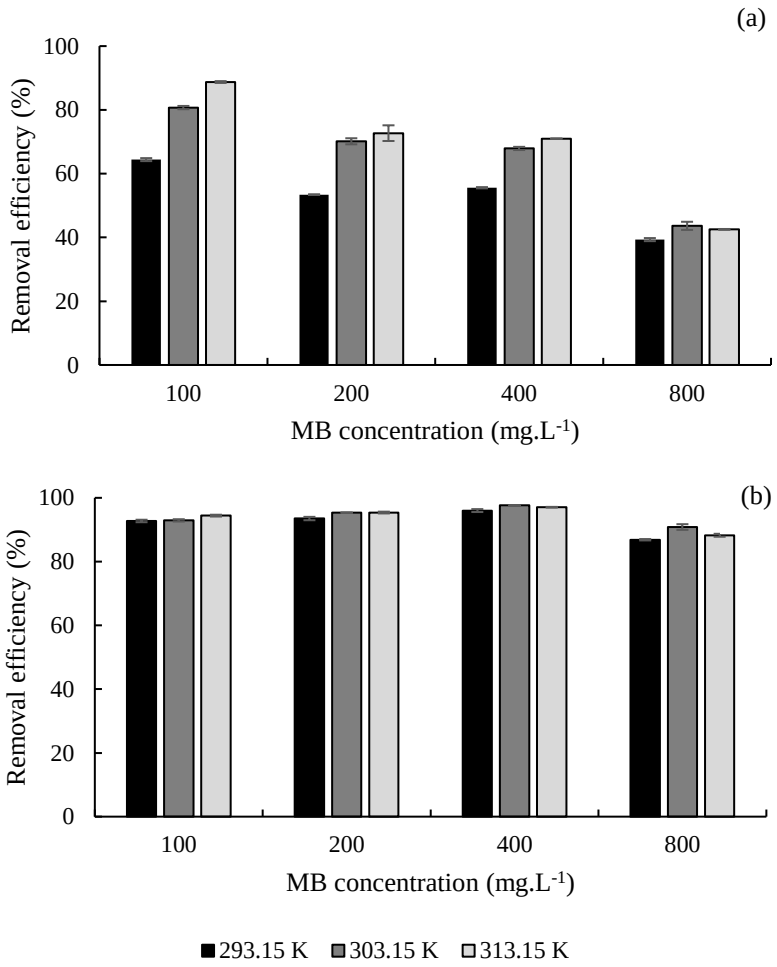

Figure 7.10: Influence of initial MB concentration and temperature on MB adsorption removal efficiency onto: (a) RDF char and (b) RDF char-KOH.

Removal efficiency increased with temperature for both chars but especially for the non-treated RDF char. This is an indication that the adsorption process has an endothermic nature (Cherifi *et al.*, 2013). According to Han *et al.* (2011), increased removal at higher temperature could be related with the activation energy necessary to establish bonds between MB and the active sites of the chars, that is more available at higher temperatures.

According to Bouaziz *et al.* (2015) initial dye concentration provides a driving force to overcome mass transfer resistance of the molecules between the aqueous and solid phases. Results show that increasing MB concentration from 100 $mg.L^{-1}$to 800 $mg.L^{-1}$ decreased removal efficiency for the RDF char, from 64.4 to 39.3 % at 20 ºC and from 88.7 to 42.5 % at 40 ºC, an evidence of the limited capacity of this char to remove MB from the aqueous solution. The MB removal efficiency of the RDF char-KOH, increased when MB initial concentration increased from 100 $mg.L^{-1}$ to 400 $mg.L^{-1}$ and only decreased when dye concentration reached 800 $mg.L^{-1}$. Furthermore, the MB removal efficiencies of RDF char-KOH were always higher than 86 % for all MB concentrations and temperatures tested. The reduction in removal efficiency at higher MB concentrations is largely due to saturation at the surface of the adsorbent (Othman *et al.*, 2018) and this saturation occurs at a significantly lower concentration (100 $mg.L^{-1}$) for the sample RDF char than for the sample RDF char-KOH (800 $mg.L^{-1}$). The amount of MB in the char (q, $mg.g^{-1}$) as represented in Figure 7.11, increased for both chars as the MB concentration increased, especially for 400$mg.L^{-1}$ and 800 $mg.L^{-1}$.

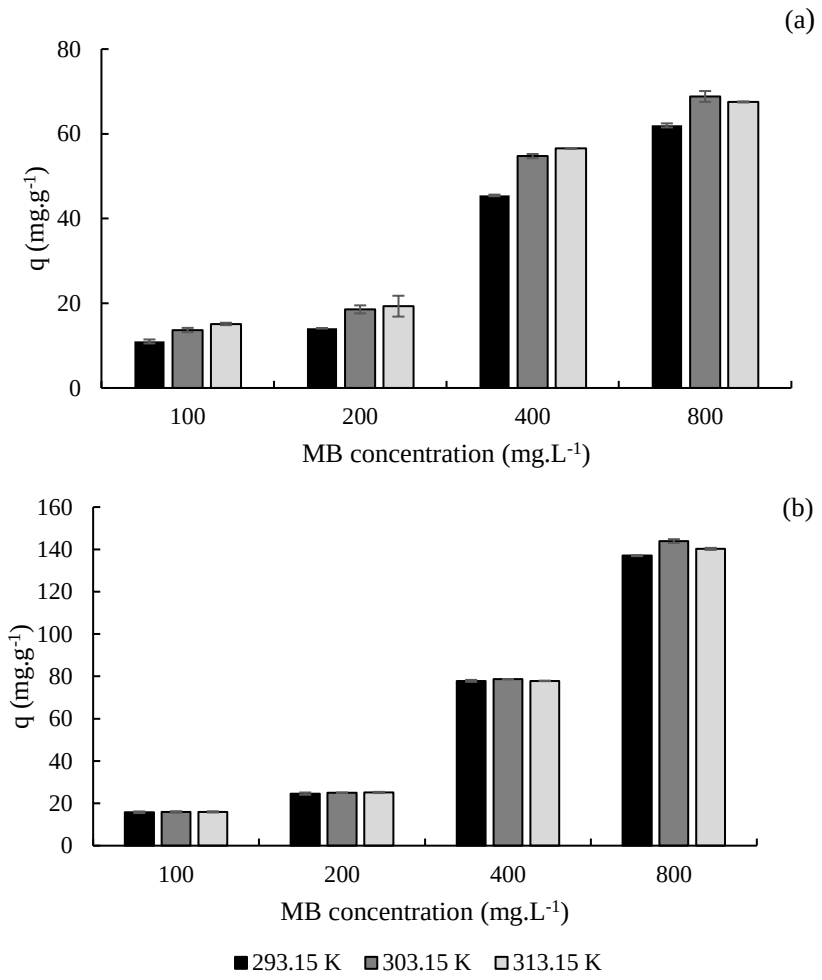

Figure 7.11: Influence of initial MB concentration and temperature on amount of MB adsorbed onto: (a) RDF char and (b) RDF char-KOH.

Maximum MB concentration in the non-treated RDF char was 68.8 $mg.g^{-1}$, obtained at 30 ºC for an MB initial concentration of 800 $mg.L^{-1}$, while for the RDF char-KOH the highest MB amount in the char was of 143.9 $mg.g^{-1}$, also obtained at 30 ºC and the same MB initial concentration. These results indicate that although presenting similar adsorption mechanisms, the two chars have surfaces with different functionalities, which translates into a higher capacity of the RDF char-KOH to adsorb MB.

Isotherm study

The nature of the interaction that is established between the MB molecules and the adsorbents can be understood from the adsorption isotherms. According to Narvekar *et al.* (2018) an adsorption isotherm refers to a graphic relating the amount of substance that is adsorbed to the equilibrium concentration of the adsorbate molecules in the solution, in this case MB, at a specified temperature. The obtained data were fitted using three isotherms models, namely, Langmuir (Equation 7.7), Freundlich (Equation 7.8) and Temkin (Equation 7.9).

The Langmuir adsorption isotherm assumes that adsorption takes place at specific homogeneous sites within the adsorbent and the adsorption of each molecule onto the surface has equal adsorption activation energy (Bulut and Ayd, 2006). The results of data fitting onto Langmuir isotherm are shown in

Figure 7.12 and Table 7.3. Values of K_L and q_m were obtained from the intercept and the slope of the plot of C_e/q_e against C_e, respectively.

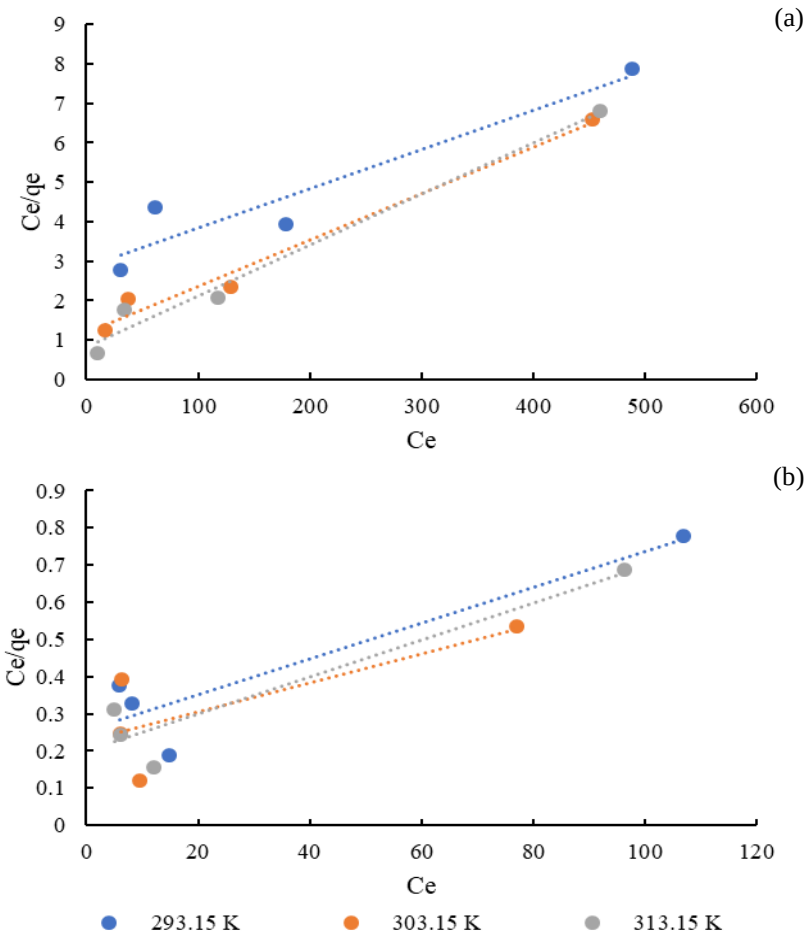

Figure 7.12: Langmuir isotherms of MB dye adsorption onto (a) RDFchar and (b) RDFchar-KOH. MB concentrations =100, 200, 400 and 800 mg.L^{-1}, T= 293.15, 303.15, 313.15 K, contact time = 24 h, adsorbent dosage = 5g.L^{-1}, no pH adjustment.

Table 7.3: Model parameters estimated for the Langmuir adsorption isotherm of MB onto RDF char and RDF char-KOH, for concentrations between 100-800 mg.L^{-1}, and temperatures 293.15 K, 303.15 K and 313.15 K.

Isotherm parameters		Sample					
		RDF char			RDF char-KOH		
		293.15 K	303.15 K	313.15 K	293.15 K	303.15 K	313.15 K
K_L (L.mg^{-1})		0.004	0.010	0.016	0.006	0.007	0.006
$q_{máx}$ (mg.g^{-1})		100.000	84.746	76.923	208.333	256.410	204.082
R_L	100 mg.L^{-1}	0.0318	0.0556	0.0916	0.144	0.138	0.167
	200 mg.L^{-1}	0.0160	0.0257	0.0284	0.110	0.140	0.140
	400 mg.L^{-1}	0.0160	0.0077	0.0084	0.064	0.096	0.076
	800 mg.L^{-1}	0.0056	0.0022	0.0022	0.009	0.013	0.010
R^2		0.8998	0.9817	0.9813	0.8512	0.5806	0.8841

The results show that the Langmuir isotherm resulted in poor fits for RDF char-KOH with R^2 values of 0.8512, 0.5806 and 0.8841 at 293.15 K, 303.15 K and 313.15 K, respectively, over the whole tested MB concentration range. On the other hand, RDF char adsorption behavior was better described by the Langmuir isotherm, having R^2 value above 0.98 at 303.15 K and 313.15 K and of around 0.89 at 293.15 K. High R^2 values are related with the homogeneous nature of the adsorbent surface. R_L values (Table 7.4) indicate if the adsorption is unfavorable (R_L>1), linear (R_L = 1), favorable (0<R_L<1), or irreversible (RL=0) (Pathania *et al.*, 2017; Zhang *et al.*, 2012). The obtained R_L values, for both chars at the three temperatures and four MB concentrations, show that the adsorption is favorable, falling in the interval between 0-1 (Rangabhashiyam and Balasubramanian, 2018). Moreover, R_L values also reveal that the adsorption process becomes more favorable with increasing initial MB concentration, as reported by other authors (Kumar and Kumaran, 2005; Peydayesh and Rahbar-Kelishami, 2015).

According to Zhang *et al.* (2012), the Freundlich isotherm is used for non-ideal adsorption that involves heterogeneous surface energy systems. The results for the fitting of the obtained data into the Freundlich isotherm are depicted in Figure 7.13 and the calculated isotherm parameters are shown in Table 7.4.

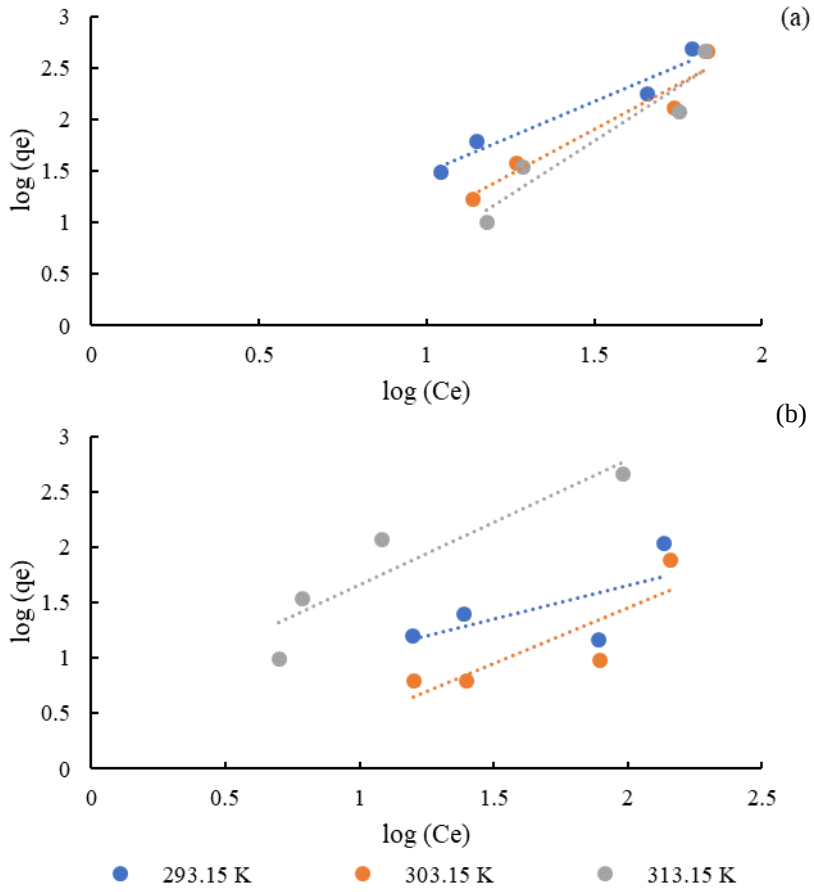

Figure 7.13: Freundlich isotherms of MB dye adsorption onto (a) RDF char and (b) RDF char-KOH. MB concentrations =100, 200, 400 and 800 $mg.L^{-1}$, T= 293.15, 303.15, 313.15 K, contact time = 24 h, adsorbent dosage = $5g.L^{-1}$, no pH adjustment.

Table 7.4: Model parameters estimated for the Freundlich adsorption isotherm of MB onto RDF char and RDF char-KOH, for concentrations between 100-800 $mg.L^{-1}$, and temperatures 293.15 K, 303.15 K and 313.15 K.

Isotherm parameters	Sample					
	RDF char			RDF char-KOH		
	293.15 K	303.15 K	313.15 K	293.15 K	303.15 K	313.15 K
K_f	1.101	0.487	0.265	1.562	1.710	0.574
1/n	0.721	0.572	0.481	1.653	0.890	0.998
R^2	0.9467	0.9332	0.9041	0.4301	0.8504	0.7098

Freundlich constant K_F can be used as an indicator of adsorption capacity, whereas 1/n can be related with adsorption intensity. These parameters are calculated from the intercept and slope of the plots in Figure 7.13. R^2 values for the RDF char were found to be 0.9467, 0.9332, and 0.9041 for the adsorption at 293.15, 303.15, and 313.15 K, respectively. On the other hand, the Freundlich isotherm gave a poor fit for RDF char-KOH adsorption data with very low R^2 values of 0.4301, 0.8504 and 0.7084 at 293.15, 303.15, and 313.15 K, respectively, demonstrating the weak applicability of this model to the adsorption of MB onto RDF char-KOH.

The calculated 1/n was found to be in the range of 0.481-0.721 for RDF char and 0.890-1.653 for RDF char-KOH. When this parameter presents values between 0 and 1, indicates that the adsorption process involved chemical interactions between adsorbent and analytes (Zhang *et al.*, 2012).

Temkin isotherm contains a factor that explicitly takes into the account interactions between analytes and adsorbents. This isotherm assumes that the heat of adsorption of all the molecules in the layer decreases linearly with coverage due to adsorbent-adsorbate interactions, and that the adsorption is characterized by a uniform distribution of binding energies, up to a maximum binding energy (Gouamid *et al.*, 2013). The Temkin constants B_T and K_T were calculated from the slope and intercept of the plot qe vs ln Ce (Figure 7.14) and are shown in Table 7.5.

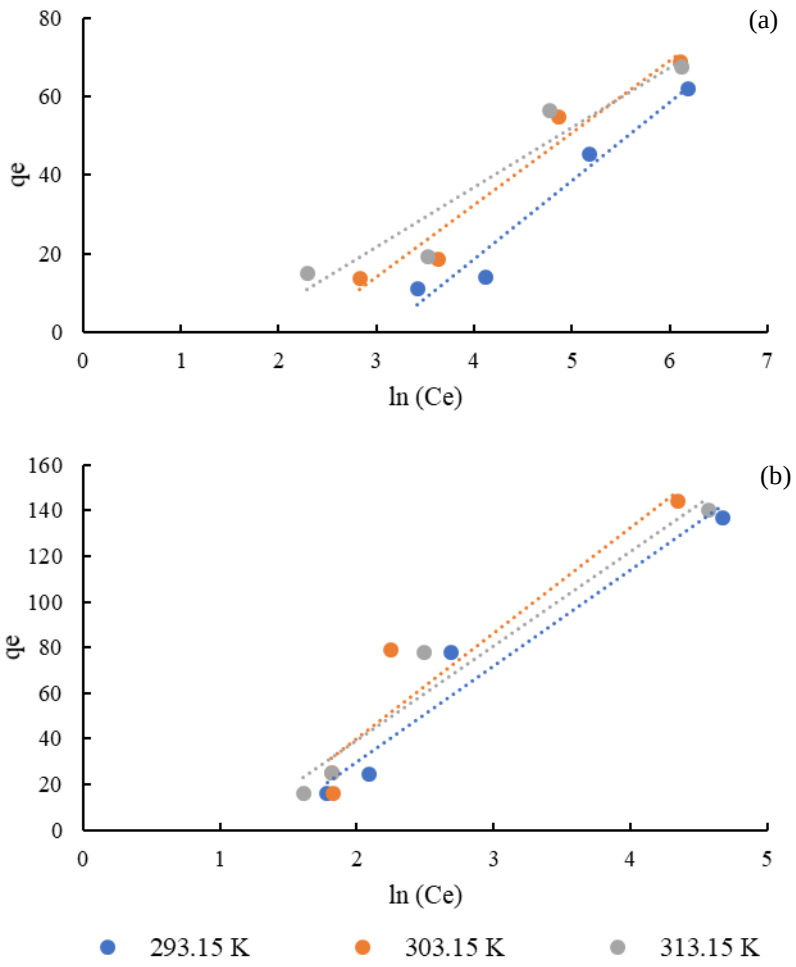

Figure 7.14: Temkin isotherms of MB dye adsorption onto (a) RDF char and (b) RDF char-KOH. MB concentrations =100, 200, 400 and 800 mg.L^{-1}, T= 293.15, 303.15, 313.15 K, contact time = 24 h, adsorbent dosage = 5g.L^{-1}, no pH adjustment.

Table 7.5: Model parameters estimated for the Temkin adsorption isotherm of MB onto RDF char and RDF char-KOH, for concentrations between 100-800 mg.L^{-1}, and temperatures 293.15 K, 303.15 K and 313.15 K.

Isotherm parameters	Sample					
	RDF char			RDF char-KOH		
	293.15 K	303.15 K	313.15 K	293.15 K	303.15 K	313.15 K
K_T (L.g^{-1})	0.047	0.106	0.206	0.276	0.321	0.348
B_T (J.mol^{-1})	122.278	137.246	171.004	58.055	54.464	62.948
R^2	0.9602	0.9511	0.9067	0.9473	0.8970	0.9542

The Temkin constant B_T was 122.278, 137.246, and 171.004 J.mol^{-1} at 293.15 K, 303.13 K and 313.16 K, respectively, for RDF char. The B_T values for RDF char-KOH were lower, 58.055, 54.464 and 62.948 J.mol^{-1} for the same order of temperatures.

The R^2 values obtained with this isotherm for both chars are more homogeneous, when compared with the previous two isotherms. For RDF char, R^2 values were above 0.90 for the three tested temperatures, and for RDF char-KOH at 293.15 K and 313.15 K R^2 was also above 0.90. According to Baghapour *et al.* (2013), high R^2 values in this model also indicate that the adsorption probably follows

a chemical mechanism. The fact that both chars present very significant B_T values, is also an indication of chemisorption, since a high B_T value is indicative of the chemical nature of the adsorption process (Bouaziz *et al.*, 2015; Kallel *et al.*, 2016). Furthermore, the Temkin isotherm model mainly describes chemical adsorption process as electrostatic interactions, and given the obtained R^2 values, this type of interaction may be an important mechanism affecting the adsorption of MB mainly onto RDF char, since RDF char-KOH presented lower B_T values (Fan *et al.*, 2017)

From the three tested isotherm models at three temperatures, with four MB dye concentrations, it was possible to assess that RDF char and RDF char-KOH have different adsorption behaviors between themselves. RDF char fits well in the Langmuir isotherm at 303.15 K and 313.15 K, presenting R^2 values > 0.98. On the other hand, RDF char-KOH presented the best correlation for all temperatures with the Temkin isotherm. This can be related with the basic treatment, yielding chemical alterations in the char, that led to a higher removal capacity due to mixed adsorbent-adsorbate interactions, involving both pore adsorption and surface interactions mediated by specific functional groups.

For sake of comparison, Table 7.6 presents different adsorbents used for MB remediation, with their maximum adsorption uptakes. The adsorbents tested in this study presented values within the range of several biomass wastes as well as activated carbons produced from low-cost precursors.

Table 7.6: Comparison of the maximum monolayer adsorption of MB onto various adsorbents (293.15 K).

Adsorbent	$q_{máx}$ (mg/g)	Reference
Refuse derived fuel char	100.0	This work
Treated Refuse derived fuel char	208.3	This work
Almond gum	250.0	(Bouaziz *et al.*, 2015)
Mango seed kernel powder	142.9	(Kumar and Kumaran, 2005)
Acid treated kenaf fiber char	18.18	(Mahmoud *et al.*, 2012)
Oil palm leaves	103.0	(Setiabudi *et al.*, 2016)
Casuarina seed-biochar	4.69	(Bharti *et al.*, 2019)
Fly ash	0.0727	(Potgieter *et al.*, 2018)
Activated carbon from pineapple waste	288.3	(Mahamad *et al.*, 2015)
Activated carbon from coconut shell	62.1	(Aljeboree *et al.*, 2017)
Activated carbon from buriti shells	274.6	(Pezoti *et al.*, 2014)
Activated carbon from waste paper	99.0	(Reza and Ahmaruzzaman, 2015)

Thermodynamic study

Operating temperature has considerable importance in order to estimate the thermodynamic parameters for the adsorption equilibrium. Thermodynamic calculations, namely ΔG, ΔH and ΔS were determined. Gibbs free energy was determined according to Equation 7.10 and the values of ΔH and ΔS were calculated from the slope and the intercept of the linear plot of ln K_C as a function of 1/T, via the van´t Hoff equation (Equation 7.12). Results are shown in Table 7.7.

Table 7.7: Thermodynamic parameters for the adsorption of MB onto RDF char and RDF char-KOH.

Adsorbent	Temperature	ΔG (kJ.mol^{-1})	ΔH (kJ.mol^{-1})	ΔS (J.mol^{-1}.K)	R^2
RDF char	293.15	-10.41	54.41	221.3	0.9966
	303.15	-12.81			
	313.15	-14.91			
RDF char-KOH	293.15	-14.97	14.09	75.5	0.5586
	303.15	-15.71			
	313.15	-16.99			

The values of ΔG were found to be negative for all studied temperatures indicating the spontaneous and favorable nature of MB adsorption onto RDF char and RDF char-KOH. Meanwhile, with the increase in temperature, ΔG values decreased further, implying that higher temperature favors MB adsorption. The positive value of ΔH suggests that the adsorption of MB onto the studied chars was endothermic, and the positive value of ΔS indicates an increase in the degree of randomness (or disorder) at the solid/solution interface during the adsorption process. ΔS also indicates that MB shows significant affinity for the used adsorbents. These results are in line with several studies conducted with different adsorbents using MB (Bulut and Ayd, 2006; Fan *et al.*, 2017; Ghosh and Bandyopadhyay, 2017; Han *et al.*, 2009, 2011; Mahmoud *et al.*, 2012).

According to Ghosh and Bandyopadhyay (2017), there are three regimes describing the adsorption mechanism based on the values of ΔH: if ΔH presents a value between 0-20 kJ.mol^{-1} van der Waals forces are predominant; if ΔH ranges between 20-80 kJ.mol^{-1} there is a contribution of electrostatic interactions, and lastly for ΔH between 80-450 kJ.mol^{-1} chemisorption occurs. As seen from Table 7.7, the studied chars fall into different regimes. RDF char presents a ΔH of 54.41 kJ.mol^{-1} and RDF char-KOH has a ΔH value of 14.09 kJ.mol^{-1}, meaning that the non-treated char presents a contribution of electrostatic interactions and the KOH treated char has a predominance in van der Waals forces. These results are in accordance with the previous findings in the isotherm and kinetic studies as well as FT-IR analysis, since RDF char took longer to reach equilibrium and presented higher B_T values in the Temkin isotherm. These results are also in line with the difference between chars regarding temperature, since the effect of temperature in the adsorption was more evident for RDF char. This is evident from the correlation for RDF char-KOH, which does not represent a good fit (R^2=0.5586), in practical terms this means that whereas RDF char presented significantly decreasing C_e values, RDF char-KOH removed almost the same amount of MB regardless of the varying temperature, presenting very little variation in C_e values. The lack of fit of RDF char throughout the studies performed, reveals a more complex nature on the adsorption process for this particular waste-derived char.

7.3.3. Fixed-column experiments

Batch studies are useful to compare adsorbents, to evaluate the influence of different adsorption parameters and to establish adsorption equilibrium conditions. On the other hand, batch adsorption is difficult to apply to industrial treatment systems due to associated costs and complexity at a larger scale (Potgieter *et al.*, 2018; Russo *et al.*, 2016).

Adsorption in a fixed-bed column allows to evaluate adsorption in a dynamic mode, which is relevant for the adaptation of the process to an industrial scale (Chen *et al.*, 2012).

In that sense, after performing batch studies, the adsorbent RDF char-KOH was chosen to proceed to column studies due to its effectiveness, faster removal rate and higher removal efficiencies towards MB. Moreover, this adsorbent was also tested for its removal capacity of Cr (VI), since most effluents

do not contain solely dyes. Industrial effluents are very complex mixtures usually containing organic and inorganic components (Rangabhashiyam and Balasubramanian, 2018; Saranya *et al.*, 2018).

The breakthrough curves obtained for different bed heights with RDF char-KOH using MB as an adsorbate are shown in Figure 7.15, and the breakthrough curve obtained for Cr (VI) at a fixed bed height is shown on Figure 7.16.

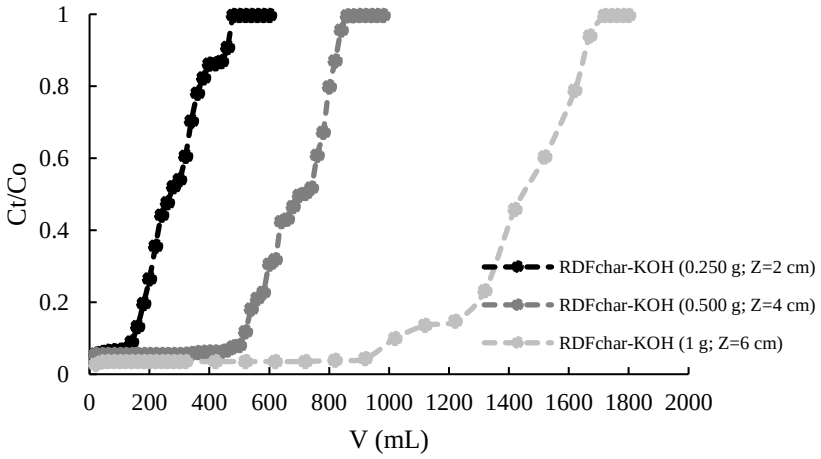

Figure 7.15: Effect of bed height on the breakthrough curves of MB dye, with initial MB concentration of 100 mg.L^{-1} and a flow rate of 2.5 mL.min^{-1}.

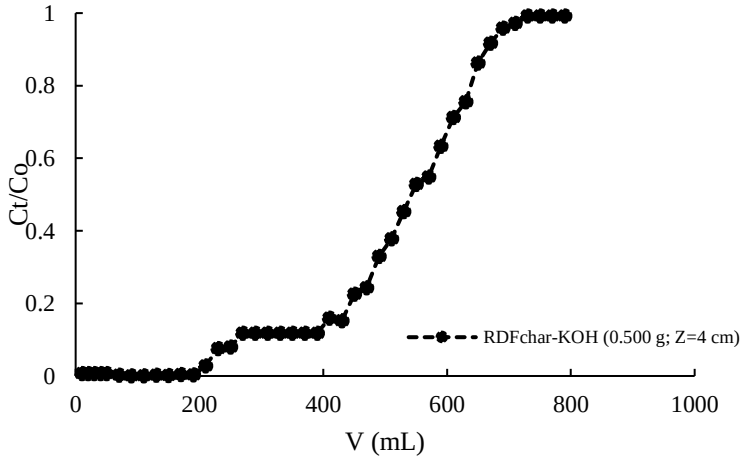

Figure 7.16: Breakthrough curves of Cr (VI) 10 mg/L, pH=2 and a flow rate of 2.5 mL.min^{-1}.

The adsorbent masses of 0.250 g, 0.500 g and 1 g correspond to bed heights of 2, 4 and 6 cm (Figure 7.15). Data extracted from the breakthrough curves can be found in Table 7.8.

Table 7.8: Adsorption breakthrough data for MB adsorptions tests in fixed-bed column varying adsorbent mass, and for Cr (VI) adsorption test.

Data	RDF char-KOH			
	MB			Cr (VI)
C_0 (mg.L^{-1})	100	100	100	10
pH	6.5	6.5	6.5	2
Z (cm)	2	4	6	4
Q (mL/min)	2.5	2.5	2.5	2.5
Breakthrough time (min)	4	128	368	92
Saturation time (min)	188	336	683	276
V_{eff} (mL)	460	840	1670	690
q_{total} (mg)	18.0	32.3	67.5	8.3
W_{total} (mg)	38.2	68.3	138.8	17.3
q_{eq} (mg/g)	70.7	64.3	64.3	16.5
R (%)	22.2	47.3	48.6	47.9
MTZ (cm)	2.0	2.5	2.8	2.7
EBCT (min)	3.9	7.9	11.8	7.9

The breakthrough curves are almost similar to an "S" shape profile, which is normally produced in adsorption systems. The results indicate that the breakthrough volume varies with bed height, which means that a higher volume of MB solution is remediated with a higher bed height (that in turn corresponds to a higher amount of adsorbent). With a higher bed height, the influent MB solution had more contact time with a higher amount of adsorbent, resulting in a better removal efficiency. These results are similar with other reports found in the literature for chitosan– glutaraldehyde biosorbent with Direct blue 71 (López-Cervantes *et al.*, 2018) or peanut husk with MB (Song *et al.*, 2011). When the bed height is decreased, the removal percentage is decreased from 48.6 % (Z=6) to 22.2 % (Z=2), and the total weight of MB adsorbed by RDF char-KOH in the column (q_{total}) is also decreased from 67.5 to 18 mg. The EBCT also increased from 3.9 min to 11.8 min with the bed depth increasing from 2 cm to 6 cm.

Furthermore, the slope of the breakthrough curve, meaning, the fact that the front of the "S" shape is deviated to the right is related with mass transfer phenomena, since the mass transfer zone is broadened, as seen from the MTZ values, that increase with increasing bed height (Song *et al.*, 2011; Taty-Costodes *et al.*, 2005). The slope deviation can also be related with an increase in the axial dispersion of the dye over the column with an increase in bed height (Song *et al.*, 2011) .

Cr (VI) removal in fixed-column mode had an efficiency of 47.9 %, with a bed height of 4 cm (~0.500 g of adsorbent). It was found that the column got saturated at about 276 min for a saturation volume of 690 mL. This experiment was conducted in order to assess if this particular adsorbent had the ability to also adsorb a heavy metal, like Cr (VI), which it proved to have, albeit in a concentration that was ten times inferior to the one used for MB adsorption. Furthermore, the pH of the Cr (VI) solution was adjusted to an acidic value (pH = 2) in order to guarantee that the phenomena that was being observed was indeed adsorption and not metal precipitation, when in contact with the adsorbent. This was a limiting step in this experiment, since pH is well below the pHpzc of the used adsorbent (6.8), which means that at that particular pH the net surface charge of RDF char-KOH was positive (Sumalinog *et al.*, 2018) thus, not favoring interaction with other positively charged species such as Cr (VI). Nevertheless, the adsorption mechanism involves more than electrostatic interactions, justifying some removal from the influent.

Breakthrough curve modelling

The Thomas model is a widely used theoretical method to describe column performance (Chen *et al.*, 2012; Chowdhury *et al.*, 2016; Gong *et al.*, 2015; López-Cervantes *et al.*, 2018; Song *et al.*, 2011). According to different authors this model assumes plug flow behavior in the bed. It also assumes no axial dispersion, stating that adsorption is the rate driving force and it obeys second-order reversible reaction kinetics. This model is applicable to both favourable or unfavourable isotherms (López-Cervantes *et al.*, 2018; Song *et al.*, 2011). The model was applied through equation 7.21, and the values of k_{TH} and q_0 were determined from the linear plot of ln $[(C_0/C_t) - 1]$ against t. Results are shown in Table 7.9.

Table 7.9: Parameters of Thomas model for MB column adsorption under different bed heights, and for CR (VI) column adsorption.

Adsorbate	C_0 (mg.L^{-1})	Z (cm)	k_{TH} (mL.min^{-1}.mg^{-1})	q_0 (mg.g^{-1})	R^2
MB	100	2	0.529	81.38	0.9333
		4	0.281	182.13	0.7529
		6	0.137	338.99	0.7586
Cr (VI)	10	4	3.353	19.66	0.9001

As the bed height increased, the values of k_{TH} decreased and the value of q_0 increased, which is due to the fact that adsorption capacity depended mainly of the amount of the adsorbent available for adsorption. As seen in the above table, the R^2 values were more significant for the MB adsorption with Z=2 and for Cr (VI) adsorption with Z=4. Also, q_0 values for these two experiments are closer to the ones determined experimentally (Table 7.9). These differences mean that the Thomas model did not give a good prediction of the breakthrough curve for all the tested conditions. As stated by López-Cervantes *et al.* (2018) the main limitation of this model is that it is based on second-order kinetics and it considers that the adsorption is not limited by chemical interactions, and it is only controlled by the mass transfer at the interface.

7.4. Conclusions

In this chapter, the application of RDF char as a low-cost adsorbent was studied. The removal efficiency of the RDF char was evaluated as produced and after activation by Soxhlet extraction with acetone and extraction with aqueous KOH using a fast adsorption test, that led to the conclusion that basic (KOH) treatment resulted in higher MB removal efficiencies. Hence, further batch adsorption studies were conducted with the RDF char as produced (sample RDF char) and with the alkali treated char (RDF char-KOH).

Both adsorbents were characterized regarding their proximate and ultimate analysis which enabled the conclusion that although the torrefaction process increased carbon content it also increased ash content, which deems these chars difficult to use in energy applications, justifying the study of their properties as low-cost adsorbents. For adsorption purposes the chars were characterized regarding FT-IR and pH_{pzc}, denoting the presence of important functional groups for electrostatic interactions that would exhibit negative charges above pH 6.5 and 6.8 increasing the propensity of the adsorbent surface to attract cationic molecules, such as MB, leading to their adsorption.

MB adsorption onto RDF char and RDF char-KOH was investigated in batch and column modes and the kinetic, equilibrium and breakthrough curves were discussed. The kinetic process was better

described by the pseudo-second-order kinetic model for both chars with R^2 values above 0.97. Adsorption isotherm was fairly described by the Langmuir isotherm at 303.15 K and 313.15 K for RDF char, while RDF char-KOH was better described by the Temkin isotherm with R^2 values above 0.90 for all temperatures. Nevertheless, none of the tested isotherms presented excellent correlations for both chars (R^2>0.99), denoting differences between the adsorption process in both adsorbents and suggesting the occurrence of multiple forms of adsorption that are difficult to describe with a single model.

Thermodynamic studies showed that the adsorption of MB onto RDF char and RDF char-KOH was spontaneous ($\Delta G<0$) and endothermic ($\Delta H>0$).

For the fixed-column adsorption tests, the removal efficiency of RDF char-KOH towards MB and Cr (VI) was tested by establishing the corresponding breakthrough curves using different adsorbent masses and bed heights. The study showed that breakthrough curves were significantly affected by bed height, and the column data were fitted by the Thomas models, yielding good fits for MB adsorption with a bed height of 2 cm and for Cr (VI) adsorption with a bed height of 4 cm.

Adsorption of complex systems such as industrial effluents, containing multiple molecules, from dyes (cationic and anionic) to heavy metals, needs further study, because in multi-component solutions, antagonistic effects, like competition between cationic species could occur. Furthermore, different activation methods could be tested in order to achieve a more defined adsorption mechanism. Still, using RDF as a low-cost adsorbent or as an activated carbon precursor for methylene blue has proven to be efficient and brings the clear advantage of using a raw material with associated low cost, as well as offering a valorization solution for a material that if not used for energy production, would be considered and treated as a waste.

Chapter 8

Conclusions and future work

8.1. Conclusions

The main objective of the present thesis was to study the thermochemical upgrading of RDF and the potential valorization of RDF chars in energy production systems (gasification) or as low-cost adsorbents, in order to validate the upgrading processes. Torrefaction, carbonization and hydrothermal carbonization were the thermochemical conversion processes used in RDF upgrading. Effectively, the applied processes yielded chars with significant enhancements in their fuel properties when compared to the starting materials.

Chars produced via conventional torrefaction and carbonization showed increased homogeneity, grindability, apparent density, fixed carbon (8.3 - 25.8 wt.%, db), carbon content (43.4 – 84.9 wt.%, daf) and high heating value (17.6 – 26.2 $MJ.kg^{-1}$, db).

The RDF chars presented reduced oxygen contents (between 5.4-49.5 wt.%, daf), giving them a fuel profile similar to some fossil fuels, like lignite (char produced at 300 ºC) or bituminous coal (char produced at 400 ºC). Nevertheless, these chars also presented increased ash and chlorine contents, which are disadvantageous fuel characteristics regarding associated emissions and operational problems.

Ash contents of the RDF chars were determined in the range of 8.2 - 26.0 wt.%, db and the chlorine contents reached values between 0.7-3.1 wt.%, db. The increase in chlorine content was not consistent with several reports in the literature stating that the thermochemical processes reduce chlorine content. But the great majority of the works are conducted in reactors that include an inert gas purging system which, although beneficial in the removal of some volatile and problematic species, also makes the process costly and less scalable. Not using an inert atmosphere allows for some of the condensable species to deposit on the surface of the char yielding a two-fold effect: increased chlorine (on the surface, or possibly in the pore structure of the char) and an increased mass yield. Leaching behavior of the raw RDF and of the chars produced by the dry processes showed that chlorine and ash contents could be reduced by water washing (49.9 - 71.6 % for chlorine removal and 1 - 3 % for ash removal), while also increasing the high heating value of the chars (increases between 9.4 and 13.8 %). The leaching results also showed that some of the more problematic mineral components existing in the studied samples, such as heavy metals, are more retained by the chars than by the raw RDF. The main implication of this observation is that RDF chars (if no other valorization in available) can be deposited in a landfill, without severe leaching of these harmful components.

On the other hand, the hydrochars, when compared with the chars obtained in the dry processes, presented higher volatile matter content (79.6 - 82.7 wt.%, db), and their fixed carbon contents were of the same order regarding the operating temperature range (13.4-16.9 wt.%). Carbon contents reached by the hydrochars were also comparable to those obtained with the dry processes, in the same temperature range. Calorific value values of the hydrochars were generally higher that the ones obtained for the dry processes (the highest measured HHV was 28.1 $MJ.kg^{-1}$) and this increase can be related with the reduction in inorganic material in the hydrochar.

The most positive feature determined in the hydrochars was the significant decrease in ash and chlorine contents. Ash content was reduced up to 30.8 % when compared with raw RDF and the

dechlorination efficiency of the HTC process reached a maximum value of 55 %. This effect is opposite to what was detected in the chars obtained by torrefaction or carbonization where both these parameters had increased concentrations.

Similar to the chars produced in the dry processes, the hydrochars showed similarities with fossil fuels such as lignite, because they also presented reduced oxygen contents, although to a less extent than in the chars, since oxygen contents in the hydrochars were found to be between 23.5 - 28.5 wt.%. Moreover, the hydrochars have distinct thermal degradation profiles from the raw RDF. The morphological characteristics assessed by SEM showed the extent of the physical transformations brought by the HTC process, since RDF presented a fibrous structure that was clearly decomposed after HTC since the hydrochars presented more random structures with indications of pore development.

Overall, given their reduced ash and chlorine contents, but improved fuel properties such as carbon content and HHV, the hydrochars presented higher potential for energy applications than the chars produced via dry torrefaction or carbonization.

The assessment of process performances showed that there was a distinct behavior between torrefaction and carbonization conditions, and between dry and wet processes. For the dry processes, at temperatures of 200 ºC and 250 ºC, process energy efficiency and energy yields were high (> 85 % for process energy efficiency and > 96.3 % for energy yield), which was related with the high mass yields that were obtained at those conditions (90.0 – 96.8 %), but the high heating value of the produced chars was low (17.6-19.4 $MJ.kg^{-1}$), because their oxygen content was still significant.

On the other hand, at 300, 350 and 400 ºC lower process energy efficiency values (70.8-79.2 %), and lower energy yields (89.5 – 91.7 %), were obtained but those values corresponded to RDF chars that had a higher calorific value (20.1-26.2 $MJ.kg^{-1}$), and therefore better fuel quality.

Process performance for HTC was heavily dependent on the amount of water used in the experiments. Conditions yielding positive net energies were the ones where the solid-to-water ratio was lower (8.5 MJ), and where mass yield was more significant (0.24 MJ). Mass yields are also very different between the dry processes and HTC, since the use of water and the auto-generated pressure entailed a more extensive decomposition of the feedstock, and therefore, reduced mass yields (47.6 – 53.7 %). As a consequence, the process energy efficiency (32.3 – 52.6 %) of the HTC process was lower than that of torrefaction or carbonization.

As expected from torrefaction and carbonization, the gas product (non-condensable phase) was mostly composed of carbon dioxide and carbon monoxide, with smaller amounts of methane and hydrogen (more significant at the higher process temperature). In the HTC process, the amount of produced gas was negligible.

Both processes involved the production of an associated aqueous effluent. In the case of the dry processes these are the condensable gases (condensates) and in the case of HTC it corresponds to the process water. Both effluents presented acidic pH values, high chemical oxygen demand values (the highest measured values were 69.3 $gO_2.L^{-1}$ for carbonization and 27.2 $gO_2.L^{-1}$ for HTC) and were mostly composed by water and organic oxygenated compounds such as acids, furans and phenols. Given their high-water content and significant organic load, these effluents can be problematic regarding their valorization. Nevertheless, the dry processes produced lower amounts of condensates (635 mL and 992 mL for the processes at 300 and 400 ºC, respectively, with 5 kg of RDF) when comparing with the amount of process water used in the HTC process (solid-to-water ratio 1:15 and 1:5). The amount of water produced during HTC is the main constraint of large-scale implementation of this system, because water treatment means added costs, and more emissions, decreasing the sustainability of the process.

As assessed in this work, the remediation of HTC process water can be quite challenging, but it was possible to verify that both RDF hydrochar and conventional RDF char showed potential as low-cost adsorbents for process water treatment (sample H-300-30/15 removed 38.5 % phenolic compounds and 61.5 % COD, whereas RDF char removed 50.5 % phenolic compounds and 7.8 % COD), although these

are lower removal efficiencies than the obtained with commercial activated carbon (95.5 and 75.4 % removal for phenolic compounds and COD, respectively).

After testing different thermochemical processes for RDF upgrading, RDF chars produced via conventional torrefaction (300 ºC for 30 min) were evaluated as fuels for gasification. Because of their properties, the RDF chars were mixed with pine wastes, with the purpose of diluting some of the more problematic features, such as the high ash content. The production of blends of RDF char with more innocuous biomass wastes, can represent one of the ways to valorize these chars, without decreasing the efficiency of this energy conversion system. Effectively, the incorporation of RDF char in biomass pellets can be a viable pathway for its energetic valorization, although it should be done in moderate incorporation ratios. The use of RDF char instead of raw RDF presents advantages, since the more problematic polymeric fraction is degraded after torrefaction or carbonization, which can positively influence the pelletization process by avoiding problems regarding clogging or coiling of the plastics in critical areas of some types of feeding systems. The obtained results showed that higher temperature and lower equivalence ratios, yielded a better conversion performance for the pellets with RDF char incorporation. Nevertheless, the addition of RDF char also caused the formation of heavier aromatic hydrocarbons in the gasification tars.

Lastly, material valorization of the RDF chars was assessed by testing their adsorption capacity towards methylene blue and chromium ions. The adsorption tests were conducted with RDF char as produced and after activation treatments. . Methylene blue adsorption onto treated and non-treated RDF char clearly showed the potential of the char as a low-cost adsorbent. The treatment with aqueous KOH gave the RDF char new characteristics, and as such the adsorption behaviors between the chars were slightly different, but both indicated that the adsorption process involved chemical interactions. The adsorption of methylene blue was more expressive than the chromium adsorption, probably because it could be evaluated at pH values more adequate for cation adsorption in these chars.

Thermochemical conversion processes such as torrefaction, carbonization and hydrothermal carbonization are gaining more notoriety as pre-treatments, particularly for very heterogeneous and complex matrixes such as the one studied in this thesis. These processes are flexible enough to accommodate different waste typologies, which is of great importance given the amounts of different wastes that are produced. Char, or at least biochar, is becoming increasingly relevant in the market (mostly due to its multiple applications), and as such, studies regarding large scale implementation and different feedstocks will certainly be needed in the future. These processes also have the advantage of enabling the production of chars with specific features by adjusting process parameters.

Upgrading of RDF is particularly important because this waste derived fuel, which is intended for energy purposes, does not always present adequate fuel characteristics. This results in accumulation of large quantities of RDF, loss of its value and ultimately, deposition of a large fraction of the produced RDF in landfills, a non-sustainable solution that should be avoided whenever possible. Using the studied thermochemical conversion processes, RDF could be transformed into a char, and with its new characteristics it could be more versatile in energy recovery systems and it could also be used for material valorization. This approach could imply the actual valorization of the RDF that is produced in diverse applications including energy recovery, production of low-cost adsorbents and others. This concept is in line with the increase in sustainability of waste management practices, that need to be implemented in order to recover as much value as possible from all the produced wastes.

Wastes need to be faced as potential raw materials for different technologies, they have tremendous potential for energy provision and material production thus, their upgrading represents a way to open a wider array of possibilities for their valorization.

8.2. Future work

Considering the importance of RDF upgrading in the current context of waste management, further studies are needed in order to fully create measures to build a sustainable upgrading system. Suggestions on future work in this area are as follows:

- Water washing for chlorine removal of RDF chars can represent more costs associated with the process, and an integration of this treatment in the overall upgrading system should be studied, in order to achieve high dechlorination without excessive expenditure or large effluent production.

- The recirculation of the gas product within the reactor could assure the absence of oxygen in substitution of an inert atmosphere. The application of the gas product in a combustion chamber in order to use the produced heat to sustain the torrefaction or carbonization process.

- Condensates of the dry processes should be studied for their remediation (through adsorption, phytoremediation, or bioremediation), for their use as fertilizers or for their application in energy production by anaerobic digestion. These condensates could also be tested as a moisture source for the HTC process.

- In the HTC process, testing lower solid-to-water ratios could lead to better process performances, such as higher mass yields or higher process energy efficiencies. Also, mixing the RDF with other wastes, for instance lipidic wastes, could help to decrease the energy requirements of the process, but also to maintain the good fuel properties of the hydrochars.

- Using RDF char in adsorption of complex systems such as industrial effluents, containing multiple molecules, from dyes (cationic and anionic) to heavy metals; Assess different activation methods for the RDF char.

- Validation of the use of RDF chars in combustion, by preparing pellets with incorporation of RDF char and evaluating its performance in combustion conditions, including evaluation of the associated emissions and of the ash composition is necessary to demonstrate the viability of this valorization pathway.

- The incorporation of RDF and RDF chars in construction materials may be an exploitable application since the combination of biomass, polymers and mineral components, including diverse waste materials is a recent trend of that field, meant to reduce costs and increase sustainability of that sector.

References

Abdel-Shafy, H.I., Mansour, M.S.M., 2016. A review on polycyclic aromatic hydrocarbons: Source, environmental impact, effect on human health and remediation. Egypt. J. Pet. 25, 107–123. doi:10.1016/j.ejpe.2015.03.011

Abdullah, N., Gerhauser, H., Bridgwater, A. V, 2007. Bio-oil from fast pyrolysis of oil palm empty fruit bunches. J. Phys. Sci. 18, 57–74.

Abood, A.R., Bao, J., Du, J., Zheng, D., Luo, Y., 2014. Non-biodegradable landfill leachate treatment by combined process of agitation, coagulation, SBR and filtration. Waste Manag. 34, 439–447. doi:10.1016/j.wasman.2013.10.025

Ábrego, J., Plaza, D., Luño, F., Atienza-Martínez, M., Gea, G., 2018. Pyrolysis of cashew nutshells: Characterization of products and energy balance. Energy 158, 72–80. doi:10.1016/j.energy.2018.06.011

Acharya, B., Dutta, A., Minaret, J., 2015. Review on comparative study of dry and wet torrefaction. Sustain. Energy Technol. Assessments 12, 26–37. doi:10.1016/j.seta.2015.08.003

Agência Portuguesa do Ambiente, 2014. Estratégia para os Combustíveis Derivados de Resíduos (CDR) [WWW Document]. URL http://apambiente.pt/_zdata/Politicas/Residuos/Planeamento/PERSU_II/Enquadramento_Estrategia_CDR.pdf

Agon, N., Hrabovský, M., Chumak, O., Hlína, M., Kopecký, V., Mašláni, A., Bosmans, A., Helsen, L., Skoblja, S., Van Oost, G., Vierendeels, J., 2016. Plasma gasification of refuse derived fuel in a single-stage system using different gasifying agents. Waste Manag. 47, 246–255. doi:10.1016/j.wasman.2015.07.014

Agraniotis, M., Nikolopoulos, N., Nikolopoulos, A., Grammelis, P., Kakaras, E., 2010. Numerical investigation of Solid Recovered Fuels' co-firing with brown coal in large scale boilers – Evaluation of different co-combustion modes. Fuel 89, 3693–3709. doi:10.1016/j.fuel.2010.07.030

Ahmad, M., Upamali, A., Eun, J., Zhang, M., Bolan, N., Mohan, D., Vithanage, M., Soo, S., Sik, Y., 2014. Biochar as a sorbent for contaminant management in soil and water: A review. Chemosphere 99, 19–33. doi:10.1016/j.chemosphere.2013.10.071

Ahn, S.Y., Eom, S.Y., Rhie, Y.H., Sung, Y.M., Moon, C.E., Choi, G.M., Kim, D.J., 2013. Application of refuse fuels in a direct carbon fuel cell system. Energy 51, 447–456. doi:10.1016/j.energy.2012.12.025

Akdag, A.S., Atimtay, A., Sanin, F.D., 2016. Comparison of fuel value and combustion characteristics of two different RDF samples. Waste Manag. 47, 217–224. doi:10.1016/j.wasman.2015.08.037

Aljeboree, A.M., Alshirifi, A.N., Alkaim, A.F., 2017. Kinetics and equilibrium study for the adsorption of textile dyes on coconut shell activated carbon. Arab. J. Chem. 10, S3381–S3393. doi:10.1016/j.arabjc.2014.01.020

Almeida, A., Neto, P., Pereira, I., Ribeiro, A., Pil, R., 2019. Effect of temperature on the gasification of olive bagasse particles. J. Energy Inst. 92, 153–160. doi:10.1016/j.joei.2017.10.012

Anthraper, D., McLaren, J., Baroutian, S., Munir, M.T., Young, B.R., 2018. Hydrothermal deconstruction of municipal solid waste for solid reduction and value production. J. Clean. Prod. 201, 812–819. doi:10.1016/j.jclepro.2018.08.116

Areeprasert, C., Ma, D., Prayoga, P., Yoshikawa, K., 2016. A review on pilot-scale applications of hydrothermal treatment for upgrading waste materials. Int. J. Environ. Sci. Dev. 7, 425–430. doi:10.7763/IJESD.2016.V7.813

Arena, U., 2012. Process and technological aspects of municipal solid waste gasification . A review. Waste Manag. 32, 625–639. doi:10.1016/j.wasman.2011.09.025

Arena, U., 2011. Gasification : An alternative solution for waste treatment with energy recovery. Waste Manag. 31, 405–406. doi:10.1016/j.wasman.2010.12.006

Arena, U., Di Gregorio, F., 2016. Fluidized bed gasification of industrial solid recovered fuels. Waste Manag. 50, 86–92. doi:10.1016/j.wasman.2016.02.011

Arena, U., Di Gregorio, F., 2014. Gasification of a solid recovered fuel in a pilot scale fluidized bed reactor. Fuel 117, 528–536. doi:10.1016/j.fuel.2013.09.044

Arena, U., Zaccariello, L., Mastellone, M.L., 2010. Fluidized bed gasification of waste-derived fuels. Waste Manag. 30, 1212–1219. doi:10.1016/j.wasman.2010.01.038

Astrup, T.F., Tonini, D., Turconi, R., Boldrin, A., 2014. Life cycle assessment of thermal Waste-to-Energy technologies: Review and recommendations. Waste Manag. 37, 104–115. doi:10.1016/j.wasman.2014.06.011

Bach, Q.V., Skreiberg, Ø., Lee, C.J., 2017. Process modeling and optimization for torrefaction of forest residues. Energy 138, 348–354. doi:10.1016/j.energy.2017.07.040

Baghapour, M.A., Djahed, B., Ranjbar, M., 2013. Removal of methylene blue from aqueous solutions by waste paper derived activated carbon. J. Heal. Sci. Surveill. Syst. 1, 48–56.

Barba, D., Capocelli, M., Cornacchia, G., Matera, D.A., 2016. Theoretical and experimental procedure for scaling-up RDF gasifiers: The Gibbs Gradient Method. Fuel 179, 60–70. doi:10.1016/j.fuel.2016.03.014

Barka, N., Ouzaouit, K., Abdennouri, M., El, M., 2013. Dried prickly pear cactus (Opuntia ficus indica) cladodes as a low-cost and eco-friendly biosorbent for dyes removal from aqueous solutions. J. Taiwan Inst. Chem. Eng. 44, 52–60. doi:10.1016/j.jtice.2012.09.007

Basu, P., 2010. Biomass gasification and pyrolysis: practical design and theory, 2nd ed. Elsevier Inc., USA.

Basu, P., Rao, S., Acharya, B., Dhungana, A., 2013. Effect of torrefaction on the density and volume changes of coarse biomass particles. Can. J. Chem. Eng. 91, 1040–1044. doi:10.1002/cjce.21817

Bedin, K.C., Martins, A.C., Cazetta, A.L., Pezoti, O., Almeida, V.C., 2016. KOH-activated carbon prepared from sucrose spherical carbon: Adsorption equilibrium, kinetic and thermodynamic studies for methylene blue removal. Chem. Eng. J. 286, 476–484. doi:10.1016/j.cej.2015.10.099

Belgiorno, V., Feo, G. De, Rocca, C. Della, Napoli, R.M.A., 2003. Energy from gasification of solid wastes. Waste Manag. 23, 1–15. doi:10.1016/S0956-053X(02)00149-6

Benavente, V., Fullana, A., Berge, N.D., 2017. Life cycle analysis of hydrothermal carbonization of olive mill waste: Comparison with current management approaches. J. Clean. Prod. 142, 2637–2648. doi:10.1016/j.jclepro.2016.11.013

Berge, N.D., Li, L., Flora, J.R. V, Ro, K.S., 2015. Assessing the environmental impact of energy production from hydrochar generated via hydrothermal carbonization of food wastes. Waste Manag. 43, 203–217. doi:10.1016/j.wasman.2015.04.029

Berge, N.D., Ro, K.S., Mao, J., Flora, J.R. V., Chappell, M.A., Bae, S., 2011. Hydrothermal carbonization of municipal waste streams. Environ. Sci. Technol. 45, 5696–5703. doi:10.1021/es2004528

Bergman, P.C.., Boersma, R., Zwart, R.W.R., Kiel, J.H., 2005. Torrefaction for biomass co-firing in existing coal-fired power stations - "Biocoal."

Bharti, V., Vikrant, K., Goswami, M., Tiwari, H., Kumar, R., Lee, J., Tsang, D.C.W., Kim, K., Saeed, M., 2019. Biodegradation of methylene blue dye in a batch and continuous mode using biochar as packing media. Environ. Res. 171, 356–364. doi:10.1016/j.envres.2019.01.051

Białowiec, A., Pulka, J., Stępień, P., Manczarski, P., Gołaszewski, J., 2017. The RDF/SRF torrefaction: An effect of temperature on characterization of the product – Carbonized Refuse Derived Fuel. Waste Manag. 70, 91–100. doi:10.1016/j.wasman.2017.09.020

Blanco, P.H., Wu, C., Onwudili, J.A., Williams, P.T., 2012. Characterization of tar from the pyrolysis/gasification of Refuse Derived Fuel : Influence of process parameters and catalysis. Energy&Fuels 26, 2107–2115. doi:10.1021/ef300031j

Bolyard, S.C., Reinhart, D.R., 2016. Application of landfill treatment approaches for stabilization of municipal solid waste. Waste Manag. 55, 22–30. doi:10.1016/j.wasman.2016.01.024

Bouaziz, F., Koubaa, M., Kallel, F., Chaari, F., Driss, D., Ghorbel, R.E., Chaabouni, S.E., 2015. Efficiency of almond gum as a low-cost adsorbent for methylene blue dye removal from aqueous solutions. Ind. Crops Prod. 74, 903–911. doi:10.1016/j.indcrop.2015.06.007

Brás, I., Silva, M., Lobo, G., Cordeiro, A., Faria, M., Lemos, L., 2017. Refuse Derived Fuel from Municipal Solid Waste rejected fractions - a Case Study. Energy Procedia 120, 349–356. doi:10.1016/j.egypro.2017.07.227

Broch, A., Jena, U., Hoekman, S.K., Langford, J., 2014. Analysis of solid and aqueous phase products from hydrothermal carbonization of whole and lipid-extracted algae. Energies 7, 62–79. doi:10.3390/en7010062

Buah, W.K., Williams, P.T., 2010. Activated carbons prepared from refuse derived fuel and their gold adsorption characteristics. Environ. Technol. 31, 125–37. doi:10.1080/09593330903386741

Bulut, Y., Ayd, H., 2006. A kinetics and thermodynamics study of methylene blue adsorption on wheat shells. Desalination 194, 259–267. doi:10.1016/j.desal.2005.10.032

Caputo, A.C., Pelagagge, P.M., 2002. RDF production plants: I Design and costs. Appl. Therm. Eng. 22, 423–437. doi:10.1016/S1359-4311(01)00100-4

Cardona, S., Gallego, L.J., Valencia, V., Martínez, E., Rios, L.A., Javier, L., Valencia, V., Martínez, E., Alberto, L., 2019. Torrefaction of eucalyptus-tree residues: A new method for energy and mass balances of the process with the best torrefaction conditions. Sustain. Energy Technol. Assessments 31, 17–24. doi:10.1016/j.seta.2018.11.002

Carrier, M., Loppinet-Serani, A., Denux, D., Lasnier, J.-M., Ham-Pichavant, F., Cansell, F., Aymonier, C., 2011. Thermogravimetric analysis as a new method to determine the lignocellulosic composition of biomass. Biomass and Bioenergy 35, 298–307. doi:10.1016/j.biombioe.2010.08.067

Casado, R.R., Rivera, J.A., García, E. borjabad, Cuadrado, R.E., Llorente, M.F., Sevillano, R.B., Delgado, A.P., 2016. Classification and characterisation of SRF produced from different flows of processed MSW in the Navarra region and its co-combustion performance with olive tree pruning residues. Waste Manag. 47, 206–216. doi:10.1016/j.wasman.2015.05.018

Catalkopru, A.K., Kantarli, I.C., Yanik, J., 2017. Effects of spent liquor recirculation in hydrothermal carbonization. Bioresour. Technol. 226, 89–93. doi:10.1016/j.biortech.2016.12.015

Çepeliogullar, Ö., Haykırı-Açma, H., Yaman Istanbul, S., 2016. Kinetic modelling of RDF pyrolysis: Model-fitting and model-free approaches. Waste Manag. 48, 275–284. doi:10.1016/j.wasman.2015.11.027

Chandra, T.S., Mudliar, S.N., Vidyashankar, S., Mukherji, S., Sarada, R., Krishnamurthi, K., Chauhan, V.S., 2015. Defatted algal biomass as a non-conventional low-cost adsorbent: Surface characterization and methylene blue adsorption characteristics. Bioresour. Technol. 184, 395–404. doi:10.1016/j.biortech.2014.10.018

Chang, Y., Lai, J.Y., Lee, D.J., 2016. Thermodynamic parameters for adsorption equilibrium of heavy metals and dyes from wastewaters: Research updated. Bioresour. Technol. 222, 513–516. doi:10.1016/j.biortech.2016.09.125

Chen, D., Cen, K., Cao, X., Li, Y., Zhang, Y., Ma, H., 2018a. Restudy on torrefaction of corn stalk from the point of view of deoxygenation and decarbonization. J. Anal. Appl. Pyrolysis 135, 1–9. doi:10.1016/j.jaap.2018.09.015

Chen, D., Gao, A., Ma, Z., Fei, D., Chang, Y., Shen, C., 2018b. In-depth study of rice husk torrefaction: Characterization of solid , liquid and gaseous products , oxygen migration and energy yield. Bioresour. Technol. 253, 148–153. doi:10.1016/j.biortech.2018.01.009

Chen, D., Mei, J., Li, H., Li, Y., Lu, M., Ma, T., Ma, Z., 2017. Combined pretreatment with torrefaction and washing using torrefaction liquid products to yield upgraded biomass and pyrolysis products. Bioresour. Technol. 228, 62–68. doi:10.1016/j.biortech.2016.12.088

Chen, D., Yin, L., Wang, H., He, P., 2014. Pyrolysis technologies for municipal solid waste: A review. Waste Manag. 34, 2466–2486. doi:https://doi.org/10.1016/j.wasman.2014.08.004

Chen, S., Yue, Q., Gao, B., Li, Q., Xu, X., Fu, K., 2012. Adsorption of hexavalent chromium from aqueous solution by modified corn stalk : A fixed-bed column study. Bioresour. Technol. 113, 114–120. doi:10.1016/j.biortech.2011.11.110

Chen, W.-H., Liu, S.-H., Juang, T.-T., Tsai, C.-M., Zhuang, Y.-Q., 2015a. Characterization of solid and liquid products from bamboo torrefaction. Appl. Energy 160, 829–835. doi:10.1016/j.apenergy.2015.03.022

Chen, W.-H., Peng, J., Bi, X.T., 2015b. A state-of-the-art review of biomass torrefaction, densification and applications. Renew. Sustain. Energy Rev. 44, 847–866. doi:10.1016/j.rser.2014.12.039

Cherifi, H., Fatiha, B., Salah, H., 2013. Kinetic studies on the adsorption of methylene blue onto vegetal fiber activated carbons. Appl. Surf. Sci. 282, 52–59. doi:10.1016/j.apsusc.2013.05.031

Chew, J.J., Doshi, V., 2011. Recent advances in biomass pretreatment – Torrefaction fundamentals and technology. Renew. Sustain. Energy Rev. 15, 4212–4222. doi:10.1016/j.rser.2011.09.017

Chiou, B.-S., Valenzuela-Medina, D., Bilbao-Sainz, C., Klamczynski, A.P., Avena-Bustillos, R.J., Milczarek, R.R., Du, W., Glenn, G.M., Orts, W.J., 2016. Torrefaction of almond shells : Effects of torrefaction conditions on properties of solid and condensate products. Ind. Crop. Prod. 86, 40–48. doi:10.1016/j.indcrop.2016.03.030

Chowdhury, S., Yasin, M., Uddin, M.T., Islam, M.A., 2016. Batch and continuous (fixed bed column) adsorption of methylene blue by rubber leaf powder. Int. J. Integr. Sci. Technol. 2, 24–28.

Chua, Y.W., Yu, Y., Wu, H., 2017. Thermal decomposition of pyrolytic lignin under inert conditions at low temperatures. Fuel 200, 70–75. doi:10.1016/j.fuel.2017.03.035

Chyang, C.S., Han, Y.L., Wu, L.W., Wan, H.P., Lee, H.T., Chang, Y.H., 2010. An investigation on pollutant emissions from co-firing of RDF and coal. Waste Manag. 30, 1334–1340. doi:10.1016/j.wasman.2009.11.018

Ciceri, G., Martignon, G., 2015. Solid Recovered Fuels production and use in Europe, in: IEA Bioenergy Conference. Berlin.

Cimpan, C., Wenzel, H., 2013. Energy implications of mechanical and mechanical-biological treatment compared to direct waste-to-energy. Waste Manag. 33, 1648–58. doi:10.1016/j.wasman.2013.03.026

Clausen, L.R., 2014. Integrated torrefaction vs. external torrefaction - A thermodynamic analysis for the case of a thermochemical biorefinery. Energy 77, 597–607. doi:10.1016/j.energy.2014.09.042

CMP-Cimentos Maceira e Pataias, S.A., 2011. Declaração Ambiental - Fábrica Cibra, Pataias.

Coates, J., 2000. Interpretation of Infrared Spectra, A Practical Approach. Encycl. Anal. Chem. doi:10.1002/9780470027318

Collazo, J., Pazó, J.A., Granada, E., Saavedra, Á., Eguía, P., 2012. Determination of the specific heat of biomass materials and the combustion energy of coke by DSC analysis. Energy 45, 746–752. doi:10.1016/j.energy.2012.07.018

Cook, E., Wagland, S., Coulon, F., 2015. Investigation into the non-biological outputs of mechanical-biological treatment facilities. Waste Manag. 46, 212–226. doi:10.1016/j.wasman.2015.09.014

Corella, J., Toledo, J.M., Molina, G., 2008. Performance of CaO and MgO for the hot gas clean up in gasification of a chlorine-containing (RDF) feedstock. Bioresour. Technol. 99, 7539–44. doi:10.1016/j.biortech.2008.02.018

Correia, R., Gonçalves, M., Nobre, C., Mendes, B., 2017. Impact of torrefaction and low-temperature carbonization on the properties of biomass wastes from Arundo donax L. and Phoenix canariensis. Bioresour. Technol. 223, 210–218. doi:http://dx.doi.org/10.1016/j.biortech.2016.10.046

Council of Ministers Presidency, 2017. Council of Ministers Resolution n.º 190-A/2017- Action Plan for Circular

Economy, Diary of the Republic, 1st seris.
Couto, N.D., Silva, V.B., Rouboa, A., 2016. Thermodynamic evaluation of Portuguese municipal solid waste gasification. J. Clean. Prod. 139, 622–635. doi:10.1016/j.jclepro.2016.08.082
Cozzani, V., Petarca, L., Tognotti, L., 1995. Devolatilization and pyrolysis of refuse derived fuels: characterization and kinetic modelling by a thermogravimetric and calorimetric approach. Fuel 74, 903–912. doi:10.1016/0016-2361(94)00018-M
da Silva, C.M.S., Carneiro, A. de C.O., Vital, B.R., Figueiró, C.G., Fialho, L. de F., de Magalhães, M.A., Carvalho, A.G., Cândido, W.L., 2017. Biomass torrefaction for energy purposes - Definitions and an overview of challenges and opportunities in Brazil. Renew. Sustain. Energy Rev. 82, 2426–2432. doi:10.1016/j.rser.2017.08.095
Dalai, A.K., Batta, N., Eswaramoorthi, I., Schoenau, G.J., 2009. Gasification of refuse derived fuel in a fixed bed reactor for syngas production. Waste Manag. 29, 252–258. doi:10.1016/j.wasman.2008.02.009
Das, O., Sarmah, A.K., Bhattacharyya, D., 2015. Biocomposites from waste derived biochars: Mechanical, thermal, chemical, and morphological properties. Waste Manag. doi:10.1016/j.wasman.2015.12.007
De la Rubia, M.A., Villamil, J.A., Rodriguez, J.J., Borja, R., Mohedano, A.F., 2018. Mesophilic anaerobic co-digestion of the organic fraction of municipal solid waste with the liquid fraction from hydrothermal carbonization of sewage sludge. Waste Manag. 76, 315–322. doi:10.1016/j.wasman.2018.02.046
Devi, R., Dahiya, R.P., 2006. Chemical oxygen demand (COD) reduction in domestic wastewater by fly ash and brick kiln ash. Water. Air. Soil Pollut. 174, 33–46. doi:10.1007/s11270-005-9022-9
Di Lonardo, M.C., Franzese, M., Costa, G., Gavasci, R., Lombardi, F., 2016. The application of SRF vs. RDF classification and specifications to the material flows of two mechanical-biological treatment plants of Rome: Comparison and implications. Waste Manag. 47, 195–205. doi:10.1016/j.wasman.2015.07.018
Dias, S., Silva, R., Barreiro, F., Costa, M., 2006. Avaliação do potencial de produção e utilização de CDR em Portugal Continental - Estudos base [WWW Document]. URL http://groups.ist.utl.pt/enverg/PDF/Potencial CDR v1 06_06.pdf
Dillibabu, V., Natarajan, E., 2014. Effect of temperature and equivalence ratio on gasification of biomass. J. Chem. Pharm. Sci. 45, 141–143.
Domeño, C., Nerín, C., 2003. Fate of polyaromatic hydrocarbons in the pyrolysis of industrial waste oils. J. Anal. Appl. Pyrolysis 67, 237–246.
Duan, F., Liu, J., Chyang, C.-S., Hu, C.-H., Tso, J., 2013. Combustion behavior and pollutant emission characteristics of RDF (refuse derived fuel) and sawdust in a vortexing fluidized bed combustor. Energy 57, 421–426. doi:10.1016/j.energy.2013.04.070
Dunnu, G., Maier, J., Scheffknecht, G., 2010. Ash fusibility and compositional data of solid recovered fuels. Fuel 89, 1534–1540. doi:10.1016/j.fuel.2009.09.008
Dunnu, G., Panopoulos, K.D., Karellas, S., Maier, J., Touliou, S., Koufodimos, G., Boukis, I., Kakaras, E., 2012. The solid recovered fuel Stabilat®: Characteristics and fluidised bed gasification tests. Fuel 93, 273–283. doi:10.1016/j.fuel.2011.08.061
Edo, M., Skoglund, N., Gao, Q., Persson, P., Jansson, S., 2017. Fate of metals and emissions of organic pollutants from torrefaction of waste wood , MSW , and RDF. Waste Manag. 68, 646–652. doi:10.1016/j.wasman.2017.06.017
Efika, E.C., Onwudili, J. a., Williams, P.T., 2015. Products from the high temperature pyrolysis of RDF at slow and rapid heating rates. J. Anal. Appl. Pyrolysis 112, 14–22. doi:10.1016/j.jaap.2015.01.004
Ekholm, E., 2005. RDF treatment methods in Finland, in: Jaakko Pöyry Infra - Soil and Water. Tallinn.
Erdogan, E., Atila, B., Mumme, J., Reza, M.T., Toptas, A., Elibol, M., Yanik, J., 2015. Characterization of products from hydrothermal carbonization of orange pomace including anaerobic digestibility of process liquor. Bioresour. Technol. 196, 35–42. doi:10.1016/j.biortech.2015.06.115
Eseyin, A., Steele, P., Pitman Jr., C., 2015. Current trends in the production and applications of torrefied wood/biomass - A Review. Bioresources.com 10, 8812–8858.
European Comission, 2014. Comission decision of December 18th 2014/955/UE, updating the European Waste List. Off. J. Eur. Union 370, 44–86.
European Union, 2015. Proposal for a Directive of the European Parliament and of the Council amending Directive 2008/98/EC on waste. doi:10.1007/s13398-014-0173-7.2
Fabry, F., Rehmet, C., Rohani, V., Fulcheri, L., 2013. Waste gasification by thermal plasma: A review. Waste and Biomass Valorization 4, 421–439. doi:10.1007/s12649-013-9201-7
Fagërnas, L., Kuoppala, E., Arpiainen, V., 2015. Composition, utilization and economic assessment of torrefaction condensates. Energy&Fuels 29, 3134–3142. doi:10.1021/acs.energyfuels.5b00004
Fan, S., Wang, Y., Wang, Z., Tang, Jie, Tang, Jun, Li, X., 2017. Removal of methylene blue from aqueous solution by sewage sludge-derived biochar : Adsorption kinetics , equilibrium , thermodynamics and mechanism. J. Environ. Chem. Eng. 5, 601–611. doi:10.1016/j.jece.2016.12.019
Fang, J., Zhan, L., Ok, Y.S., Gao, B., 2018. Minireview of potential applications of hydrochar derived from

hydrothermal carbonization of biomass. J. Ind. Eng. Chem. 57, 15–21. doi:10.1016/j.jiec.2017.08.026
Faria, P., Órfão, J., Pereira, M., 2004. Adsorption of anionic and cationic dyes on activated carbons with different surface chemistries. Water Res. 38, 2043–2052. doi:10.1016/j.watres.2004.01.034
Fernandes, A.C., Guerra, M.D., Ribeiro, R., Rodrigues, S., 2018. Relatório do Estado do Ambiente.
Fernandez, M., Nunell, G., Bonelli, P., Cukierman, A., 2014. Activated carbon developed from orange peels: Batch and dynamic competitive adsorption of basic dyes. Ind. Crops Prod. 62, 437–445. doi:10.1016/j.indcrop.2014.09.015
Foo, K.Y., Hameed, B.H., 2009. An overview of landfill leachate treatment via activated carbon adsorption process. J. Hazard. Mater. 171, 54–60. doi:10.1016/j.jhazmat.2009.06.038
Funke, A., Reebs, F., Kruse, A., 2013. Experimental comparison of hydrothermal and vapothermal carbonization. Fuel Process. Technol. 115, 261–269. doi:10.1016/j.fuproc.2013.04.020
Funke, A., Ziegler, F., 2010. Hydrothermal carbonization of biomass: A summary and discussion of chemical mechanisms for process engineering. Biofuels, Bioprod. Biorefining 4, 160–177. doi:10.1002/bbb.198
Galvagno, S., Casciaro, G., Casu, S., Martino, M., Mingazzini, C., Russo, a., Portofino, S., 2009. Steam gasification of tyre waste, poplar, and refuse-derived fuel: A comparative analysis. Waste Manag. 29, 678–689. doi:10.1016/j.wasman.2008.06.003
Gao, P., Zhou, Y., Meng, F., Zhang, Y., Liu, Z., Zhang, W., Xue, G., 2016. Preparation and characterization of hydrochar from waste eucalyptus bark by hydrothermal carbonization. Energy 97, 238–245. doi:10.1016/j.energy.2015.12.123
Garcia-Valls, R., Hatton, T.A., 2003. Metal ion complexation with lignin derivatives. Chem. Eng. J. 94, 99–105. doi:10.1016/S1385-8947(03)00007-X
Genon, G., Brizio, E., 2008. Perspectives and limits for cement kilns as a destination for RDF. Waste Manag. 28, 2375–85. doi:10.1016/j.wasman.2007.10.022
George, J., Arun, P., Muraleedharan, C., 2018. Experimental investigation on co-gasification of coffee husk and sawdust in a bubbling fluidised bed gasifier. J. Energy Inst. doi:10.1016/j.joei.2018.10.014
Ghosh, S.K., Bandyopadhyay, A., 2017. Adsorption of methylene blue onto citric acid treated carbonized bamboo leaves powder : Equilibrium , kinetics , thermodynamics analyses. J. Mol. Liq. 248, 413–424. doi:10.1016/j.molliq.2017.10.086
Gong, J.L., Zhang, Y.L., Jiang, Y., Zeng, G.M., Cui, Z.H., Liu, K., Deng, C.H., Niu, Q.Y., Deng, J.H., Huan, S.Y., 2015. Continuous adsorption of Pb(II) and methylene blue by engineered graphite oxide coated sand in fixed-bed column. Appl. Surf. Sci. 330, 148–157. doi:10.1016/j.apsusc.2014.11.068
Gopu, C., Gao, L., Volpe, M., Fiori, L., Goldfarb, J.L., 2018. Valorizing municipal solid waste: Waste to energy and activated carbons for water treatment via pyrolysis. J. Anal. Appl. Pyrolysis 133, 48–58. doi:10.1016/j.jaap.2018.05.002
Gouamid, M., Ouahrani, M.R., Bensaci, M.B., 2013. Adsorption equilibrium, kinetics and thermodynamics of methylene blue from aqueous solutions using Date palm Leaves. Energy Procedia 36, 898–907. doi:10.1016/j.egypro.2013.07.103
Grammelis, P., 2013. Report on RDF/SRF utilization applications and technical specifications. Ptolemais.
Grammelis, P., Basinas, P., Malliopoulou, a., Sakellaropoulos, G., 2009. Pyrolysis kinetics and combustion characteristics of waste recovered fuels. Fuel 88, 195–205. doi:10.1016/j.fuel.2008.02.002
Granados, D.A., Velásquez, H.I., Chejne, F., 2014. Energetic and exergetic evaluation of residual biomass in a torrefaction process. Energy 74, 181–189. doi:10.1016/j.energy.2014.05.046
Grootjes, S., 2012. Solid Phase Adsorption (SPA) method for tar and sulphr compounds, in: 20th European Biomass Conference & Exhibition. Milan.
Gu, H., Tang, Y., Yao, J., Chen, F., 2018. Study on biomass gasification under various operating conditions. J. Energy Inst. 1–8. doi:10.1016/j.joei.2018.10.002
Guo, F., Wang, X., Yang, X., 2017. Potential pyrolysis pathway assessment for microalgae-based aviation fuel based on energy conversion efficiency and life cycle. Energy Convers. Manag. 132, 272–280. doi:10.1016/j.enconman.2016.11.020
Gupta, V.K., Suhas, 2009. Application of low-cost adsorbents for dye removal – A review. J. Environ. Manage. 90, 2313–2342. doi:10.1016/j.jenvman.2008.11.017
Hadjittofi, L., Prodromou, M., Pashalidis, I., 2014. Activated biochar derived from cactus fibres - Preparation, characterization and application on Cu(II) removal from aqueous solutions. Bioresour. Technol. 159, 460–4. doi:10.1016/j.biortech.2014.03.073
Hajizadeh, Y., Williams, P.T., 2013. Activated carbon production from RDF and its use for dioxin removal from flue gas of waste incinerators. Int. J. Environ. Health Eng. 1, 1–10. doi:10.4103/2277-9183.110131
Han, B., Chen, Y., Wu, Y., Hua, D., Chen, Z., Feng, W., Yang, M., Xie, Q., 2014. Co-pyrolysis behaviors and kinetics of plastics-biomass blends through thermogravimetric analysis. J. Therm. Anal. Calorim. 115, 227–235. doi:10.1007/s10973-013-3228-7
Han, R., Zhang, J., Han, P., Wang, Y., Zhao, Z., Tang, M., 2009. Study of equilibrium, kinetic and thermodynamic

parameters about methylene blue adsorption onto natural zeolite. Chem. Eng. J. 145, 496–504. doi:10.1016/j.cej.2008.05.003
Han, X., Wang, W., Ma, X., 2011. Adsorption characteristics of methylene blue onto low cost biomass material lotus leaf. Chem. Eng. J. 171, 1–8. doi:10.1016/j.cej.2011.02.067
Haykiri-Acma, H., Kurt, G., Yaman, S., 2017. Properties of biochars obtained from RDF by carbonization: Influences of devolatilization severity. Waste and Biomass Valorization 8, 539–547. doi:10.1007/s12649-016-9610-5
Haykırı-Açma, H., Kurt, G., Yaman, S., 2017. Properties of biochars obtained from RDF by carbonization: Influences of devolatilization severity. Waste and Biomass Valorization 8, 539–547. doi:10.1007/s12649-016-9610-5
Hernandez-Atonal, F.D., Ryu, C., Sharifi, V.N., Swithenbank, J., 2007. Combustion of refuse-derived fuel in a fluidised bed. Chem. Eng. Sci. 62, 627–635. doi:10.1016/j.ces.2006.09.025
Ho, Y.S., McKay, G., 1999. Pseudo-second order model for sorption processes. Process Biochem. 34, 451–465. doi:10.1016/S0032-9592(98)00112-5
Hossain, A.K., Davies, P.A., 2013. Pyrolysis liquids and gases as alternative fuels in internal combustion engines - A review. Renew. Sustain. Energy Rev. 21, 165–189. doi:10.1016/j.rser.2012.12.031
Huang, Q., Tang, Y., Lu, S., Wu, X., Chi, Y., Yan, J., 2015. Characterization of tar derived from principle components of Municipal Solid Waste. Energy & Fuels 29, 7266–7274. doi:10.1021/acs.energyfuels.5b01152
Huang, R., Fang, C., Zhang, B., Tang, Y., 2018. Transformations of phosphorus speciation during (hydro) thermal treatments of animal manures. Environ. Sci. Technol. 52, 3016–3026. doi:10.1021/acs.est.7b05203
Hwang, I.-H., Kobayashi, J., Kawamoto, K., 2014. Characterization of products obtained from pyrolysis and steam gasification of wood waste, RDF, and RPF. Waste Manag. 34, 402–10. doi:10.1016/j.wasman.2013.10.009
Hwang, I.-H.H., Kawamoto, K., 2010. Survey of carbonization facilities for municipal solid waste treatment in Japan. Waste Manag. 30, 1423–1429. doi:10.1016/j.wasman.2010.01.017
Hwang, I.H., Aoyama, H., Matsuto, T., Nakagishi, T., Matsuo, T., 2012. Recovery of solid fuel from municipal solid waste by hydrothermal treatment using subcritical water. Waste Manag. 32, 410–416. doi:10.1016/j.wasman.2011.10.006
Hwang, I.H., Matsuto, T., 2008. Evaluation of carbonization as a thermal pretreatment method for landfilling by column leaching tests. Waste Manag. 28, 3–14. doi:10.1016/j.wasman.2006.11.007
Hwang, I.H., Matsuto, T., Tanaka, N., 2006. Water-soluble characteristics of chlorine in char derived from municipal solid wastes. Waste Manag. 26, 571–579. doi:10.1016/j.wasman.2005.04.012
Hwang, I H, Matsuto, T., Tanaka, N., Sasaki, Y., Tanaami, K., 2007. Characterization of char derived from various types of solid wastes from the standpoint of fuel recovery and pretreatment before landfilling. Waste Manag. 27, 1155–66. doi:10.1016/j.wasman.2006.05.013
Hwang, I. H., Matsuto, T., Tanaka, N., Sasaki, Y., Tanaami, K., 2007. Characterization of char derived from various types of solid wastes from the standpoint of fuel recovery and pretreatment before landfilling. Waste Manag. 27, 1155–1166. doi:10.1016/j.wasman.2006.05.013
Idowu, I., Li, L., Flora, J.R. V, Pellechia, P.J., Darko, S.A., Ro, K.S., Berge, N.D., 2017. Hydrothermal carbonization of food waste for nutrient recovery and reuse. Waste Manag. 69, 480–491. doi:10.1016/j.wasman.2017.08.051
Jeguirim, M., Trouvé, G., 2009. Pyrolysis characteristics and kinetics of Arundo donax using thermogravimetric analysis. Bioresour. Technol. 100, 4026–4031. doi:10.1016/j.biortech.2009.03.033
Junming, X., Jianchun, J., Yanju, L., Jie, C., 2009. Liquid hydrocarbon fuels obtained by the pyrolysis of soybean oils. Bioresour. Technol. 100, 4867–70. doi:10.1016/j.biortech.2009.04.055
Kallel, F., Chaari, F., Bouaziz, F., Bettaieb, F., Ghorbel, R., Chaabouni, S.E., 2016. Sorption and desorption characteristics for the removal of a toxic dye, methylene blue from aqueous solution by a low cost agricultural by-product. J. Mol. Liq. 219, 279–288. doi:10.1016/j.molliq.2016.03.024
Kambo, H.S., Dutta, A., 2015. A comparative review of biochar and hydrochar in terms of production , physico-chemical properties and applications. Renew. Sustain. Energy Rev. 45, 359–378. doi:10.1016/j.rser.2015.01.050
Kambo, H.S., Minaret, J., Dutta, A., 2017. Process water from the hydrothermal carbonization of biomass: A waste or a valuable product? Waste and Biomass Valorization 9, 1181–1189. doi:10.1007/s12649-017-9914-0
Kanaly, R., Harayama, S., 2000. Biodegradation of high-molecular-weight polycyclic aromatic hydrocarbons by bacteria. J. Bacteriol. 182, 2059–2067. doi:10.1128/JB.182.8.2059-2067.2000
Kara, M., 2012. Environmental and economic advantages associated with the use of RDF in cement kilns. Resour. Conserv. Recycl. 68, 21–28. doi:10.1016/j.resconrec.2012.06.011
Karnib, M., Kabbani, A., Holail, H., Olama, Z., 2014. Heavy Metals Removal Using Activated Carbon, Silica and Silica Activated Carbon Composite. Energy Procedia 50, 113–120. doi:10.1016/j.egypro.2014.06.014
Khadhri, N., El, M., Saad, K., Moussaoui, Y., 2019. Batch and continuous column adsorption of indigo carmine

onto activated carbon derived from date palm petiole. J. Environ. Chem. Eng. 7, 102775. doi:10.1016/j.jece.2018.11.020
Kim, D., Park, K.Y., Yoshikawa, K., 2017. Conversion of Municipal Solid Wastes into biochar through hydrothermal carbonization, in: Huang, W.-J. (Ed.), Engineering Applications of Biochar. IntechOpen. doi:10.5772/intechopen.68221
Kim, S.S., Kim, S.H., 2000. Pyrolysis kinetics of waste automobile lubricating oil. Fuel 79, 1943–1949. doi:10.1016/S0016-2361(00)00028-4
Kumar, A., Jena, H.M., 2016. Removal of methylene blue and phenol onto prepared activated carbon from Fox nutshell by chemical activation in batch and fixed-bed column. J. Clean. Prod. 137, 1246–1259. doi:10.1016/j.jclepro.2016.07.177
Kumar, A., Jones, D.D., Hanna, M.A., 2009. Thermochemical biomass gasification: A review of the current status of the technology. Energies 2, 556–581. doi:10.3390/en20300556
Kumar, K.V., Kumaran, A., 2005. Removal of methylene blue by mango seed kernel powder. Biochem. Eng. J. 27, 83–93. doi:10.1016/j.bej.2005.08.004
Kumar, M., Olajire Oyedun, A., Kumar, A., 2018. A review on the current status of various hydrothermal technologies on biomass feedstock. Renew. Sustain. Energy Rev. 81, 1742–1770. doi:10.1016/j.rser.2017.05.270
Kurniawan, T.A., Lo, W.H., Chan, G.Y.S.G.Y., 2006. Physico-chemical treatments for removal of recalcitrant contaminants from landfill leachate. J. Hazard. Mater. 129, 80–100. doi:10.1016/j.jhazmat.2005.08.010
Kuzmina, J.S., Director, L.B., Shevchenko, A.L., Zaichenko, V.M., 2016. Energy efficiency analysis of reactor for torrefaction of biomass with direct heating. J. Phys. Conf. Ser. 774. doi:10.1088/1742-6596/774/1/012138
Kwant, K.W., Knoef, H., 2004. Status of gasification in countries participating in the IEA and GasNet activity.
Lee, J., Lee, K., Sohn, D., Kim, Y.M., Park, K.Y., 2018. Hydrothermal carbonization of lipid extracted algae for hydrochar production and feasibility of using hydrochar as a solid fuel. Energy 153, 913–920. doi:https://doi.org/10.1016/j.energy.2018.04.112
Li, B., Wang, Q., Guo, J.-Z., Huan, W.-W., Liu, L., 2018. Sorption of methyl orange from aqueous solution by protonated amine modified hydrochar. Bioresour. Technol. 268, 454–459. doi:https://doi.org/10.1016/j.biortech.2018.08.023
Li, L., Diederick, R., Flora, J.R.V., Berge, N.D., 2013. Hydrothermal carbonization of food waste and associated packaging materials for energy source generation. Waste Manag. 33, 2478–2492. doi:10.1016/j.wasman.2013.05.025
Li, M., Li, W., Liu, S., 2011. Hydrothermal synthesis , characterization , and KOH activation of carbon spheres from glucose. Carbohydr. Res. 346, 999–1004. doi:10.1016/j.carres.2011.03.020
Lima, D.G., Soares, V.C.D., Ribeiro, E.B., Carvalho, D. a., Cardoso, É.C.V., Rassi, F.C., Mundim, K.C., Rubim, J.C., Suarez, P. a. Z., 2004. Diesel-like fuel obtained by pyrolysis of vegetable oils. J. Anal. Appl. Pyrolysis 71, 987–996. doi:10.1016/j.jaap.2003.12.008
Lin, K.S., Wang, H.P., Liu, S.H., Chang, N. Bin, Huang, Y.J., Wang, H.C., 1999. Pyrolysis kinetics of refuse-derived fuel. Fuel Process. Technol. 60, 103–110. doi:10.1016/S0378-3820(99)00043-0
Lin, Y., Ma, X., Peng, X., Hu, S., Yu, Z., Fang, S., 2015. Effect of hydrothermal carbonization temperature on combustion behavior of hydrochar fuel from paper sludge. Appl. Therm. Eng. 91, 574–582. doi:https://doi.org/10.1016/j.applthermaleng.2015.08.064
Lin, Y., Ma, X., Peng, X., Yu, Z., 2017. Hydrothermal carbonization of typical components of municipal solid waste for deriving hydrochars and their combustion behavior. Bioresour. Technol. 243, 539–547. doi:10.1016/j.biortech.2017.06.117
Liu, Z., Quek, A., Hoekman, S.K., Balasubramanian, R., Kent Hoekman, S., Balasubramanian, R., 2013. Production of solid biochar fuel from waste biomass by hydrothermal carbonization. Fuel 103, 943–949. doi:10.1016/j.fuel.2012.07.069
Lokahita, B., Aziz, M., Yoshikawa, K., Takahashi, F., 2017. Energy and resource recovery from Tetra Pak waste using hydrothermal treatment. Appl. Energy 207, 107–113. doi:10.1016/j.apenergy.2017.05.141
Lombardi, L., Carnevale, E., Corti, A., 2014. A review of technologies and performances of thermal treatment systems for energy recovery from waste. Waste Manag. 37, 26–44. doi:10.1016/j.wasman.2014.11.010
Lonappan, L., Rouissi, T., Kumar, R., Brar, S.K., Avalos, A., Verma, M., Surampalli, R.Y., Valero, J.R., 2016. Adsorption of methylene blue on biochar microparticles derived from different waste materials. Waste Manag. 49, 537–544. doi:10.1016/j.wasman.2016.01.015
López-Cervantes, J., Sánchez-Machado, D., Sánchez-Duarte, R., Correa-Murrieta, M., 2018. Study of a fixed-bed column in the adsorption of an azo dye from an aqueous medium using a chitosan – glutaraldehyde biosorbent. Adsorpt. Sci. Technol. 36, 215–232. doi:10.1177/0263617416688021
Lopez-Urionabarrenechea, A., De Marco, I., Caballero, B.M., Laresgoiti, M.F., Adrados, A., 2012. Catalytic stepwise pyrolysis of packaging plastic waste. J. Anal. Appl. Pyrolysis 96, 54–62.

doi:10.1016/j.jaap.2012.03.004
López, A., Marco, I. De, Caballero, B.M., Laresgoiti, M.F., Adrados, A., 2011. Influence of time and temperature on pyrolysis of plastic wastes in a semi-batch reactor. Chem. Eng. J. 173, 62–71. doi:10.1016/j.cej.2011.07.037
Lu, L., Namioka, T., Yoshikawa, K., 2011. Effects of hydrothermal treatment on characteristics and combustion behaviors of municipal solid wastes. Appl. Energy 88, 3659–3664. doi:10.1016/j.apenergy.2011.04.022
Lu, X., Flora, J.R. V, Berge, N.D., 2014. Influence of process water quality on hydrothermal carbonization of cellulose. Bioresour. Technol. 154, 229–239. doi:10.1016/j.biortech.2013.11.069
Lucian, M., Volpe, M., Gao, L., Piro, G., Goldfarb, J.L., Fiori, L., 2018. Impact of hydrothermal carbonization conditions on the formation of hydrochars and secondary chars from the organic fraction of municipal solid waste. Fuel 233, 257–268. doi:10.1016/j.fuel.2018.06.060
Ma, W., Hoffmann, G., Schirmer, M., Chen, G., Rotter, V.S., 2010. Chlorine characterization and thermal behavior in MSW and RDF. J. Hazard. Mater. 178, 489–98. doi:10.1016/j.jhazmat.2010.01.108
Ma, X., Zhou, B., Budai, A., Jeng, A., Hao, X., Wei, D., Zhang, Y., Rasse, D., 2016. Study of biochar properties by Scanning Electron Microscope – Energy Dispersive X-Ray spectroscopy (SEM-EDX). Commun. Soil Sci. Plant Anal. 47, 593–601. doi:10.1080/00103624.2016.1146742
Mahamad, M.N., Zaini, M.A.A., Zakaria, Z.A., 2015. Preparation and characterization of activated carbon from pineapple waste biomass for dye removal. Int. Biodeterior. Biodegradation 102, 274–280. doi:10.1016/j.ibiod.2015.03.009
Mahmoud, D.K., Salleh, M.A.M., Karim, W.A.W.A., Idris, A., Abidin, Z.Z., 2012. Batch adsorption of basic dye using acid treated kenaf fibre char: Equilibrium, kinetic and thermodynamic studies. Chem. Eng. J. 181–182, 449–457. doi:10.1016/j.cej.2011.11.116
Mäkelä, M., Benavente, V., Fullana, A., 2015. Hydrothermal carbonization of lignocellulosic biomass: Effect of process conditions on hydrochar properties. Appl. Energy 155, 576–584. doi:10.1016/j.apenergy.2015.06.022
Mäkelä, M., Forsberg, J., Söderberg, C., Larsson, S.H., Dahl, O., 2018. Process water properties from hydrothermal carbonization of chemical sludge from a pulp and board mill. Bioresour. Technol. 263, 654–659. doi:10.1016/j.biortech.2018.05.044
Manna, S., Roy, D., Saha, P., Gopakumar, D., Thomas, S., 2017. Rapid methylene blue adsorption using modified lignocellulosic materials. Process Saf. Environ. Prot. 107, 346–356. doi:10.1016/j.psep.2017.03.008
Manyà, J.J., García-Ceballos, F., Azuara, M., Latorre, N., Royo, C., 2015. Pyrolysis and char reactivity of a poor-quality refuse-derived fuel (RDF) from municipal solid waste. Fuel Process. Technol. 140, 276–284. doi:10.1016/j.fuproc.2015.09.014
Manyuchi, M.M., Mbohwa, C., Muzenda, E., 2018. Potential to use municipal waste bio char in wastewater treatment for nutrients recovery. Phys. Chem. Earth 107, 92–95. doi:10.1016/j.pce.2018.07.002
Marçal, A., Mateus, I., Silva, F., 2014. Relatório Anual Resíduos Urbanos, Relatório Anual Resíduos Urbanos 2014. Amadora.
Marçal, A., Teixeira, A.R., 2017. Relatório Anual de Resíduos Urbanos. Amadora.
Marsh, R., Griffiths, a. J., Williams, K.P., Wilcox, S.J., 2007. Physical and thermal properties of extruded refuse derived fuel. Fuel Process. Technol. 88, 701–706. doi:10.1016/j.fuproc.2007.01.015
Mastellone, M., Zaccariello, L., Arena, U., 2010. Co-gasification of coal , plastic waste and wood in a bubbling fluidized bed reactor. Fuel 89, 2991–3000. doi:10.1016/j.fuel.2010.05.019
Materazzi, M., Lettieri, P., Mazzei, L., Taylor, R., Chapman, C., 2015. Fate and behavior of inorganic constituents of RDF in a two stage fluid bed-plasma gasification plant. Fuel 150, 473–485. doi:10.1016/j.fuel.2015.02.059
Materazzi, M., Lettieri, P., Taylor, R., Chapman, C., 2016. Performance analysis of RDF gasification in a two stage fluidized bed-plasma process. Waste Manag. 47, 256–266. doi:10.1016/j.wasman.2015.06.016
Matsakas, L., Gao, Q., Jansson, S., Rova, U., Christakopoulos, P., 2017. Green conversion of municipal solid wastes into fuels and chemicals. Electron. J. Biotechnol. 26, 69–83. doi:10.1016/j.ejbt.2017.01.004
Mau, V., Gross, A., 2018. Energy conversion and gas emissions from production and combustion of poultry-litter-derived hydrochar and biochar. Appl. Energy 213, 510–519. doi:10.1016/j.apenergy.2017.11.033
Meili, L., Lins, P.V.S., Costa, M.T., Almeida, R.L., Abud, A.K.S., Soletti, J.I., Dotto, G.L., Tanabe, E.H., Sellaoui, L., Carvalho, S.H. V, Erto, A., 2018. Adsorption of methylene blue on agroindustrial wastes: Experimental investigation and phenomenological modelling. Prog. Biophys. Mol. Biol. 1–12. doi:10.1016/j.pbiomolbio.2018.07.011
Mihajlović, M., Petrović, J., Maletić, S., Isakovski, M.K., Stojanović, M., Lopičić, Z., Trifunović, S., 2018. Hydrothermal carbonization of Miscanthus × giganteus: Structural and fuel properties of hydrochars and organic profile with the ecotoxicological assessment of the liquid phase. Energy Convers. Manag. 159, 254–263. doi:https://doi.org/10.1016/j.enconman.2018.01.003
Miller, G.L., 1959. Use of dinitrosalicylic acid (DNS) reagent for determination of reducing sugar. Anal. Chem.

31, 426–428. doi:10.1021/ac60147a030
Minaret, J., Dutta, A., 2016. Comparison of liquid and vapor hydrothermal carbonization of corn husk for the use as a solid fuel. Bioresour. Technol. 200, 804–811. doi:10.1016/j.biortech.2015.11.010
Ministry of Environment Regional Ordinance and Regional Development, 2009. Decree-Law n.º183/2009.
Ministry of the Environment, 1998. Decree-Law n.º 236/98, Diary of the Republic.
Miskolczi, N., Buyong, F., Angyal, a., Williams, P.T., Bartha, L., 2010. Two stages catalytic pyrolysis of refuse derived fuel: Production of biofuel via syncrude. Bioresour. Technol. 101, 8881–8890. doi:10.1016/j.biortech.2010.06.103
Missaoui, Ayoub, Bostyn, S., Belandria, V., Cagnon, B., Sarh, B., 2017. Hydrothermal carbonization of dried olive pomace : Energy potential and process performances. J. Anal. Appl. Pyrolysis 128, 281–290. doi:10.1016/j.jaap.2017.09.022
Missaoui, A, Bostyn, S., Belandria, V., Sarh, B., Gökalp, I., 2017. Assessing the Heat and Energy Balances of Hydrochar Production via Hydrothermal Carbonization of Olive Pomace. Proceeding 25th Eur. Biomass Conf. Exhib. 1393–1398.
Mohan, D., Sarswat, A., Ok, Y.S., Pittman, C.U., 2014. Organic and inorganic contaminants removal from water with biochar, a renewable, low cost and sustainable adsorbent - A critical review. Bioresour. Technol. 160, 191–202. doi:10.1016/j.biortech.2014.01.120
Molino, A., Iovane, P., Donatelli, A., Braccio, G., Chianese, S., Musmarra, D., 2013. Steam gasification of refuse-derived fuel in a rotary kiln pilot plant: Experimental tests. Chem. Eng. Trans. 32, 337–342. doi:10.3303/CET1332057
Monteiro, E., Ismail, T.M., Ramos, A., El-salam, M.A., Brito, P., Rouboa, A., 2018. Experimental and modeling studies of Portuguese peach stone gasification on an autothermal bubbling fluidized bed pilot plant. Energy 142, 862–877. doi:10.1016/j.energy.2017.10.100
Mu'min, F.G., Prawisudha, P., Zaini, N.I., Aziz, M., Pasek, D.A., 2017. Municipal solid waste processing and separation employing wet torrefaction for alternative fuel production and aluminum reclamation. Waste Manag. 67, 106–120. doi:10.1016/j.wasman.2017.05.022
Municipality of Lisbon, 1991. Regulation for the release of industrial efluents in the network of collectors of Lisbon - Ed n.º156/91. Lisbon.
Murugan, S., Ramaswamy, M.C., Nagarajan, G., 2008. The use of tyre pyrolysis oil in diesel engines. Waste Manag. 28, 2743–9. doi:10.1016/j.wasman.2008.03.007
Nakagawa, K., Namba, A., Mukai, S.R., Tamon, H., Ariyadejwanich, P., Tanthapanichakoon, W., 2004. Adsorption of phenol and reactive dye from aqueous solution on activated carbons derived from solid wastes. Water Res. 38, 1791–1798. doi:10.1016/j.watres.2004.01.002
Nakagawa, K., Tamon, H., Suzuki, T., Nagano, S., 2002. Preparation and Characterization of Activated Carbons from Refuse Derived Fuel (RDF). J. Porous Mater. 9, 25–33. doi:10.1023/A:1014395520344
Nakason, K., Panyapinyopol, B., Kanokkantapong, V., 2018. Characteristics of hydrochar and liquid fraction from hydrothermal carbonization of cassava rhizome. J. Energy Inst. 91, 184–193. doi:10.1016/j.joei.2017.01.002
Nakason, K., Panyapinyopol, B., Kanokkantapong, V., Viriya-empikul, N., Kraithong, W., Pavasant, P., 2017. Hydrothermal carbonization of unwanted biomass materials: Effect of process temperature and retention time on hydrochar and liquid fraction. J. Energy Inst. 91, 786–796. doi:10.1016/j.joei.2017.05.002
Narvekar, A.A., Fernandes, J.B., Tilve, S.G., 2018. Adsorption behavior of methylene blue on glycerol based carbon materials. J. Environ. Chem. Eng. 6, 1714–1725. doi:10.1016/j.jece.2018.02.016
Nasrullah, M., Vainikka, P., Hannula, J., Hurme, M., 2015. Elemental balance of SRF production process: Solid recovered fuel produced from commercial and industrial waste. Fuel 145, 1–11. doi:10.1016/j.fuel.2014.12.071
Nasrullah, M., Vainikka, P., Hannula, J., Hurme, M., Kärki, J., 2014. Mass, energy and material balances of SRF production process. Part 1: SRF produced from commercial and industrial waste. Waste Manag. 34, 1398–407. doi:10.1016/j.wasman.2014.06.009
Nerín, C., Domeño, C., Moliner, R., Lázaro, M., Suelves, I., Valderrama, J., 2000. Behaviour of different industrial waste oils in a pyrolysis process : metals distribution and valuable products. J. Anal. Appl. Pyrolysis 55, 171–183.
Nhuchhen, D.R., Afzal, M.T., 2017. HHV Predicting Correlations for Torrefied Biomass Using Proximate and Ultimate Analyses. Bioengineering 4. doi:10.3390/bioengineering4010007
Niu, Y., Tan, H., Hui, S., 2016. Ash-related issues during biomass combustion: Alkali-induced slagging, silicate melt-induced slagging (ash fusion), agglomeration, corrosion, ash utilization, and related countermeasures. Prog. Energy Combust. Sci. 52, 1–61. doi:10.1016/j.pecs.2015.09.003
Nizamuddin, S., Baloch, H.A., Griffin, G.J., Mubarak, N.M., Bhutto, A.W., Abro, R., Mazari, S.A., Ali, B.S., 2017. An overview of effect of process parameters on hydrothermal carbonization of biomass. Renew. Sustain. Energy Rev. 73, 1289–1299. doi:10.1016/j.rser.2016.12.122
Nobre, C., Gonçalves, M., Resende, D., Vilarinho, C., Mendes, B., 2016. Removal of Chromium and Aluminum

from Aqueous Solutions Using Refuse Derived Char, in: Camarinha-Matos, L.M., Falcão, A.J., Vafaeu, N., Najdi, S. (Eds.), Technological Innovation for Cyber-Physical Systems: 7th IFIP WG 5.5/SOCOLNET Advanced Doctoral Confenrece on Computing, Electrical and Industrial Systems. Springer Nature. doi:10.1007/978-3-319-31165-4

Nobre, C., Gonçalves, M., Vilarinho, C., 2019a. A brief assessment on the application of torrefaction and carbonization for refuse derived fuel upgrading. Lect. Notes Electr. Eng. 505, 633–640. doi:10.1007/978-3-319-91334-6_86

Nobre, C., Vilarinho, C., Alves, O., Mendes, B., Gonçalves, M., 2019b. Upgrading of refuse derived fuel through torrefaction and carbonization: Evaluation of RDF char fuel properties. Energy 181, 66–76. doi:10.1016/j.energy.2019.05.105

Nutalapati, D., Gupta, R., Moghtaderi, B., Wall, T.F.F., 2007. Assessing slagging and fouling during biomass combustion: A thermodynamic approach allowing for alkali/ash reactions. Fuel Process. Technol. 88, 1044–1052. doi:10.1016/j.fuproc.2007.06.022

Ohliger, A., Förster, M., Kneer, R., 2013. Torrefaction of beechwood: A parametric study including heat of reaction and grindability. Fuel 104, 607–613. doi:10.1016/j.fuel.2012.06.112

OJEC, 2003. Council Decision 2003/33/CE of 19 December 2002 on Waste landfilling. European Comunity.

Olufemi, A.S., 2017. Comparative study of temperature effect on gasification of solid wastes in a fixed bed. Austin Chem. Eng. 4, 2–5.

Osipovs, S., 2013. Comparison of efficiency of two methods for tar sampling in the syngas. Fuel 103, 387–392. doi:10.1016/j.fuel.2012.05.021

Osswald, T., Hernández-Ortiz, J.P., 2006. Chapter 2: Processing properties, in: Polymer Processing: Modeling and Simulation. Hanser, Munich, pp. 37–47.

Othman, N.H., Alias, N.H., Shahruddin, M.Z., Fitrah, N., Bakar, A., Raikhan, N., Him, N., Jye, W., 2018. Adsorption kinetics of methylene blue dyes onto magnetic graphene oxide. J. Environ. Chem. Eng. 6, 2803–2811. doi:10.1016/j.jece.2018.04.024

Oyedun, A.O., Tee, C.Z., Hanson, S., Hui, C.W., 2014. Thermogravimetric analysis of the pyrolysis characteristics and kinetics of plastics and biomass blends. Fuel Process. Technol. 128, 471–481. doi:10.1016/j.fuproc.2014.08.010

Pala, M., Kantarli, I.C., Buyukisik, H.B., Yanik, J., 2014. Hydrothermal carbonization and torrefaction of grape pomace: A comparative evaluation. Bioresour. Technol. 161, 255–262. doi:10.1016/j.biortech.2014.03.052

Park, K.Y., Lee, K., Kim, D., 2018. Characterized hydrochar of algal biomass for producing solid fuel through hydrothermal carbonization. Bioresour. Technol. 258, 119–124. doi:https://doi.org/10.1016/j.biortech.2018.03.003

Park, S.S., Seo, D.K., Lee, S.H., Yu, T.U., Hwang, J., 2012. Study on pyrolysis characteristics of refuse plastic fuel using lab-scale tube furnace and thermogravimetric analysis reactor. J. Anal. Appl. Pyrolysis 97, 29–38. doi:10.1016/j.jaap.2012.06.009

Park, S.W., Jang, C.H., 2011. Characteristics of carbonized sludge for co-combustion in pulverized coal power plants. Waste Manag. 31, 523–529. doi:10.1016/j.wasman.2010.10.009

Pathania, D., Sharma, S., Singh, P., 2017. Removal of methylene blue by adsorption onto activated carbon developed from Ficus carica bast. Arab. J. Chem. 10, S1445–S1451. doi:10.1016/j.arabjc.2013.04.021

Petrovic, J., Perisic, N., Maksimovic, J.D., Maksimovic, V., Kragovic, M., Stojanovic, M., Lausevic, M., Mihajlovic, M., 2016. Hydrothermal conversion of grape pomace: Detailed characterization of obtained hydrochar and liquid phase. J. Anal. Appl. Pyrolysis 118, 267–277. doi:10.1016/j.jaap.2016.02.010

Peydayesh, M., Rahbar-Kelishami, A., 2015. Adsorption of methylene blue onto Platanus orientalis leaf powder: Kinetic, equilibrium and thermodynamic studies. J. Ind. Eng. Chem. 21, 1014–1019. doi:10.1016/j.jiec.2014.05.010

Pezoti, O., Cazetta, A.L., Souza, I.P. a F., Bedin, K.C., Martins, A.C., Silva, T.L., Almeida, V.C., 2014. Adsorption studies of methylene blue onto ZnCl2-activated carbon produced from buriti shells (Mauritia flexuosa L.). J. Ind. Eng. Chem. 20, 4401–4407. doi:10.1016/j.jiec.2014.02.007

Phillips, J.A., 1998. Managing America ' s Solid Waste [WWW Document]. Natl. Renew. Energy Lab. URL https://www.csu.edu/cerc/researchreports/documents/ManagingAmericasSolidWaste1998.pdf (accessed 4.20.14).

Pinto, F., André, R.N., Carolino, C., Miranda, M., Abelha, P., Direito, D., Perdikaris, N., Boukis, I., 2014. Gasification improvement of a poor quality solid recovered fuel (SRF). Effect of using natural minerals and biomass wastes blends. Fuel 117, 1034–1044. doi:10.1016/j.fuel.2013.10.015

Pinto, S., 2009. Caracterização de Combustíveis Derivados de Resíduos obtidos a partir de resíduos industriais não perigosos. Master Thesis. NOVA University of Lisbon.

Poerschmann, J., Weiner, B., Woszidlo, S., Koehler, R., Kopinke, F.D., 2015. Hydrothermal carbonization of poly(vinyl chloride). Chemosphere 119, 682–689. doi:10.1016/j.chemosphere.2014.07.058

Postai, D.L., Demarchi, C.A., Zanatta, F., Melo, D., Rodrigues, C., 2016. Adsorption of rhodamine B and

methylene blue dyes using waste of seeds of Aleurites Moluccana, a low cost adsorbent. Alexandria Eng. J. 55, 1713–1723. doi:10.1016/j.aej.2016.03.017
Potgieter, J.H., Pearson, S., Pardesi, C., 2018. Kinetic and thermodynamic parameters for the adsorption of methylene blue using fly ash under batch , column , and heap leaching configurations. Coal Combust. Gasif. Porducts 10, 23–33. doi:10.4177/CCGP-D-17-00011.1
Prawisudha, P., Namioka, T., Yoshikawa, K., 2012. Coal alternative fuel production from municipal solid wastes employing hydrothermal treatment. Appl. Energy 90, 298–304. doi:https://doi.org/10.1016/j.apenergy.2011.03.021
Prins, M.J., Ptasinski, K.J., Janssen, F.J.J.G., 2006a. Torrefaction of wood. Part 1. Weight loss kinetics. J. Anal. Appl. Pyrolysis 77, 28–34. doi:10.1016/j.jaap.2006.01.002
Prins, M.J., Ptasinski, K.J., Janssen, F.J.J.G., 2006b. Torrefaction of wood. Part 2. Analysis of products. J. Anal. Appl. Pyrolysis 77, 35–40. doi:10.1016/j.jaap.2006.01.001
Puccini, M., Ceccarini, L., Antichi, D., Seggiani, M., Tavarini, S., Latorre, M.H., Vitolo, S., 2018. Hydrothermal carbonization of municipal woody and herbaceous prunings: Hydrochar valorisation as soil amendment and growth medium for horticulture. Sustainability 10. doi:10.3390/su10030846
Puccini, M., Stefanelli, E., Hiltz, M., Seggiani, M., 2017. Activated carbon from hydrochar produced by hydrothermal carbonization of wastes. Chem. Eng. Trans. 57, 169–174. doi:10.3303/CET1757029
Qi, J., Zhao, J., Xu, Y., Wang, Y., Han, K., 2018. Segmented heating carbonization of biomass: Yields, property and estimation of heating value of chars. Energy 144, 301–311. doi:10.1016/j.energy.2017.12.036
Qian, W.-C., Luo, X.-P., Wang, X., Guo, M., Li, B., 2018. Removal of methylene blue from aqueous solution by modified bamboo hydrochar. Ecotoxicol. Environ. Saf. 157, 300–306. doi:https://doi.org/10.1016/j.ecoenv.2018.03.088
Rabou, L.P.L.M., 2005. Biomass tar recycling and destruction in a CFB gasifier. Fuel 84, 577–581. doi:10.1016/j.fuel.2004.10.013
Rada, E.C., Andreottola, G., 2012. RDF/SRF: which perspective for its future in the EU. Waste Manag. 32, 1059–1060. doi:10.1016/j.wasman.2012.02.017
Rafatullah, M., Sulaiman, O., Hashim, R., Ahmad, A., 2010. Adsorption of methylene blue on low-cost adsorbents: A review. J. Hazard. Mater. 177, 70–80. doi:10.1016/j.jhazmat.2009.12.047
Ramos, A., Monteiro, E., Silva, V., Rouboa, A., 2018. Co-gasification and recent developments on waste-to-energy conversion: A review. Renew. Sustain. Energy Rev. 81, 380–398. doi:10.1016/j.rser.2017.07.025
Rangabhashiyam, S., Balasubramanian, P., 2018. Adsorption behaviors of hazardous methylene blue and hexavalent chromium on novel materials derived from Pterospermum acerifolium shells. J. Mol. Liq. 254, 433–445. doi:10.1016/j.molliq.2018.01.131
Recari, J., Berrueco, C., Abelló, S., Montané, D., Farriol, X., 2016. Gasification of two solid recovered fuels (SRFs) in a lab-scale fluidized bed reactor: Influence of experimental conditions on process performance and release of HCl, H2S, HCN and NH3. Fuel Process. Technol. 142, 107–114. doi:10.1016/j.fuproc.2015.10.006
Recari, J., Berrueco, C., Puy, N., Alier, S., Bartrolí, J., Farriol, X., 2017. Torrefaction of a solid recovered fuel (SRF) to improve the fuel properties for gasification processes. Appl. Energy 203, 177–188. doi:10.1016/j.apenergy.2017.06.014
Reddy, P.M.K., Verma, P., Subrahmanyam, C., 2015. Bio-waste derived adsorbent material for methylene blue adsorption. J. Taiwan Inst. Chem. Eng. 58, 500–508. doi:10.1016/j.jtice.2015.07.006
Regmi, P., Garcia Moscoso, J.L., Kumar, S., Cao, X., Mao, J., Schafran, G., 2012. Removal of copper and cadmium from aqueous solution using switchgrass biochar produced via hydrothermal carbonization process. J. Environ. Manage. 109, 61–69. doi:10.1016/j.jenvman.2012.04.047
Ren, J., Wang, F., Zhai, Y., Zhu, Y., Peng, C., Wang, T., Li, C., Zeng, G., 2017. Effect of sewage sludge hydrochar on soil properties and Cd immobilization in a contaminated soil. Chemosphere 189, 627–633. doi:https://doi.org/10.1016/j.chemosphere.2017.09.102
Renou, S., Poulain, S., Givaudan, J.G., Sahut, C., Moulin, P., 2009. Lime treatment of stabilized leachates. Water Scinece Technol. 59, 673–685. doi:10.2166/wst.2009.014
Reza, M.T., Lynam, J.G., Uddin, M.H., Coronella, C.J., 2013. Hydrothermal carbonization: Fate of inorganics. Biomass and Bioenergy 49, 86–94. doi:10.1016/j.biombioe.2012.12.004
Reza, R.A., Ahmaruzzaman, M., 2015. Comparative study of waste derived adsorbents for sequestering methylene blue from aquatic environment. Biochem. Pharmacol. 3, 395–404. doi:10.1016/j.jece.2014.06.006
Ribeiro, J.M.C., Godina, R., Matias, J.C. de O., Nunes, L.J.R., 2018. Future perspectives of biomass torrefaction: Review of the current state-of-the-art and research development. Sustainability 10, 1–17. doi:10.3390/su10072323
Richter, H., Howard, J.B., 2000. Formation of polyciclic aromatic hydrocarbons and their growth to soot - a review of chemical reaction pathways. Prog. Energy Combust. Sci. 26, 565–608. doi:https://doi.org/10.1016/S0360-1285(00)00009-5

Rivas, F.J., Beltrán, F.J., Gimeno, O., Frades, J., Carvalho, F., 2006. Adsorption of landfill leachates onto activated carbon: Equilibrium and kinetics. J. Hazard. Mater. 131, 170–178. doi:10.1016/j.jhazmat.2005.09.022

Rotter, V.S., Kost, T., Winkler, J., Bilitewski, B., 2004. Material flow analysis of RDF-production processes. Waste Manag. 24, 1005–21. doi:10.1016/j.wasman.2004.07.015

Russo, V., Masiello, D., Trifuoggi, M., Di Serio, M., Tesser, R., 2016. Design of an adsorption column for methylene blue abatement over silica: From batch to continuous modeling. Chem. Eng. J. 302, 287–295. doi:10.1016/j.cej.2016.05.020

Saha, N., Saba, A., Reza, M.T., 2018. Effect of hydrothermal carbonization temperature on pH, dissociation constants, and acidic functional groups on hydrochar from cellulose and wood. J. Anal. Appl. Pyrolysis 1–8. doi:10.1016/j.jaap.2018.11.018

Samad, N.A.F.A., Jamin, N.A., Saleh, S., 2017. Torrefaction of municipal solid waste in Malaysia. Energy Procedia 138, 313–318. doi:10.1016/j.egypro.2017.10.106

Saqib, N.U., Baroutian, S., Sarmah, A.K., 2018. Physicochemical, structural and combustion characterization of food waste hydrochar obtained by hydrothermal carbonization. Bioresour. Technol. 266, 357–363. doi:https://doi.org/10.1016/j.biortech.2018.06.112

Saranya, N., Ajmani, A., Sivasubramanian, V., Selvaraju, N., 2018. Hexavalent chromium removal from simulated and real effluents using Artocarpus heterophyllus peel biosorbent - Batch and continuous studies. J. Mol. Liq. 265, 779–790. doi:10.1016/j.molliq.2018.06.094

Sarc, R., Lorber, K.E., 2013. Production, quality and quality assurance of Refuse Derived Fuels (RDFs). Waste Manag. 33, 1825–34. doi:10.1016/j.wasman.2013.05.004

Sarvaramini, A., Larachi, F., 2014. Integrated biomass torrefaction - Chemical looping combustion as a method to recover torrefaction volatiles energy. Fuel 116, 158–167. doi:10.1016/j.fuel.2013.07.119

Schipfer, F., Vakkilainen, E., Proskurina, S., Heinim, J., 2017. Biomass for industrial applications: The role of torrefaction. Renew. Energy 111, 265–274. doi:10.1016/j.renene.2017.04.015

Sermyagina, E., Saari, J., Zakeri, B., Kaikko, J., Vakkilainen, E., 2015. Effect of heat integration method and torrefaction temperature on the performance of an integrated CHP-torrefaction plant. Appl. Energy 149, 24–34. doi:10.1016/j.apenergy.2015.03.102

Setiabudi, H.D., Jusoh, R., Suhaimi, S.F.R.M., Masrur, S.F., 2016. Adsorption of methylene blue onto oil palm (Elaeis guineensis) leaves: Process optimization, isotherm, kinetics and thermodynamic studies. J. Taiwan Inst. Chem. Eng. 000, 1–8. doi:10.1016/j.jtice.2016.03.035

Séverin, M., Velis, C. a, Longhurst, P.J., Pollard, S.J.T., 2010. The biogenic content of process streams from mechanical-biological treatment plants producing solid recovered fuel. Do the manual sorting and selective dissolution determination methods correlate? Waste Manag. 30, 1171–82. doi:10.1016/j.wasman.2010.01.012

Sharma, B.K., Moser, B.R., Vermillion, K.E., Doll, K.M., Rajagopalan, N., 2014. Production, characterization and fuel properties of alternative diesel fuel from pyrolysis of waste plastic grocery bags. Fuel Process. Technol. 122, 79–90. doi:10.1016/j.fuproc.2014.01.019

Shehzad, A., Bashir, M.J.K., Sethupathi, S., Lim, J.-W., 2015. An overview of heavily polluted landfill leachate treatment using food waste as an alternative and renewable source of activated carbon. Process Saf. Environ. Prot. 98, 309–318. doi:10.1016/j.psep.2015.09.005

Shen, D.K., Gu, S., 2009. The mechanism for thermal decomposition of cellulose and its main products. Bioresour. Technol. 100, 6496–6504. doi:10.1016/j.biortech.2009.06.095

Shen, Y., Yu, S., Ge, S., Chen, X., Ge, X., Chen, M., 2017. Hydrothermal carbonization of medical wastes and lignocellulosic biomass for solid fuel production from lab-scale to pilot-scale. Energy 118, 312–323. doi:10.1016/j.energy.2016.12.047

Shi, Y., Zhang, T., Ren, H., Kruse, A., Cui, R., 2018. Polyethylene imine modified hydrochar adsorption for chromium (VI) and nickel (II) removal from aqueous solution. Bioresour. Technol. 247, 370–379. doi:https://doi.org/10.1016/j.biortech.2017.09.107

Sikarwar, V.S., Zhao, M., Clough, P., Yao, J., Zhong, X., Memon, M.Z., Shah, N., Anthony, E.J., Fennell, P.S., 2016. An overview of advances in biomass gasification. Energy Environ. Sci. 9, 2939–2977. doi:10.1039/C6EE00935B

Silva, R.B., Fragoso, R., Sanches, C., Costa, M., Martins-Dias, S., 2014. Which chlorine ions are currently being quantified as total chlorine on solid alternative fuels? Fuel Process. Technol. 128, 61–67. doi:10.1016/j.fuproc.2014.07.003

Silva, R.B., Martins-Dias, S., Arnal, C., Alzueta, M.U., Costa, M., 2015. Pyrolysis and char characterization of refuse-derived fuel components. Energy and Fuels 29, 1997–2005. doi:10.1021/ef502011f

Singh Kambo, H., Dutta, A., 2015. Comparative evaluation of torrefaction and hydrothermal carbonization of lignocellulosic biomass for the production of solid biofuel. Energy Convers. Manag. 105, 746–755. doi:10.1016/j.enconman.2015.08.031

Singleton, V.L., Orthofer, R., Lamuela-Raventós, R.M., 1998. Analysis of total phenols and other oxidation

substrates and antioxidants by means of Folin-Ciocalteu reagent. Methods Enzymol. 299, 152–178. doi:10.1016/S0076-6879(99)99017-1
Smith, A.M., Ross, A.B., 2016. Production of bio-coal , bio-methane and fertilizer from seaweed via hydrothermal carbonisation. Algal Res. 16, 1–11. doi:10.1016/j.algal.2016.02.026
Smith, A.M., Singh, S., Ross, A.B., 2016. Fate of inorganic material during hydrothermal carbonisation of biomass: Influence of feedstock on combustion behaviour of hydrochar. Fuel 169, 135–145. doi:https://doi.org/10.1016/j.fuel.2015.12.006
Song, J., Zou, W., Bian, Y., Su, F., Han, R., 2011. Adsorption characteristics of methylene blue by peanut husk in batch and column modes. Desalination 265, 119–125. doi:10.1016/j.desal.2010.07.041
Stelte, W., 2012. Torrefaction of unutilized biomass resources and characterization of torrefaction gases. Resultat Kontrakt (RK) Report - Danish Technological Institute.
Stemann, J., Putschew, A., Ziegler, F., 2013. Hydrothermal carbonization: Process water characterization and effects of water recirculation. Bioresour. Technol. 143, 139–146. doi:10.1016/j.biortech.2013.05.098
Stemann, J., Ziegler, F., 2011. Assessment of the energetic efficiency of a continuously operating plant for hydrothermal carbonisation of biomass, in: World Renewable Energy Congress. Linköping, Sweden, pp. 125–132.
Stępień, P., Białowiec, A., 2018. Kinetic parameters of torrefaction process of alternative fuel produced from Municipal Solid Waste and characteristic of carbonized Refuse Dervied Fuel. Detritus 3, 75–83. doi:10.31025/2611-4135/2018.13702
Sumalinog, D., Capareda, S., de Luna, M., 2018. Evaluation of the effectiveness and mechanisms of acetaminophen and methylene blue dye adsorption on activated biochar derived from municipal solid wastes. J. Environ. Manage. 210, 255–262. doi:10.1016/j.jenvman.2018.01.010
Sun, R.-Q., Sun, L.-B., Chun, Y., Xu, Q.-H., 2008. Catalytic performance of porous carbons obtained by chemical activation. Carbon N. Y. 46, 1757–1764. doi:https://doi.org/10.1016/j.carbon.2008.07.029
Tag, A.T., Duman, G., Yanik, J., 2018. Influences of feedstock type and process variables on hydrochar properties. Bioresour. Technol. 250, 337–344. doi:10.1016/j.biortech.2017.11.058
Tagoe, S.O., Horiuchi, T., Matsui, T., 2008. Preliminary evaluation of the effects of carbonized chicken manure, refuse derived fuel and K fertilizer application on the growth, nodulation, yield, N and P contents of soybean and cowpea in the greenhouse. African J. Agric. Res. 3, 759–774.
Tantemsapya, N., 2004. Removal of color, COD and lignin of pulp and paper wastewater using wood ash. Songklanakarin J. Sci. Technol. 26, 1–12.
Taty-Costodes, V.C., Fauduet, H., Porte, C., Ho, Y.S., 2005. Removal of lead (II) ions from synthetic and real effluents using immobilized Pinus sylvestris sawdust: Adsorption on a fixed-bed column. J. Hazard. Mater. 123, 135–144. doi:10.1016/j.jhazmat.2005.03.032
Teixeira, S., Monteiro, E., Silva, V., Rouboa, A., 2014. Prospective application of municipal solid wastes for energy production in Portugal. Energy Policy 71, 159–168. doi:10.1016/j.enpol.2014.04.002
Thommes, M., Kaneko, K., Neimark, A. V, Olivier, J.P., Rodriguez-reinoso, F., Rouquerol, J., Sing, K.S.W., 2015. Physisorption of gases , with special reference to the evaluation of surface area and pore size distribution (IUPAC Technical Report). Pure Appl. Chem. 87, 1051–1069. doi:10.1515/pac-2014-1117
Togashi, T., Miyazaki., T., Yoshimura, J., Yudate, K., Cox, P.A., 2007. Using carbonized refuse derived fuel to restore seaweed forests: A potential conservation technique. Appl. Ecol. Environ. Res. 5, 19–26.
Tovar-gómez, R., Rivera-ramírez, D.A., Hernández-montoya, V., Bonilla-petriciolet, A., 2012. Synergic adsorption in the simultaneous removal of acid blue 25 and heavy metals from water using a Ca (PO 3) 2 -modified carbon. J. Hazard. Mater. 199–200, 290–300. doi:10.1016/j.jhazmat.2011.11.015
Tradler, S.B., Mayr, S., Himmelsbach, M., Priewasser, R., Baumgartner, W., Stadler, A.T., 2018. Hydrothermal carbonization as an all-inclusive process for food-waste conversion. Bioresour. Technol. Reports 2, 77–83. doi:10.1016/j.biteb.2018.04.009
Tran, H.N., You, S.J., Chao, H.P., 2016. Thermodynamic parameters of cadmium adsorption onto orange peel calculated from various methods: A comparison study. J. Environ. Chem. Eng. 4, 2671–2682. doi:10.1016/j.jece.2016.05.009
Tran, K.-Q., 2018. Chapter 10 - Process Intensification and Process Integration for Hydrothermal Processing of Forest Residues and Agricultural Wastes, in: Bhaskar, T., Pandey, A., Mohan, S.V., Lee, D.-J., Khanal, S.K. (Eds.), Waste Biorefinery. Elsevier, pp. 299–322. doi:https://doi.org/10.1016/B978-0-444-63992-9.00010-0
Tumuluru, J.S., Sokhansanj, S., Hess, J.R., Wright, C.T., Boardman, R.D., 2011. A review on biomass torrefaction process and product properties for energy applications. Ind. Biotechnol. 7, 384–401. doi:10.1089/ind.2011.0014
Van de Velden, M., Baeyens, J., Brems, A., Janssens, B., Dewil, R., 2010. Fundamentals, kinetics and endothermicity of the biomass pyrolysis reaction. Renew. Energy 35, 232–242. doi:10.1016/j.renene.2009.04.019

van der Stelt, M., Gerhauser, H., Kiel, J., Ptasinski, K., 2011. Biomass upgrading by torrefaction for the production of biofuels: A review. Biomass and Bioenergy 35, 3748–3762. doi:10.1016/j.biombioe.2011.06.023
Vanjara, A.K., 1998. Colour removal from textile effluent using Refuse Derived Fuel as an adsorbent. Indian J. Chem. Technol. 5, 53–55.
Vassilev, S. V., Baxter, D., Andersen, L.K., Vassileva, C.G., 2010. An overview of the chemical composition of biomass. Fuel 89, 913–933. doi:10.1016/j.fuel.2009.10.022
Vassilev, S. V., Braekman-Danheux, C., Laurent, P., Thiemann, T., Fontana, a., 1999. Behaviour, capture and inertization of some trace elements during combustion of refuse-derived char from municipal solid waste. Fuel 78, 1131–1145. doi:10.1016/S0016-2361(99)00043-5
Vassilev, S. V, Braekman-Danheux, C., Laurent, P., 1999. Characterization of refuse-derived char from municipal solid waste 1 . Phase-mineral and chemical composition. Fuel Process. Technol. 59, 95–134.
Velis, C. a., Longhurst, P.J., Drew, G.H., Smith, R., Pollard, S.J.T., 2010. Production and Quality Assurance of Solid Recovered Fuels Using Mechanical—Biological Treatment (MBT) of Waste: A Comprehensive Assessment. Crit. Rev. Environ. Sci. Technol. 40, 979–1105. doi:10.1080/10643380802586980
Verhoeff, F., Adell i Arnuelos, A., Boersma, A.R., Pels, J.R., Lensselink, J., Kiel, J.H.A., Schukken, H., 2011. TorTech: Torrefaction technology for the production of solid bioenergy carriers from biomass and waste. ECN-E-11-039.
Vieira, C., Machado, B., Ferraz, N., Monteiro, J., Roque, S., 2011. Manual de Gestão de Resíduos Industriais. doi:ISBN: 978-972-8702-70-0
Vollhardt, K.P.C., Schore, N.E., 2007. Organic Chemistry: Structure and Function. W. H. Freeman, New York.
Volpe, R., Messineo, A., Millan, M., Volpe, M., Kandiyoti, R., 2015. Assessment of olive wastes as energy source: pyrolysis , torrefaction and the key role of H loss in thermal breakdown. Energy 82, 119–127. doi:10.1016/j.energy.2015.01.011
Wahid, F.R.A.A., Harun, N.H.H.M., Rashid, S.R.M., Samad, N.A.F.A., Saleh, S., 2017. Physicochemical property changes and volatile analysis for torrefaction of oil palm frond. Chem. Eng. Trans. 56, 199–204. doi:10.3303/CET1756034
Waldheim, L., Nilsson, T., 2001. Heating value of gases from gasification - IEA Bioenergy Agreement, Task 20 - Thermal gasification of biomass.
Wang, L., Barta-Rajnai, E., Skreiberg, O., Khalil, R., Czégény, Z., Jakab, E., Barta, Z., Grønli, M., 2017. Impact of torrefaction on woody biomass properties. Energy Procedia 105, 1149–1154. doi:10.1016/j.egypro.2017.03.486
Wang, S., Wu, H., 2006. Environmental-benign utilisation of fly ash as low-cost adsorbents. J. Hazard. Mater. 136, 482–501. doi:10.1016/j.jhazmat.2006.01.067
Wang, T., Zhai, Y., Zhu, Y., Li, C., Zeng, G., 2018a. A review of the hydrothermal carbonization of biomass waste for hydrochar formation: Process conditions , fundamentals , and physicochemical properties. Renew. Sustain. Energy Rev. 90, 223–247. doi:10.1016/j.rser.2018.03.071
Wang, Tengfei, Zhai, Y., Zhu, Y., Peng, C., Xu, B., Wang, Tao, 2018b. Influence of temperature on nitrogen fate during hydrothermal carbonization of food waste. Bioresour. Technol. 247, 182–189. doi:10.1016/j.biortech.2017.09.076
Wasielewski, R., Stelmach, S., Sobolewski, A., 2011. Production and use of solid recovered fuels. Chemik 65, 572–579.
Weber, K., Quicker, P., 2018. Properties of biochar. Fuel 217, 240–261. doi:10.1016/j.fuel.2017.12.054
Weber, R., Kupka, T., Zając, K., 2009. Jet flames of a refuse derived fuel. Combust. Flame 156, 922–927. doi:10.1016/j.combustflame.2008.12.011
Weide, T., Brügging, E., Wetter, C., 2019. Anaerobic and aerobic degradation of wastewater from hydrothermal carbonization (HTC) in a continuous , three-stage and semi-industrial system. J. Environ. Chem. Eng. 7, 102912. doi:10.1016/j.jece.2019.102912
White, R.H., Dietenberger, M.A., 2001. Wood Products : Thermal Degradation and Fire. Encycl. Mater. Sci. Technol. 48, 9712–9716.
Whyte, H.E., Loubar, K., Awad, S., Tazerout, M., 2015. Pyrolytic oil production by catalytic pyrolysis of refuse-derived fuels: Investigation of low cost catalysts. Fuel Process. Technol. 140, 32–38. doi:10.1016/j.fuproc.2015.08.022
Wilén, C., 2004. Review of waste processing technology for SRF [WWW Document]. IEA Bioenergy Agreem. - Task 36. URL http://www.ieabioenergytask36.org/Publications/2001-2003/Publications/Review_of_Waste_Processing_Technology_for_SRF.pdf
Wilk, M., Magdziarz, A., Jayaraman, K., Szymańska-Chargot, M., Gökalp, I., 2019. Hydrothermal carbonization characteristics of sewage sludge and lignocellulosic biomass. A comparative study. Biomass and Bioenergy 120, 166–175. doi:10.1016/j.biombioe.2018.11.016
Wilk, M., Magdziarz, A., Kalemba, I., 2015. Characterisation of renewable fuels' torrefaction process with different instrumental techniques. Energy 87, 259–269. doi:https://doi.org/10.1016/j.energy.2015.04.073

Wilk, M., Magdziarz, A., Kalemba, I., Gara, P., 2016. Carbonisation of wood residue into charcoal during low temperature process. Renew. Energy 85, 507–513. doi:http://dx.doi.org/10.1016/j.renene.2015.06.072
Wirth, B., Mumme, J., 2013. Anaerobic gigestion of waste water from hydrothermal carbonization of corn silage. Appl. Bioenergy 1–10. doi:10.2478/apbi-2013-0001
Work Group for the preparation of PERSU 2020+, 2018. Persu 2020+ - Document for Public Discussion [WWW Document]. URL https://www.apambiente.pt/_zdata/DESTAQUES/2019/PERSU2020/PERSU2020_Audicao_Publica_dez2018.pdf (accessed 4.15.19).
Wu, F.-C., Wu, P.-H., Tseng, R.-L., Juang, R.-S., 2014. Use of refuse-derived fuel waste for the adsorption of 4-chlorophenol and dyes from aqueous solution: Equilibrium and kinetics. J. Taiwan Inst. Chem. Eng. 45, 2628–2639. doi:10.1016/j.jtice.2014.07.007
Wu, Q., Yu, S., Hao, N., Wells, T., Meng, X., Li, M., Pu, Y., Liu, S., Ragauskas, A.J., 2017. Characterization of products from hydrothermal carbonization of pine. Bioresour. Technol. 244, 78–83. doi:10.1016/j.biortech.2017.07.138
Wüst, D., Rodriguez, C., Uwe, K., Köhler, H., Kruse, A., 2019. Hydrothermal carbonization of dry toilet residues as an added-value strategy – Investigation of process parameters. J. Environ. Manage. 234, 537–545. doi:10.1016/j.jenvman.2019.01.005
Xu, X., Jiang, E., 2017. Treatment of urban sludge by hydrothermal carbonization. Bioresour. Technol. 238, 182–187. doi:10.1016/j.biortech.2017.03.174
Xue, G., Kwapinska, M., Horvat, A., Kwapinski, W., Rabou, L.P.L.M., Dooley, S., Czajka, K.M., Leahy, J.J., 2014. Gasification of torrefied Miscanthus×giganteus in an air-blown bubbling fluidized bed gasifier. Bioresour. Technol. 159, 397–403. doi:10.1016/j.biortech.2014.02.094
Xue, Gang, Kwapinska, M., Kwapinski, W., Czajka, K.M., Kennedy, J., Leahy, J.J., 2014. Impact of torrefaction on properties of Miscanthus×giganteus relevant to gasification. Fuel 121, 189–197. doi:10.1016/j.fuel.2013.12.022
Xue, Y., Gao, B., Yao, Y., Inyang, M., Zhang, M., Zimmerman, A.R., Ro, K.S., 2012. Hydrogen peroxide modification enhances the ability of biochar (hydrochar) produced from hydrothermal carbonization of peanut hull to remove aqueous heavy metals: Batch and column tests. Chem. Eng. J. 200–202, 673–680. doi:https://doi.org/10.1016/j.cej.2012.06.116
Yan, W., Perez, S., Sheng, K., 2017. Upgrading fuel quality of moso bamboo via low temperature thermochemical treatments: Dry torrefaction and hydrothermal carbonization. Fuel 196, 473–480. doi:10.1016/j.fuel.2017.02.015
Yao, Z., Ma, X., 2018. Characteristics of co-hydrothermal carbonization on polyvinyl chloride wastes with bamboo. Bioresour. Technol. 247, 302–309. doi:10.1016/j.biortech.2017.09.098
Yasuhara, A., Amano, Y., Shibamoto, T., 2010. Investigation of the self-heating and spontaneous ignition of refuse-derived fuel (RDF) during storage. Waste Manag. 30, 1161–4. doi:10.1016/j.wasman.2009.11.003
Yeoh, K., Sha, S.A., Al-attab, K.A., Zainal, Z.A., 2018. Upgrading agricultural wastes using three different carbonization methods: Thermal, hydrothermal and vapothermal. Bioresour. Technol. 265, 365–371. doi:10.1016/j.biortech.2018.06.024
Yorgun, S., Vural, N., Demiral, H., 2009. Preparation of high-surface area activated carbons from Paulownia wood by ZnCl2 activation. Microporous Mesoporous Mater. 122, 189–194. doi:10.1016/j.micromeso.2009.02.032
Yu, Y., Lei, Z., Yang, Xi, Yang, Xiaojing, Huang, W., Shimizu, K., Zhang, Z., 2018. Hydrothermal carbonization of anaerobic granular sludge: Effect of process temperature on nutrients availability and energy gain from produced hydrochar. Appl. Energy 229, 88–95. doi:10.1016/j.apenergy.2018.07.088
Yuan, H., Wang, Y., Kobayashi, N., Zhao, D., Xing, S., 2015. Study of fuel properties of torrefied municipal solid waste. Energy & Fuels 29, 4976–4980. doi:10.1021/ef502277u
Yue, Y., Singh, H., Singh, B., Mani, S., 2017. Torrefaction of sorghum biomass to improve fuel properties. Bioresour. Technol. 232, 372–379. doi:10.1016/j.biortech.2017.02.060
Zhai, Y., Peng, C., Xu, B., Wang, T., Li, C., Zeng, G., Zhu, Y., 2017. Hydrothermal carbonisation of sewage sludge for char production with different waste biomass: Effects of reaction temperature and energy recycling. Energy 127, 167–174. doi:10.1016/j.energy.2017.03.116
Zhang, C., Ho, S.H., Chen, W.H., Xie, Y., Liu, Z., Chang, J.S., 2018. Torrefaction performance and energy usage of biomass wastes and their correlations with torrefaction severity index. Appl. Energy 220, 598–604. doi:10.1016/j.apenergy.2018.03.129
Zhang, Y.Z.H., Liang, H.Z.M., Lu, R., 2012. Adsorption of chromium (VI) from aqueous solution by the iron (III)-impregnated sorbent prepared from sugarcane bagasse. Int. J. Environ. Sci. Technol. 9, 463–472. doi:10.1007/s13762-012-0043-9
Zhang, Z., Hara, I.M.O., Kent, G.A., Doherty, W.O.S., 2013. Comparative study on adsorption of two cationic dyes by milled sugarcane bagasse. Ind. Crop. Prod. 42, 41–49. doi:10.1016/j.indcrop.2012.05.008
Zhao, K., Li, Y., Zhou, Y., Guo, W., Jiang, H., Xu, Q., 2018. Characterization of hydrothermal carbonization products (hydrochars and spent liquor) and their biomethane production performance. Bioresour. Technol.

267, 9–16. doi:10.1016/j.biortech.2018.07.006
Zhou, C., Yang, W., 2015. Effect of heat transfer model on the prediction of refuse-derived fuel pyrolysis process. Fuel 142, 46–57. doi:10.1016/j.fuel.2014.10.079
Zhu, Y., Yi, B., Yan, S., Yuan, Q., Wu, Y., 2018. Removal of methylene blue from aqueous solution by cattle manure-derived low temperature biochar. RSC Adv. 8, 19917–19929. doi:10.1039/c8ra03018a
Zhuang, X., Zhan, H., Huang, Y., Song, Y., Yin, X., Wu, C., 2018. Conversion of industrial biowastes to clean solid fuels via hydrothermal carbonization (HTC): Upgrading mechanism in relation to coalification process and combustion behavior. Bioresour. Technol. 267, 17–29. doi:10.1016/j.biortech.2018.07.002
Zornoza, R., Moreno-Barriga, F., Acosta, J.A., Muñoz, M.A., Faz, A., 2016. Stability, nutrient availability and hydrophobicity of biochars derived from manure, crop residues, and municipal solid waste for their use as soil amendments. Chemosphere 144, 122–130. doi:10.1016/j.chemosphere.2015.08.046
Zwart, R., Heijden, S. Van Der, Dahlman, R.E., Dall, J., Dall, B., Dfbt, P.S., Anhydro, J.K., 2010. Tar removal from low-temperature gasifiers.

Appendix

A.1 – Chapter 3

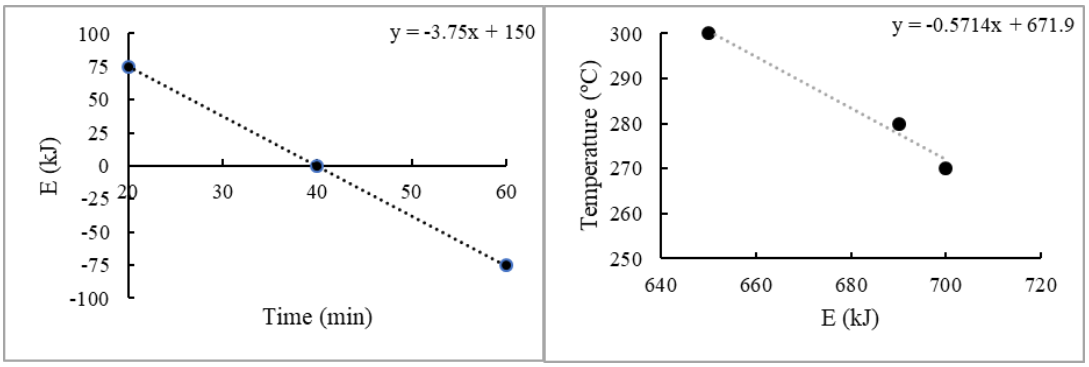

Figure A.1: Linear regressions used for the calculations of the heat of torrefaction/carbonization (Q_4) in Chapter 3, based on values from (Ohliger *et al.*, 2013).

Table A.1: Estimated valued for the thermal loses (Q_5), expressed in %, from the process performance in Chapter 3.

Temperature (ºC)	Residence Time (min)		
	15	30	60
200	25	30	35
250	30	35	40
300	35	40	45
350	40	45	50
400	45	50	55

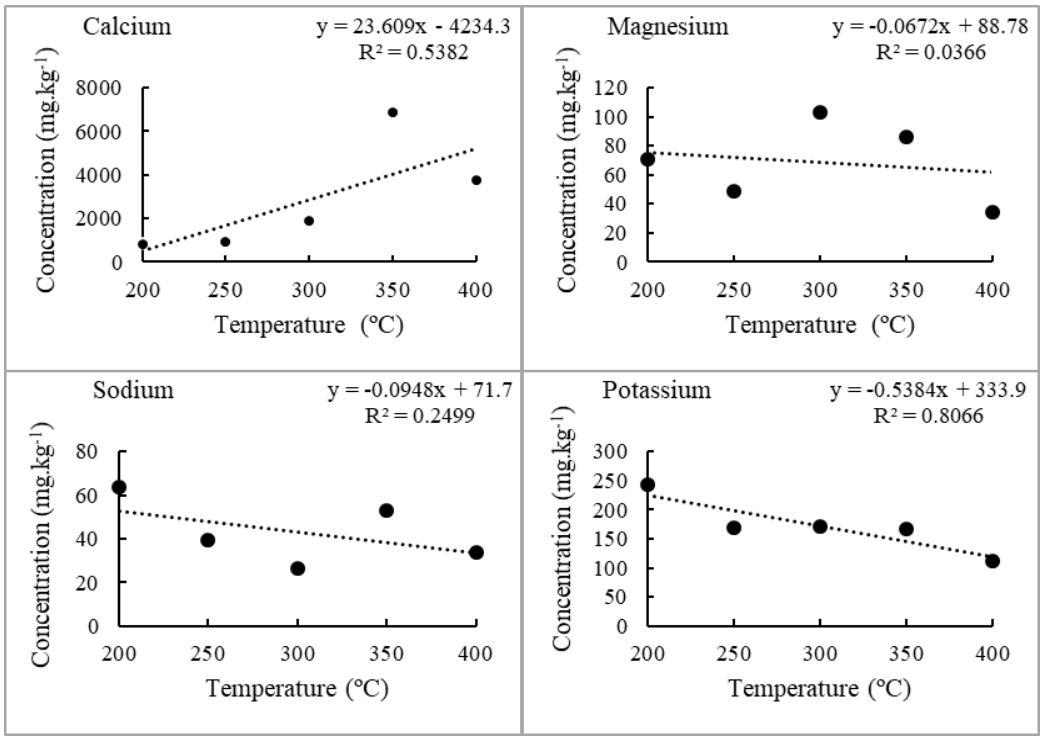

Figure A.2: Correlations between the concentrations of alkali and alkali-earth metals and process temperature, in the RDF chars' leachates from Chapter 3.

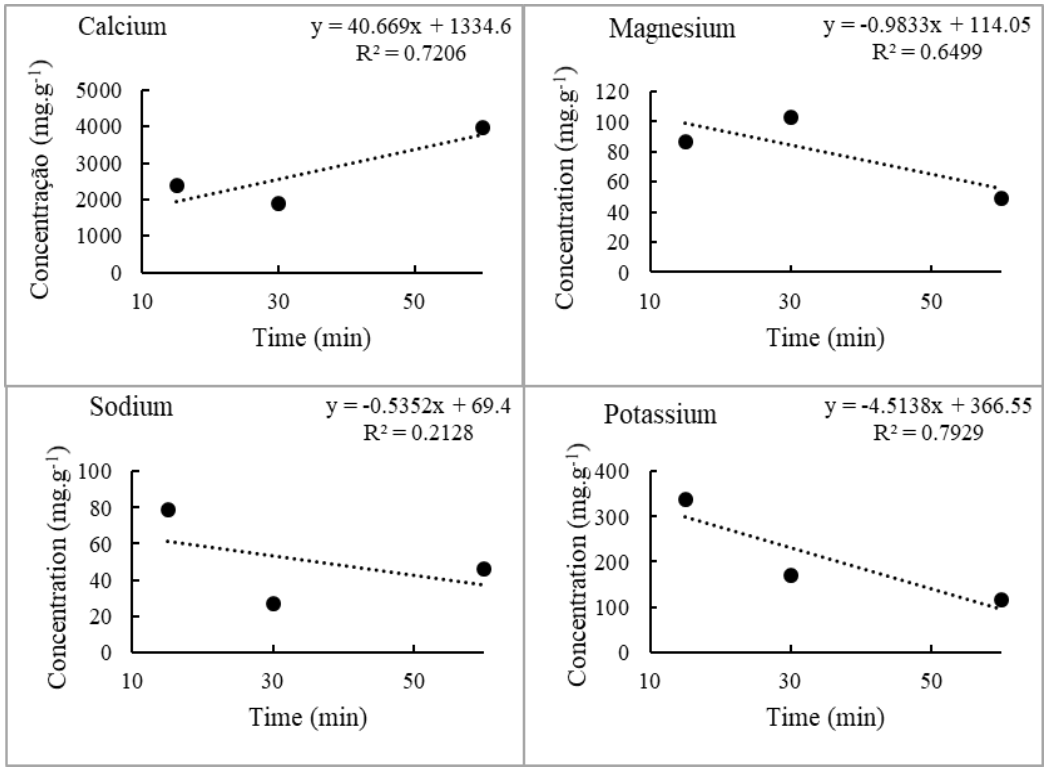

Figure A.3: Correlations between the concentrations of alkali and alkali-earth metals and process residence time, in the RDF chars' leachates from Chapter 3.

Table A.2: Pearson correlation coefficients determined through Figures A.2 and A.3.

Element	Pearson correlation coefficient (ρ)	
	Temperature	Time
Ca	0.734	0.849
Mg	0.191	0.806
K	0.898	0.461
Na	0.500	0.890

A.2 – Chapter 4

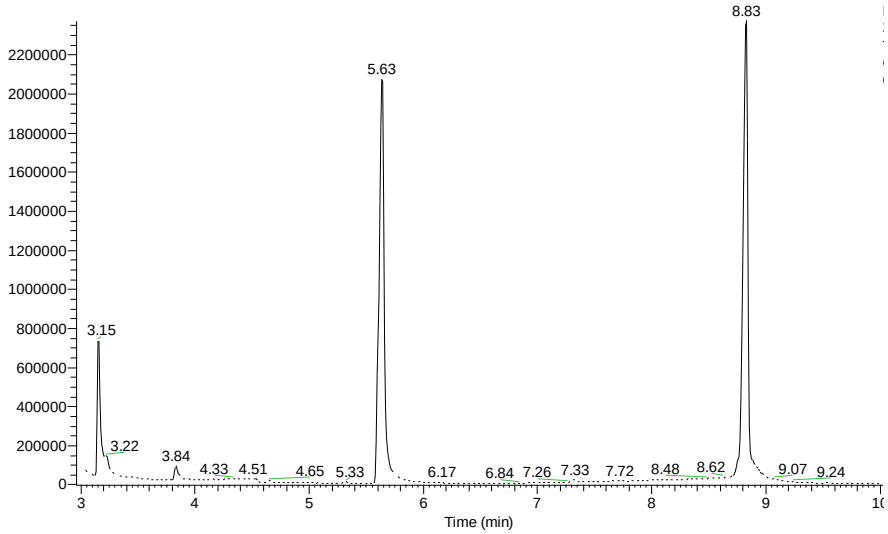

Figure A.4: Organic acids, peaks labeled with retention times (RT): acetic acid (RT=3.15), propionic acid (RT=5.63) and butyric acid (RT=8.83), used for identification in the chromatograms of Chapter 4.

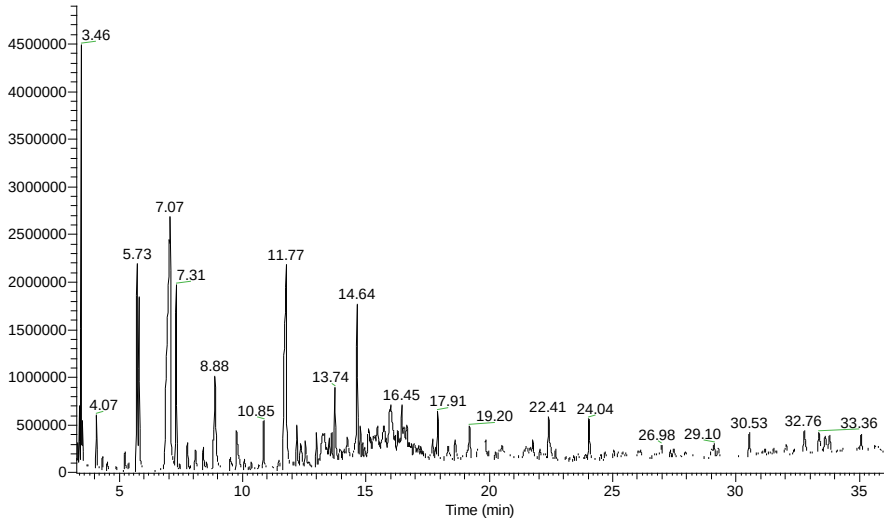

Figure A.5: Representative normalized chromatogram from the organic extract of the condensates from the 2nd collection point of the carbonization test conducted at 400 ºC and 30 minutes from Chapter 4. Peaks labeled with retention times (RT).

Table A.3: Identified peaks from Figure A.5.

Compound	Retention time (min)
Oxalic acid (TMS)	3.11
Acetic acid (TMS)	3.46
4,4-dimethyl-2-pentynal	4.07
Butanol (TMS)	5.73
Propionic acid (TMS)	5.81
3-Furancarboxaldehyde	7.07
2-chloroethanol (TMS)	7.31
Ethylbenzene	7.76
Xylene	8.09
Styrene	8.88
2-acetylfuran	9.76
3-carene	10.85
2,4,6-trimethyl -(2a, 4a,6a)-1,3-dioxane	10.99
Cumene	11.47
5-methyl-2-furaldehyde	11.77
2-propenyl-benzene	12.19
Benzonitrile	12.35
1-ethyl-2-methylbenzene	12.54
Phenol	13.25
2-ethylcyclopentanone	14.24
Phenol (TMS)	14.64
2,2-Dihydroxy-1-phenyletanone	15.1
3-hydroxy-2-methyl-4H-pyran-4-one	16
Octanol (TMS)	16.45
Naphtalene	18.61
Benzoic acid	19.86
1,1'-Biphenyl	24.04
Guaiacylacetone	28.03
Phenantrene	33.36

Note: Oxalic acid peak is omitted due to its larger area at the beginning of the chromatogram. Some retention times are not shown in the chromatogram due to the small area of the peaks. TMS stands for trimethylsilyl derivative.

A.3 – Chapter 5

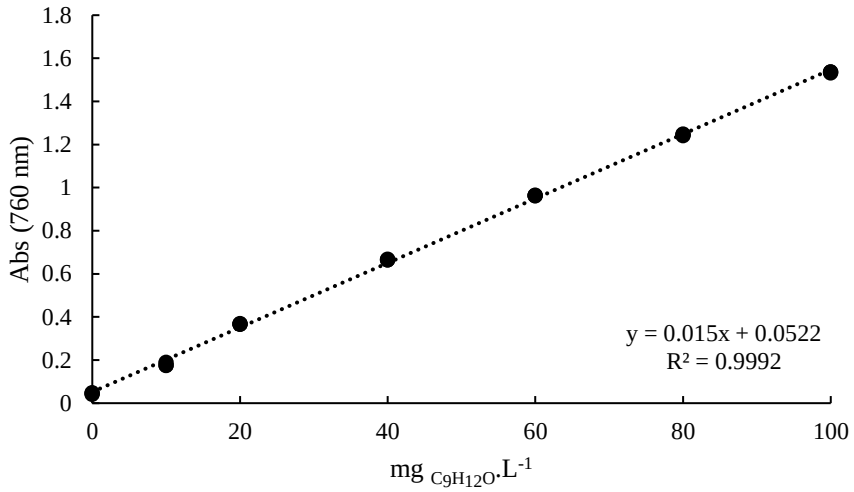

Figure A.6: Calibration curve used for the determination of total phenolic compounds, using the Folin-Ciocalteu method, with 2,4,6-trimethylphenol as a standard (Chapter 5).

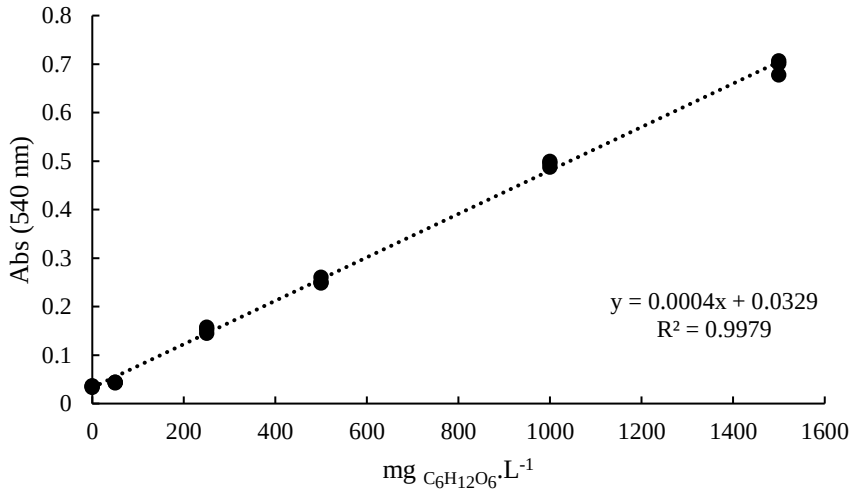

Figure A.7: Calibration curve used for the determination of total reducing sugars, using the DNS method, with glucose as a standard (Chapter 5).

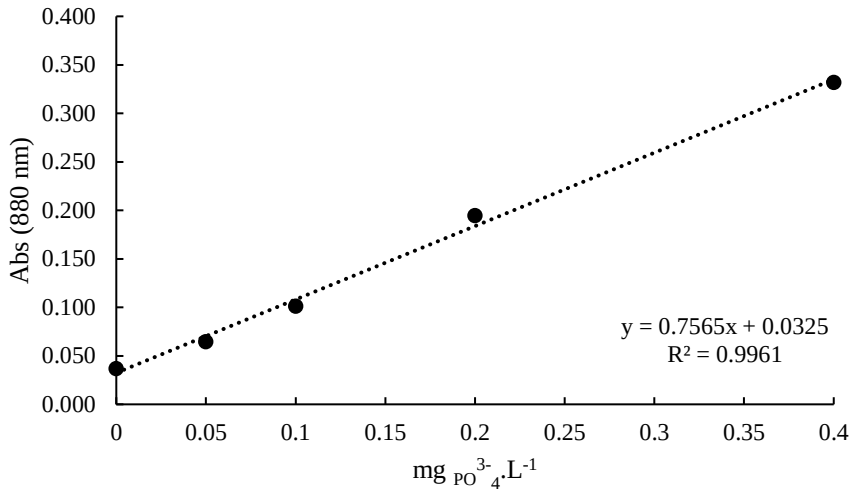

Figure A.8: Calibration curve used for the determination of total phosphorous, using the ascorbic acid method, with phosphate as a standard (Chapter 5).

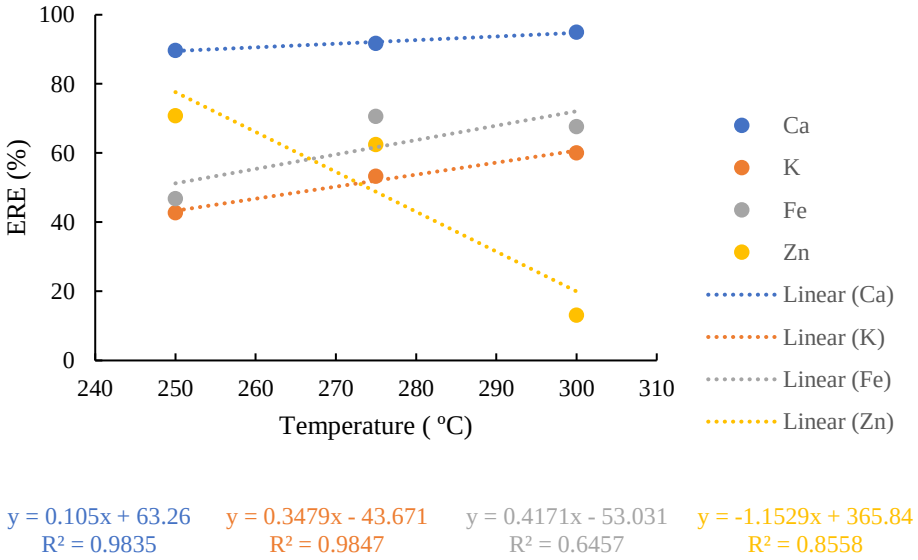

Figure A.9: Correlations between element removal efficiency (ERE, %) and temperature for the hydrochars produced in Chapter 5 (Ca, K, Fe, Zn).

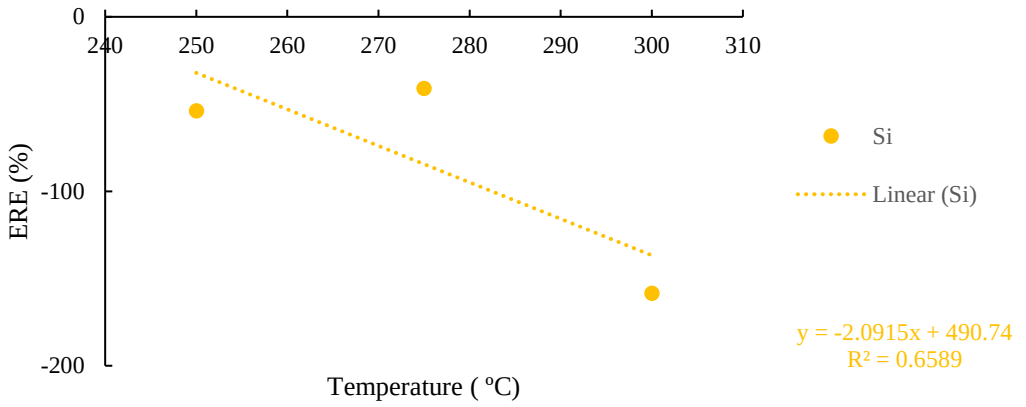

Figure A.10: Correlations between element removal efficiency (ERE, %) and temperature for the hydrochars produced in Chapter 5 (Ti, Pb, Cu, Cr).

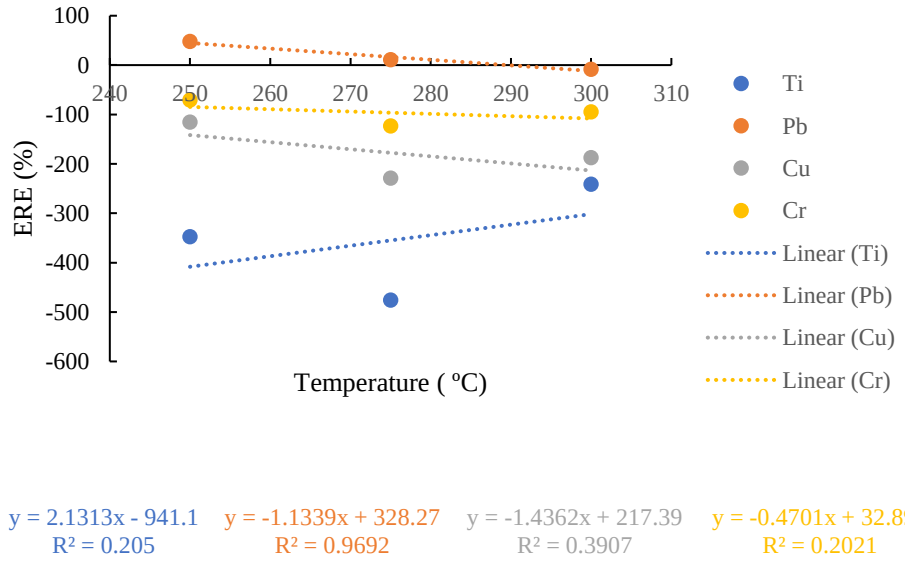

Figure A.11: Correlations between element removal efficiency (ERE, %) and temperature for the hydrochars produced in Chapter 5 (Ti, Pb, Cu, Cr).

Table A.4: Correlation coefficients determined from Figures A.9, A.10 and A.11.

Metal	Pearson correlation coefficient (ρ)
Ca	0.992
K	0.992
Fe	0.804
Zn	0.925
Ti	0.453
Pb	0.984
Cu	0.625
Cr	0.450
Si	0.812

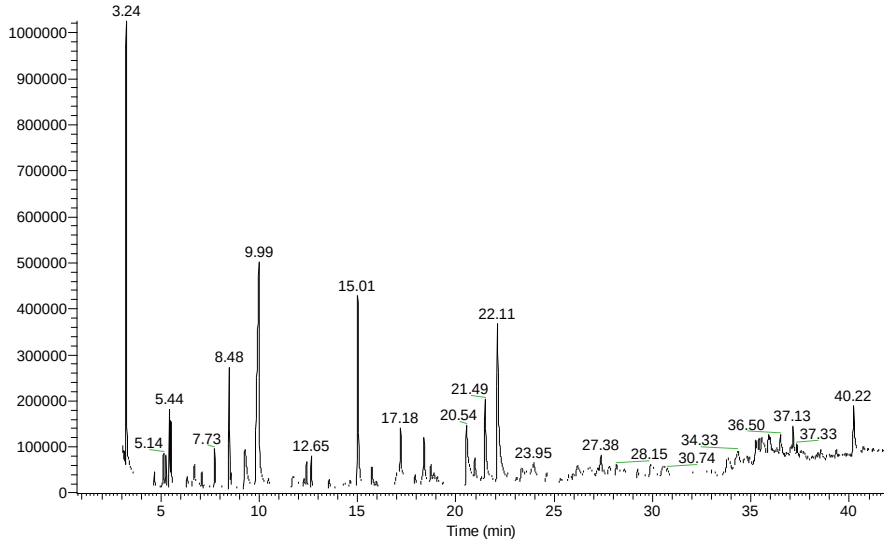

Figure A.12: Representative normalized chromatogram from the organic extract of HTC process water obtained from the process at 300 ºC for 120 minutes, from Chapter 5, labeled with retentions times (RT).

Table A.5: Identified peaks from Figure A.12.

Compounds	Retention time (min)
Acetic acid (TMS)	3.24
2-Propenoic acid (TMS)	5.14
Butanol (TMS)	5.44
Propanoic acid (TMS)	5.51
Isobutyric acid (TMS)	6.71
3-Furaldehyde	7.07
3-hydroxy-3-buten-2-one (TMS)	7.73
Pentanol (TMS)	8.48
2,4-dimethylfuran	9.27
2-Methyl-2-cyclopentenone	9.99
2,2,7,7-Tetramethyloctane	12.4
Phenol (TMS)	15.01
Octanol (TMS)	17.18
1-cyclohexen-1-yl methyl ketone	17.93
p-Methylphenol	18.37
o-Methylphenol	18.72
Sorbic acid (TMS)	20.54
2-(phenylmethyl)-phenol	20.95
2-Methoxyphenol (TMS)	21.49
Benzoic acid (TMS)	22.11
1-Benzyl-2,4-dimethylbenzene	23.34
2-hydroxy-benzophenone	23.95
2,4,6-Trimethoxytoluene	26.15
2,6-dimethoxy-phenol	26.78
1,4-Dihydroxybenzene (TMS)	27.38
Acetophenone (TMS)	27.78
1-Ethyl-2-methylphenanthrene	28.15
9-Acetylphenanthrene	29.89
2,3,4,6-Tetramethoxystyrene	30.55
m-Anisaldehyde (TMS)	32.14
1,1-di-3,4-xylyl-ethane	33.82

Note: Some retention times are not shown in the chromatogram due to the small area of the peaks. TMS stands for trimethylsilyl derivative.

A.4 – Chapter 6

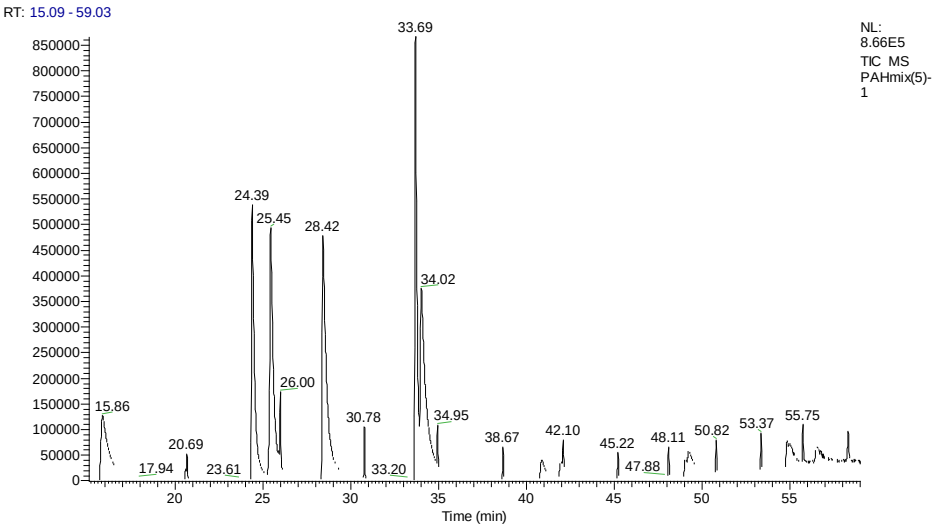

Figure A.13: PAHs mix standard solution (Chem Service) used for identification in the tar samples from Chapter 6.

Table A.6: Identified PAHs from Figure A.13.

Compound	Retention Time (min)
Naphtalene	15.86
Acenaphtylene	24.39
Acenaphtene	25.45
Fluorene	28.42
Phenantrene	33.69
Anthracene	34.02
Fluoranthene	38.67
Pyrene	42.10
Benzanthracene	45.22
Chrysene	48.11
Benzo(k)fluoroanthene	50.82
Benzo(b)fluorathene	53.37
Benzo(a)pyrene	55.75

A.5 – Chapter 7

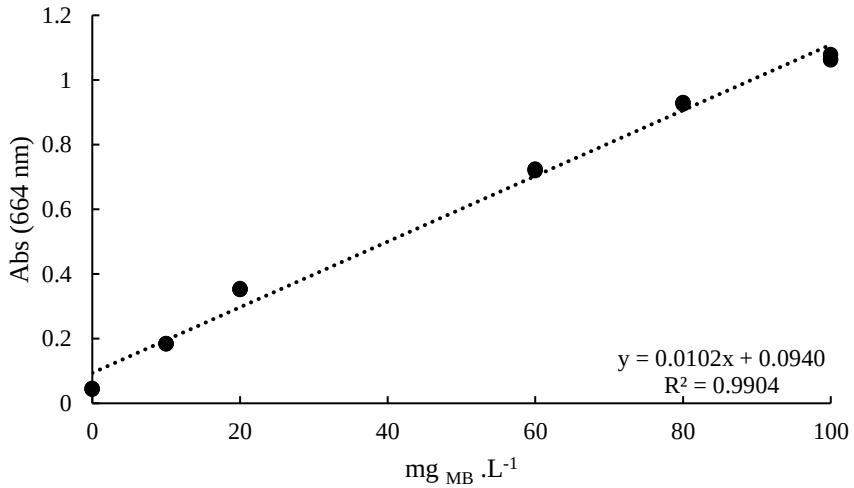

Figure A.14: Example of calibration curve for methylene blue (MB) used in Chapter 7.

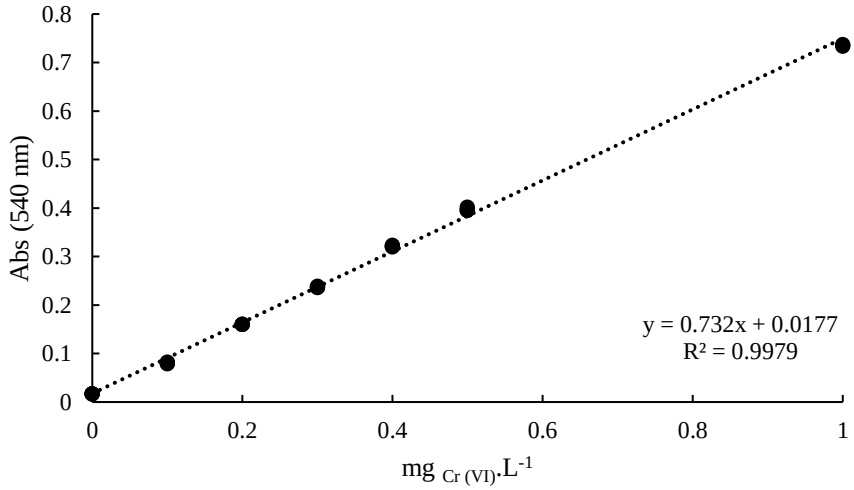

Figure A.15: Example of calibration curve for chromium (VI), obtained through the 1,4-diphenylcarbizide method, used in Chapter 7.